Membrane Based Intensification of Ammonia Removal from Wastewater

BY

Azel Almutairi

Submitted to the graduate degree program in Chemical & Petroleum Engineering and the Graduate Faculty of the University of Kansas in partial fulfillment of the requirements for the degree of Doctor of Philosophy

Chairperson, Dr. Laurence Weatherley

Dr. Craig Adams

Dr. Karen Nordheden

Dr. Shapour Vossoughi

Dr. Russell Ostermann

12/15/2011

Date defended

The Dissertation Committee for Azel Almutairi certifies that this is the approved version of the following dissertation:

Membrane Based Intensification of Ammonia Removal from Wastewater

Chairperson, Dr. Laurence Weatherley

12/15/2011

Date approved

Abstract

The aim of this research was to study a novel membrane based oxygen intensification system to enhance a biological wastewater treatment process for ammonia removal. Specifically, this work is concerned with the biological nitrification process which occurs in ion exchange packed columns during ammonia removal from wastewater.

Two types of commercial clinoptilolite were used, namely KMI and BIT, as ion exchangers. Removal of ammonium ion by ion exchange offers a number of advantages such as the capability to handle shock loadings and to purify wastewater to a very high specification. Also, ion exchangers can be used to provide a solid surface for bacterial growth which enhances performance.

The uptake removal rates of ammonium ions onto KMI and BIT clinoptilolite using DI water, RO water, and filtered tap water were examined. The presence of major metal ions that normally exist in wastewater such as K^{+}, Ca^{++}, and Mg^{++} and their impact on ammonia adsorption was tested. The experimental data were fitted using Langmuir and Freundlich isotherms and compared to related works done previously. KMI clinoptilolite exhibited the highest uptake capacity, and KMI clinoptilolite preference for the metal ions was found to be in the order $Mg^{++} \approx K^{+} > Ca^{++}$.

The kinetics of the ammonium ion removal were studied at bench scale using KMI and BIT clinoptilolite. The process variables include: initial ammonia concentration, amount of clinoptilolite in contact with the solution, clinoptilolite particle size, and mixing speed. To model the kinetics removal rates two types of diffusion was assumed to be possible rate limiting steps, namely the external film diffusion and the intraparticle diffusion. Two models were selected to

fit the controlled diffusion resistances, Furusawa-Smith to model the external film resistance and McKay model to model the intraparticle film resistance. The values of the external and internal mass transfer coefficients were calculated and tabulated.

Five air permeable membranes were used, four porous membranes and a dense membrane. The porous membranes were Polyethersulfone (PES), Polytetrafluoroethylene (PTFE), Polypropylene (PP), and Nylon. The dense membrane was a silicon tube membrane. All membranes were assessed for aeration. The overall mass transfer coefficients were calculated using the two-film theory model. The highest oxygen transfer rate was observed in PTFE membrane, and in the following order of lower performance PP > PES > Nylon > silicon tube.

For the column studies, different loading rates were used, 0.96, 0.25, and 0.03 Kg N/(m^3day) depending on the type of the experiment. For the bacteria-free silicon membrane column, the inlet ammonia concentration, bed height, and inlet flowrate were examined. Biologically activated silicon membrane column exhibited no difference in the ammonia removal comparing to bacteria-free column under the same operating conditions.

The porous membrane columns were designed to enhance the aeration for the combined biologically active ion exchanger packed bed column. It was found that the porous membrane columns were significantly enhanced by introducing the nitrifying bacteria into the columns. For example, the uptake capacity of PP membrane column was increased from 0.43 to 0.67 meq/g by introducing the biological material into the PP column. The breakthrough bed volumes (BVs) were estimated and the uptake column capacities were calculated for all the used columns. The breakthrough curves were modeled using the Bohart-Adams and Thomas models.

To assess the bio-regeneration as an alternative to the chemical regeneration, nitrifying bacteria circulated in PP and PES columns to treat exhausted KMI clinoptilolite. The results showed that some regeneration may be achieved, but complete regeneration would require higher concentrations of biomass which is recommended for future study.

Dedication

This work is dedicated to my parents Joza and Fihan Almutairi

Acknowledgement

I would like to acknowledge my advisor, Professor Laurence Weatherley, for giving me the opportunity to work with him and for his continuous support and encouragement over the last four years. His input to all the work presented here was critical.

I would like to offer thanks to my committee members Dr. Craig Adams, Dr. Karen Nordheden, Dr. Shapour Vossoughi, and Dr. Russell Ostermann for their time and input to this research.

Thanks must be offered to Kuwait University for the funding they provided to me.

The following people provided help for this research and I need to pass thanks to them: Alan walker, Dr. Karen Peltier, Dr. Belinda Sturm, Mohammad Almishwat, Dr. Philip Gao., Neeraja Vajrala, and Prem Thapa.

My family deserves special thanks, My mother Joza Almutairi, my brother Bo Fihan Mubarak, My sisters Alia and Mariam. To my wife Hessa, my daughters Asma, Amar, and Shaikhah, and my son Jarrah I would say: Thank you, you are gifts from God.

To my friends, in Kuwait and in Lawrence, thank you.

Table of Contents

List of Figures

List of Tables

1 Introduction

1.1 Wastewater treatment and the environment

Water is what distinguishes earth from other planets and it is essential for man's, plant, and animal life continuation. Due to man's use and influence, water resources are threatened by continuing degradation. Therefore, to protect the water bodies, many water quality regulations were enacted in the middle of the 20th century. As an example, the 1948 Water Pollution Control Act was originated as the first federal water pollution program [1]. This law was amended several times which indicates that water quality became an increasing concern [2]. In 1970, the Environmental Protection Agency (EPA) was established as an indicator of the awareness of environmental problems including the presence of wastes in water. EPA and other international environmental agencies, such as The Council of European Committees, have set standards to satisfy the removal of pollutants from wastewater. Among these pollutants, ammonia has attracted significant attention and is considered to be a toxic contaminant which is ubiquitous in domestic and municipal wastewater. EPA has set an effluent concentration limit of 0.5 mg as N/l throughout for all sewage treatment works [3]. The potential future application of many parts of the work carried out in this research is expected to be integrated into the wastewater treatment process.

1.1.1 Wastewater treatment plant

Wastewater treatment is an important engineering task used to fulfill society's need for clean water. Conventionally, the wastewater treatment plant consists of four major steps: preliminary treatment, primary treatment, secondary treatment, and tertiary treatment. The preliminary treatment is where the raw waste water passes through screens, grit chambers, comminuting devices, pre-aeration tanks, equalization tanks, and sedimentation tanks. The primary treatment

mainly has the following functions: (1) removal of all settleable suspended organic solids and heavy inorganic; (2) removal of excessive amount of oils and greases. Secondary treatment depends on biological oxidation to reduce the biological oxygen demand (BOD) by converting the organic matter in presence of microbes to CO_2 and H_2O. The most commonly used methods in secondary treatment are the trickle filter system and the activated sludge process. The removal percentage of total nitrogen, in secondary treatment, varies from 10-25% [4]. Tertiary treatments are introduced for further disinfection and for the removal of remaining pathogens prior to discharging the wastewater into receiving water bodies. Figure 1.1 shows the main stages discussed above.

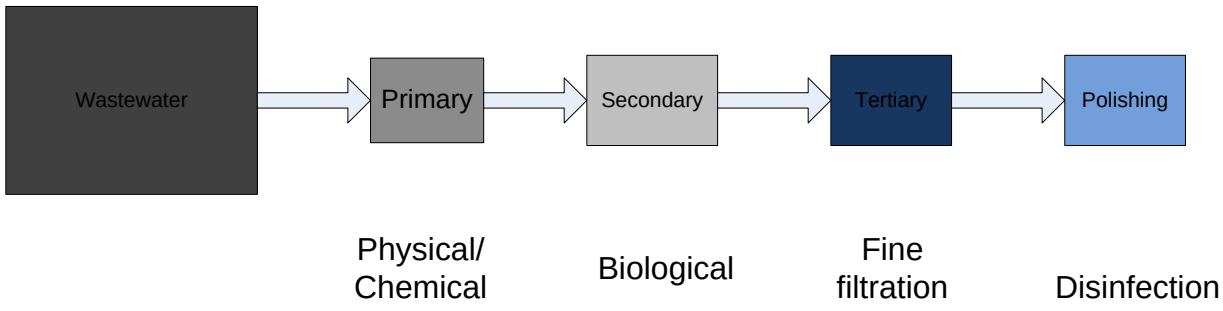

Figure 1.1: A schematic diagram of a water treatment plant.

1.2 Ammonia in environment

Nitrogen is one of the principal nutrients found in wastewater and it can severely damage water bodies . Ammonia is the most commonly occurring nitrogenous pollutant in wastewater [4]. The chemical form of ammonia in water exists into two forms, the more abundant of which is the ionized form, the ammonium ion (NH_4^+), and the less abundant of which is the unionized form, the ammonia molecule (NH_3). The pH is a critical variable which determines the proportion of each form. The equilibrium of these two forms can be represented by the following equations:

$$NH_4^+ \leftrightarrow NH_3 + H^+ \quad (1.1)$$

Equation (1.1) can be written in the thermodynamic equilibrium constant, *K*, as:

$$K = \frac{(NH_3)(H^+)}{(NH_4^+)} \quad (1.2)$$

Where the symbol (…) indicates the activity, *a*, which has the units of mol/l and,

$$a = \gamma C \quad (1.3)$$

or in symbolic form,

$$(\quad) = \gamma[\quad] \quad (1.4)$$

where γ is the activity coefficient, and C or [ ] is the concentration in mol/l. Normally, the activity coefficient of water equals to1 if the solution is considered as an ideal solution. Accordingly, Equation (1.2) can be rewritten as the following,

$$K = \frac{[NH_3][H^+]}{[NH_4^+]} \quad (1.5)$$

As Equation (1.4) suggested, the dissociation of ammonia into NH_3 or NH_4^+ highly depends on both the pH and the temperature of the medium. Figure 1.2 describes the effect of pH and

temperature on ammonia/ammonium equilibrium [5].

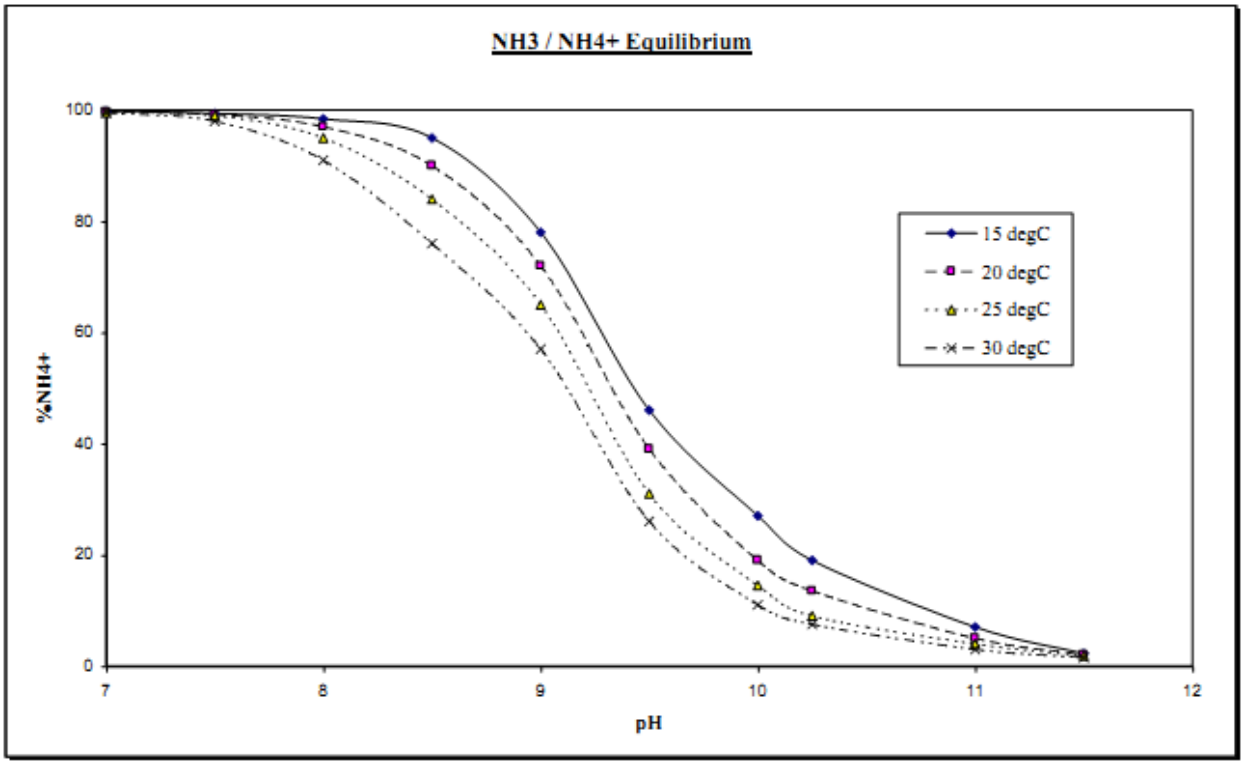

Figure 1.2: The effect of pH and temperature on ammonia/ammonium equilibrium [5].

The free unionized ammonia is considerably harmful and more toxic than the ionic form [3, 6]. Therefore, the equilibrium should be maintained towards the ionic form, i.e. pH<8, not only for safety reason but also for removal by ion exchange [3]. EPA criterion for fresh water aquatic life is 0.02 mg/l of unionized ammonia.

1.3 The nitrogen cycle

Nitrogen is an element of high importance as it is one of the building blocks of life in the majority of living systems [3]. It is present in DNA, RNA, and proteins [7]. The fundamental structure of nitrogen is behind its unique importance. The ground state of electron configuration of nitrogen is $1s^2\ 2s^2\ 2p^3$ and each of the *p*-orbitals is occupied by one electron ($2px^1\ 2py^1\ 2pz^1$)

which allow nitrogen to produce a total of eight oxidation states that varies from -3 to +5 [8] as shown in Table 1.1.

Table 1.1: Oxidation states of nitrogen [8].

Nitrogen:	$1s^2\ 2s^2\ 2p^3$	
Valance	Compound	Formula
-3	Ammonia	NH_3
-1	Hydroxylamine	$HONH_2$
0	Nitrogen gas	N_2
+1	Nitroxyl	HNO
+3	Nitrite ion	NO_2^-
+5	Nitrate ion	NO_3^-

Atmospheric nitrogen gas, N_2, consists 79% of the atmosphere. Although that, it is not available to higher plants or animals unless it combines with other compounds of nitrogen fixation [9]. Figure 1.3 shows the main four steps in the nitrogen cycle, which are nitrogen fixation, decay, nitrification, and denitrification [4].

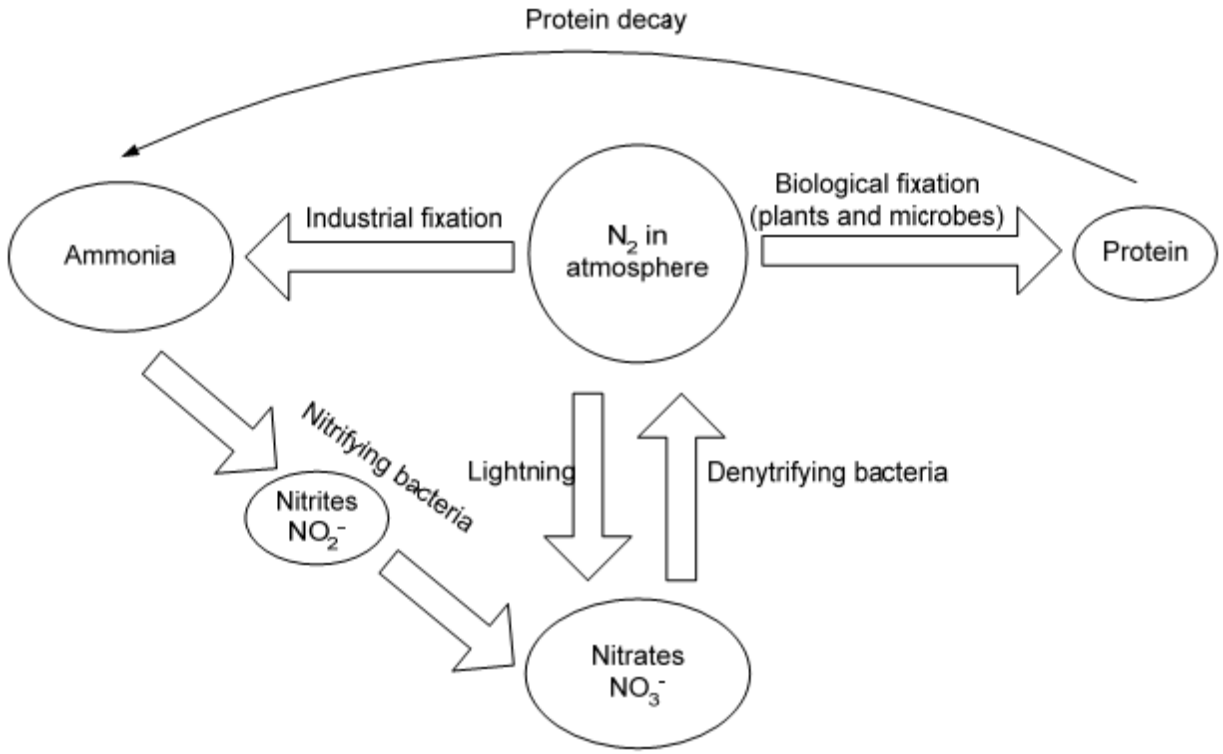

Figure 1.3: Simplified nitrogen cycle [4].

Nitrogen in the atmosphere is fixed by nitrogen fixing microorganisms into organic nitrogen which is incorporated into plant tissue (This known as the biological fixation step). When proteins enter the food chain, it is returned to soil as organic nitrogen from plant decay or human and animal wastes where the microorganisms break down the organic molecules into ammonia (Decay step). Then, ammoniacal nitrogen is oxidized to nitrite and nitrate by nitrifying bacteria (Nitrification step). In the denitrification step, nitrate is reduced to nitrogen by denitrifying bacteria, and nitrogen is returned to atmosphere. Lightning strikes, closer to earth, split water atoms into hydrogen (H) and hydroxyl radical (OH^-) which is highly reactive and ready to react with nitrogen to form nitric acid which is adsorbed by air's moisture and then precipitated into earth (Lightning step) [4]. The nitrification step is discussed in details in section 1.2.1 due to its importance to this work.

1.3.1 Nitrification

There are several means to remove ammonia from wastewater. Currently, the biological nitrification process is the most economical and common mean used in wastewater treatment [10]. Nitrification may defined as the microbiological oxidation of ammoniacal nitrogen to nitrite (NO_2^-) by ammonia oxidizing bacteria (AOB) and nitrite to nitrate (NO_3^-) by nitrite oxidizing bacteria (NOB) in presence of oxygen. Two bacterial groups participate in each step of the oxidation process, namely *Nitrosomonas* and *Nitrobacter*. Equations 1.6 and 1.7 describe the two stages of nitrification process.

$$NH_4^+ + \frac{3}{2}O_2 \xrightarrow{Nitrosomonas} NO_2^- + 2H^+ + H_2O \quad (1.6)$$

$$NO_2^- + \frac{1}{2}O_2 \xrightarrow{Nitrobacter} NO_3^- \quad (1.7)$$

The oxidation of ammonia to nitrite (Equation 1.7) is the rate limiting step and thus this step determines the overall kinetics [4]. Based on Equation 1.7 and 1.8, a large amount of dissolved oxygen is needed to perform the nitrification reactions (4.27g of O_2 per 1.0g of NH_4^+) [5].

1.3.2 Nitrifying bacteria

Many bacterial species have the capability to oxidize inorganic nitrogen to nitrite and nitrate. As a matter of fact, as many as 404 bacterial species that could accomplish this type of oxidation were reported [11]. The bacterial family of *Nitrobacteraceae* is composed of two groups which are *Nitrosomonas*, as AOB and *Nitrobacter*, as NOB [8]. Typically, AOB have a genus name begins with "*Nitroso-*", and *Nitrosomonas* is the famous genera of AOB [7] while Nitrobacter is the genus of bacteria that is associated with NOB [10]. Other common AOB genera are

Nitrosococcus, *Nitrosospira*, and *Nitrosolobus* [12]. More specifically, *Nitrosomonas europea*, *Nitrosomonas monella*, *Nitrosococcus sp.*, *Nitrosospira sp.*, *Nitrosocystic sp.*, and *Nitrosogloea sp.* are able to function as AOB, while *Nitrobacter Winogradskyi, Nitrobacter agile*, and *Nitrobacter sp.* are considered as NOB [11]. In literature, *Nitrosomonas europea* and *Nitrobacter Winogradskyi* are suggested to be used in nitrification process rather than other types [3-8]. *Nitrosomonas europea* has a centerline length of from 1.0 to 2.0 µm and a width of 0.8 to 0.9 µm [8]. *Nitrosomonas europea* and *Nitrobacter Winogradskyi* are shown in Figure 1.4 and 1.5 respectively.

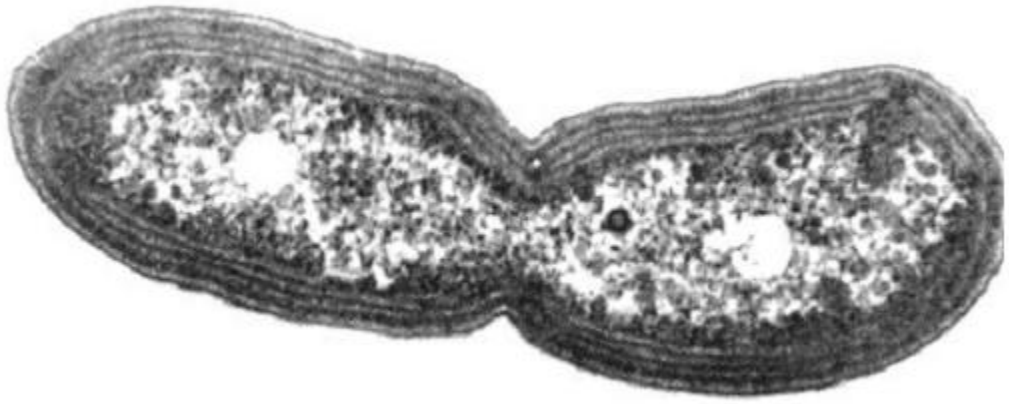

Figure 1.4: Nitrosomonas europea, Magnification X 32,500[3].

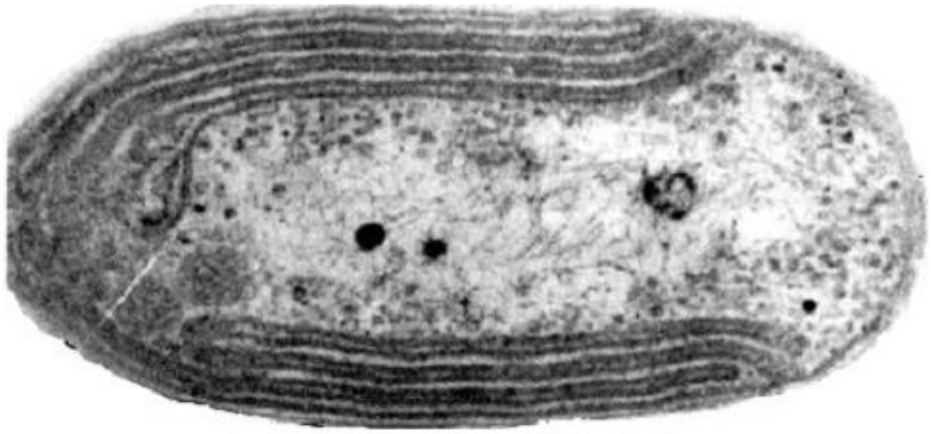

Figure 1.5: Nitrobacter Winogradskyi, Magnification X 63,000 [3].

Some characteristics of *Nitrosomonas europea* and *Nitrobacter Winogradskyi* are provided in Table 1.2.

Table 1.2: Characteristics of *Nitrosomonas europea* and *Nitrobacter Winogradskyi*. Obtained from [3] unless mentioned otherwise.

	Nitrosomonas europea	*Nitrobacter Winogradskyi*
Cell shape	Ovoid to rod-shape	Ovoid to rod-shape
centerline length	1.0 – 1.5 µm 1.0 – 2.0 µm [9]	0.5 – 1.0 µm
Width	0.8 - 0.9 µm [9]	-
Gram test	Negative	Negative
Generation time	8-36 hr	12-59 hr
DO requirements	Strict aerobe	Strict aerobe

Nitrifying bacteria are aerobes that have the following characteristics; they are: *autotrophs*: i.e., they fix and reduce inorganic carbon, *chemolithotrophs*: their nitrogen electron donor is oxidized in the cell, and *obligate*: they use O_2 for respiration and as an electron acceptor [11, 13].

During nitrification, some of the consumed nitrogen is built up into bacterial protoplasm with an empirical cell formulation of $C_5H_7O_2N$, and the production of the biomass can be written as [4]:

$$5CO_2 + NH_4^+ + 2H_2O \rightarrow C_2H_7O_2N + 5O_2 + H^+ \quad (1.8)$$

where $C_5H_7O_2N$, the biomass, counts for both *Nitrosomonas* and *Nitrobacter*.

The oxidation reactions of ammonia and nitrite are represented by the following equations [4]:

$$55NH_4^+ + 5CO_2 + 76O_2 \rightarrow C_2H_7O_2N + 54NO_2^- + 52H_2O + 109H^+ \quad (1.9)$$

$$400NO_2^- + 5CO_2 + NH_4^+ + 195O_2 + 2H_2O \rightarrow C_2H_7O_2N + 400NO_3^- + H^+ \quad (1.10)$$

In the case of noninhibition behavior, the oxidation reactions are expected to follow the pattern indicated in Figure 1.6. This suggests that ammonia concentration should fall with time while the concentrations of nitrite and nitrate accumulate until certain level then, nitrite concentration will decline and nitrate concentration will continue increasing [4, 14].

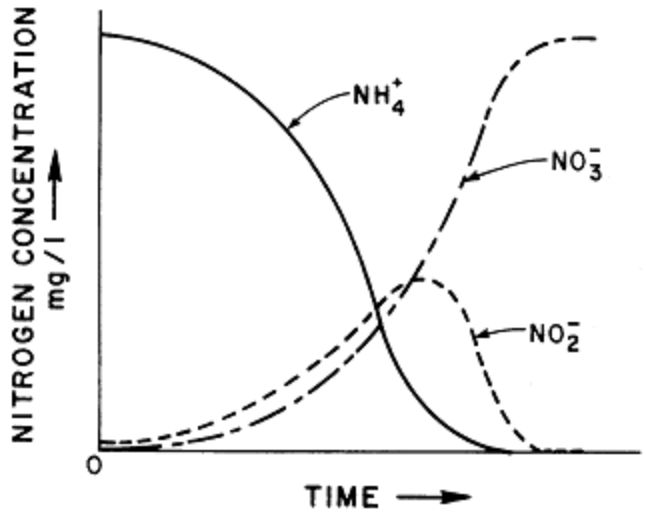

Figure 1.6: Transformations of nitrogen during noninhibited nitrification, batch experiment[14].

1.3.3 Nitrifying bacteria kinetics

As a classical concept, the growth of bacterial culture has several distinguishing phases that are characterized by variation of the growth rate [15]. These phases are defined as follows:

1. Lag phase: after bacteria have been inoculated, growth rate null;
2. Acceleration phase: growth rate increases;
3. Exponential phase: bacteria population is increasing at a constant growth rate;
4. Retardation phase: growth rate decreases;
5. Stationary phase: reproduction and death rates are equal, growth rate null;
6. Decline phase: the death rate is greater than the reproduction rate, growth rate negative [4, 15].

The main phases of bacterial life cycle are represented in Figure 1.7.

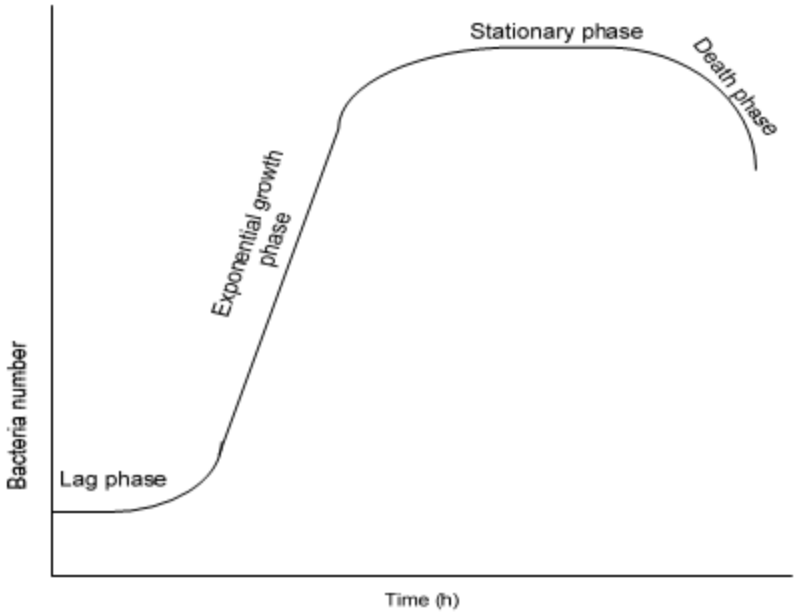

Figure 1.7: Phases of growth [4].

Usually, the discussion of bacterial growth starts from the exponential growth equation:

$$\frac{1}{X}\frac{dX}{dt} = \frac{d(log_e X)}{dt} = \mu = \frac{log_e 2}{t_d} \qquad (1.11)$$

where:

X- bacterial mass concentration, g l^{-1} at time *t;*

dX/dt- growth rate, g l^{-1} hr^{-1};

μ- specific growth rate, hr^{-1};

t_d- doubling time, hr, the time required for the concentration of organisms to double [16].

The rate of ammonia or nitrite utilization is highly dependent on the concentration of these substrates in the bulk solution [17]. In 1942, Monod was the first scientist who showed that there

is a simple relationship between the specific growth rate and the concentration of limiting food substrate as follows [4, 16, 17]:

$$\mu = \frac{\mu_{max} S}{K_s + S} \tag{1.12}$$

where:

μ_{max}- maximum growth rate constant, hr^{-1};

S- limiting substrate concentration, g l^{-1},

K_s- half saturation constant, g l^{-1}, numerically equal to the substrate concentration at which $\mu = \frac{1}{2}\mu_{max}$ as shown in Figure 1.8.

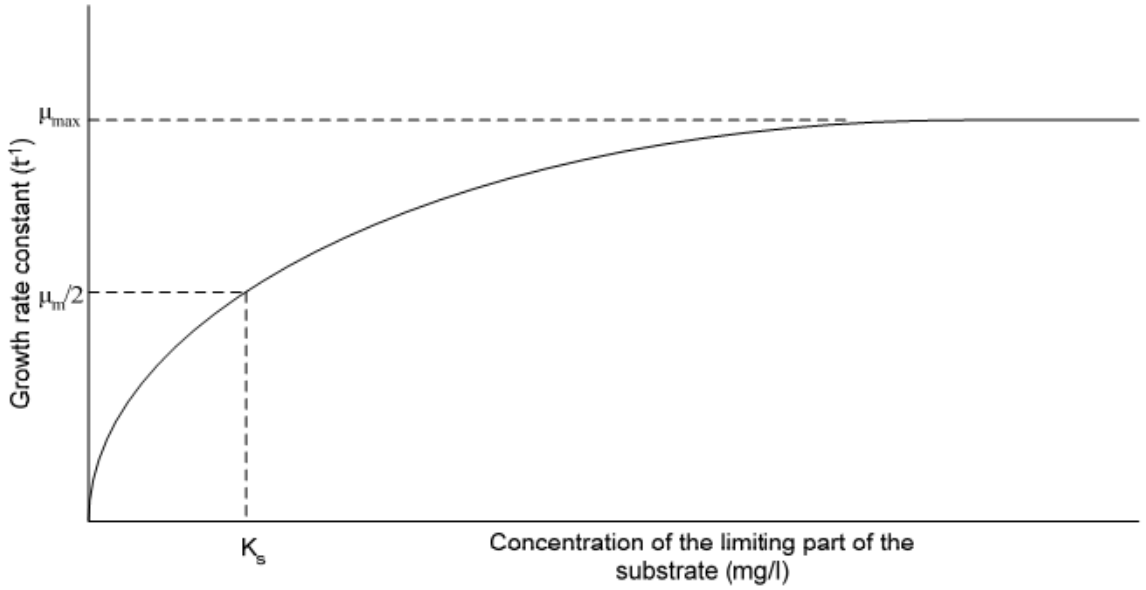

Figure 1.8: Monod description for the bacterial growth [4].

Also, Monod introduced the *yield constant*, *Y*, a parameter that relates the bacterial growth to the utilization of the substrate according to the following equation:

$$\frac{dX}{dt} = -Y\frac{ds}{dt} \tag{1.13}$$

Over a finite period of growth:

$$Y = \frac{weight\ of\ bacteria\ formed}{weight\ of\ substrate\ used}, \text{g cell g}^{-1}\text{substrate} \tag{1.14}$$

Monod's equation can be used to represent the kinetics of two stages of nitrification; ammonia as a growth limiting substrate for *Nitrosomonas* and nitrite as a growth limiting substrate for *Nitrobacter* [8, 13, 17]. Equation 1.15 represents the substrate removal rate, *R*, :

$$R = \mu_{max}\frac{X}{Y}\frac{S}{K_s + S} \tag{1.15}$$

where *R* has the units of g l^{-1} hr^{-1}. It has been found that the Monod equation can adequately represent batch and continuous cultures [18]. Substrate also can be referred to in terms of oxygen, and Equation 1.15 can be used to describe the oxygen consumed by bacteria.

1.4 Ion exchange

Based on origin and structure, ion exchange materials can be divided into different categories: mineral ion exchange materials, synthetic inorganic ion exchange materials, ion exchange resins (hydrocarbon chains form the 3D matrix), ion exchange coals, and liquid ion exchangers [3, 4, 19].

Most natural ion exchange minerals are crystalline, hydrated, aluminosilicates of alkali and alkaline earth cations or anions, having a three dimensional structures formed by AlO4 and SiO4

that are connected by sharing oxygen atoms and water molecules [1, 4, 19]. This type of natural material is known as zeolite. Clinoptilolite, mordenite, analcite, chabazite, erionite, heulandite, and laumonite are the most common types of zeolites [4, 19]. Figure 1.9 shows some of the zeolitic structures.

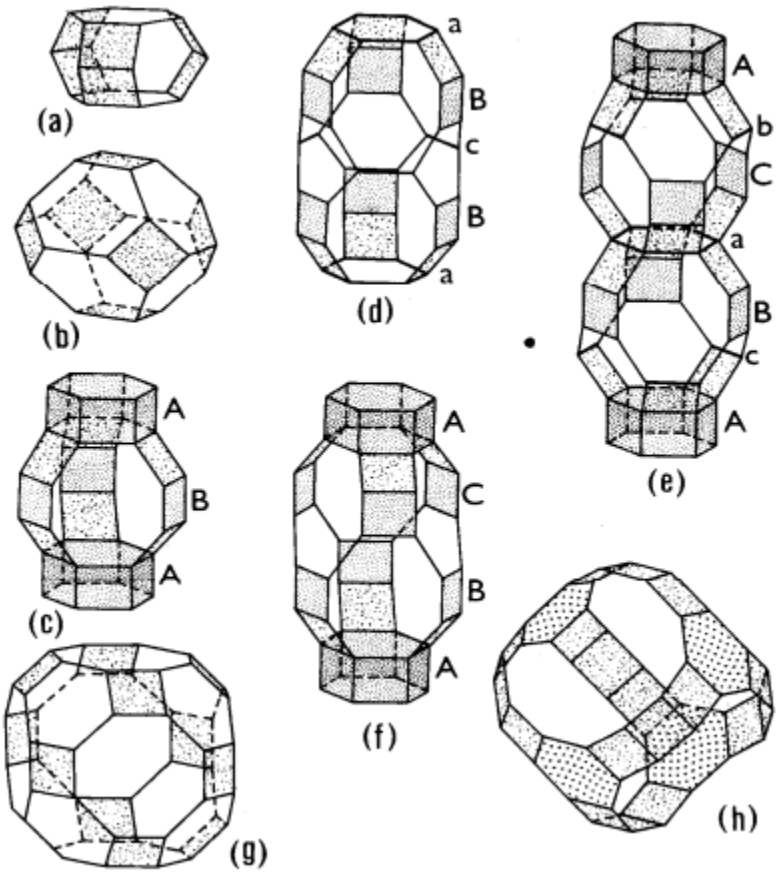

Figure 1.9: different zeolitic structure [5].

Zeolites have been used in many scientific disciplines: organic/inorganic chemistry, biochemistry, catalysis, chemical engineering processes, mineralogy, and agriculture. Also, zeolites have been used in a wide variety of applications such as separation and recovery of normal paraffinic hydrocarbons, catalysis of hydrocarbons, demineralization of feed water to the

boiler in power stations, separation of air components, as carriers for catalysts used in the curing of plastics rubber, removing CO2 and S compounds from natural gas, removal of atmospheric pollutants such as SO2, and more important to this research, for removing ammonium ion, NH4+, from waste water [1, 4, 20, 21].

An ion exchange process can be defined as "a process where an insoluble substance removes ions of positive or negative charge from an electrolytic solution and releases other ions of like charge into solution in a chemically equivalent amount" [22]. Applying this definition to the ion exchange materials, we say that: ion exchange materials are insoluble solids that have a charged framework and mobile ions which neutralize the charge. When an ion exchange material comes into contact with a solution, the mobile ions dissociate in the solution providing there are ions in the solution which can replace those in the exchanger so the overall charge is maintained neutral [5, 12].

The ion exchange material is called a "cationic exchanger" if the framework is negatively charged and the "cations" are available for exchange, and the opposite is true for the "anionic exchanger" where the framework is positively charged and the ion that available for exchange is "anion". The general reaction for the exchange of ion A and B on a cationic exchange material can be represented as follows:

$$nR^{-}A^{+} + B^{n+} \longleftrightarrow R_n^{-}B^{n+} + nA^{+} \qquad (1.16)$$

Where R^{-} is an anionic group attached to the ion exchange material, A^{+} is the mobile ion in the ion exchange material, and B^{+} is the ion in the solution or the aqueous phase. Also, A^{+} and B^{+} are known as counter ions. As Equation (1.16) suggested, the ion exchange process is a stoichiometric process, i.e., during the ion exchange process, the overall charge in the ion

exchange matrix and the aqueous phase must be zero. This is true because the ions removed from the aqueous phase are replaced by the mobile ions in the matrix [4, 22].

1.4.1 Clinoptilolite: Description

The ion exchange material used in this research is clinoptilolite. Next, origin, occurrence, and description of clinoptilolite are presented to provide an understanding of the ion exchange material used throughout this research.

Clinoptilolite, which means "oblique feather stone" in Greek [23], is the most abundant zeolite of natural zeolite [3], and it is a secondary mineral formed from rocks in lacustrine, fluviatile, and marine environments [1, 3]. Water passes downward and laterally through beds of formation at depths of 400 to 1200 m and at temperatures 25-50 ºC and pressures 35 to 120 atm, as a result clinoptilolite was precipitated [1]; high silica and alkali is solution are necessary conditions for this precipitation. The solubility of SiO_2 and Al_2O_3 increases in a basic solution and a pH 8.5 or above should be maintained [24].

Occurrences of clinoptilolite have been reported subsequently from sedimentary rocks especially those rich in silicic vitric material (high silica content and glassy appearance) [1]. Clinoptilolite was formed before the consolidation of the sediment to rock. Originally, clinoptilolite was described as a material from volcanic basalt rocks in Wyoming, and it has been found in rocks of the Jurassic Period in New Mexico [1]. Figure 1.10 gives a glance of the clinoptilolite's occurrence in United States.

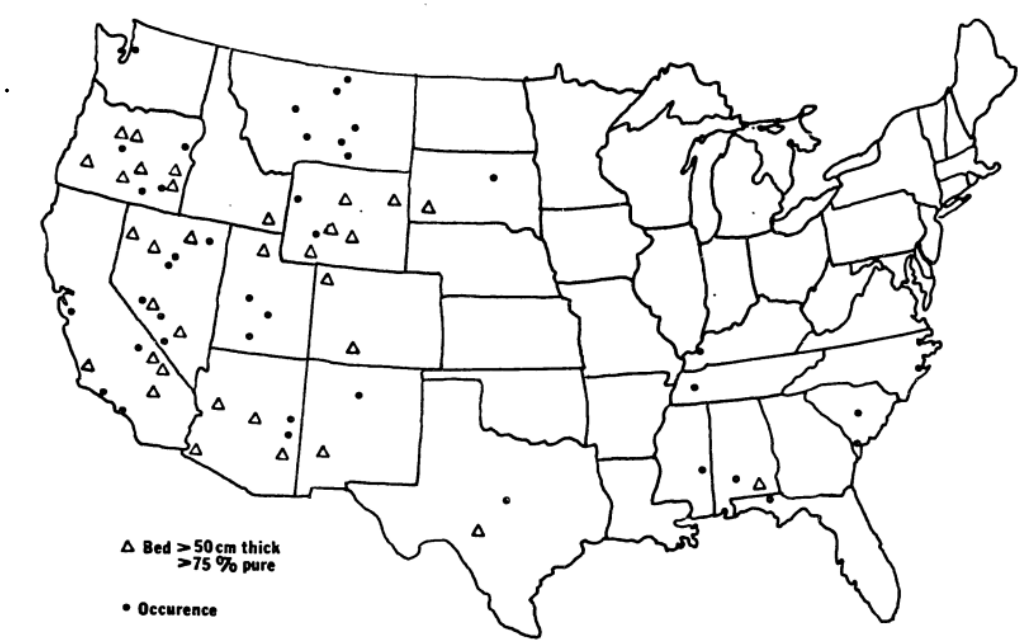

Figure 1.1: Occurrence of Clinoptilolite in USA [1].

There are three prerequisites zeolite have to meet to be classified as a clinoptilolite [25]:

- Si/Al ratio should be greater than four;
- (Na+K)/(Ca+Mg+Sr+Ba) should be greater than one and
- Polymorphism should not be manifested.

To describe a zeolite's structure, the chemical and physical composition must be specified. The molecular formula of clinoptilolite as provided by the KMI company is $(Na,K,Ca)_6(Si,Al)_{36}O_{72}.2H_2O$, this formula was also reported by Miladinovic 2005. Fe^{3+}, Sr^{2+}, and Ba^{2+} can also be found in natural clinoptilolite. As natural zeolite, clinoptilolite can contain large amount of impurities [5]. Based on the test results provided by the companies which supplied the zeolite, the clinoptilolite used in this work was 90%-95% pure which is quite high. Figure 1.11 shows the crystalline structure of clinoptilolite.

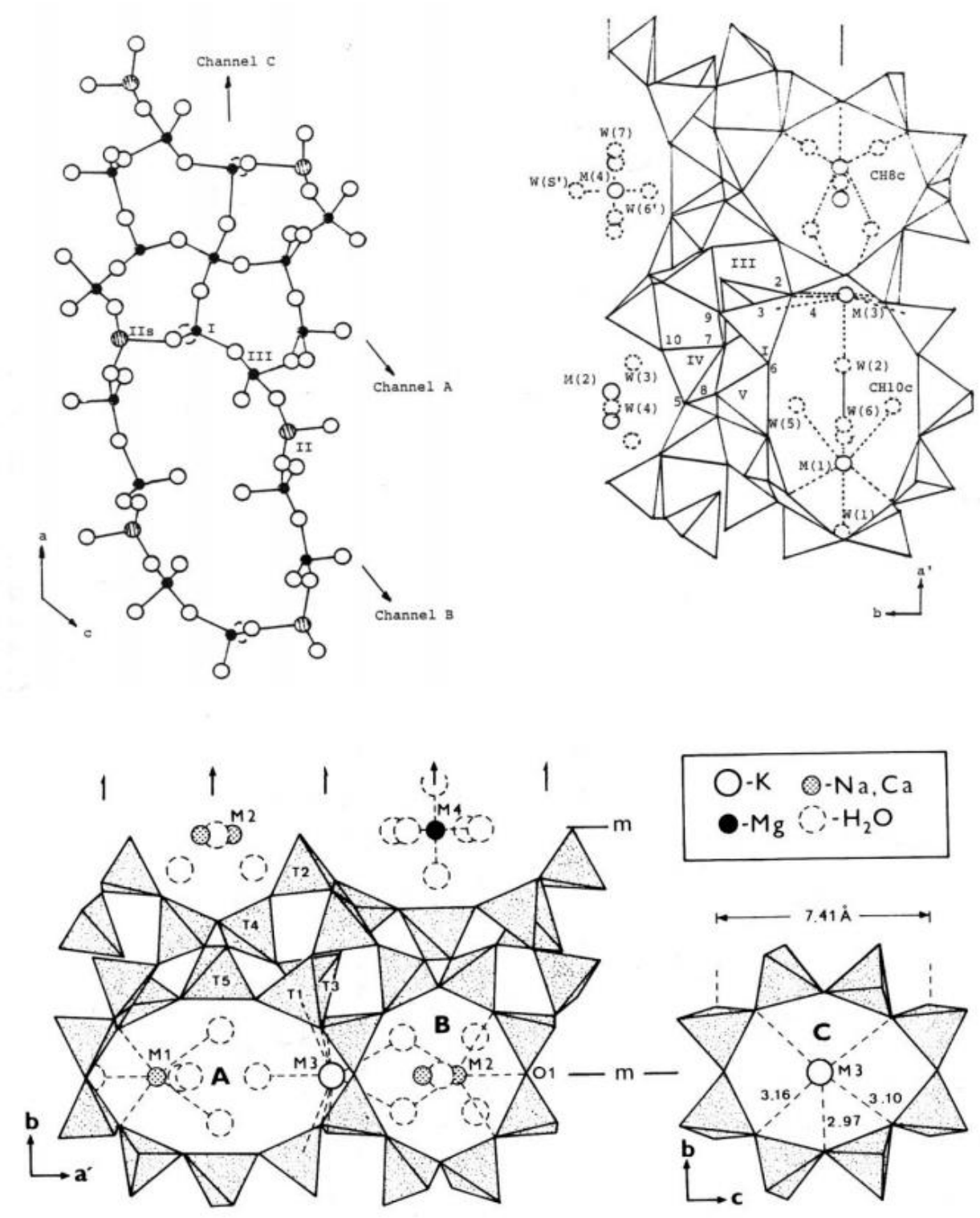

Figure 1.11: Crystalline structure of clinoptilolite [26].

Previous studies of clinoptilolite [26] identified four types of site at which cation exchange may take place. These sites are designated M1, M2, M3, and M4. Sodium and calcium are located in M1 and M2, with preferences for sodium to be positioned in M1 and calcium in M2. M3 and M4 occupy potassium and magnesium. M3 has a preference for potassium and M4 for magnesium [26].

1.4.2 Ion exchange equilibrium

The exchange of ions *A* and *B* in a binary system, which is represented by Equation 1.16, is a reversible reaction. Figure 1.12 shows the zeolite containing initially counter cations A+, and an aqueous solution containing B+ cations. When the solution contact the zeolite, a Fickian diffusion occurs due to a concentration gradient, and at a later stage equilibrium is achieved [3].

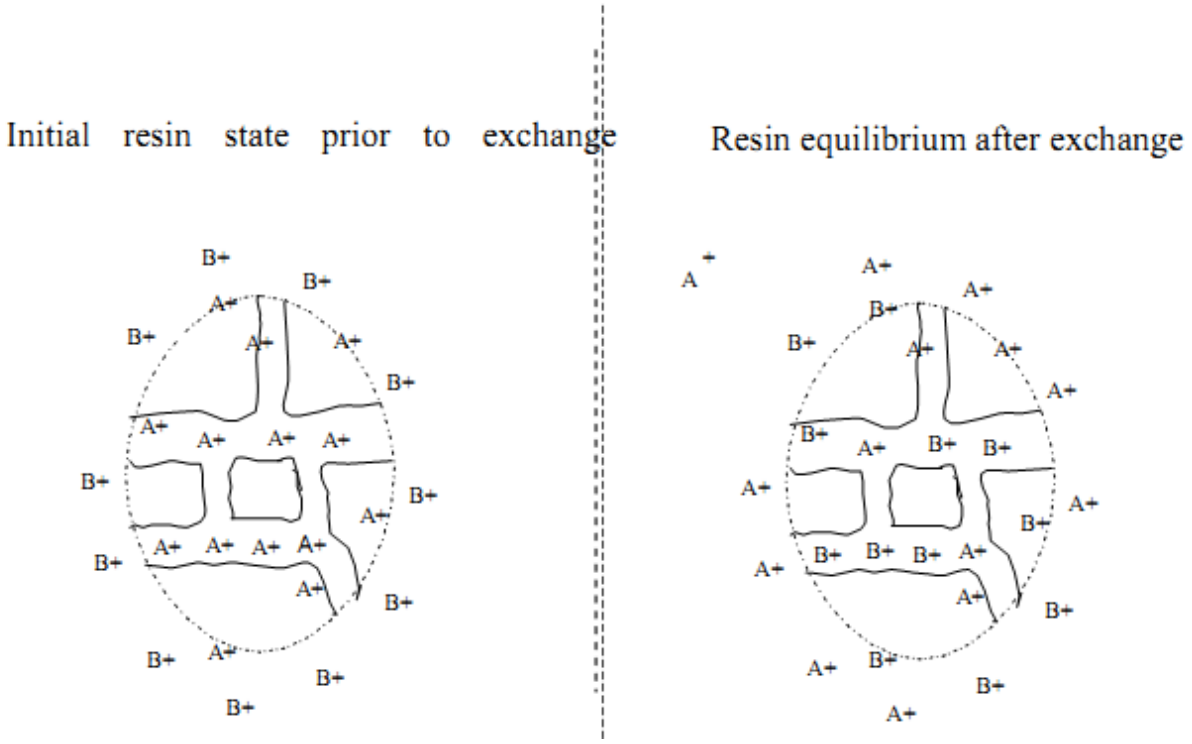

Figure 1.12: Zeolite initial and equilibrium states [3].

1.4.3 Ion exchange capacity

An ion exchanger material is a reservoir of exchangeable counter ions. The counter-ion content is one of the most important characteristics of an ion exchanger [19]. Thus, *capacity* is a major parameter, in the ion exchange process, that is used for two purposes: for characterizing ion exchange materials and, for use in the process design. Therefore, several definitions appear in the literature to reflect these two purposes. The three most common capacity definitions will be discussed here.

Ion exchange capacity, or *maximum capacity*, is the definition that used to characterize an ion exchange material, and can be defined as the number of counter ions per specified amount of ion exchanger. The maximum capacity is expressed in milli-equivalents per gram (meq/g). An equivalent is an amount of material that will release or react with an Avogadro's number of electrical charges on particles. The amount of substance expressed in units of equivalents has a very small magnitude, so the maximum capacity is rather described in terms of "m"lliequivalents"; where the prefix *milli* is denoting that the measure is divided by 1000. A specimen calculation is provided below:

The mass concentration of 60 mg/l of Ca^{++} can be converted to milliequivalent by knowing that the atomic weight of Ca^{++} ion is 40 g/mol and that calcium is a *divalent* cation:

$$\frac{60\ mg/l}{\frac{40\ mg/mmol}{2meq/mmol}} = \frac{60\ mg/l}{20\ mg/meq} = 3\ meq/l$$

Breakthrough capacity is "the value obtained in column experiments when capacity is calculated at the point when the breakthrough of the column starts" [4] normally at 5% exhaustion.

Breakthrough capacity is used for the determination of selectivity series and for the design of column operations [19]. Sorption capacity is "the amount of solute, taken up by sorption rather than by ion exchanger, per specified amount of ion exchanger" [19].

Capacity, defined as the amount of ions taken up per g of ion exchanger, is normally determined on the basis of dry mass of ion exchanger but zeolites have water molecules incorporated in their framework and still hydrated [3, 4]. Capacity highly depends on the Si:Al ratio because the charge imbalance is greater if the ion exchanger has more aluminum, and as a result more cations are needed to neutralize the negative charge [4]. There are also several factors that capacity depends on such as the purity of the material, the ionic form in which the material is present, ion exchanger's particle size, pretreatment of the ion exchanger before use, competing cations present in the aqueous phase, and the experimental procedure [4].

1.4.4 Ion exchange selectivity

The selectivity is defined as "a measure of the preference that the ion exchanger has for an ion over the others" [5]. It is characterized by the equilibrium constant for charge equilibria expression, Equation 1.16. The equilibrium constant for Equation 1.16 is defined thus:

$$K_{A^+}^{B^{n+}} = \frac{(R_n^- B^{n+})_R (A^+)_S^n}{(R^- A^+)_R^n (B^{n+})_S} \tag{1.17}$$

where,

$(R_n^- B^{n+})_R$ is the activity of B^{n+} in the ion exchanger;

$(B^{n+})_S$ is the activity of B^{n+} in the solution;

$(R^-A^+)_R$ is the activity of A^+ in the ion exchanger,

$(A^+)_S$ is the activity of A^+ in the solution.

This equilibrium constant depends on experimental conditions; therefore, it is not actually a constant. Rather, it is referred to as a selectivity coefficient [22]. If the solution phase is diluted, the activity coefficients can be ignored, and the equilibrium constant become Q_s or selectivity quotient. The data for ion exchanger removal at equilibrium is normally presented in the form of an "isotherm" which represents the relationship of the aqueous phase and the ion exchanger at equilibrium [26]. Isotherms are constructed from a number of separate ion exchange equilibria, by measuring the ratio of initial concentration to equilibrium concentration of each cation [26]. Figure 1.13 shows generalized ion exchange isotherms.

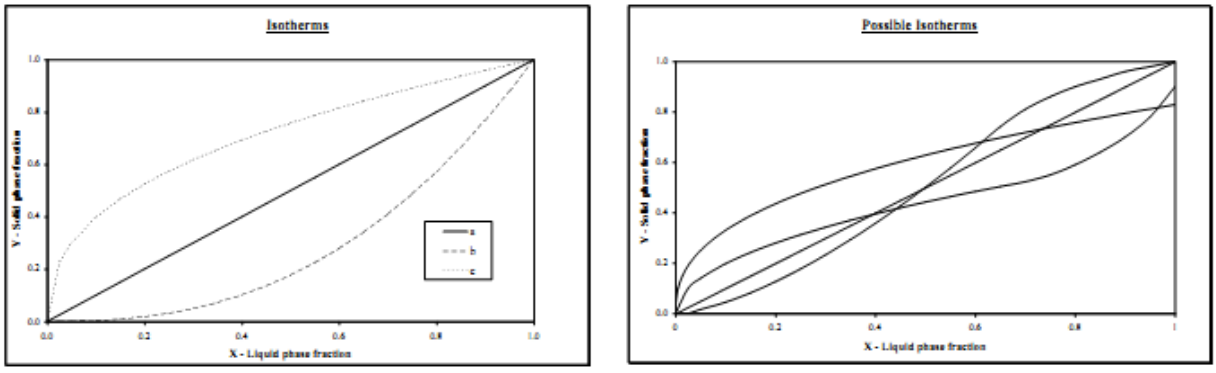

Figure 1.13: Generalized ion exchange isotherms [5]. (a) Binary isotherm, mole fraction; (b) other possible isotherms.

What makes the selectivity quotient, Q_s, a useful factor is that it indicates the preference of the ion exchanger for one ion relative to another. Selectivity quotient, Q_s, can be defined as in Equation 1.18:

$$Q_s = \frac{(R_n^- B^{n+})_R (A^+)_S}{(R^- A^+)_R (B^{n+})_S} \quad (1.18)$$

If Q_s>1, then the ion B^{n+} is preferred over the ion A^+ (curve "c" in Figure 1.13(a)); if Q_s<1, the ion exchanger prefers A^+ ion over B^{n+} (curve "b" in Figure 1.13(a)); if Q_s=1, there is an equal preference for each ion (curve "a" in Figure 1.13(a)) [22]. As shown in Figure 1.13(b), not all isotherms are simples. Indeed, some isotherms have complex behavior, and in such behavior a selectivity cross-over is expected [5, 22].

Benefield et al listed the rules that generally explain the affinity of an ion for an ion exchanger:

1) Ions of high valence are preferred over ions of low valence (e.g. Fe^{3+}>Mg^{2+}, Na^+; PO_4^{3-} >SO_4^{2-}, NO_3^-). An increase in the total ionic concentration of the solution yields to a decrease in this preference.
2) For ions of the same valence, the extent of the ion exchange increases with decreasing hydrated radius and increasing atomic number (e.g., Ca^{2+}>Mg^{2+}>Be^{2+}; K^+>Na^+>Li^+). This is due to the swelling pressure within the ion exchanger; since ions of larger hydrated radius increase the swelling pressure.
3) For a solution with high total ionic concentration the behavior of the ion exchange is unpredictable and is often reversed.
4) In ion exchangers with a high degree of crosslinking, the ions may be too large to penetrate into the matrix of the exchanger.
5) If the lattice forces of the ion exchanger are sufficient to overcome the hydration energy, then the cation may enter the ion exchanger lattice [19].

Clinoptilolite selectivity behavior has been investigated by many researchers [1, 3-5, 20-24, 27-29]. Clinoptilolite's preference for the ions that might be present in wastewater is shown in Equation 1.19:

$$Cs^{+} > K^{+} > NH_4^{+} > Ba^{2+} > Na^{+} > Ca^{2+} > Fe^{3+} > Al^{3+} > Mg^{2+} \quad (1.19)$$

Table 1.3 shows the ionic radius, hydrated radius, and hydration energy of some important ions in wastewater treatment.

Table 1.3: Cation size and hydration energy [5].

	Ionic radius (Å)	Hydrated radius (Å)	Hydration energy (kJ/g)
K^{+}	1.33	5.30	394
NH_4^{+}	1.43	5.35	364
Na^{+}	0.95	7.90	477
Ca^{2+}	0.99	9.60	1717
Mg^{2+}	0.66	10.80	2051

1.4.5 Adsorption

Adsorption is defined as "the taking up of molecules by the external or internal surface of solids or by the surface of liquids"[22], and it is an important process in industrial and pollution control

processes. There are differences and similarities when comparing to ion exchange. For adsorption to occur, there must be an attractive force between the adsorbate (the substance adsorbed or solute) and the adsorbent (the solid phase). The various forces able to cause adsorption are usually divided into two classes: physical and chemical, which result in physisorption and chemisorption.

Physisorption: physisorption occurs through dipole/dipole interactions which are commonly referred to as Van der Waals or London interactions. These forces are relatively weak and thermodynamically reversible. When these forces overcome the kinetic forces of the adsorbate in the liquid, physisorption occurs.

Chemisorption: the chemical forces associated with covalent bonds which are highly specific, i.e., they occur only between certain molecules. Chemical forces are very short range forces and the two molecules involved must be close enough to share electrons. They could be reversible or irreversible forces.

In both types, for adsorption to occur, the adsorptive forces (physical or chemical) must be strong enough not only to bind the adsorbate to the adsorbent but also to overcome the affinity of adsorbate for the solvent and to displace the solvent from the adsorbent surface. Thus, the selectivity of adsorption depends on the adsorbate, the adsorbent, and the solvent [5]. In wastewater treatment, most adsorption processes are a combination of the physisorption and the chemisorption [22].

Three distinct steps must take place for adsorption to occur [22]:

1) The adsorbate molecule must pass through a film of solvent that surrounds the adsorbent particle (film diffusion).

2) The adsorbate molecule must be transferred to an adsorption site (pore diffusion).
3) The solute must become attached to the surface of the particle.

Adsorption is quantified by adsorption isotherms which are mathematical descriptions of the relationship between the solid and liquid phase concentrations. More specifically, these isotherms relate the liquid phase concentration of adsorbate to the mass of the adsorbate in the solid phase. Adsorption isotherms are linear for many adsorption phenomena involving very low concentrations but at higher concentrations a non-ideal behavior is generally observed.

There are many isotherm models but the two most commonly applied are the Langmuir isotherm and the Freundlich isotherm. Also, these two models are commonly used to model the adsorption of various cations onto zeolite [4].

Langmuir Isotherm: the Langmuir model is written as shown in Equation 1.20.

$$Q_e = \frac{KbC_e}{1 + KC_e} \; ; \quad or \qquad \frac{1}{Q_e} = \frac{1}{KbC_e} + \frac{1}{b} \tag{1.20}$$

where:

- Q_e- concentration of adsorbate on the adsorbent (mg/g) at equilibrium, also known as *adsorptive capacity* also known as *surface* or *solid phase concentration*,
- C_e- equilibrium liquid phase concentration of adsorbate (mg/l),
- *K*- Langmuir constant (l/mg),
- *b*- Langmuir adsorption capacity constant (mg/g)

The Langmuir isotherm is based on the assumption that all sites have equal affinity for molecules of the adsorbate. This is what is known as a homogenous surface. Also, it is assumed that the

presence of adsorbed molecules at one site will not affect the adsorption of molecules at adjacent site, i.e., the adsorbed layer will be one molecule thick [4, 22].

Freundlich Isotherm: The Freundlich isotherm is used when the adsorbent surface is heterogeneous, i.e., composed of different classes of adsorption sites. The Freundlich isotherm is given by Equation 1.21:

$$Q_e = kC_e^{1/n}\,; or \quad \log Q_e = \log k + \frac{1}{n}\log C_e \tag{1.21}$$

where:

- Q_e and C_e- are described above.
- *k* and *n*- are constant that must be evaluated for each solute.

Note that in the whole work, the expression *log* refers to log_{10}. All the assumptions that are given by these isotherms work well with ion exchange and thus many researchers have used these two models to describe the solute equilibrium between the solid and liquid phases involved in ion exchange.

1.4.6 Ion exchange kinetics

Kinetics is an important aspect that should be understood for process design. Having very high kinetics is a desirable demand for ion exchange processes. A high exchange rate requires short time to achieve maximum breakthrough capacity which yields to ion exchange improvement and better process optimization. Diffusion plays an important role in the ion exchange process. The steps that describe the transport of exchanging ions to and from the inter-phase boundary of the ion exchanger are as follows:

- Transport of the exchanging ions to and from the vicinity of the ion exchanger surface (bulk diffusion).
- Transport of the exchanging ions through the hypothetical film (or boundary layer) at the surface of the particle (film diffusion).
- Pore transport of the exchanging ions to the sites of active exchange (pore diffusion or particle diffusion).
- The actual rate of exchange process; reaction between counterions and fixed groups, which are the only chemical interactions that can affect the overall rate of the ion exchange.

In a well stirred batch system, agitation can balance any concentration differences in the bulk solution; therefore, the rate limiting step is determined by film diffusion and/or by particle diffusion [19]. For the general exchange reaction given by Equation 1.16, n=1, that's occurring in a batch reactor, evaluation of the following relationship will indicate which diffusion process controls the rate of exchange:

$$\xi = \frac{\pi D_r \delta [RB]_R}{3 D_o r [B]_S} \tag{1.21}$$

where:

- $[RB]_R$- the final equilibrium concentration of the exchanging ion in the ion exchanger (meq/l);
- $[B]_S$- the final equilibrium concentration of the exchanging ion in the solution (meq/l);
- D_r- the diffusion constant of the exchanging ion in the ion exchanger (cm^2/sec);
- D_o- the diffusion constant of the exchanging ion in the ion solution (cm^2/sec);

- δ- the thickness of the film (cm)
- *r*- the radius of the ion exchanger particle (cm).

If the value of ξ is:

- less than 1, particle diffusion is the rate limiting step;
- greater than 1, film diffusion is the rate limiting step;
- near to 1, both steps exert about the same effect [22].

The rate of film diffusion can be enhanced by many means such as [19, 22]:

1) Increasing agitation to reduce the film thickness.
2) Increasing the concentration of the exchanging ions in the solution.
3) Decreasing the size of the particle to increase the total surface area.
4) Increasing the mobility of the ions by increasing the temperature.

The film diffusion will be a rate limiting step, if any of these factors are missing.

On the other hand, if particle diffusion is the rate limiting step then the flux is:

- proportional to the concentration of fixed charges;
- inversely proportional to particle radius and;
- independent of: the film thickness, concentration of the exchanging ions in the solution, and film diffusion coefficient [4].

A number of models have been used to simulate kinetics of mass transfer ion exchange process. Here, two models will be discussed briefly, namely the *film diffusion model* and the *particle diffusion model*.

Film diffusion model

This model was introduced by Furusawa and Smith (1973), and it was applied for an adsorption system. Because of the similarities that exist between the ion exchange system and the adsorption system, this model is also applicable to ion exchange and it is expected to give a good accuracy since it uses parameters from either the Langmuir or Freundlich adsorption isotherms [4].

This model is a result of solving partial differential mass balance equations of exchanging ions in the solution and around the particles. The film diffusion model has the following expression [30]:

$$\ln\left[\frac{C_t}{C_0} - \frac{1}{1+m_s K}\right] = \ln\left[\frac{m_s K}{1+m_s K}\right] + \left[\frac{-1+m_s K}{m_s K} k_f S_s t\right] \qquad (1.22)$$

$$\text{where} \qquad m_s = \frac{M}{V} \quad and \quad S_s = \frac{6m_s}{d_p \rho_p} \qquad (1.23)$$

where:

- d_p- particle diameter (cm)
- K- Langmuir constant (l/g)
- k_f- mass transfer coefficient between liquid outer surface of the particle (cm/s)
- M- mass of ion exchanger (g)
- m_s- concentration of the particle in the free liquid
- S_s- specific surface area available for mass transfer (cm^{-1})
- t- time (sec)

- V- volume of the particle free liquid (cm^3)
- ρ- particle density (g/cm^3)
- C_0- initial solute concentration (mg/l)
- C_t- liquid phase concentration at time t (mg/l).

The mass transfer coefficient, k_f, can be determined from the slop of plotting the left side of the equation versus time.

Particle diffusion model

This model was introduced by McKay et al (1983) and assumes that most of the diffusional resistance lies in the solid phase and it is based on the following assumptions:

- solute concentration is uniform and equal zero in the particle at t=0;
- diffusion is radial with no concentration variation in the angular direction;
- the external mass transfer resistance is significant only in the early stages of the process and;
- for ion exchange, D is the intraparticle diffusion coefficient and it is a function of the self-diffusion coefficients of the exchanging counter ions [4].

The model has the following expression:

$$k_d = \frac{1}{t^{0.5}} Q_t \qquad (1.24)$$

where:

- k_d- mass transfer coefficient within the particle ($mg/gmin^{0.5}$);
- Q_t- solid phase concentration at the particle (mg/g);

- *t*- time (min).

1.4.7 Ion exchange regeneration

As stated previously, the ion exchange process is a reversible process. In order for an exhausted bed to be reused, the bed must be regenerated. Regeneration displaces ions exchanged and uptaken during service run and returns the ion exchanger to its initial exchange capacity. Regeneration is an expensive process and it might cost about 50% of the total ion exchange process [3]. The main types of regeneration are discussed below.

1.4.7.1 Chemical regeneration

When the column cycles reach the breakthrough point which is the point where the column is unable to accommodate the exchange zone length [19], the bed must be regenerated. Chemical regeneration is when the exhausted bed is treated with NaCl and/or NaOH solutions; also, known as alkaline regeneration.

During the regeneration, the regenerant solution, NaCl for example, is passed through the exhausted column so that the sodium ions displace the ammonium ions until the bed becomes saturated with sodium ions.

Usually, the regenerant solution is a mixture of sodium chloride, to provide bulk of Na+, and sodium hydroxide, to provide high pH [5]. However, exposing zeolites to NaOH solution could cause mass loss [4]; therefore, a small amount of NaOH is usually used. A high pH value is required to transform ammonia to the unionized form so that the unionized form will not be held by the negatively charged zeolite framework and as a result the regeneration process will be enhanced. Clinoptilolite has a higher affinity for NH_4^+ ions over Na^+ ions; therefore, a high

concentration of regenerant ions are required. In the case of high pH regeneration, NH_4^+ ions are expected to be removed easily, hence, obviating the need for a high concentration of the regenerant solution.

Economics play an important role in determining the degree of regeneration as the regeneration process may not be taken to completion. One way to reduce the cost of regeneration is to reuse the regenerant solution after the exhausted ammonium ions has been removed.

1.4.7.2 Bio-regeneration

The cost of the chemical regeneration is considerably high. A potential solution to this problem is to use the nitrifying bacteria to oxidize ammonia to nitrate. A possible scenario to operate the bioregeneration process is to load the nitrifying bacteria to the exhausted bed and a $NaHCO_3$ solution is passed through the column. While sodium ions displace the ammonium ions, nitrifying biomass consumes the released NH_4^+. This approach is known in the literature as in-situ bioregeneration process. The other scenario for the bioregeneration setup is the ex-situ regeneration where the nitrifying biomass is located in a separated reactor.

Semmens and Goodrich [31] first studied the regeneration of clinoptilolite loaded with ammonium ions. They observed 80% regeneration of 5g saturated clinoptilolite with ammonium ions over a period of 1-3 hr by using 1L of nitrifying bacteria at 27 ºC. The factors affecting the bioregeneration process are the same factors that affect the nitrification process. Section 2.1 discusses these factors in detail.

1.5 Other methods for ammonia removal

Besides nitrification and ion exchange process, there are other methods for ammonia removal presented in the literature such as ozonation, breakpoint chlorination, and air stripping.

Ozonation oxidizes ammonia to nitrate by ozone which is a strong oxidizing agent that has been used in water treatment for disinfection and decomposition [3]. The rate of converting ammonia to nitrate by ozonation is very slow and cannot be expected to remove ammonia effectively [4].

Breakpoint chlorination is the chlorination of a water containing ammonia resulting in an initial increase in combined chlorine residual, followed by a decrease in the combined chlorine residual along with ammonia concentrations, followed by an increase in free chlorine residual and near complete removal of ammonia as nitrogen gas [4]. For this process pH control is required. The process is effective but free chlorine which is produced during the treatment must be removed since it is toxic to aquatic life [6].

Air stripping is a process operated at high pH (10.8 -11.5) [4] where free ammonia is stripped out through packed bed column with air or steam [5]. The process is not economic for low ammonia concentrations of 25-60 mg NH_4^+/l [4].

1.6 Process intensification

The term *process intensification, PI,* started to appear in the scientific literature in the mid of 1960s as equivalent to *process improvement* [32] in the metallurgical processing field. Colin Ramshaw, one of the pioneers in the field, defined PI as a "reduction in plant size by at least a factor 100" [33] thirty five years ago. These days, chemical engineers define process intensification as a process by which transport rates are enhanced and every molecule, in the process, is given the same processing experience [34]. By such, the ultimate target of PI can be achieved, which is the reduction in capital cost. Figure 1.14 shows the main elements of process intensification.

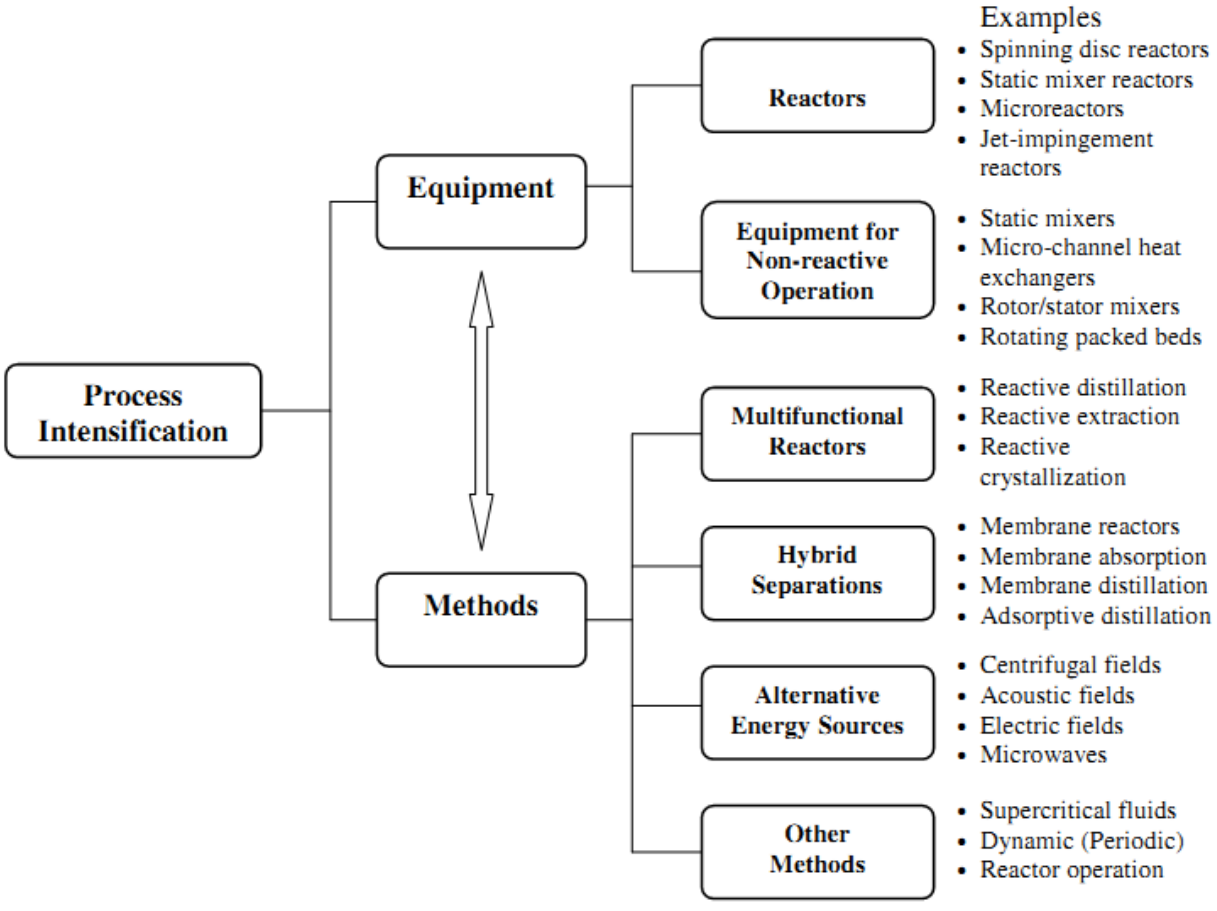

Figure 1.14: Process intensification tools [35].

Separations, after reactions, are the most important unit operations within the chemical industry [34]. Membrane processes have already provided interesting solutions to some of major problems in industry including separation processes. Membrane technology is now competing with other separation technology in terms of energy efficiency, separation capacity and selectivity, and capital investment [33, 36]. The components of a gas or liquid mixture are separated on the basis of their different permeabilities through the membranes. Membrane processes have the ability to replace conventional energy-consuming techniques, to efficiently enhance the transport of specific components, and to improve the rate of reaction [33]. For those reasons, membrane processes meet the requirements of PI.

1.7 Research objectives

The objectives of the research conducted in this work are as follows:

- To study the kinetics and ammonia removal by KMI and BIT clinoptilolite. KMI and BIT clinoptilolite are defined in Section 3.1.
- To examine the performance of KMI and BIT clinoptilolite in a packed bed column with and without the presence of nitrifying bacteria, and to examine the ability of KMI and BIT clinoptilolite as solid supports for nitrifying bacteria.
- To evaluate the oxygen concentration enhancement in the biologically active packed bed column using in-situ membrane aeration unit that consists of dense and porous gas permeable membranes. The gas permeable membranes are defined in Section 3.2.3.

To achieve these objectives, the following topics will be studied:

- Measurement of ammonium ion exchange capacities of KMI and BIT clinoptilolite.
- Measurement of the impact of K^{+}, Ca^{++}, and Mg^{++} on ammonium ion exchange equilibria.
- Study the diffusion of ammonium ion through the KMI and BIT clinoptilolite by considering the external and internal mass transfer resistances. Evaluation of the uptake removal rate constants.
- Evaluation the performance of the chosen gas permeable membranes in clean water.
- Determination of the breakthrough behavior of uptake removal of ammonia in packed bed columns.

- Study the bio-regeneration of the exhaustion clinoptilolite as an option of the chemical regeneration. Locate where the nitrifying bacteria might inoculate on the packed bed column.

2 Literature Review

2.1 Nitrification

Nitrification is the microbiological oxidation of ammoniacal nitrogen to nitrite (NO_2^-) by Ammonia Oxidizing Bacteria, AOB, Equation 1.6, and nitrite to nitrate (NO_3^-) by Nitrite Oxidizing Bacteria, NOB, Equation 1.7, in the presence of oxygen. The first step of nitrification process is known as *partial nitrification*, and this process was recently the focus of much research [37-43]. Figure 2.1 shows the difference between full and partial nitrification. It is worth mentioning that, Equation 1.6 & 1.7 and Figure 2.1 are approximate representations of the nitrification process as it is known that many intermediates are formed during these reactions, particularly during the oxidation of ammonia to nitrite.

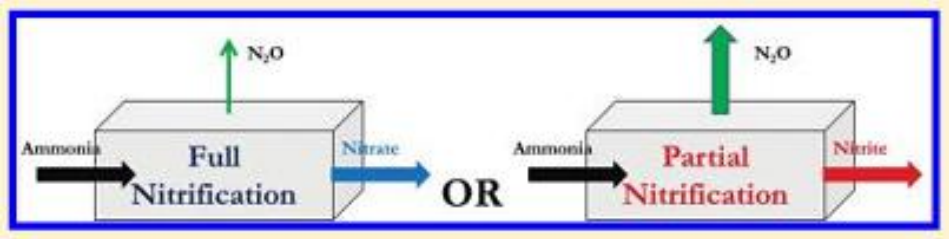

Figure 2.1: Comparison between full and partial nitrification [39].

In the past, there was confusion on the usage of the words *inhibition* and *toxicity* in nitrification literature. Toxicity is explained as permanent damage or change in the metabolic activity compared to inhibition which is commonly interpreted as an interference with the general metabolism of the cells. Probably the first observation inhibition during nitrification may goes back to the late 1800s when Schloesing and Muntz (1877) carried out their work on inhibiting nitrifiers with chloroform during soil percolation experiments. Edwards [44] proposed a growth

kinetics model that accounts for inhibition and he reported that a microbial system could be affected by one of the following possible types of inhibitory actions:

- Modify chemical potential of substrates, intermediates, or products.
- Alter cell's permeability.
- Dissociation of one or more enzymes or metabolic aggregates.
- Influence functional activity of the cell.

Inhibitors which cause inhibition by interference with the general metabolism of the cell would not necessarily cause short term effects while inhibitors that interfere with the primary oxidation reactions would cause immediate effects [45] since the oxidation of NH_4^+ and NO_2^- would stop.

The AOB growth rate might be inhibited by several factors, such as: ammonia concentration, pH, oxygen concentration, temperature, microbial composition of the growing environment, chemicals other than ammonia present in the solution, and the surface available for bacteria growth. These factors will be discussed here in details.

2.1.1 Substrate inhibition

Ammonia oxidizing bacteria (AOB) play a critical role in the global nitrogen cycle and the removal of nitrogen from wastewater treatment plants. *Nitrosomonas europaea*, a model AOB, has been found to be a key AOB in terrestrial and freshwater habitats [46]. AOB depends on ammonium for nitrogen assimilation and for energy generation. In general, AOB are poor competitors for limiting amounts of substrate, i.e., ammonia [47] and therefore; ammonia concentration is an important element in the design of biological nitrification processes since substrate concentration may inhibit AOB from breaking down ammonia to nitrite. In other words it may inhibit the nitrification process.

Nitrosomonas europaea uses an enzyme called ammonia monooxygenase (AMO) to oxidize ammonia to nitrite as their source of energy for growth and metabolism [48]. Indeed, the oxidation of ammonia to nitrite is a two-step process, the oxidation of ammonia to hydroxylamine (NH_2OH) is catalyzed by AMO while the oxidation of NH_2OH to nitrite is performed by hydroxylamine oxidoreductase (HAO) enzyme [48].

In 1913, L. Michaelis and M. Menten developed a general theory of enzyme action and kinetics. The Michaelis-Menten model is described below:

$$v = v_m \frac{S}{K_m + S} \tag{2.1}$$

where:

v: is the velocity of the enzyme reaction;

v_m: is the maximum velocity of the enzyme reaction;

K_m: is the Michaelis-Menten coefficient,

S: is the substrate concentration.

This model defines the quantitative relationship between the substrate concentration and the reaction rate in relation to maximum possible rate [13].

Over a limited low range of substrate concentration, many enzyme conform to Michaelis-Menten kinetics but at high substrate concentrations enzymes deviate in that the rate is drops off and the maximal rate is not attained [45]. This phenomenon is named substrate inhibition.

Leyden Webb [49] introduced several mechanisms that might be responsible for substrate inhibition:

1. The substrate in the active Enzyme-Substrate (ES) complex forms a multipoint attachment to the enzyme, so at high substrate concentration it is possible that two or more substrate molecules can be bound simultaneously at the active center which leads to in active complexes and a reduction of available enzyme.
2. The substrate may react with an activator and at high concentration deplete the system of the activator so the enzyme becomes inactive.
3. The substrate may combine at sites in various spatial relationships to the active sites, which leads to interference with either the binding of the substrate in an active ES complex or interference with its reaction.
4. At high concentrations, the substrate may interfere with the binding of a co-enzyme or acceptor in transfer reactions.
5. The true substrate for the enzyme may be a complex of the added substrate with an activator, so at high concentrations the substrate may compete with this complex for binding to the enzyme.
6. The ionic strength may be increased due to increase of the substrate concentration which may modify the rate independently of any direct or specific effects of the substrate.

It was found that free ammonia, NH_3, rather than ammonium ion, NH_4^+, is the substrate for AOB [50, 51]. The inhibition behavior in nitrification processes due to substrate (as free ammonia) concentration was extensively studied by Anthonisen in 1976 [14]. Since then, literature has reflected contradictory conclusions about substrate inhibition effects on nitrification. Numerous

studies [52-56] observed inhibitory effects on the nitrification process due to substrate concentration, while others [3, 57, 58] did not report any substrate inhibition effects.

Anthonisen concluded that the free ammonia concentration that inhibits AOB ranges from 10 to 150 mg/l while that inhibits the Nitrobacter is in the range of 0.1-1.0 mg/l. Bae et al [59] supported this observation by reporting that nitrite accumulation occurred at an initial free ammonia concentration of around 4.7 mg/l in a batch reactor. Chung et al [60] found that the optimum free ammonia concentration for the inhibition of nitrite oxidation without slowing down the rate of ammonia oxidation was 5-10 mg/l. Turk et al [61] explained that free ammonia concentration in the range of 0.1-10 mg/l inhibited the nitrite oxidation in the beginning but the NOB can adapt to a free ammonia concentration as high as 22 mg/l. An an excessively high free ammonia concentration level above 10-150 mg/l may lead to ammonia oxidation inhibition. Castens et al [62] observed a decrease in nitrification rate as free ammonia concentration was increased. Tora et al [63] found that the AOB inhibition by free ammonia is somewhat increased under total inorganic carbon limitation. According to literature [3, 62, 64], the Haldane model is suggested to model ammonia removal rates in the case of substrate inhibition, which is represented by the following equation:

$$\mu = \frac{\mu_{max} S}{K_s + S + \frac{S^2}{K_i}} \tag{2.2}$$

where K_i is the inhibition constant (mg/l) and the other parameters were explained previously. By using this model, a reduction in the nitrification rate after the peak is reached is predicted because of the high ammonia concentration [4].

On the other hand, substrate inhibition effects were not observed by several researchers even if high free ammonia concentrations were used (200 mg/l) such as in the work carried out by Tanka et al [57]. Kim et al [64] reported that the free ammonia concentration showed no effect on the nitrite accumulation rate. Contreras et al [65] used a free ammonia concentration of 135 mg/l and stated that this concentration was not toxic nor inhibitory for the nitrifying bacteria. McVeigh et al [3] and Miladinovic et al [58] employed ammonium inlet concentrations in the range of 20-40 mg/l without any substrate inhibition was reported. Miladinovic summarized that if the initial ammonia concentration is not high enough, the nitrification process might be inhibited by the retention of NH4+ on the clinoptilolite sites where the nitrifying bacteria cannot reach it. Park et al [66] concluded that the effect of free ammonia inhibition becomes insignificant in an acidic environment (e.g. pH 6).

Based on this review, the maximum inlet ammonia concentration, in this work, was chosen to be 40 mg N-NH_4^+/l with pH of 8 to avoid high free ammonia concentrations, and since no inhibition was expected the Monod model was adopted to model bacteria growth.

2.1.2 pH role in nitrification process

pH plays a major role in process of nitrification as it has an effect on the enzyme function which depends on the maintenance of a special spatial configuration and access to special chemical groups that bind the enzyme and the substrate together as well as special groups at which the reactions take place [3, 45]. Many ionizable groups exist in the enzyme protein, and the ionization of these groups depends on the pH of the environment [14, 45]. Severe changes in pH may affect the protein structure of the enzyme and may change the mode of binding of enzyme and substrate which eventually slow down the rate of reaction. Another major role that pH plays

in nitrification process is that the pH value in the system affects the NH_3/NH_4^+ and HNO_2/NO_2^- equilibrium.

The narrow range of pH values at which the rate of nitrification is maximum is called the optimum range pH range. Generally, the rate of nitrification (or partial nitrification) exhibits a plateau over a limited pH range and decreases steadily on both sides of the plateau. Figure 2.2 show the expected effect of pH on the Nitrosomonas activity

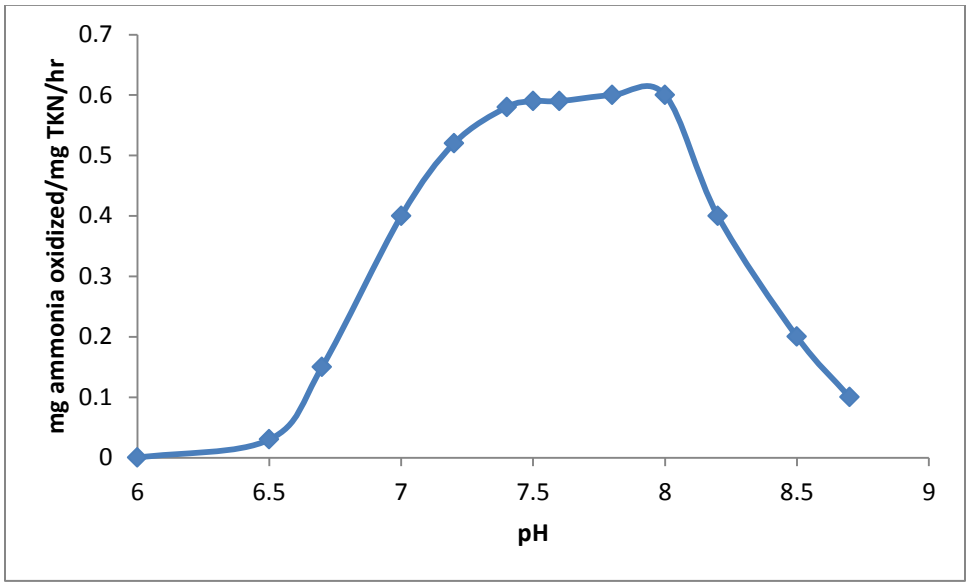

Figure 2.2: Effects of pH upon the activity of Nitrosomonas (reproduced from [67]).

The pH for optimal rate of nitrification has been reported by many investigators. Table 2.1 shows the optimum pH range for optimal rate of nitrification of recent publications. It has been found that most of publications, either old or recent publications, agreed with optimum range of pH in Figure 2.2.

Table 2.1: : Optimum pH for optimal rate of nitrification.

pH range or value	Reference
7.5-8.5	[68]
7.5	[69]
7.85±0.5	[70]
8	[43]
7.5	[58]

As Equation 1.6 suggests, the first step in the nitrification process, with Nitrosomonas function, is a hydrogen ion producing step. The pH of the reaction medium will be decreased if the medium is not well buffered, and there is a general agreement that as pH moves towards the acidic range, the rate of nitrification declines as Figure 2.2 showed that. Therefore, the alkalinity of the process is an important consideration as it acts as a buffer to maintain the pH levels slightly alkaline in order to counteract any addition of acid.

2.1.3 Temperature effect on nitrification

Nitrification is a process driven by mesophilic bacteria. Generally, biochemical reactions are dependent on the temperature but the influence of temperature on the nitrification process is particularly important because of the slower rate of activity of nitrifiers compared to the heterotrophs. For example, Uhl et al [71] mentioned that lower rate of nitrification is observed during winter as the ammonia inlet concentration would normally be in the range of 4.2 mg/l while this concentration falls down during summer to 0.05 mg/l. The influence of temperature on the nitrification process can easily be noticed but the exact influence is difficult to determine because of its interaction with mass transfer, chemical equilibria, and growth rate [72]. Therefore, usually the effect of temperature is related to the rate of nitrification or consumption kinetics. Kim et al [64] studied the effect of temperature on ammonia oxidation rate and nitrite oxidation rate in a batch system over the temperature range of 10-30 ºC, and they found that the optimum rate of nitrification was at 30 ºC, within that range, as shown in Figure 2.3.

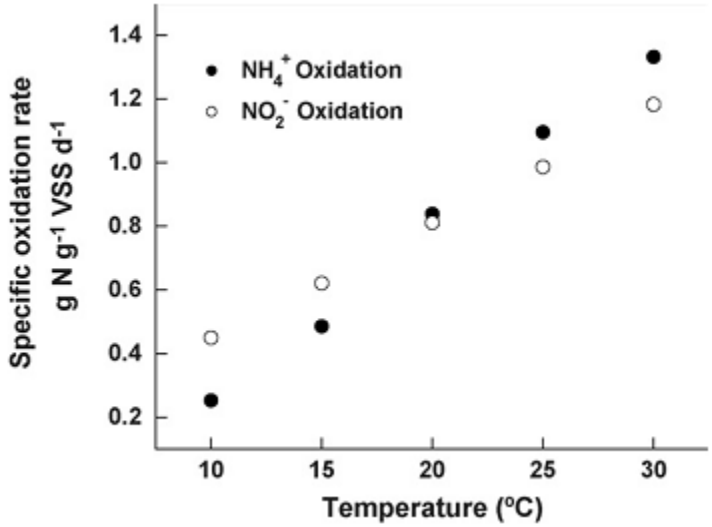

Figure 2.3: Specific ammonium and nitrite oxidation rate at different temperatures [64].

Downing et al [73] found that the ammonium oxidation rate doubled as temperature increased by 10 ºC over the temperature range of 5-30 ºC. Groeneweg et al [50] obtained similar results since they reported that the ammonium consumption kinetics increased by a factor of 3 as the temperature increased from 10 to 30 ºC. Wang et al [74] found that the ammonium oxidation rate increased by a factor of 4.5 when temperature increased from 12 to 30 ºC.

Wild et al [75] claimed that the rate of nitrification increase through the range of 5-30 ºC in reasonable agreement with the Van't Hoff-Arrhenius Law which correlate the temperature of the reaction to the activation energy. The activation energy of a reaction can be determined graphically by taking the natural logarithm of the Arrhenius equation as shown in the following equation [76]:

$$\ln K = \frac{-E_a}{RT} + \ln A \qquad (2.3)$$

where

K: the reaction rate constant, s^{-1};

E_a: the activation energy, kJ/mol;

R: the universal gas constant, $JK^{-1}mol^{-1}$;

T: temperature, K;

A: frequency factor for the reaction, s^{-1}.

Kim et al [64] obtained results on the activation energy for ammonia and nitrite oxidation over the temperature range of 10-30 ºC. These agree with the claims of Wild et al [75]. These results are presented in Table 2.2.

Table 2.2: Activation energy over temperature range of 10-30 ºC for both ammonia and nitrite oxidation [64].

	Temperature (ºC)	E_a (kJ/mol)
Ammonia oxidation	10-20	87.1
	20-30	38.6
Nitrite oxidation	10-20	34.2
	20-30	34.2

Based on these results, the activation energy of ammonia oxidation at the higher temperature range (20-30 ºC) dropped almost to half that at the lower range of temperature (10-20 ºC). Moreover, this difference in activation energy between the two ranges of temperatures of the ammonia oxidation step is strong evidence that the mechanism of ammonia conversion to nitrite is a two-step process as indicated previously unlike the NOB which shows the same activity over the entire temperature range (10-30 ºC). Guo et al [76] worked at a temperature range of (5-35 ºC) and they came also to similar results ,to those of Kim et al, when they reported that the energy of activation of ammonia oxidation at the lower temperature range (5-20 ºC) was greater by a factor of 2.5 compared to the higher temperature range (20-35 ºC).

2.1.4 Oxygen concentration

AOB and NOB are *obligate* aerobes, therefore; oxygen is a major requirement for nitrifiers, and they are intolerant of low dissolved oxygen concentrations. The importance of oxygen in the nitrification process and oxygen limitations are discussed in the next sections.

2.1.4.1 Role of oxygen in nitrification

Microorganisms, including AOB and NOB, gain the energy released from oxidation-reduction reactions. In terms of chemistry, molecular oxygen (O_2) has two unpaired electrons in the π*Y antibonding orbital and one in the π*Z antibonding orbital; the σ*Z is empty. These unpaired electrons have the same parallel spins so oxygen cannot easily oxidize another molecule by accepting a pair of electrons and, thus, oxygen is not reactive with most molecules, except radicals [77]. For this reason, the aerobic respiration process of reducing O_2 to H_2O takes place in a series of reactions. The overall net reaction which involve the acceptance of four electrons and has the form (O_2+4H+4e^- ➔ 2H_2O) is central to aerobic respiration. The detailed series reactions are shown in Equations 2.4 to 2.7:

$$O_2 + e^- \rightarrow O_2^- \ (superoxide) \tag{2.4}$$

$$O_2^- + e^- + 2H^+ \rightarrow H_2O_2 \ (hydrogen\ peroxide) \tag{2.5}$$

$$H_2O_2 + e^- + H^+ \rightarrow H_2O + OH^- \tag{2.6}$$

$$OH^- + e^- + H^- \rightarrow H_2O\ (water) \tag{2.7}$$

It is worth mentioning that if the conditions are acidic, the superoxide, O_2^-, can gain a hydrogen atom to form a highly reactive hyperoxyl radical, HOO^-, which has a pK_a value of 4.8 [77].

In terms of energy capture, electrons removed from the primary electron donor, ammonia, and transferred to intracellular electron carriers namely NAD+, nicotinamide-adenin dinucleotide, NAPD+, nicotinamide-adenin dinucleotide phosphate, NADH dehydrogenases, and others carriers. The carriers transport the electrons to the terminal electron acceptor, oxygen, and the energy released can be determined from the overall free energy change of NADH and oxygen half reactions as shown in Equation 2.8 to 2.10 [13]:

$$NADH + H^+ \rightarrow NAD^+ + 2H^+ + 2e^- \quad \Delta G^\circ = -62\ \text{kJ} \tag{2.8}$$

$$\frac{1}{2}O_2 + 2H^+ + 2e^- \rightarrow H_2O \qquad \Delta G^\circ = -157\ \text{kJ} \tag{2.9}$$

$$\text{Net: } NADH + \tfrac{1}{2}O_2 + H^+ \rightarrow NAD^+ + H_2O \qquad \Delta G^\circ = -219\ \text{kJ} \tag{2.10}$$

The energy is captured by transferring the energy from intermediate electron carriers, adenosine triphosphate (ATP) known as a primary example, to energy carrier as in Equation 2.10, and the energy released is used to add a phosphate group to adenosine diphosphate, ADP as presented in Equation 2.11 [13]:

$$ADP + H_3PO_4 \rightarrow ATP + H_2O \quad \Delta G^{\circ} = +32 \text{ kJ} \tag{2.11}$$

Theoretically six moles of ATP could be formed under aerobic conditions from each mole of NADH, yet, only three moles are actually formed as the real reactions capture less than 100 % of the standard free energy [13].

2.1.4.2 Oxygen limitations

Of many factors discussed in this work that are known to affect nitrifiers, dissolved oxygen concentration is one of the more important. AOB and NOB require a certain minimum (critical) level of dissolved oxygen to survive. The required stoichiometric quantities, according to Equations 1.6 and 1.7, are 3.43 mg O_2/mg NH_4^+-N for conversion to nitrite, and 1.14 mg O_2/mg NO_2^--N to be converted to nitrate. That is 4.57 mg O_2 needed to oxidize 1.0 mg NH_4^+-N to NO_3^- in a complete nitrification process. Several investigators [78-82] have questioned the amount of oxygen required, and suggested that less than the stoichiometric amount of oxygen required. Buswell et al [79] introduced the first attempt to figure out this discrepancy, and they claimed that since oxygen is released from carbon dioxide in the synthesis of cell material, less than the stoichiometric quantity of oxygen is required for the oxidation process. Montgomery et al [82] attempted to quantify the oxygen production from CO2 reduction based on equation 1.8, and they found it equals to 3.23 and 1.12 instead of 3.43 and 1.14 for oxidation of ammonia and nitrite, respectively. Adams et al [80] came up with much less value when they reported the oxygen requirement as 3.9 mg O_2/mg NH_4^+-N instead of 4.57 mg O_2/mg NH_4^+-N. Bryant et al [81] reported another value which is 4.26 mg O_2/mg NH_4^+-N.

It appears to be generally accepted that the nitrification rate increase with increasing concentration of dissolved oxygen up to a certain level, above which further increase in oxygen concentration have little or no effect (maximum). In literature, the observed nitrification rate-limiting dissolved oxygen concentration varies widely (minimum) as is now discussed.

The reported values of dissolved oxygen, DO, that have been applied in the nitrification process, in literature, vary from 0.05 mg O_2/l [83] to 60 mg O_2/l [84]. Abeliovich [83] reported that nitrification was observed for a certain time at dissolved oxygen concentration of 0.05 mg/l. In a sequencing batch reactor (SBR), Guo et al [76] carried out their work under low dissolved oxygen concentration (0.4-0.8) mg O_2/l, and they conclude that low dissolved oxygen did not produce sludge. Therefore, Yusof et al [68] stated that complete nitrification at higher loading rate was achieved by maintaining dissolved oxygen in the range of 2.0 to 5.0 mg O_2/l, and the minimum dissolved oxygen must be maintain at 2.0 mg O_2/l. The NH_4^+-N removal efficiency, in their work, was 99%. Aslan et al [69] used a fluidized bed reactor, and the dissolved oxygen was varied from 1.5 to 2.5 mg O_2/l at the top of the reactor and 4 to 6 mg O_2/l in the recycling tank of the nitrification column. Under these conditions, their reactor achieved NH_4^+-N removal efficiency of 90%. Stenstrom and Poduska [85] cited five references that observed inhibitory effect on nitrification process when dissolved oxygen was in the range of 0.2 to 0.7 mg O_2/l. This finding supported by Knowles et al [86] when they stated that nitrification ceased entirely below 0.2 mg O_2/l. On other hand, the effect of high dissolved oxygen concentration was studied by Haug and McCarty [84], and they found no inhibition at dissolved oxygen up to 60 mg O_2/l. A summary of recent researches of the dissolved oxygen effects on nitrification process is presented in Table 2.3.

Table 2.3: Summary of the effects of DO on nitrification.

Dissolved Oxygen Parameter			Reactor Type	Conditions and Remarks	Reference
DO, mg/l	K_o(DO), mg/l	k_La, hr^{-1}			
7.5	0.2	2.77	SBR	DO at saturation T=30 ºC, pH=7.5-8.0 Culture is a sludge from WWTP	[87]
3.0	48.3±4.2		Continuous flow reactor	T=23ºC, 45% NH_4^+-N removal	[88]
0.4-0.8			SBR	Seeding sludge, pH=7.0-7.8, no sludge was produced	[76]
0.3-1.2			Aerated pond	Nitrification inhibited,	[89]
2.5-3.0	0.65 for Nitrosomonas, 0.23 for Nitrobacter		Batch reactor	Seeding sludge, T=20 ºC, pH=7.2, K_o is an average value	[90]

Table 2.3: Summary of the effects of DO on nitrification *continued*

Dissolved Oxygen Parameter			Reactor Type	Conditions and Remarks	Reference
DO, mg/l	K_o(DO), mg/l	k_La, hr^{-1}			
2.0-5.0			Activated sludge system	Seeding sludge from landfill, pH=7.5, 99% NH_4^+-N removal	
9.5					[3]

Satnkewich [91] studied the effect of dissolved oxygen on the growth rate of nitrifiers, and postulated a relationship between growth rate and the dissolved oxygen based on Monod-type model as shown in Figure 2.4.

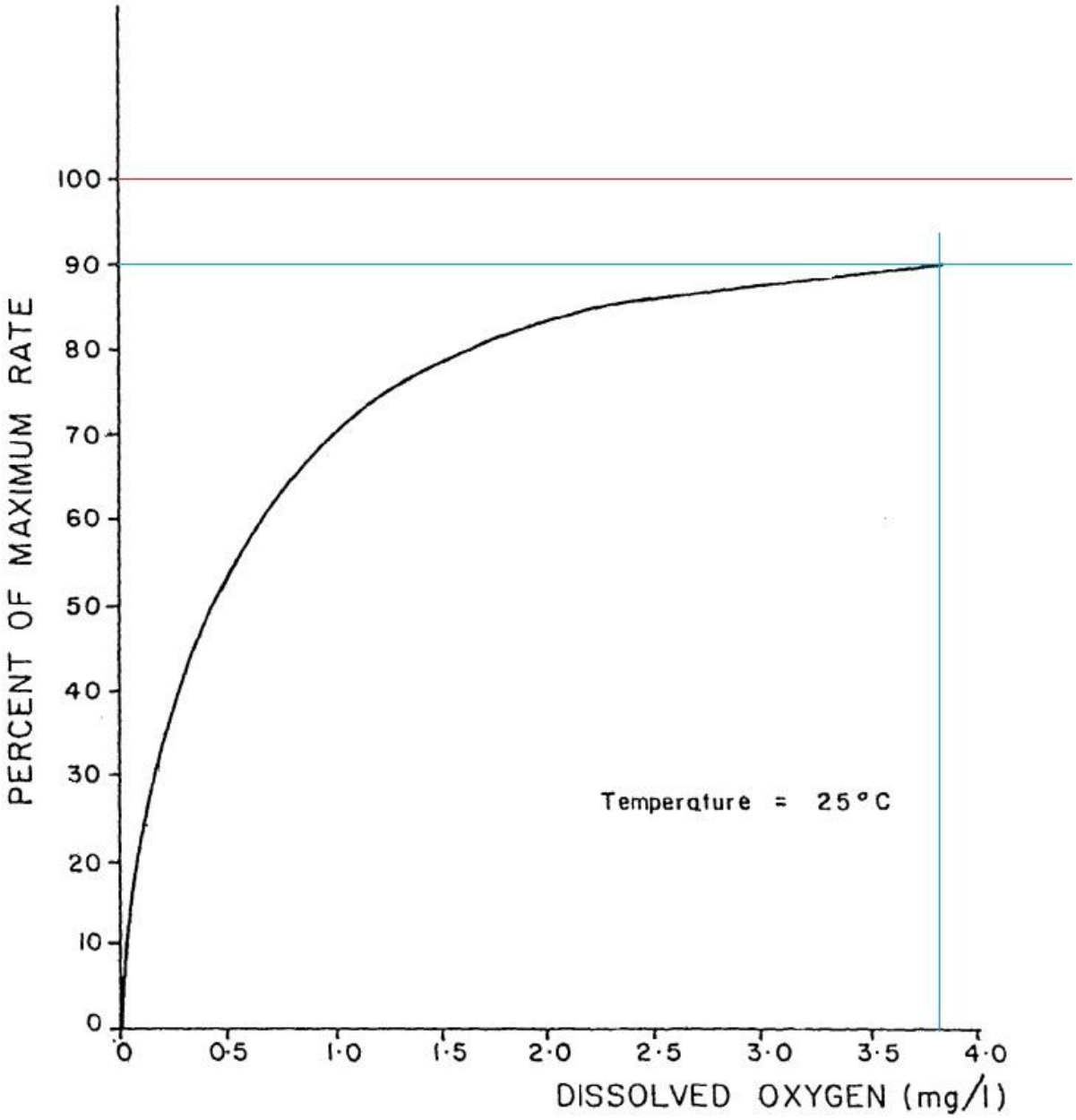

Figure 2.4: Effect of dissolved oxygen on the growth rate of nitrifiers [91].

2.2 Ion Exchange

2.2.1 Removal of ammonia by ion exchange

Removal of ammonia by ion exchange has received a great attention since the Clean Air Act and the Clean Water Act were passed in the 1970s [58], since then, natural zeolites such as clinoptilolite have been widely used as materials with a great affinity for ammonium ions [26]. A review of the literature indicates a significant amount of recent research has been focused on using clinoptilolite in wastewater treatment [92-107]. The majority of the research on using clinoptilolite for NH_4^+ removal has been on municipal wastewater [92, 94, 96-98, 101, 102, 106, 107], although some [99, 100] has investigated its use to treat landfill leachates or for sorption of contaminants in the ground water [102]. Most of these studies have used the same principle idea of experimental setups which consist of a clinoptilolite column through which is fed the wastewater to be treated until a specified NH_4^+ breakthrough value is reached the effluent end. Then, the ion exchange material is regenerated to restore its capacity and reused in the column for another cycle. Although, the experimental setups were similar, in principle, different parameters were reported under varying conditions. In the next sections, these parameters are discussed.

2.2.2 Clinoptilolite's capacity

Reported data for the capacity clinoptilolite's in the literature are varied. These variations lead us to the factors that affect the clinoptilolite's capacity. Klieve and Semmens [108] claimed that these variations are due to the different measurement techniques employed. Hedstrom and Amofah [97] discussed, in column experiment, the factors affecting the clinoptilolite's capacity such as influent ammonium concentration, retention time, clinoptilolite particle size, type of

solution (ammonium solutions or wastewater), pretreatment of clinoptilolite, and design of column (height, diameter, etc.). These workers varied some of these factors, and they obtained different clinoptilolite's capacities. Their work is an example why different researchers reported different clinoptilolite's capacities. Table 2.4 shows a list of clinoptilolite's capacity data reported in recent literature. The source of the clinoptilolite is also a major factor, and even within the same source there may be batch to batch variation.

Table 2.4: Clinoptilolite's breakthrough capacity.

Breakthrough capacity, meq NH_4^+-N/g	Inlet concentration, mg NH_4^+/l	Remarks and conditions	Reference
1.76	40	pH=7.8, pretreated with NaCl, bed height=25 cm, BV=0.49L, 9.8BV/hr,	[3]
1.61	50	3BV/hr, pretreated with NaCl, T=20 ºC, BV=0.454L, upflow	[109]
0.76	20	2BV/hr, pretreated with NaCl, BV=0.141L, upflow	[58]
0.19	20	Particle size 4-8 mm, feed is wastewater, bed height=20cm, pH=7.0-7.5, 3BV/hr	[97]

Table 2.4: Clinoptilolite's breakthrough capacity *continued*

Breakthrough capacity, meq NH_4^+-N/g	Inlet concentration, mg NH_4^+/l	Remarks and conditions	Reference
0.69	40	Particle size 0.853mm, downflow, 12BV/hr, column height=1m, T=29±2ºC	[103]
0.72	40	Particle size 0.422mm, conditions are same as in [103]	[103]
0.88 (max. capacity)	250	Batch study, particle size 0.2-1 mm, pretreated with 2M NaCl at 25 ºC	[106]
1.31 (max. capacity)	250	Same conditions in [106] except that clinoptilolite was treated with 2M NaCl at 90 ºC *for* 7 hr in thermostat	[106]

Table 2.4 shows not only the differences in the obtained values of the breakthrough capacity, in column experiments, and maximum capacity, in batch experiments, but also how the conditions and factors vary for each experiment.

The capacity changes due to variations in the influent concentrations have been reported in literature. For example, Mclaren et al [110] reported that as the influent concentration increased from 14 to 70 mg NH_4^+-N/l, the capacity of clinoptilolite increased from 0.47 to 0.95 meq NH_4^+-N/g respectively. Vassileva and Voikov [106] in their work studied the dependence of the capacity on the ammonium initial concentration, in a batch system, and they concluded that an increase in ammonium adsorption with increasing of the initial concentration was observed as shown in Figure 2.5.

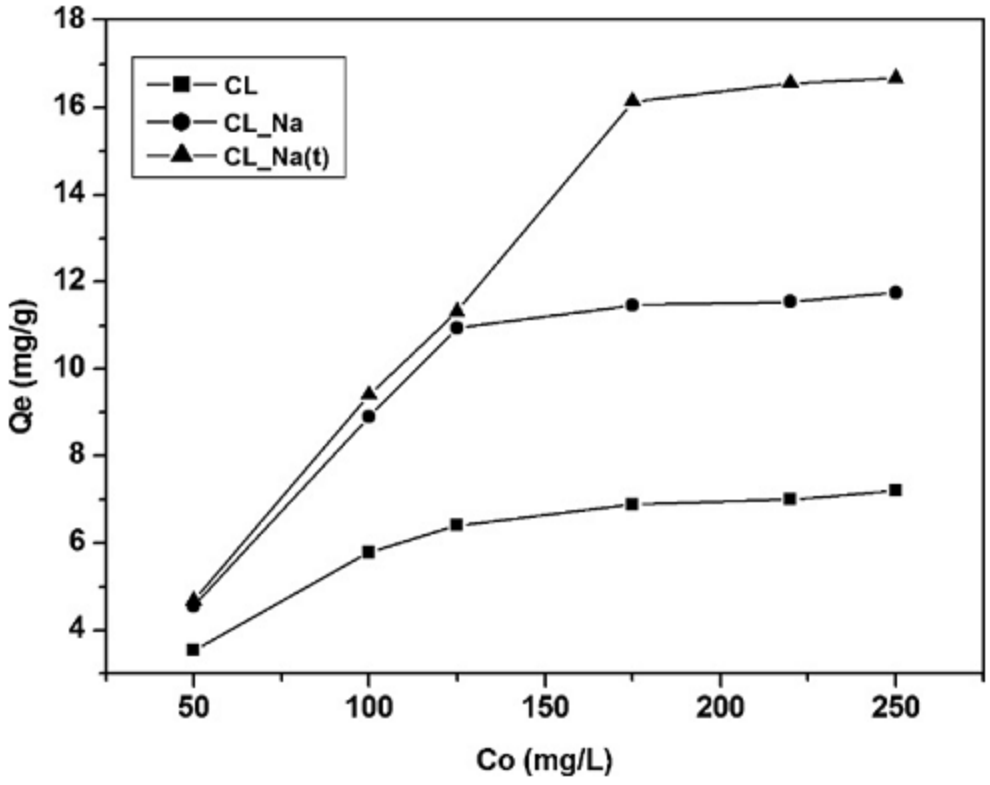

Figure 2.5: Dependence of the clinoptilolite's capacity on the initial ammonium concentration for different clinoptilolite pretreatments [106]. CL indicates for that clinoptilolite was natural and untreated, CL_Na means that clinoptilolite was treated in 2M NaCl at 25ºC, CL_Na(t) indicates that clinoptilolite was treated in 2M NaCl at 90 ºC for 7 hr [106]. Note That Q_e is the clinoptilolite's capacity in mg/g and not in meq/g, to do the conversion divide the Q_e in mg/g by molecular weight of nitrogen which is 14.

Figure 2.4 also shows the effects of pretreatment on clinoptilolite's capacity. If clinoptilolite is heated or chemically treated before being put in service, it is considered pretreated. Semmens and Martin [111] were among the earliest researchers who examined the relationship between the pretreatment and the clinoptilolite capacity, and they concluded that clinoptilolite's capacity and selectivity depends on the manner in which the clinoptilolite is pretreated. The aim of

pretreatment is to remove ions that are located on the structure of the material and relocates more easily removable ones, prior to any use. Based on the evaluation of clinoptilolite's behavior, it is desirable to let clinoptilolite have a single cation for exchange, into what is called the homoionic form [111]. However, it well known that it is very difficult to obtain clinoptilolite in a single ionic form [111], but a *near* homoionic state of clinoptilolite is possible [112]. For a chemical pretreatment, sodium chloride, NaCl, is commonly used as a pretreatment agent. Heat treatment has been found to significantly increase clinoptilolite ammonium exchange capacity as suggested by Vassileva and Voikov [106]. As shown in Table 2.4, Vassileva and Voikov reported a 49% increase in clinoptilolite capacity when clinoptilolite's was pretreated at 90 ºC instead of 25 ºC.

Another factor that might affect the clinoptilolite's capacity is the particle size. The smaller particle size has greater surface area available for ion exchange; hence, higher capacity is expected [113]. Rahmani et al [103] showed that the reduction in particle size from 0.853 to 0.422 mm increased the clinoptilolite's capacity from 0.69 to 0.72 meq NH_4^+-N/g clinoptilolite, respectively, as presented in Table 2.4. Much better results were obtained by Nguyen and Tanner [114] as they increased the breakthrough capacity 2 to 4 times by reducing the particle size of clinoptilolite from 2.83 to 2.00 mm. Hedstrom and Amofah [97] used relatively large particle size, 4-8 mm, and the clinoptilolite's capacity they observed was very low, with a reported value of 0.19 meq NH_4^+-N/g clinoptilolite.

pH, also, plays a role in clinoptilolite's capacity. As the pH of the aqueous solution controls the ammonia-ammonium equilibrium, it also controls the adsorption process. The optimum pH range for adsorption is between 4 and 8. Vassileva and Voikov [106] investigated the removal of NH_4^+-N ions by clinoptilolite at pH values from 2.5 to 9.0, and found that the maximum removal was obtained at pH=6 as shown in Figure 2.6.

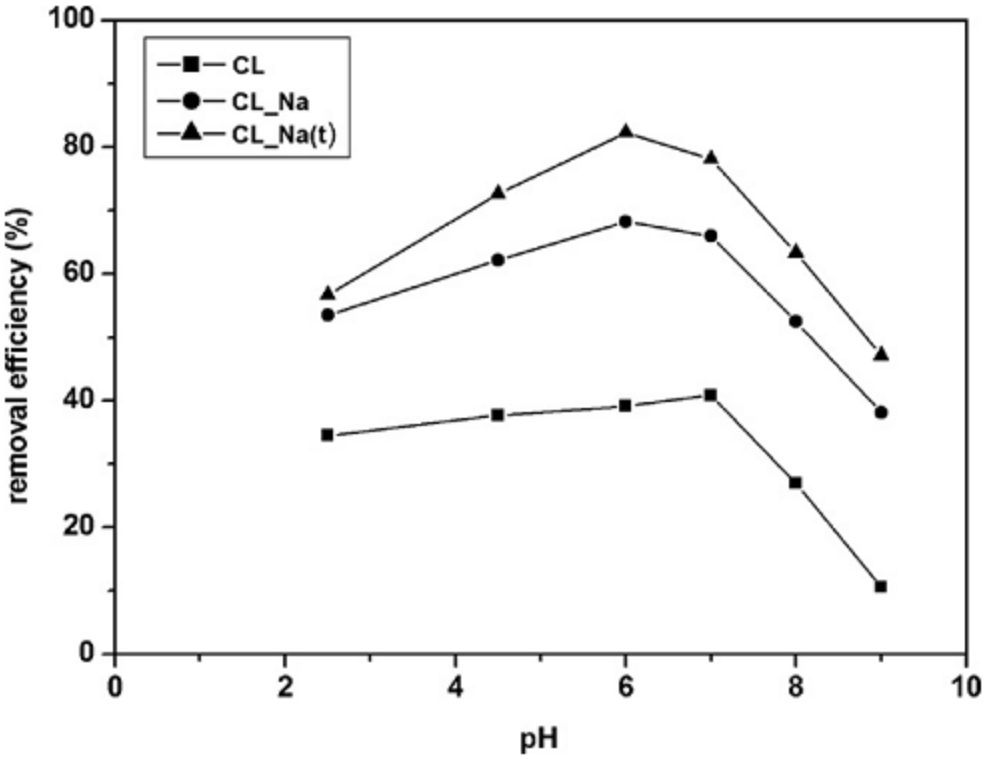

Figure 2.6: Removal efficiency of ammonium ion at different pH values [106]; CL, Cl_Na, CL_Na(t) were explained as in the case of Figure 2.4. The initial ammonium ion was 175 mg/l, and clinoptilolite used was added in an amount of 10 g clinoptilolite/l.

In Figure 2.5, the removal efficiency increases with increasing pH from 2.5 until maximum removal efficiency is reached at pH=6, then removal efficiency decreases as pH increased. The optimum pH range that suggested by Figure 2.5 is between 5 and 8. Because the of the high selectivity of clinoptilolite for H^+, H^+ ions compete with NH_4^+ ions at low pH values [115] which results in low removal efficiency. Vassileva and Voikov [106] gave two explanations for the drop in NH_4^+ removal efficiency after pH=7:

1) Partial dissolution of the clinoptilolite might occur.
2) Possible conversion of NH_4^+ into NH_3.

2.2.3 Clinoptilolite packed bed column

The batch process is important to the extent that the kinetic and thermodynamic parameters can be estimated for an adsorption reaction. These data cannot be applied for a continuous adsorption system. Therefore; ion exchange operations, whether in laboratory scale or in plant scale, are mostly carried out in columns [19]. Solution to be treated is passed through these columns until a specified NH_4^+ breakthrough value is reached in the effluent.

In order to predict the performance of a packed bed column, the equilibrium isotherm which relates the liquid phase concentration of adsorbate to the mass of the adsorbate in the solid phase, and the mechanism governing the rate of adsorption of the adsorbate onto the adsorbent are required. The equilibrium isotherms were discussed in section 1.4.5, and the rate limiting mechanism was discussed in section 1.4.6. The models governing the rate of adsorption of ammonium ion onto clinoptilolite will be discussed in the following section.

2.2.3.1 Uptake models

When a small volume of ammonium ion solution is passed through a clinoptilolite column in the sodium form, the ammonium ion will entirely replace the sodium ions in the bottom part of the column, in case of an upflow system. Above that part, a small part exists in which the ammonium ions have only partially replaced the sodium ions. Above this part of the column none of the sodium ions will have been replaced by ammonium ions. Hence, a mass transfer zone (MTZ) is established. As the ammonium solution is continuously fed to the column, the mass transfer zone travels through the bed until it eventually reaches the column outlet, and this is known as breakthrough point, as shown in Figure 2.7.

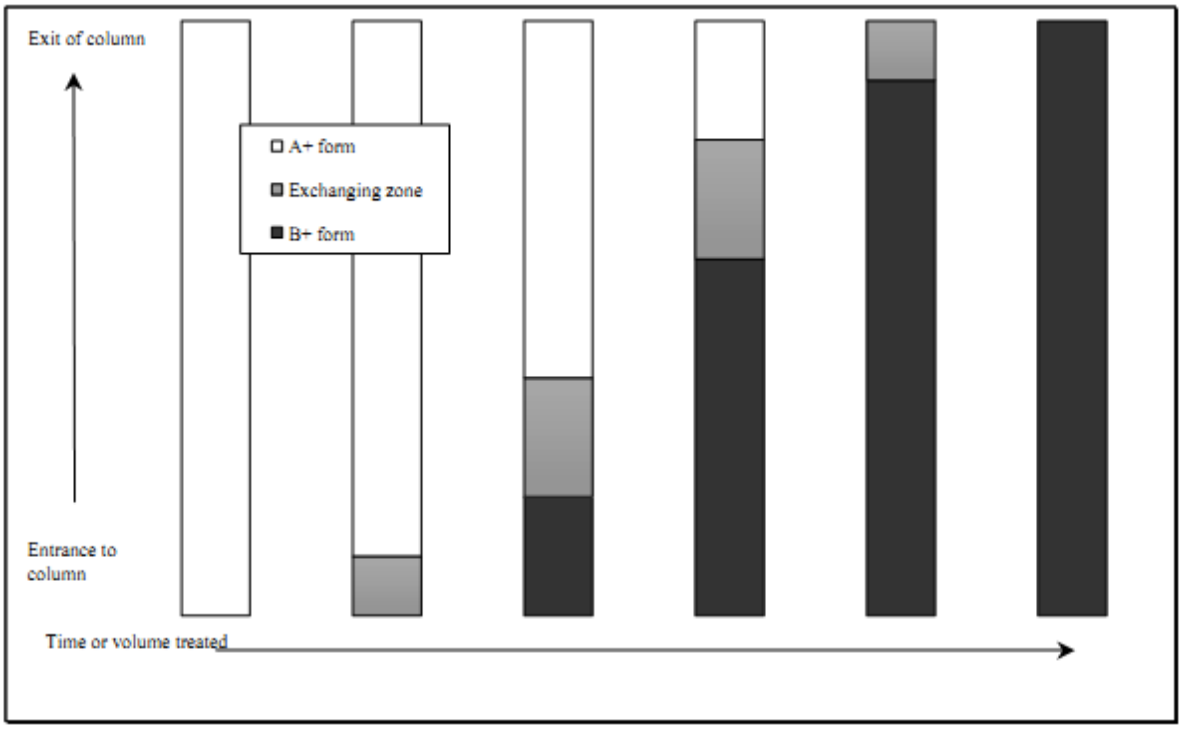

Figure 2.7: Mass transfer zone, exchanging zone, moving through a packed bed [109]. A^+ is equivalent for the sodium form and B^+ for ammonium ion.

The distribution of the ammonium ion concentration in the column can be represented by a breakthrough curve, also called S-shaped curve. A breakthrough curve describes the movement of the mass transfer zone through a packed bed. An example of a breakthrough curve is illustrated in Figure 2.8.

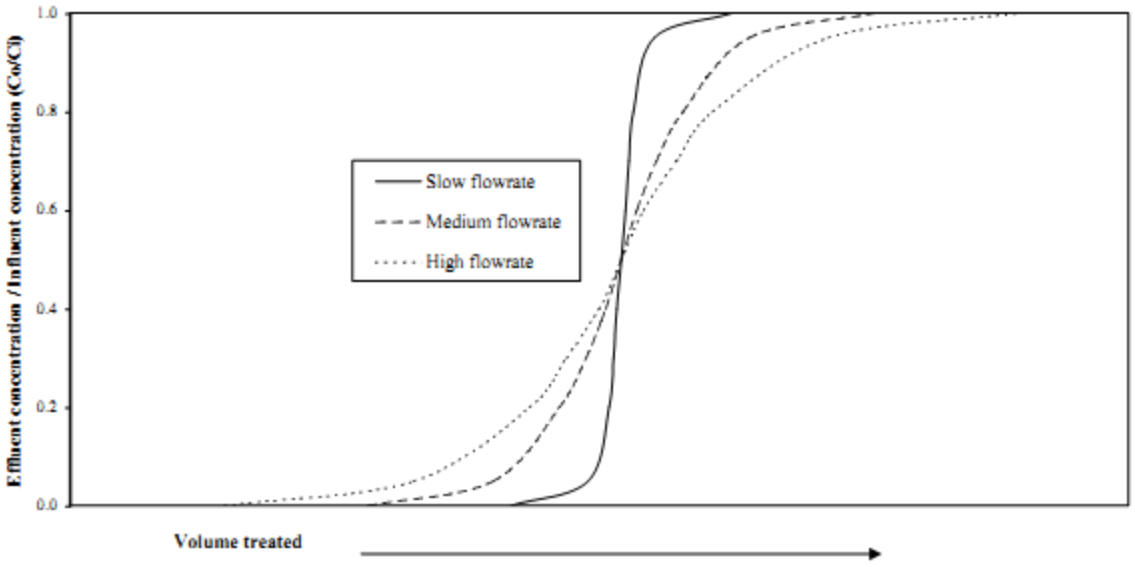

Figure 2.8: Breakthrough curves [5].

The fact that the breakthrough curves are S-shaped is evidence that there is a mass transfer resistance. There are several factors that might affect this mass transfer resistance, or in other word affect the sharpness of the S-shaped. Some of these are experimental or designed factors, while others are depends on the clinoptilolite's properties. These factors are listed below [3]:

- Packed bed volume
- Clinoptilolite particle size
- Clinoptilolite's capacity
- Clinoptilolite's selectivity
- Influent concentration
- Influent flowrate
- Temperature [22]
- Degree of clinoptilolite crosslinking [22]

A sharp MTZ indicates that most of the bed is utilized. Therefore, it is preferable to have a sharp MTZ. McVeigh and Weatherley [3], and Nguyen and Tanner [114] have found that a narrow MTZ can be achieved and more water can be treated if small particles and low flowrate were used.

The MTZ can be sharp and narrow or wide and spread out, changing as it moves through the bed depending on the clinoptilolite's selectivity [5]. If the clinoptilolite prefers ammonium ions, the MTZ will sharpen, and widen if prefers sodium ions over NH_4^+.

Thomas, *Bohart-Adams*, and *bed depth-service time* (BDST)s model are the models that are widely used in the literature to predict the breakthrough curves and to analyze the data obtained from an ion exchange column. Next, these uptake models are introduced.

Thomas Model

The adsorption rate may be controlled by more than one mechanism, but then, the solution for the adsorption rate becomes complicated. Thomas [116] assumed only one limiting mechanism which is the surface kinetics, and he used the Langmuir kinetics of adsorption-desorption to derive his model such that the rate driving force obeys second order reversible kinetics. The model equation is represented by Equation 2.12:

$$\frac{C_t}{C_0} = \frac{1}{1 + \exp\left(\frac{k_{Th} q_0 x}{v} - k_{Th} C_0 t\right)} \tag{2.12}$$

where:

- C_t- concentration of ammonium ion in the effluent, mg/l,

- C_0- concentration of ammonium ion in the influent, mg/l,
- k_{TH}- Thomas rate constant, ml/min/mg,
- q_0- the equilibrium uptake capacity, mg/g,
- x- mass of the clinoptilolite in the column, g,
- v- the flowrate, ml/min
- t- time, min. $t=V_{eff}/v$, where V_{eff} is the effluent volume in ml.

Bohart-Adams Model

This model was originally developed by Bohart and Adams [117] to describe the adsorption of chloride on charcoal, but it is widely used in literature for the quantitative description for other systems [118]. This model assumed that the adsorption rate is proportional to both the residual adsorbent and the concentration of the adsorbate [119]. The Bohart-Adams model is given by Equation 2.13:

$$\frac{C_t}{C_0} = \exp\left(k_{AB}C_0 t - k_{AB}N_{AB}\frac{Z}{F}\right) \quad (2.13)$$

where:

- C_t, C_0, and t are the same as described in Thomas model,
- k_{AB}- is the kinetic constant, L/mg/min,
- N_{AB}- is the saturation concentration, mg/l,
- Z- is the bed depth of the column,
- F- is the linear flow rate calculated by dividing the flow rate by the column cross-sectional area, cm/min.

BDST Model

This model developed by Hutchins [120] assumes, in its simple form, that the intraparticle mass transfer resistance and external film resistance are negligible, which means that the adsorbate is adsorbed on the surface of the adsorbent. This model is based physically measuring the capacity of the column at different breakthrough values. Equation 2.14 represents the BDST model.

$$t_b = \left(\frac{ZN_{BD}}{C_0 v}\right) - \frac{1}{k_{BD} C_0} \ln\left(\frac{C_0}{C_b} - 1\right) \tag{2.14}$$

where:

- C_0, Z, and v are the same as described in Thomas model,
- t_b- is the time at breakthrough point, min,
- N_{BD}- is the adsorption capacity, mg/cm3,
- k_{BD}- is the rate constant of the adsorption reaction, L/mg/min,
- C_b- is the concentration at the breakthrough point, mg/l.

2.3 Immobilization

Immobilization is a process by which an enzyme or whole cell is confined so that it may function as a biocatalytic converter for an extended period of time [121]. Methods of restraining biocatalyst are called immobilization techniques. These techniques vary widely but the fundamental aspect of each is the restriction of an enzymatic system or cell population within a defined boundary for a certain purpose [8].

Applying microbial immobilization to a biological waste treatment system is expected to give the following advantages [121]:

- Retention of biomass
- Manipulation of growth rate independent of washout
- Phase separation of cell mass
- High cell concentration within the reactor
- Possible protection from inhibitory compounds

When the microbial population is confined to a distinct phase, it is far more controlled than when dispersed in the liquid phase. Immobilization allows for high cell concentrations of slow growing cell in reactors of high flow [121].

The immobilization of viable cells is subjected to the following factors [121]:

- Cell physiology
- Immobilization method
- Mass transfer

Among these factors, the immobilization method is the most important factor to determine cell viability. For example, some methods used chemical reagents to crosslink matrices or to link cells. These compounds may affect the cell surface or may lead to complete loss of viability [121]. Cell physiology can be described as the relationship between the cell's metabolic capacity and its environment [9]. The long range viability of an immobilized cell mass is predicted on mass transfer limitations. As an example, if the substrate is not available for the bacteria, it will eventually die. So, mass transfer, especially of weakly soluble substrate such as oxygen, is important in terms of affecting the cell viability.

There are four methods of biomass immobilization as shown in Figure 2.9. These are [122]:

- Entrapment: physical entrapment in a physical matrix.
- Adsorption: attachment or adsorption to a pre-formed carrier.
- Self-aggregation: cells being aggregated by flocculation or crosslinking agents.
- Cells contained behind a barrier: such as membrane, this allows substrate to pass.

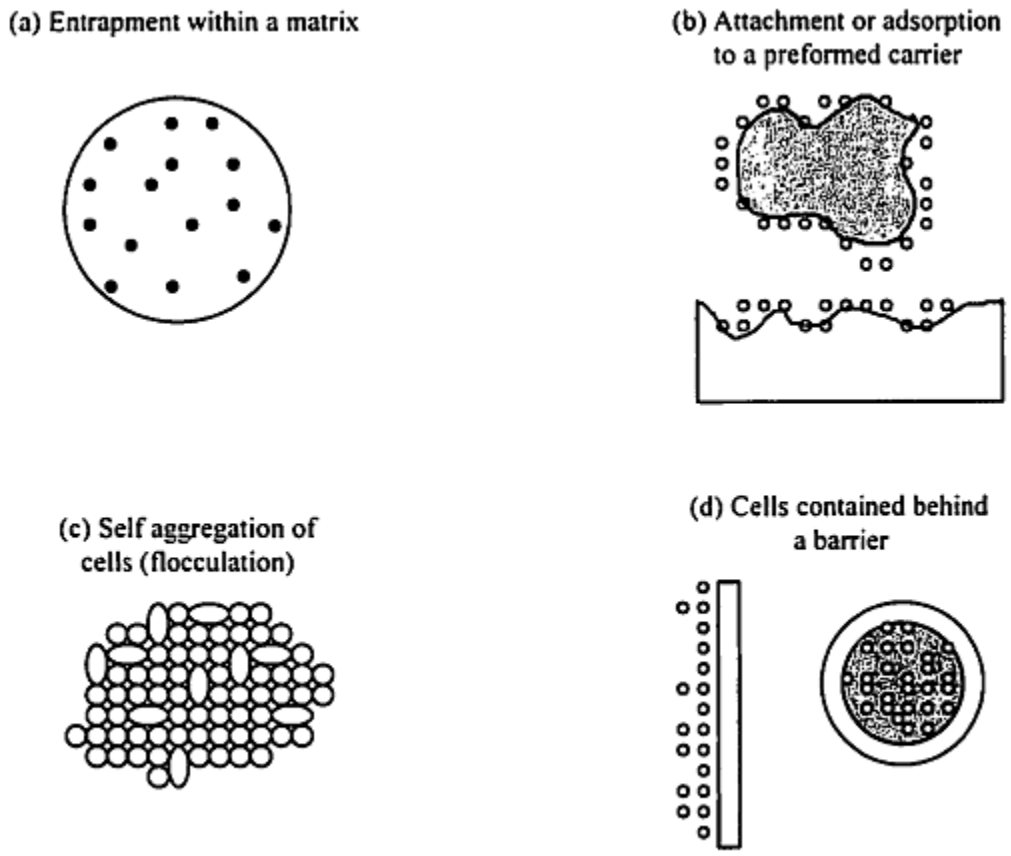

Figure 2.9: Basic methods of cell immobilization [122].

There are four criteria that must be met for an immobilization method to be considered feasible. It must be safe, simple, economical, and produce an active matrix [8].

The immobilization of nitrifying bacteria has been studied in numerous studies. Table 2.5 lists studies that deal with nitrifiers, AOB and/or NOB.

Table 2.5: List of recent researches of immobilized nitrifying bacteria.

Nitrifiers	Method of immob.	Carrier/Remarks	Reference
mixed	Entrapment	Na-alginate	[123]
mixed	Adsorption	Wood	[124]
mixed	Entrapment	Polyurethane gel	[125]
mixed	Entrapment	Polyvinyl alcohol and Na-alginate	[126]
mixed	Entrapment	Na-alginate	[43]
mixed	Adsorption	Elastic plastic filler	[127]
mixed	Encapsulation (cells behind a barrier)	Polyethylene glycol pellets	[127]
AOB	Entrapment	Ca-alginate	[128]
mixed	Entrapment	Urethane gel porous pellets	[129]
mixed	Entrapment	Ba-alginate and clinoptilolite	[9]

Table 2.5: List of recent researches of immobilized nitrifying bacteria *continued*

Nitrifiers	Method of immob.	Carrier/Remarks	Reference
mixed	Adsorption	Clinoptilolite	[3]
mixed	Adsorption	Clinoptilolite/mordenite	[58]
AOB	Entrapment	PVA-SbQ gel	[130]

Although most researchers have used the entrapment method, few found that the adsorption method was more effective. Only three studies used both nitrifying bacteria and clinoptilolite as a combination method for ammonia removal. Two of these used the adsorption method to immobilize nitrifying bacteria on clinoptilolite. Moreover, Miladinovic and Weatherley [4], one of the two studies that used the adsorption method, stated that the entrapment method was ineffective.

In Table 2.5, most researchers used mixed, AOB and NOB, nitrifiers. All the researchers in Table 2.5 obtained the mixed culture from waste treatment plants. Ginkel et al [128], Tramper et al [131], and Uemoto [130] used only an AOB, or more specifically *Nitrosomonas europaea*, as a nitrifier in their immobilization studies. Ginkel et al and Tramper et al obtained the *Nitrosomonas europaea* (ATCC 19718) they used from American Type Culture Collection (ATCC), USA, while Uemoto et al obtained it (IFO-14298) from Institute for Fermentation (IFO), Japan. The reason behind using pure strain, and not mixed, was that a better defined, controllable, and thus more suitable system for fundamental studies can be obtained using pure strain of nitrifying bacteria.

Manju et al [124] immobilized nitrifying bacteria on wood particles as the biomass support. Among the factors they studied, they examined the effect of particle size of the carrier on the nitrification rate. The particle size they used ranged as: 0.5-0.71 mm, 0.71-2.00 mm, 2.5-3.00 mm, and 0.30-1.50 mm. They found that the particle size 0.30-1.50 mm showed better performance in removing total ammonium nitrogen.

2.4 Membranes applications in bioprocesses

In 1831, over 180 years ago, J.K Mitchel conducted several experiments on how fast gases permeate through membranes and he found that CO_2 permeated faster than H_2 through natural rubber membrane. He concluded that different gases permeate through membrane at different rates [132]. Later, in 1866, S.T. Graham utilized the fact that gases have different permeability through membranes to separate a gas mixture when he showed that the oxygen concentration in air could be increased through natural rubber membranes [132].

Despite these early discoveries, economical and industrial utilization of membranes as a gas separator only came after 100 years when the development of “asymmetric” and “composite” membrane was achieved in the 1950s.

A “Bioprocess” can be defined as “any process that uses complete living cells or their components (for example, bacteria, enzymes, chloroplasts) to obtain desired products” (Wikipedia). There are different applications of membranes in bioprocesses.

One of these applications of membranes that have been used in bioprocesses is in bioseparation processes, i.e., the membranes are applied to separate living solutes. These processes are classified based on the membrane’s pore size. For example, ultrafiltration membranes have pore

sizes between 1 and 20 nm, microfiltration membranes have pore size between 0.05 and 10 µm, and virus filtration have pore size between 20 and 70 nm (also known as nanofiltration) [133].

Another application of membranes in bioprocesses that is related to this work is the use of membranes in gas separation.

The first membrane aeration study was conducted by Schaffer et al. in 1960 [134]. They examined polyethylene, ethyl cellulose, and polyethylene membrane as oxygenation tools in sewage treatment [135].

2.5 Transport phenomena in biologically active ion exchange column

2.5.1 Ion exchange mass transfer

The dynamic mathematical model for the exchange of ammonium ion in a fixed bed column can be obtained by means of mass balance equations applied to an element of volume of the column in both liquid and solid phase. For a binary ion exchange system, including NH_4^+ and Na^+, the unsteady state mass balance equation is as follows [136-140]:

$$\frac{\partial C_i}{\partial t} + u_0 \frac{\partial C_i}{\partial z} + \rho_L \frac{1}{\varepsilon} \frac{\partial Q_i}{\partial t} - D_L \frac{\partial^2 C_i}{\partial z^2} = 0 \qquad (2.15)$$

where:

- C_i- the concentration of species *i* in the liquid phase, mg/l;
- Q_i- the concentration of species *i* in the clinoptilolite, mg/g;
- ρ_L- is the bed density, g/L;
- u_0- is the interstitial velocity of the liquid phase, cm/min;
- D_L- is the axial dispersion coefficient, cm^2/min;

- ε- is the column voidage;
- *t*- time, min;
- *z*- is the space coordinate, cm.

Silva et al [139] used this model, Equation 2.15, to represent the biosorption of copper in fixed bed columns using the biomass of brown alga as a biosorbent. Later, Barros et al [140] adapted this model to express the dynamic removal of Cr^{3+} in a packed bed column with NaX zeolite. Gazola et al [136] cofirmed Barros' work. In 2011, Ostroski et al [138] studied the mass transfer mechanism of ion exchange in fixed bed columns using the same model. Many assumptions have been made to obtain this model. These are:

- isothermal and isobaric process;
- constant column void fraction;
- constant physical properties;
- negligible radial dispersion.

Back to Equation 2.15, the first and third term represents the concentration change with time, and *accumulation* of species *i* in the liquid phase and in the clinoptilolite, respectively. The second term reflects the mass transfer of species *i* in the liquid phase due to *convection*. The fourth term represents the mass transfer of species *i* due to *diffusion*, which is equal to the sum of all terms in Equation 2.15. This fact simply demonstrates that the ion exchange process is a diffusional controlled phenomenon.

There are three mass transfer resistances in the ion exchange process. Usually, researchers studied the external liquid film and/or the intraparticle diffusion as rate controlling steps.

Ion exchange process occurs in three steps as shown in Figure 2.10:

i- diffusion of ions from the bulk phase through the liquid film;

ii- diffusion of ions into the micropores of clinoptilolite;

iii- ion exchange at the fixed site.

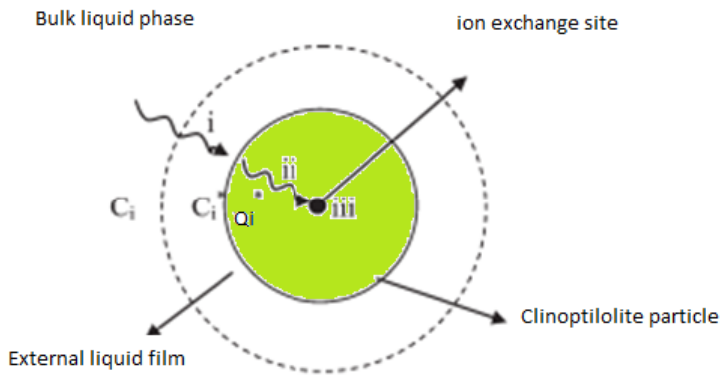

Figure 2.10: Ion exchange process steps. Adapted from Silva et al [139].

Usually the mass transfer rates in the external liquid film for NH_4^+ and Na^+ are represented by Equation 2.16 and 2.17, respectively:

$$\frac{\partial C_{NH_4^+}}{\partial t} = \frac{K_{FNH_4^+}\varepsilon}{\rho_L}\left(C_{NH_4^+} - C^*_{NH_4^+}\right) \tag{2.16}$$

$$\frac{\partial C_{Na^+}}{\partial t} = -\frac{\partial C_{NH_4^+}}{\partial t} \quad (2.17)$$

where:

- K_{FNH4+}- is the overall liquid film external mass transfer coefficient, min^{-1};
- $C^*_{NH_4^+}$- is the concentration of NH_4^+ in the liquid phase at equilibrium, mg/l.

The mass transfer rates inside the clinoptilolite particle for NH_4^+ and Na^+ are represented by Equations 2.18 and 2.19, respectively:

$$\frac{\partial Q_{NH_4^+}}{\partial t} = K_{SNH_4^+}\left(Q^*_{NH_4^+} - Q_{NH_4^+}\right) \quad (2.18)$$

$$\frac{\partial Q_{Na^+}}{\partial t} = -\frac{\partial Q_{NH_4^+}}{\partial t} \quad (2.19)$$

where:

- $K_{SNH_4^+}$- is the mass transfer coefficient in clinoptilolite, min^{-1};
- $Q^*_{NH_4^+}$- is the concentration of NH_4^+ in clinoptilolite at equilibrium, meq/g.

The relationship between *Ci** and *Qi** can be obtained using Equation 1.17.

Initial Conditions

The initial average concentrations in the liquid phase of NH_4^+ and Na^+ are expressed in Equations (2.20) and (2.21) respectively:

$$C_{\mathrm{NH_4^+}}(z,0) = 0 \tag{2.20}$$

$$C_{Na^+}(z,0) = 0 \tag{2.21}$$

The initial concentration in the solid phase of NH_4^+ and Na^+ are:

$$Q_{\mathrm{NH_4^+}}(z,0) = 0 \tag{2.22}$$

$$Q_{Na^+}(z,0) = \mathrm{CEC} \tag{2.23}$$

where CEC is the cation exchange capacity of ammonium ion in clinoptilolite.

Boundary Conditions

The boundary conditions for NH_4^+ and Na^+ ion are:

$$D_L \frac{\partial C_i}{\partial z} = u_0(C_i(t,0) - C_{i0}) \qquad z = 0 \tag{2.24}$$

$$\frac{\partial C_i}{\partial z} = 0 \qquad z = L \tag{2.25}$$

where C_{i0} is the feed concentration of species *i* in the liquid phase in mg/l.

Intraparticle Resistance Model

In this model, the intraparticle resistance is the rate controlling step, and $Ci \approx Ci^*$ (i.e. equilibrium at the interface). Equations 1.17, 2.15, 2.18-2.25 are applied.

Film and Intraparticle Resistances Model

In this model, both the external film resistance and the intraparticle resistance are considered as rate limiting steps. In this case, Equations 1.17 and 2.15-2.25 are applied.

In Equations 2.15 to 2.25, some parameters are experimentally determined such as $\rho_{L,}$ ε, and u_0, while others such as K_{Fi} and D_L can be estimated from empirical correlations.

The axial dispersion coefficient, D_L, can be estimated using the correlation that is given by Ruthven [141]:

$$\frac{D_L}{u_0 d_p} = \frac{20}{\mathrm{ReSc}} + \frac{1}{2} = \frac{20}{\varepsilon}\left(\frac{D_m}{u_0 d_p}\right) + \frac{1}{2} \tag{2.26}$$

where:

- d_p- is the particle diameter, cm;
- D_m- is the molecular diffusion of species in water, cm^2/min;
- Re- Reynolds number;
- Sc- Schmidt number;

Re and Sc numbers are defined as follows:

$$\mathrm{Re} = \frac{u_0 d_p}{\nu_s} \tag{2.27}$$

$$\mathrm{Sc} = \frac{\nu_s}{D_m} \tag{2.28}$$

where ν_s is the kinematic viscosity, cm^2/min.

The overall mass transfer coefficient, K_{Fi}, is given as:

$$K_{\mathrm{Fi}} = a_e k_{fi} \tag{2.29}$$

$$a_e = \frac{6\left(1-\varepsilon_p\right)}{d_p} \tag{2.30}$$

where:

- a_e- is the particle specific area, cm^{-1};
- k_{fi}- is the mass transfer coefficient in liquid film, cm/min;
- ε_p- particle porosity.

The mass transfer coefficient in the liquid film, k_{fi}, is commonly calculated based on the correlation developed by Wilson and Geankoplis [142]:

$$J_D = \frac{1.09}{\varepsilon \mathrm{Re}^{2/3}} \tag{2.31}$$

where J_D is the Chilton-Colburn factor and it is defined as follows:

$$J_D = \frac{\mathrm{Sh}}{\mathrm{ReSc}^{1/3}} \tag{2.32}$$

where Sh is the Sherwood number:

$$Sh = \frac{k_{fi} d_p}{D_m} \tag{2.33}$$

The Chilton-Colburn factor, J_D, Equation 2.32; can be redefined as:

$$J_D = \frac{k_{fi}}{u_0} \mathrm{Sc}^{2/3} \tag{2.34}$$

Upon rearrangement of Equations 2.31 and 2.34:

$$k_{fi} = \frac{1.09\, u_0}{\varepsilon} (\mathrm{ReSc})^{-2/3} \tag{2.35}$$

2.5.2 Oxygen mass transfer

Transport of oxygen from a gas source, a gas bubble for example, to the nitrifying bacteria is a function of several resistances as presented in Figure 2.11.

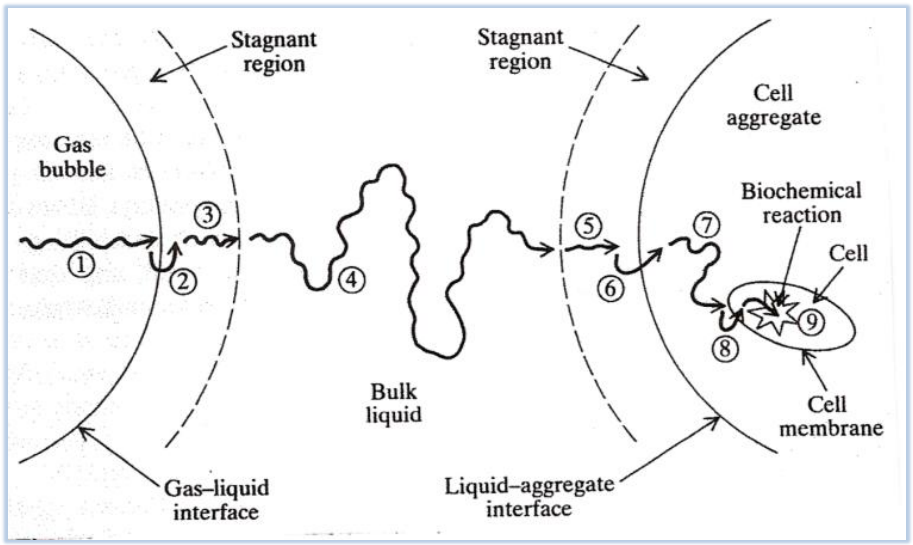

Figure 2.11: Transport of oxygen from a gas source to inside a cell [143].

If oxygen is enriched using a membrane, then the oxygen flux through the membrane can be written as:

$$J_{O_2} = K_{O_2}\left(C^*_{O_2} - C_{O_2L}\right) \quad (2.36)$$

where:

- J_{O2}- is the oxygen flux through membrane, mg/cm^2/min;
- K_{O2}- is the overall oxygen mass transfer coefficient, cm/min;
- C_{O2}^*- is the saturation concentration of oxygen in liquid, mg/l;
- C_{O2L}- is the concentration of oxygen in the liquid, mg/l;

Henry's law constant, *H*, relates the saturation concentration of oxygen in liquid, *C**, to the oxygen partial pressure in the gas phase, P_{O2}, as Equations 2.37 shows:

$$H = \frac{P_{O_2}}{C^*_{O_2}} \quad (2.37)$$

The overall oxygen mass transfer coefficient is a result of several resistances in series as shown in Equation 2.38:

$$K_{O_2} = \frac{1}{\frac{1}{Hk_G} + \frac{1}{Hk_m} + \frac{1}{k_L}} \quad (2.38)$$

where:

- k_G- is the oxygen mass transfer coefficient in the gas phase, cm/min;
- k_m- is the oxygen mass transfer coefficient in the membrane, cm/min;
- k_L- is the oxygen mass transfer coefficient in the liquid phase, cm/min;

The oxygen diffusion in the gas phase, in hydrophobic membranes, is 4 orders of magnitude faster than the liquid phase diffusion [7], and the membrane thickness used in oxygen aeration

studies are quite thin (1-100 μm). Thus, the contributions of gas-film resistance ($1/Hk_G$) and the membrane resistance ($1/Hk_m$) are negligible comparing to the liquid-film resistance ($1/k_L$). Therefore, Equation 2.38 is reduced to Equation 2.39:

$$K_{O_2} = k_L \tag{2.39}$$

2.5.3 Biofilm

Unlike the suspended cells, the immobilized biofilm provide retention of nitrifying bacteria on fixed attachment surfaces, as discussed in section 2.3.2, which makes the biofilm important for environmental applications.

Biofilms can be defined as " layerlike aggregations of microorganisms and their extracellular polymers attached to a solid surface" [13]. Biofilm systems are quite complex because of the effect of several factors on biofilm growth such as reaction rate, substrate consumption, attachment, external-internal mass transfer of substrate and products, cell death, biofilm loss, and competition between species besides process conditions such as pH, temperature, substrate concentration etc. [144]. A schematic presentation of the formation of a biofilm is shown in Figure 2.10.

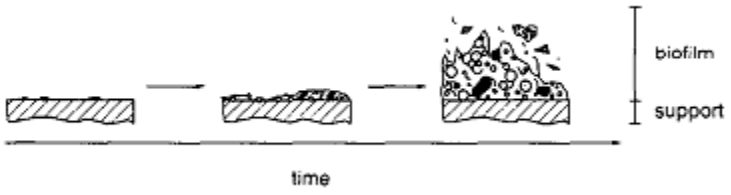

Figure 2.10: Formation of a biofilm [144].

In literature, there are several models that describe the substrate transport to and consumption by biofilms. These models are generally divided into *steady state* and *dynamic* models.

In steady state models, the biomass distribution over the entire biofilm is assumed to be homogenous [144, 145]. That means the biomass per unit surface area is constant in time, and the growth of new biomass per unit area is balanced by the losses per unit area [13].

On the other hand, dynamic models consider the bacterial growth, and the substrate consumption and growth separately [144]. Environmental conditions can cause the biofilm to grow or lose part of its biomass. A steady state model is considered in this review.

In a steady state approach, the ammonia removal and the dissolved oxygen consumption of a nitrifying biofilm can be represented in Figure 2.12.

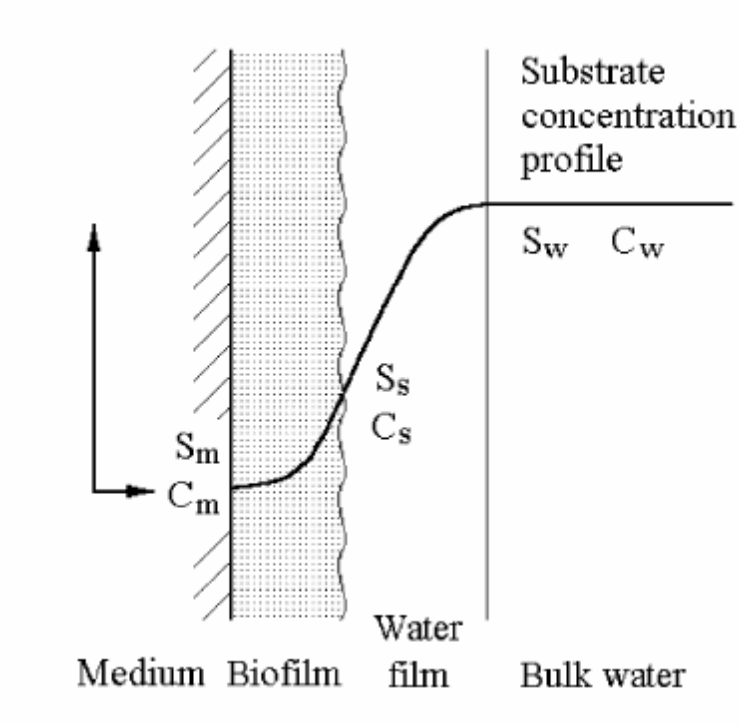

Figure 2.12: Conceptual substrate concentration profile [17].

2.5.3.1 External mass transfer

The rate of ammonia and oxygen transport from the bulk liquid to the liquid-biofilm interface can be expressed respectively as [146]:

$$J_N = \frac{D_{NL}}{l}(S_W - S_S) \tag{2.40}$$

$$J_{ox} = \frac{D_{OL}}{l}(C_W - C_S) \tag{2.41}$$

where:

- J_N- is the ammonia transport flux, mg/cm^2/min;
- D_{NL}- is the ammonia diffusion coefficient in liquid, cm^2/min;
- S_W- is the ammonia concentration in bulk liquid, mg/l;
- S_S- is the ammonia concentration at the biofilm surface, mg/l;
- J_{OX}- is the oxygen transport flux, mg/cm^2/min;
- D_{OL}- is the oxygen diffusion coefficient in liquid, cm^2/min;
- C_W- is the oxygen concentration in bulk liquid, mg/l;
- C_S- is the oxygen concentration at the biofilm surface, mg/l;
- l- is the thickness of liquid film layer, cm.

The thickness of liquid film layer, l, can be estimated using the following correlation [147]:

$$l = 1.23\left(\frac{\mu_w}{\rho_w}\right)^{1/3}\left(\frac{d_f}{u}\right)^{1/2}\varepsilon_b^{3/2}\left(\frac{D_{OL}}{86400}\right)^{1/3} \tag{2.42}$$

Where:

- μ_w- is the viscosity of water, mg/cm/min;
- ρ_w- density of water, mg/cm^3;
- d_f- characteristic length of the biofilm media, cm;
- ε_b- biofilm void fraction= 1-density of cell in biofilm/density of dry cell;
- other parameters are discussed previously.

2.5.3.2 Mass diffusion of the biofilm

Equation 1.15 can be applied to represent the oxygen consumption at any position inside the biofilm:

$$R_{Ocon} = -\mu_{max} \frac{X}{Y_O} \frac{S}{K_O + S} \tag{2.43}$$

the subscript "$_O$" stands for oxygen, and all terms are defined earlier in this work. The mines sign indicates the rate of oxygen consumption.

Oxygen transported into the biofilm by molecular diffusion and may be represented by Fick's second law as follows:

$$R_{diff} = D_{OL} \frac{d^2C}{dZ^2} \tag{2.44}$$

but diffusion and consumption occur simultaneously, so Equations 2.43 and 2.44 can be combined to give the overall mass balance of oxygen in the biofilm:

$$D_{OL} \frac{d^2C}{dZ^2} = \mu_{max} \frac{X}{Y_O} \frac{S}{K_O + S} \tag{2.45}$$

Equation 2.45 cannot be solved analytically; rather it can be integrated once to give the dissolved oxygen flux of a biofilm as expressed in Equation 2.46:

$$J_{ox} = D_{OL}\left(\frac{dC}{dZ}\right)_{Z=0} = \sqrt{2D_{OL}\frac{\mu_{max}X}{Y_O}\left(C_s - C_{ms} - K_O \ln\left(\frac{K_O + C_S}{K_O + C_{ms}}\right)\right)} \quad (2.46)$$

where C_{ms} is the oxygen concentration at the biofilm-support interface. Usually, ammonia exists in adequate concentration in the bulk liquid, therefore, oxygen is the rate limiting step, and as a result C_{ms}=0 and Equation 2.46 can be simplified as:

$$J_{ox} = D_{OL}\left(\frac{dC}{dZ}\right)_{Z=0} = \sqrt{2D_{OL}\frac{\mu_{max}X}{Y_O}\left(C_s - K_O \ln\left(\frac{K_O + C_S}{K_O}\right)\right)} \quad (2.47)$$

substituting Equation 2.41 into Equation 2.47 yields:

$$J_{ox} = D_{OL}\left(\frac{dC}{dZ}\right)_{Z=0} = \sqrt{2D_{OL}\frac{\mu_{max}X}{Y_O}\left(C_W - J_{ox}l/D_{OL} - K_O \ln\left(\frac{K_O + C_W - J_{ox}l/D_{OL}}{K_O}\right)\right)} \quad (2.48)$$

Ammonia flux can be obtained in a similar way, or more simply can be obtained according to the ratio of oxygen consumption to ammonia removal, J_{OX} = 4.57 J_N and Y_o= Y_N/4.57. Equation 2.49 expresses the ammonia flux in the biofilm as follows:

$$J_N = D_{NL}\left(\frac{dC}{dZ}\right)_{Z=0}$$

$$= 0.66\sqrt{D_{NL}\frac{\mu_{max}X}{Y_N}\left(C_W - 4.57J_N l/D_{NL} - K_O \ln\left(\frac{K_O + C_W - 4.57J_N l/D_{NL}}{K_O}\right)\right)} \quad (2.49)$$

Equations 2.48 and 2.49 can be solved with an iterative process [145].

3 Experimental Materials and Methods

3.1 Experimental materials

The ion exchange materials used in this research were two different types of clinoptilolite provided by two companies: KMI Zeolites Inc. and Boulder Innovative Technologies Inc. (BIT). Both types of clinoptilolite are referred to by abbreviated names based on the provider companies as KMI and BIT respectively. Both clinoptilolite types have a particle size of 14x40 mesh (1.41 mm-0.420 mm).

3.1.1 Ion exchange materials analysis

3.1.1.1 Electron Microscopy

A visible analysis (topography studies) of the surface of clinoptilolite was carried out in the Microscopy and Analytical Imaging Laboratory at the University of Kansas (KU). The analysis was performed using a GEMINI scanning electron microscope (SEM). A sample was put on a circular aluminum disk using a layer of epoxy resin to confirm attachment of the sample to the disk. The drying and the coating steps were carried out using a HUMMER II sputter coater. The disk containing the sample was placed on a substrate holder covered by the top cathode assembly. Drying was carried out using argon gas that introduced under vacuum to the chamber. Then, a fine layer of gold/palladium was deposited on the sample. The prepared disk was then introduced into the vacuum chamber in the SEM and exposed to the focused electron beam. This procedure was applied for all samples. The magnification used, and the value of accelerating voltage for each sample are indicated on each image.

3.1.1.2 XRF analysis

The chemical composition of the material used was obtained using an X-Ray Fluorescence Spectrophotometer, XRF. The XRF was obtained by the Mineral Lab Inc.

3.1.1.3 EDS analysis

Energy Dispersive X-ray Spectroscopy (EDS) was carried out using EDAX EDS in the Microscopy and Analytical Imaging Laboratory at KU. Although it has the ability to determine all the elements in sample, EDS was used to obtain the percentage of Si and Al existing in the samples in order to determine the Si/Al ratio.

3.1.1.4 Surface area and pore size measurements

The surface area and pore size data was obtained by the Mineral Lab Inc.

3.1.2 Material preparation

The KMI clinoptilolite was sourced from the KMI's deposits in Sandy valley, Nevada, while BIT clinoptilolite was sourced from BIT' claim deposits in Colorado. Both types have a mean particle diameter in the range of 0.420 mm-1.41 mm as delivered from the factory. For further screening a Cole-Parmer sieve # 18 was used. In general, clinoptilolite has a brittle nature and high-speed grinders could not be used as they may be expected to produce too many fines. To remove any fines and impurities, the clinoptilolite samples were washed and soaked in DI water overnight. Then, the clinoptilolite samples were soaked in a 1 M NaCl solution for 24 hours. Regular hand agitation was applied to ensure complete conditioning in the sodium form. The NaCl solution was renewed on a daily basis for a period of 6 days. Then, the clinoptilolite samples were washed several times and soaked in DI water overnight to remove the excess NaCl. The samples

were then dried overnight at 25 ºC. The conductivity of the DI water used to wash the samples was measured by conductivity meter to ensure no residual of NaCl remained. To ensure the removal of excess NaCl, the conductivity was frequently taken, using the conductivity meter.

3.2 Experimental methods

3.2.1 Batch equilibrium studies

Two different types of clinoptilolite were used:

- KMI clinoptilolite (0.420 mm – 1.41 mm)
- BIT clinoptilolite (0.420 mm – 1.41 mm).

Photographs the clinoptilolite used in this work are presented in Figure 3.1.

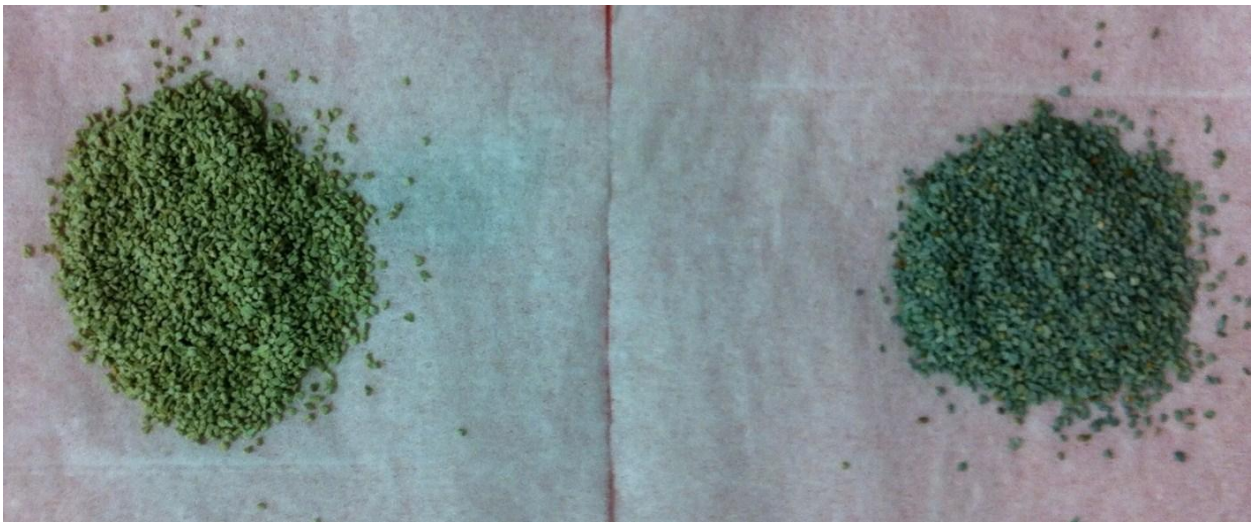

Figure 3.1: Types of clinoptilolite used in this work, KMI on the left and BIT on the right.

It is easily to distinguish the two types of clinoptilolite by colorations. KMI clinoptilolite is a light green while BIT is a dark green.

To examine the effect of the type of water on ion exchange equilibration three types of water were used: RO, DI, and tap water. Table 3.1 summarizes the batch experiments that were carried out in this work.

Table 3.1: Batch experiments summary, for both KMI and BIT clinoptilolite.

Experiment	Concentration used, mg $N\text{-}NH_4^+$/l	Water used
Equilibration	10, 40, 70, 90, 150, 200, 500, and 1000	RO
Equilibration	40, 90, 150, and 200	DI
Equilibration	40, 90, 150, and 200	Tap
Influence of other ions	20, 80, 300, and 400	DI

To obtain the desired $N\text{-}NH_4^+$ concentration, ammonium nitrogen stock solutions were made by dissolving the required amount of ammonium chloride, NH_4Cl in water (RO, DI, or tap). For example, to make a 1000 mg $N\text{-}NH_4^+$/l stock solution, 1.909 g NH_4Cl was dissolved in 500 ml in a volumetric flask.

The ion exchange equilibration measurements were carried out by contacting 1 g of clinoptilolite and 100 ml aliquots of $N\text{-}NH_4^+$ solutions in a sealed bottle having the specified concentration in each experiment as described in Table 3.1. Each sample was gently agitated by hand 4 times per day. The ammonia concentration was measured daily for each sample. In the experiment using

RO water, as a preliminary experiment, ammonia levels were measured daily over a period of up to 9 days to examine the time required for equilibrium to be reached. The $N\text{-}NH_4^+$ concentrations in the aqueous phase at equilibrium were measured and the solid phase concentrations were determined by mass balance.

In order to examine the influence of presence of other cations that are normally present in significant concentrations in wastewater such as potassium, calcium, and magnesium on ammonium ion uptake, further experiments were conducted. These experiments were designed to determine the effect of each individual cation alone upon the ammonium ion uptake. The salts used as sources for the corresponding cations are KCl, $CaCl_2.2H_2O$, and $MgCl_2.6H_2O$. Stock solutions of these salts were made, and 40 mg/l solutions were obtained from the stock salt solutions. Respectively, 2 ml of each 40 mg/l of each cation solution was added in each 100 ml sealed bottle containing different concentrations of ammonium ions as (20, 80, 300, and 400 mg $N\text{-}NH_4^+$/l), and then the sealed bottles were continuously shaken on an orbital shaker, KS-501 IKA-WERKE, at 150 rpm.

3.2.2 Kinetics studies

The apparatus used to carry out the kinetics studies is presented in Figure 3.2.

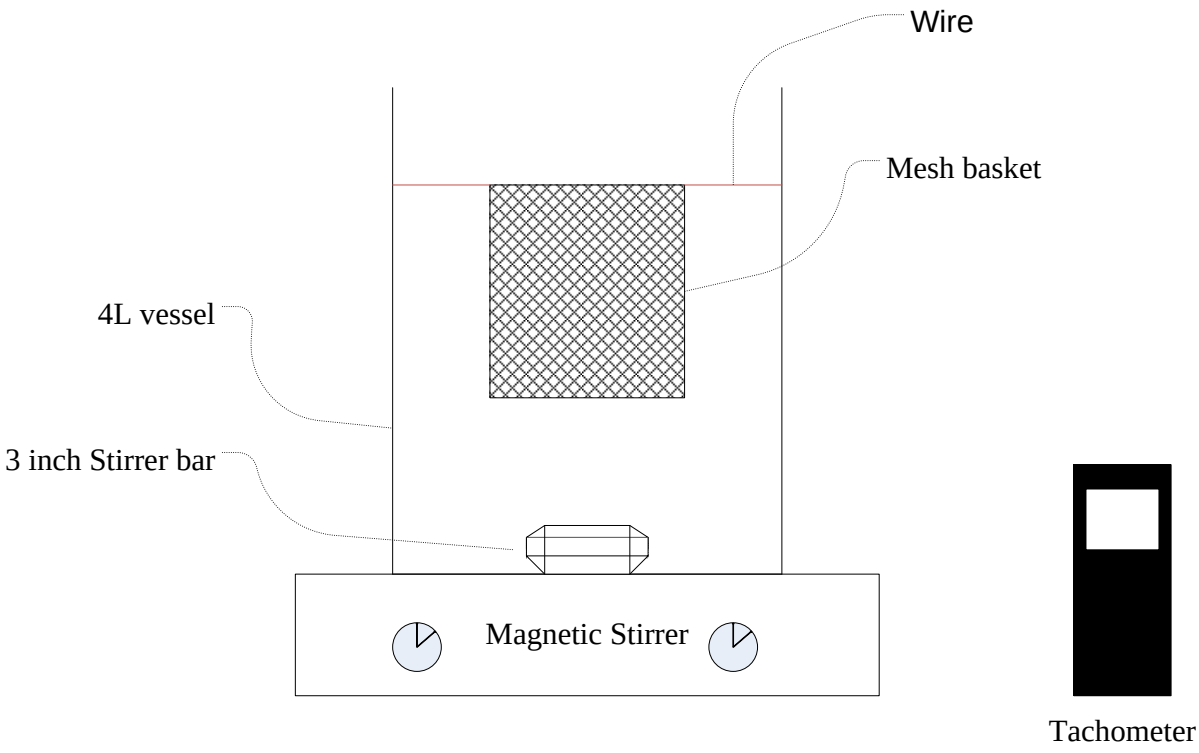

Figure 3.2: Kinetics equipment design.

The apparatus consists of 4 L glass vessel equipped with a 297 μm mesh basket which was immersed in the solution. The mesh basket was used to protect the clinoptilolite from crushing, and was connected to the vessel by a wire. The solution was stirred by a 3inch stirrer bar driven by a magnetic stirrer. The mixing speed was measured using a digital AMETEK tachometer. A red tape strip was attached to one end of the stirrer bar in order to detect the bar rotation by the tachometer. The ammonium ion solution was placed in the vessel and clinoptilolite was placed in the mesh basket. Samples of the solution were taken by a 10 ml pipet over recorded time

intervals and the ammonium ion concentration was measured according to the procedure given in section 3.3.1. Table 3.2 summaries the varying parameters studied in these experiments.

Table 3.2: Summery of kinetics studies.

	Varying parameter	Constant parameters
Part 1, C_0 is a varying parameter	150 mg/l 100 mg/l 150 mg/l	Mixing speed=1200 rpm M_{clino}= 1.5 g Particles size= 0.7-1.0 mm
Part 2, particle size is a varying parameter	0.7 - 1.0 mm 1.0 - 1.40 mm	C_0 = 50 mg/l M_{clino}= 1.5 g Mixing speed=1200 rpm
Part 3, mixing speed is a varying parameter	500 rpm 1200 rpm	C_0 = 50 mg/l M_{clino}= 1.5 g Particles size= 0.7-1.0 mm
Part 4, M_{clino} is a varying parameter	1.5 g 3.0 g 4.5 g 6.0 g	C_0 = 50 mg/l Mixing speed=1200 rpm Particles size= 0.7-1.0 mm

Different sizes of KMI clinoptilolite is introduced in Figure 3.3.

Figure 3.3: Different sizes of KMI clinoptilolite used in kinetics studies. Sizes from left to right: 0-0.7 mm. 0.7-1.0 mm, and 1.0-1.4 mm.

3.2.3 Aeration studies

The objective of the aeration studies was to examine the performance of membranes under different pressures. The apparatus used in aeration studies is presented in Figure 3.4.

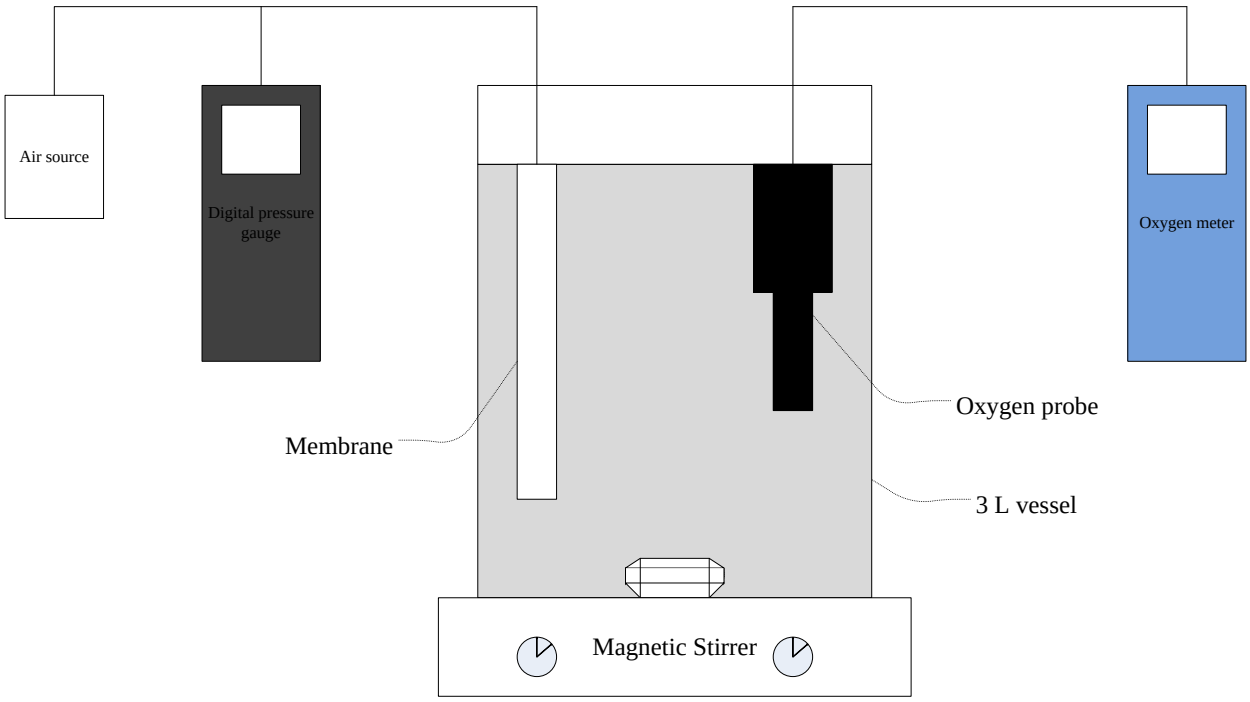

Figure 3.4: Aeration studies apparatus.

The aeration studies apparatus was constructed using the following equipment:

- 3L glass beaker as a reaction vessel;
- Sodium sulfite, Na_2SO_3;
- Compressed air cylinder, size 300, as air source;
- Air flowmeter;
- Digital manometer;
- Oxygen meter;

- Acrylic tubes as membrane module;
- Porous and non-porous membranes.

Membrane module preparation

The membrane module is a device by which a membrane flat sheet is installed in the system. The membrane modules used in this work were acrylic tubes. A total of 6 tubes was used each having a length of 15 cm and an outside diameter of 1.27 cm. One cm was left over from the top and bottom to allow a space to adhere the edges of the membranes onto the tubes. In order to let air pass through the tubes and reach to the surface of the membranes, a total of 42 equally spaced slots were made. Each slot has an area of 0.461 cm^2. Thus, the total free area of the 42 slots is 19.357 cm^2. One end of the tubes was blocked by a stopper while the other was connected to the flowmeter by a PVC tube (ID=0.635 cm). The membrane module is shown in Figure 3.4.

The membranes specifications that were used in the studies are shown in Table 3.3.

Figure 3.5: Membrane module.

Table 3.3: Membrane specifications.

	Membrane type				
Parameter	Polytetrafluoroethylene (PTFE), (or Teflon)	Polypropylene, (PP)	Polyethersulfone, (PES), (or Supor-R200)	Nylon	Silicon
Pore size (µm)	0.2	0.1	0.2	0.1	
Thickness (µm)	175	75-110	119.4-215.9		
Length (mm)	300	200	250	200	
Maximum pressure (psi)	12-23	30	20-57		
Air Flow	-	-	LPM/3.7 cm2 @ 13.5 psi		
Shape	Flat sheet	Flat sheet	Flat sheet	Flat sheet	Tube
Type	Porous	Porous	Porous	Porous	Dense
Provider (company)	STERLITECH	STERLITECH	PALL	Osmonics Inc.	Cole-Parmer

First, 2.5 L of filtered tap water were added to the 3 L glass vessel and sodium sulfite, Na_2SO_3, was then added to deoxygenate the tap water according to following Equation:

$$2Na_2SO_3 + O_2 \rightarrow 2Na_2SO_4 \quad (3.1)$$

The appropriate amount of sodium sulfite (Molecular weight = 126.1 g/mol) to deoxygenate 2.5 L tap water that has 8.5 mg/l DO can be determined using Equation 3.1as follows:

$$\frac{2 * 126.1\ \text{g}}{32.0\ \text{g}} * 8.5 \frac{\text{mg}}{\text{l}} * 2.5\ \text{l} = \ 167.5\ \text{mg}\ Na_2SO_4$$

The deoxygenation step takes time and it depends on the amount of sodium sulfite used. The DO meter was used to watch how oxygen was depleting in water. When reaching a zero concentration of dissolved oxygen, the air cylinder was used to pressurize the membrane assembly to allow oxygen to diffuse through the membrane wall to oxygenate the water. Dissolved oxygen concentration readings were then taken every 10 minutes.

SEM analysis was carried out for all membrane types in the Microscopy and Analytical Imaging Laboratory at KU following the same procedure carried out for analysis of clinoptilolite samples in Section 3.1.1.1.

3.2.4 Column studies

3.2.4.1Design of the columns

Two types of columns were used to perform the column studies. The first column, Figure 3.6, was constructed to accommodate the silicon membrane module. A cross-sectional view of this column is outlined in Figure 3.7. The second column was designed on the basis of the first column, and was introduced to operate the porous membrane modules. The second column is presented in Figure 3.8 and the cross-sectional view in Figure 3.9. The design of these columns was informed by previous experiments done by Miladinovic and Weatherley [58], Jorgenson and Weatherley [98], and McVeigh and Weatherley [3]. Membranes used in these studies have the specifications outlined in Table 3.3.

Both columns were designed to enhance the aeration within the clinoptilolite bed so that the nitrification process can proceed without being limited by the oxygen concentration. The silicon membrane's permeability was 7961×10^{10} cm^3 sec^{-1} cm^{-2} cmHg. The internal and external silicon tube diameters were 1.8 and 2.1 mm respectively, and it was curled around 35 cm module. Two

tubes were assembled in the silicon membrane column. Modules were clipped on both ends of the column. The air outlet is sealed with a metal clip to force air to diffuse through the membrane.

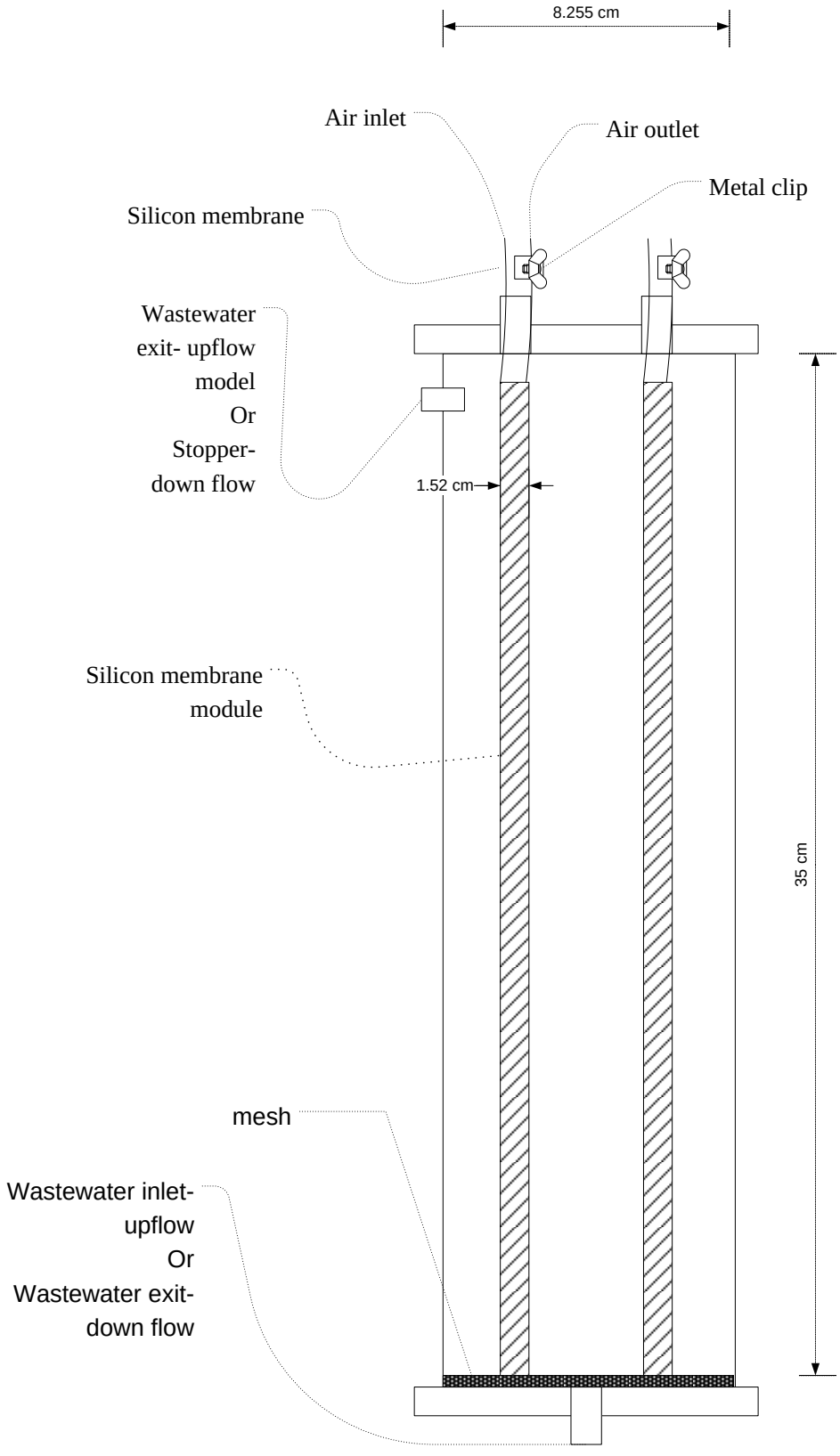

Figure 3.6: Silicon membrane module column.

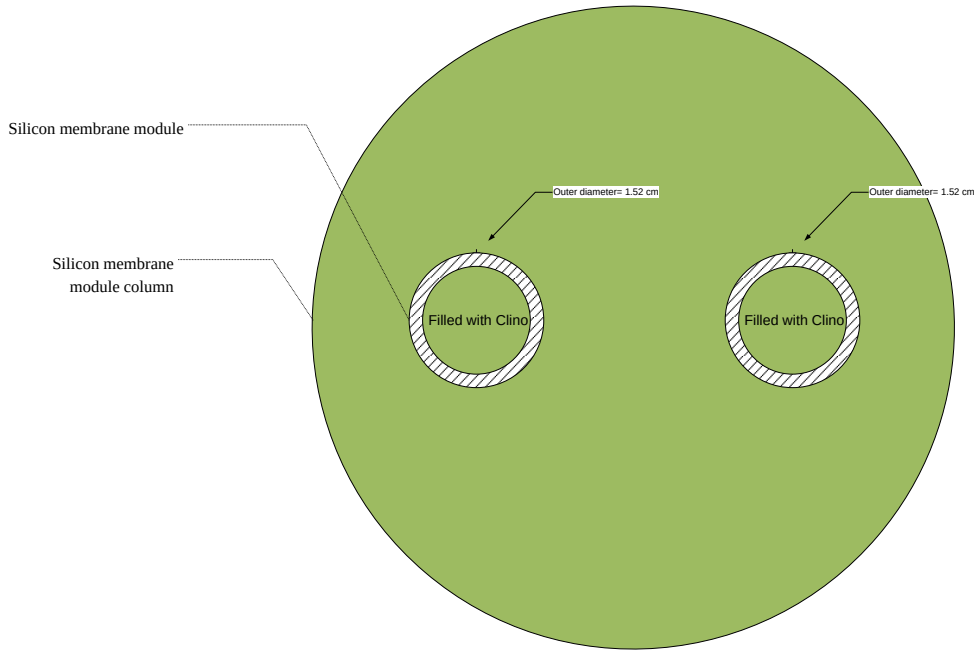

Figure 3.7: Cross-sectional view of silicon membrane module column. Clinoptilolite was filled inside and outside the membrane module.

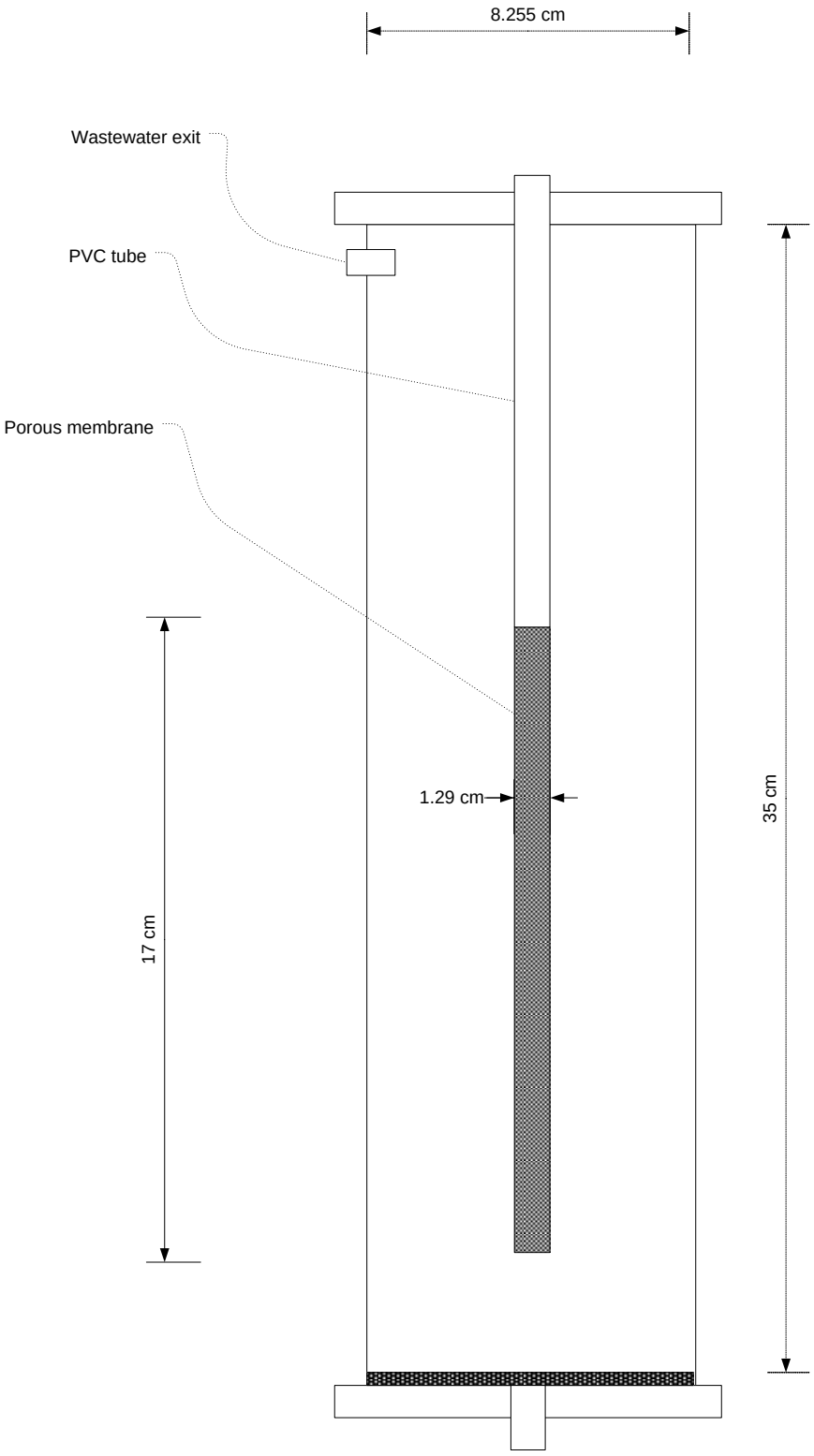

Figure 3.8: Porous membrane module column.

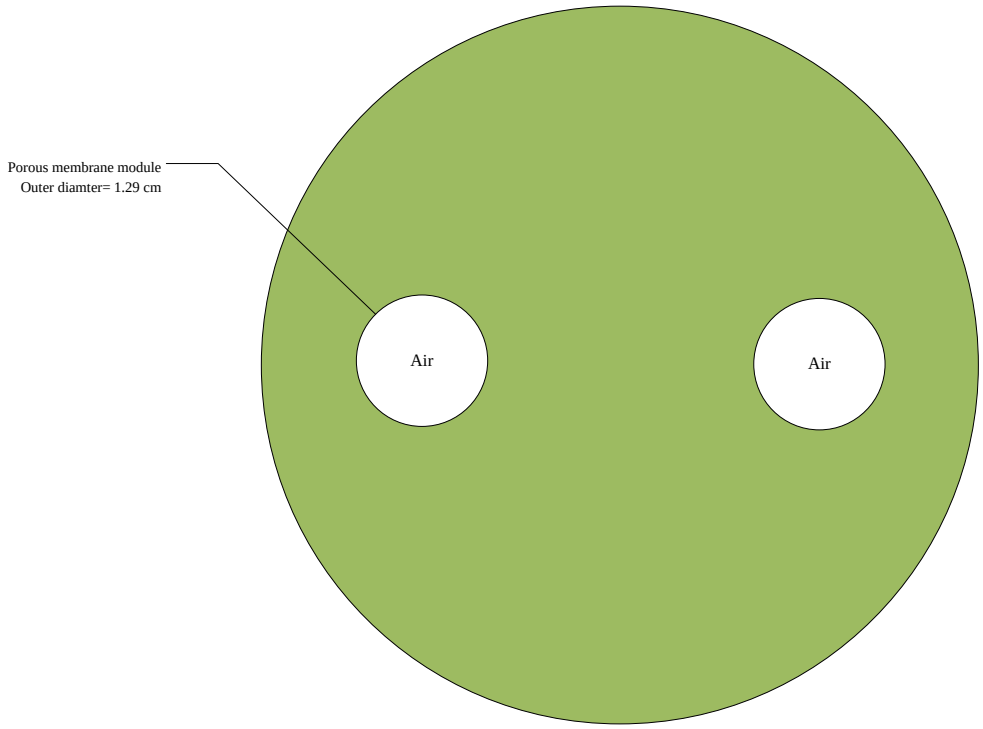

Figure 3.9: Cross-sectional view of silicon membrane module column. Clinoptilolite was filled outside the membrane module while air is pressurized inside the module.

Columns were built into a lab scale plant design, and a maximum of four columns were operated at the same time. Columns were operated under down-flow and up-flow conditions. In the down-flow condition, Figure 3.10, columns were operated based on a constant head principle. The flow rate was maintained constant by keeping the head in the feed tanks constant. Rotameters were used to adjust the inlet flow. Separate tests were carried out to find out the appropriate float height associated with the designed flowrate. It was found that when the float was at 36 mm the flowrate was 22 L/hr. In the up-flow condition, Figure 3.11, peristaltic pumps, Watson-Marlow pumps, were used to maintain the flowrates as designed. Calibration measurements for the pumps across a range of flowrates were made before each experimental set.

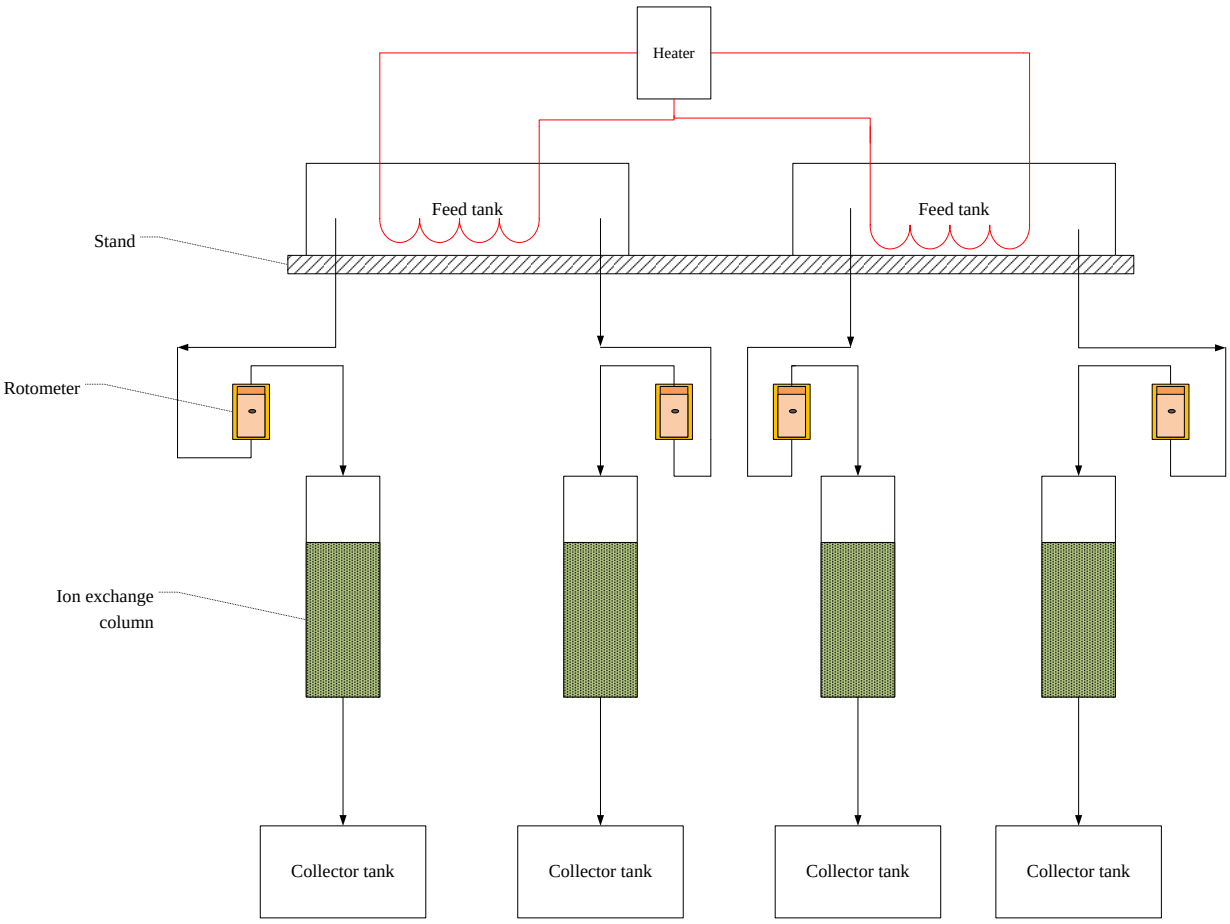

Figure 3.10: Down-flow condition. Air was supplied into the column by air cylinder.

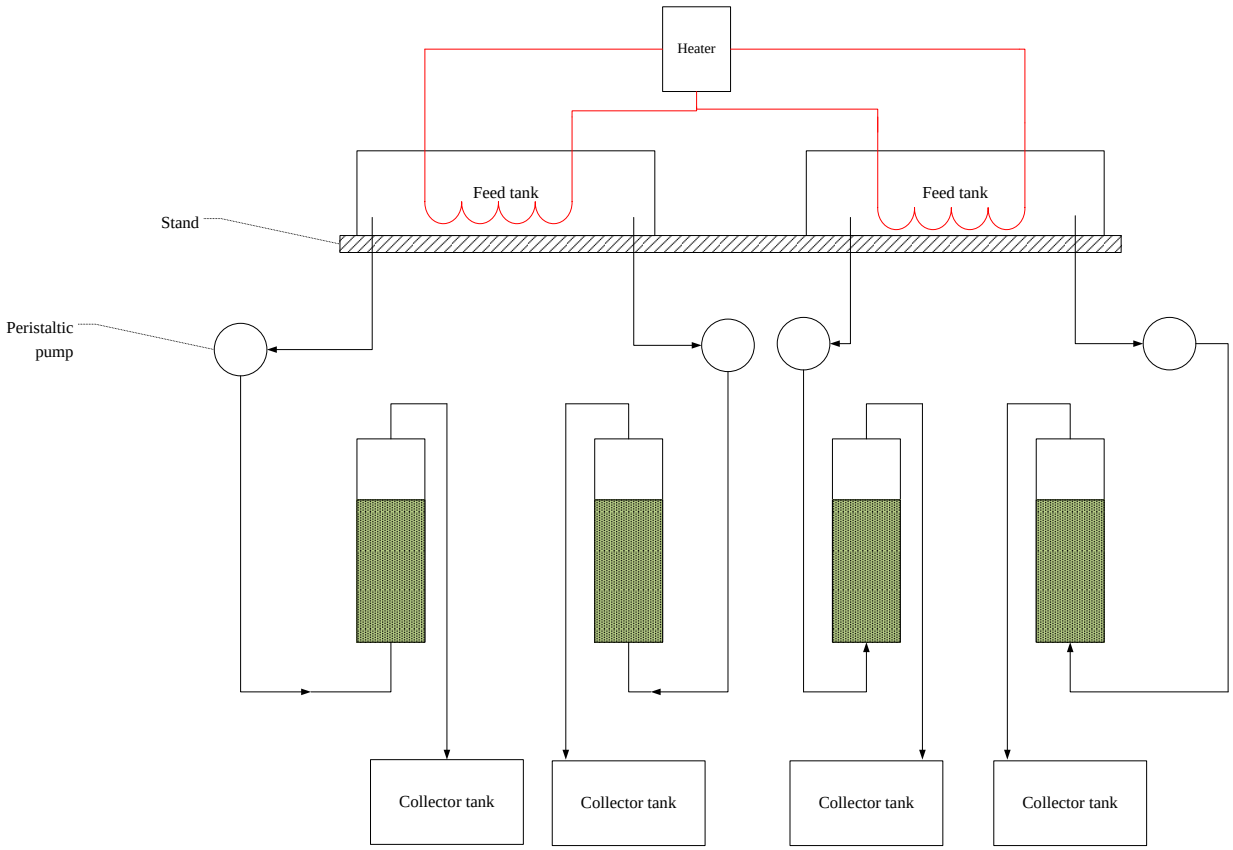

Figure 3.11: Up-flow condition. Air was supplied by air cylinder, and it depends on the column design.

A photo of a porous membrane column with an up-flow condition is shown in image 3.12.

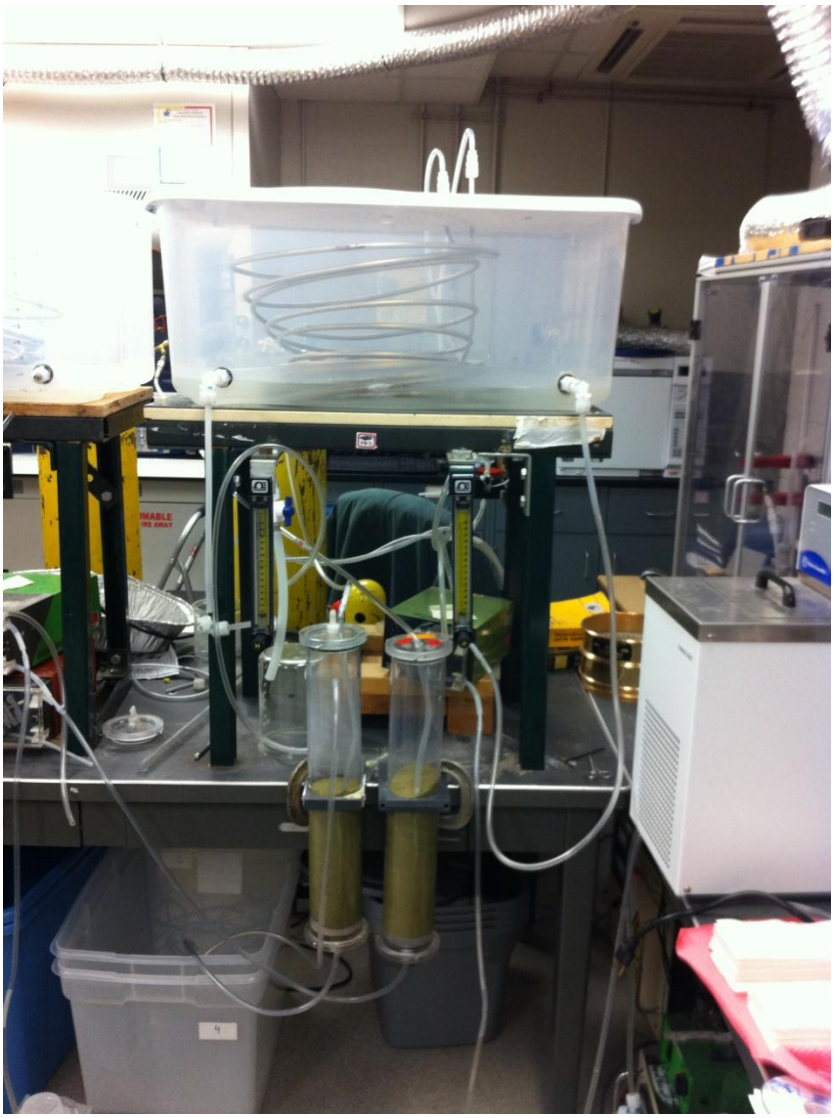

Figure 3.12: A column runs with an up-flow condition, porous membrane column design.

3.2.4.2 Service procedure

Although the used clinoptilolite came with the required particle size, 0.42-1.41 mm, further sieving was carried out using a sieve shaker, RX-29 W.S. TYLER – Geology department at KU. Prior to use, clinoptilolite was pretreated as outlined in section 3.1.2. The height of the bed was either 27 cm or 32 cm. The bed volume varied according to the variations in the bed height and the variation in the column design. The term “Bed Volume” (BV) in this study always refers to

the volume of the empty column, i.e., without packed clinoptilolite. Table 3.4 summarizes the BV used in this work. The desired flowrate was maintained in the down-flow condition by the constant head approach. The purpose of this approach is to supply the columns with a high flowrate, 14 BV/hr (22 L/hr). The up-flow condition was also used as it was expected to minimize channeling.

Table 3.4: BV variations used in this work.

Column design	Bed height, h (cm)	BV
Silicon membrane column	32	1.605 L
	27	1.355 L
Porous membrane column	27	1.455 L

To prevent air bubbles being trapped within the column, dry clinoptilolite was added to the column and the column was isolated from its inlet and outlet, then, the bed was washed with DI water several times and the column was reconnected to the inlet/outlet. The water used was tap water filtered in a commercial PUR 3-stage faucet filter. The synthetic wastewater was made up and stored in a 120 L reservoir tank, and solution concentration was measured before use. Solution was lifted up to the feed tank using a VESTIL hand winch lift truck. The feed tanks were 90 L capacity. The solution inside the feed tanks was kept at 30 ºC by using a bath circulator (Isotemp 3016p, Fisher Scientific). The solution was fed to the column and was contacted with the clinoptilolite bed. The effluent solution was accumulated in the collector tank. The collector tanks were graduated receiving tanks with a 4 L volume interval. After a specified

time interval, the effluent solution was sampled and measured for ammonium ion concentration, oxygen concentration, pH, and nitrite concentration. The analytical section provides how these parameters were measured. Experiments on biologically active clinoptilolite followed the same procedure but with aeration present.

3.2.4.3 Bacteria immobilization

One of the challenges facing the combination of ion exchange and nitrification as a combined method is establishing the growth of the biofilm on the ion exchange material without losing too much of its adsorption capacity. The adsorption method was chosen to immobilize bacteria on clinoptilolite bed. This method was used previously by Miladinovic and Weatherley [58] and McVeigh and Weatherley [3], and it was reported as an effective method when oxygen was adequately supplied to the packed column. 50 ml of bacteria rich solution was added to 2 L of low ammonium ion solution (0.5 mg N-NH_4^+/l), and the combined active solution was manually introduced to the packed bed column in the presence of aeration. Approximately, after 4 hours the effluent was re-fed to the column. This procedure lasted for 24 hours. The biomass concentration was measured, as explained in section 3.3.6, before and after bacteria were introduced to the column in order to determine how much bacteria was bound to the clinoptilolite bed. Since Nitrosomonas europea is very sensitive to light, the biologically active column was coated with aluminum foil during the experiment. For the silicon tube column, air was pressurized at 25 psi. For the porous membrane column, pressure gauge was kept at 1.5 psi.

3.2.4.4 Bacteria inoculation

The bacteria used in this work (ATCC 19718) were obtained from the American Type Culture Collection (ATCC). The medium by which the bacteria were cultured was made as follows:

Step 1: 900 ml DI water was added to 2 L Erlenmeyer flask and the following materials were added in sequence:

- 3.3 g $(NH_4)_2SO_4$ (50mM)
- 0.41 g KH_2PO_4
- 0.75 ml 1 M $MgSO_4$
- 0.2 ml 1 M $CaCl_2$
- 0.33 ml 30 mM $FeSO_4$/50 mM EDTA
- 0.01 ml 50 mM $CuSO_4$

The flask was then sterilized using an autoclave.

Step 2: 400 ml of DI water was added in a 500 ml baker, then, the following materials were added:

- 27.22 g KH_2PO_4
- 2.4 g NaH_2PO_4

pH was adjusted to 8.0 with 10 N NaOH, and the final volume was brought to a final volume of 500 ml with DI water. The solution was transferred to a 500 bottle and was sterilized.

Step 3: 500 ml of 5 % (w/v) Na_2CO_3 was prepared and sterilized.

To prepare a 1 L of inoculum, the following steps were made:

- 100 ml of solution prepared in Step 2 was added to the flask prepared in Step 1.
- 8 ml of the solution made in Step 3 was added to the flask prepared in Step 1.
- 10 ml of 3-day old culture was added to the flask prepared in Step 1, and incubate it on a rotary shaker (@150 rpm) at 30 ºC.

After 7 days of incubation, the culture was centrifuged in a SORVAL Evolution centrifuge at 5000 RCF (relative centrifugal force) for 20 minutes. The biomass was added to 50 ml DI water and either stored or used. This 50 ml of biomass is what is referred previously as a bacteria rich solution.

3.2.5 Bioregeneration column

In this part, the regeneration of exhausted clinoptilolite by nitrifying bacteria is examined. The column was uploaded with exhausted KMI clinoptilolite, and a 50 ml of rich bacteria solution added to 3 L of media solution and the combined solution circulated through the column. Over fixed time intervals, samples were taken and analyzed for nitrite. Based on the performance of membranes in aeration studies and porous membrane columns, the two membranes with the highest performance were selected to enhance aeration inside the bioregeneration columns. The bioregeneration column setup is shown in Figure 3.13. Preparing media solution and taking nitrite measurement were/are explained in Section 3.2.4.4 and 3.3.2 respectively. After few days, the column was stopped and samples from different height of the column (5, 10, 15, 20, and 27cm) were taken and equilibrated with 100 ml of ammonium ion solution (20 mg $N\text{-}NH_4^+$/l) exactly as explained previously in Section 3.2.1.

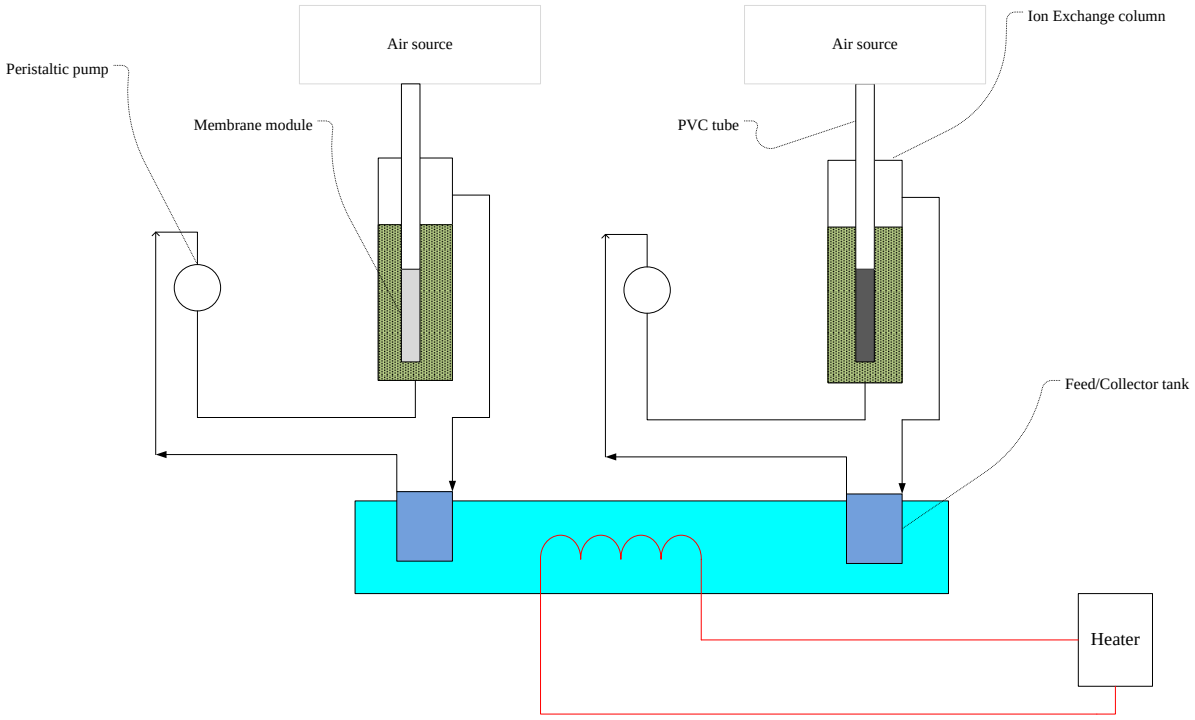

Figure 3.13: Bioregeneration column setup.

3.3 Analytical methods

3.3.1 Ammonia measurements

Ammonium ion concentration measurements were carried out using a Thermo Scientific Orion ISE *meter* 4-Star along with a Thermo Scientific Orion ammonium ion selective *electrode* (No. 9512BNWP). Figure 3.12 shows the general assembly of an ion selective electrode (ISE).

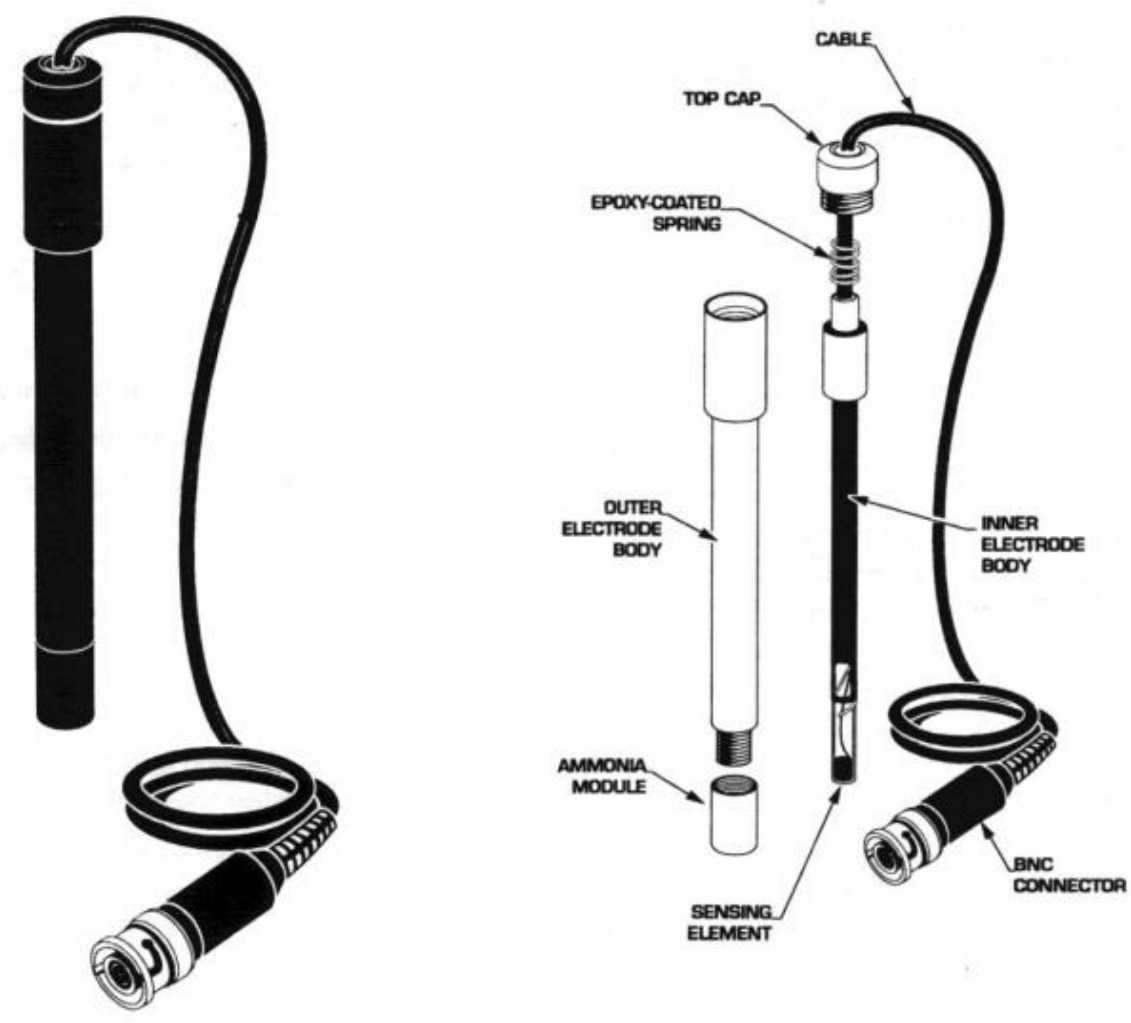

Figure 3.12: Ammonium ion selective electrode [5]

The inner body of the electrode was filled with ammonia electrode filling solution (Orion 951202), and the ammonia selective membrane (Orion 951204) was attached to the cap of the

electrode. The ammonium ion sample is measured in a 20 ml disposable scintillation vial. A pH buffer (ISA Orion 951211) added to the sample in a ratio 50:1.The principle of operation can now be described.

The ammonia membrane is a PVC hydrophobic membrane containing an ammonium carrier with a high selectivity towards ammonium ions. When ammonium ions, in the sample, are in contact with the membrane these ions diffuse from the sample solution into the internal filling solution, and an electrode potential is established against reference potential, and then ammonium ion concentration can be calculated by the Nernst equation [3, 5]:

$$E = E^0 + \left(\frac{RT}{zF} \ln a_{NH_4^+}\right) \qquad (3.2)$$

where E is the electrode potential in volt, E^0 is the standard or reference potential in volt, R is the universal gas constant (=8.314 J/K/mol), T is the temperature in ^oK, z is the valence of ammonium ion (=+1), F is the Faraday's constant (=96485 Coulombs/mol), and a is the ammonium ion activity as described in Equation 2.1.

In order to maintain precise measurements, the electrode was calibrated on a daily basis using a three point calibration that brackets the range to the expected sample concentrations. The calibration is performed using the lowest concentration standard working up to the highest concentration standard. To prevent any contamination, the electrode is washed before and after measuring the sample with DI water and dried with a lint-free tissue. All solutions, including calibration solutions, were made from ammonium chloride (NH_4Cl) assuming that 100% of ammonia dissolved was in the cationic form. A sample calculation below describes how the preparation a 1000 mg/l NH_4^+ as N was undertaken:

$$\frac{1000\ mg\ NH_4^+ as\ N}{L} * \frac{53.4915\ g\ NH_4Cl}{mol} * \frac{mol}{14.0067\ g\ NH_4^+\ as\ N} = 3819\frac{mg\ NH_4Cl}{L}$$

$$= 3.819\frac{g\ NH_4Cl}{L}$$

➔ 3.819 g of NH_4Cl was dissolved in a liter of DI water giving a solution with a concentration 1000 mg/l NH_4^+ as *N*.

3.3.2 Nitrite measurement

Nitrite (NO_2^-) was accurately determined using a UV-visible spectrophotometer following the procedure given in Simplified Procedures for Water Examination [148]. In order to establish a photometric calibration curve, a color reagent was prepared by adding 100 ml of an 85 % phosphoric acid (H_3PO_4) solution and 10 g sulfanilamide ($C_6H_8N_2S$) to 800 ml DI water. After the sulfanilamide dissolved completely, 1 g of NED dihyrdochloride was added, and the solution diluted to 1L. Standard nitrite solution was prepared by adding 1.232 g sodium nitrite ($NaNO_2$) to 1 L DI water, and diluted to the required concentrations. After removing any suspended solids by filtering through a 0.45-µm diameter pore membrane filter, the pH must be adjusted to the range of 5 to 9 with 1N hydrochloric acid (HCl) or 1N ammonium hydroxide (NH_4OH) as needed. To develop the color of the sample or standard, 2 ml color reagent was added to a 50 ml portion of sample. For different known concentrations, the absorbance was measured at 543 nm. The calibration curve was obtained by plotting the absorbance of nitrite standards against the concentration of each, and documented in Appendix I. The calculations of uncertainty of the calibration curve are given in Appendix II.

3.3.3 Oxygen measurement

Dissolved oxygen concentrations were determined by using an oxygen probe/meter, DO200, (Yellow Spring Instruments), with a built-in temperature probe for automatic temperature compensation. This probe model uses a polarographic electrode with convenient screw-on cap membranes. Before use, the probe was calibrated at 100% water-saturated air environment. This was done by calibrating the probe in the bottle that the probe is stored in.

3.3.4 pH measurement

Determination of pH was carried out by using either an Orion 4 Star pH meter along with Gel-Filled pH electrode or an OAKTON pH tester 30. Both meters have a built-in temperature probe. Both meters were calibrated using Thermo Scientific buffer solutions pH=4.01, pH=7.00, and pH=10.01.

3.3.5 Conductivity measurement

Conductivity was measured to check the presence of sodium hydroxide in the solution, and it was measured by an Orion 4 Star conductivity meter along with an Orion conductivity electrode (DuraProbe conductivity Cells 013005MD) which was calibrated by using 100 µS/cm and 1413 µS/cm Orion conductivity standards.

3.3.6 Protein measurement

Protein measurements were carried out using either a UV-visible spectrophotometer or a NanoDrop 1000 (Thermo Scientific). The samples were measured at OD600 nm (OD=optical density).

3.3.7 Temperature measurement

When needed, the temperature can be determined by using one of the meters described previously or for a quick measurement a Traceable® thermometer was used.

4 Results and Discussion

4.1 Ion exchanger analysis

4.1.1 Electron microscopy

Scanning electron microscope (SEM) pictures of KMI and BIT clinoptilolite used in this work are given in Figure 4.1 and Figure 4.2 respectively. For better comparison, both photos were taken with the same magnification (12.10 k). Clinoptilolite's structure can be seen easily for KMI, and may be more difficult for BIT. The pores are shown in the SEM photos and are noticeable. However, by comparing Figure 4.1 and Figure 4.2 it seems that BIT clinoptilolite is more porous than KMI clinoptilolite.

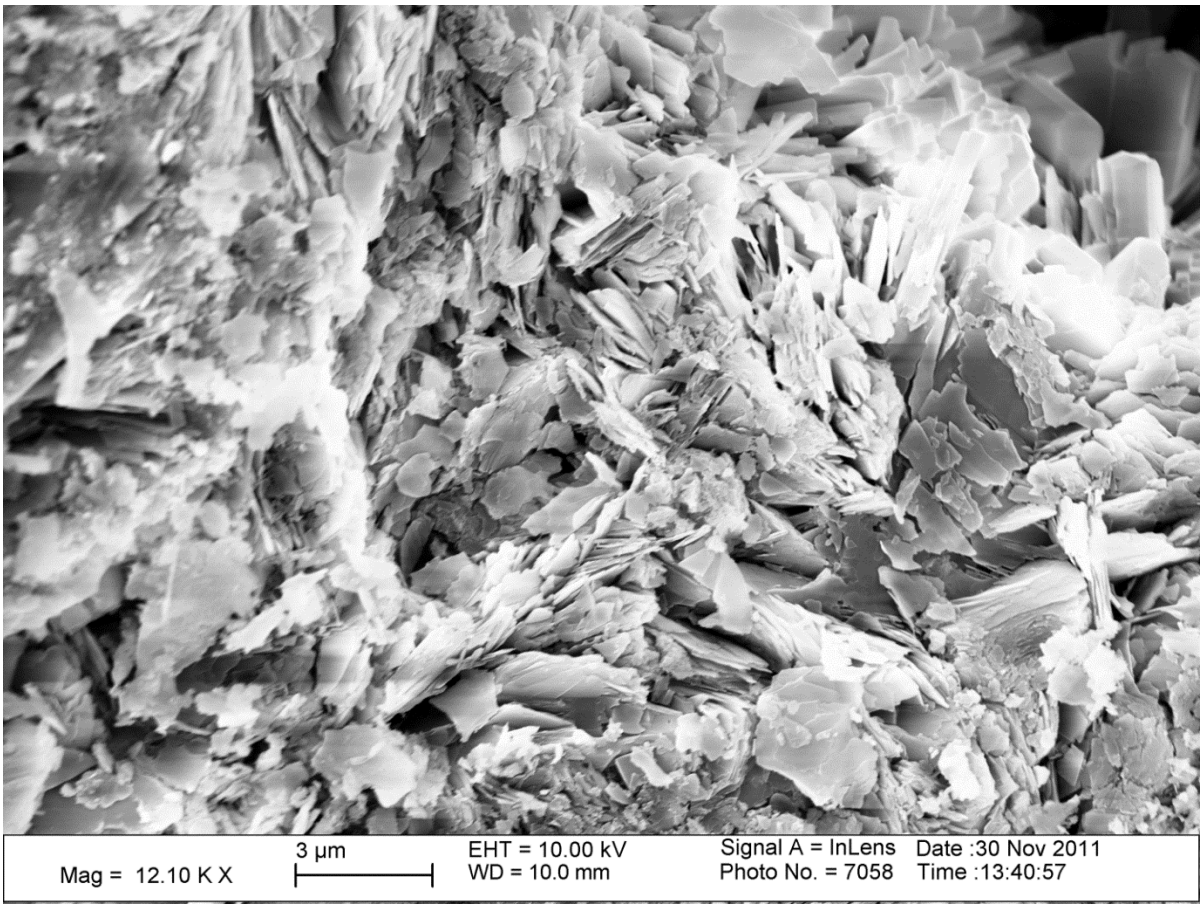

Figure 4.1: Surface photographs of KMI.

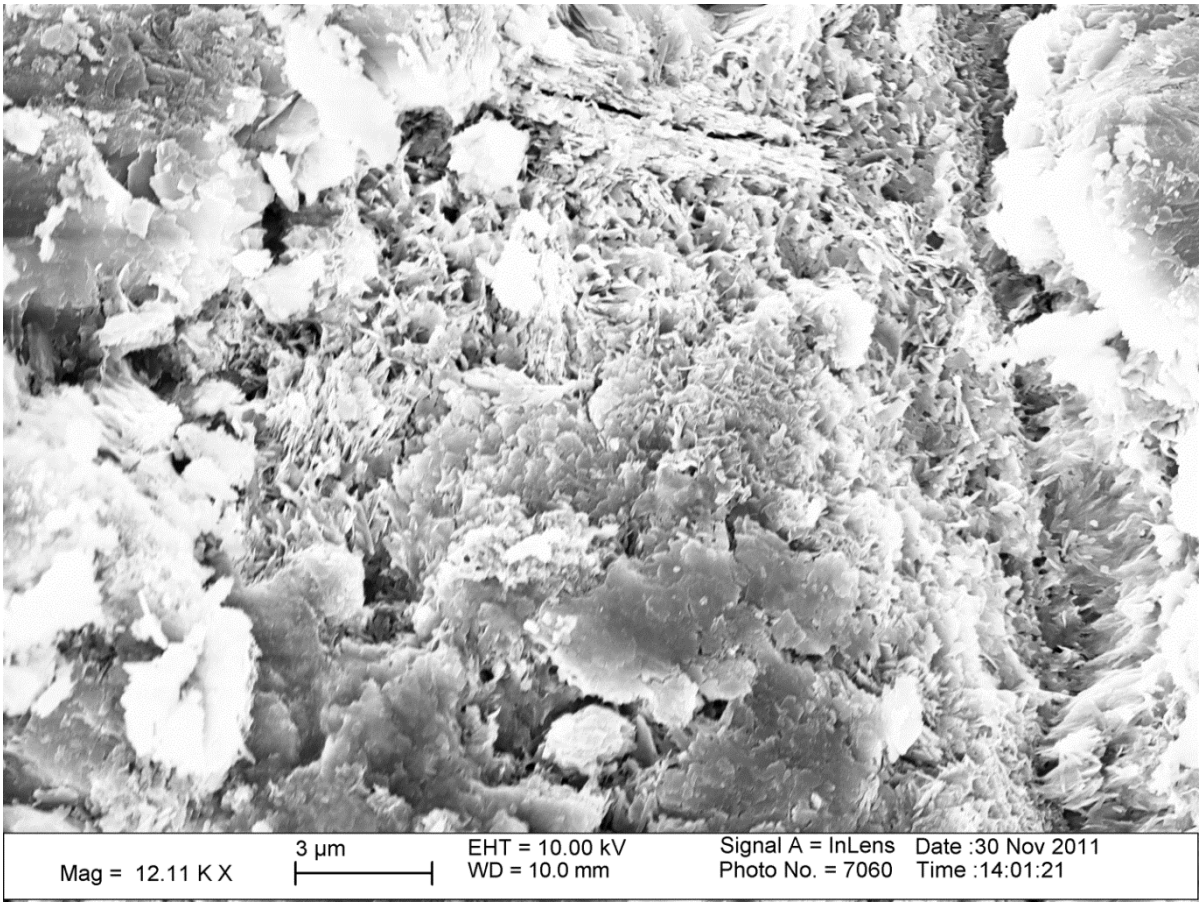

Figure 4.2: Surface photographs of BIT.

The macrospores and microporous of BIT are detected in Figure 4.2.

4.1.2 XRF analysis

Clinoptilolite is a naturally occurring ion exchanger and is likely to be of variable composition. Clinoptilolite samples were analyzed for chemical composition using X-Ray Fluorescence spectrophotometer (XRF) which can quantify the main chemical within a solid compound. The chemical composition of KMI and BIT clinoptilolite used in this work are presented in Table 4.1. XRF analysis of Hector clinoptilolite (California) and New Zealand are also presented in Table 4.1 for comparison. The Si/Al ratio is calculated and documented for all clinoptilolite types. The Si/Al ratios reported in the literature, range from 4.5 to 5.5 [4]. The Si/Al ratio of KMI and BIT

clinoptilolite is 5.13 and 5.62 respectively. Si/Al ratios of KMI lays in the middle of the range, while Si/Al ratio of BIT lays in the upper limit of the range. Both KMI and BIT Si/Al ratio is higher than the New Zealand clinoptilolite used by Miladinovic and Weatherley [58] which is 4.78. The more aluminum present in the clinoptilolite, the more cations are needed to neutralize the negative charge, hence; high capacity is expected. So, KMI clinoptilolite capacity is expected to be lower than the capacity of the New Zealand clinoptilolite and higher than the BIT clinoptilolite capacity. As expected, Na, K, Mg, and Ca are present along with other trace elements within KMI and BIT clinoptilolite. BIT clinoptilolite contains relatively large amounts of potassium.

Table 4.1: Chemical composition of clinoptilolite used in this research and that of Hector deposit.

Weight % (Normalized to 100 %)	KMI	BIT	Hector deposit (California) [26]	New Zealand [4]
SiO_2	75.61	76.99	71.01	70.75
Al_2O_3	13.01	12.11	12.09	13.04
Fe_2O_3	1.02	1.94	1.05	2.08
CaO	1.50	2.55	3.85	1.93
MgO	0.30	0.51	0.54	0.41
Na_2O	4.49	0.67	6.09	1.83
K_2O	3.88	4.79	1.70	3.64
MnO	0.028	0.01	0.02	0.14
TiO_2	0.15	0.11	0.41	0.18
P_2O_5	-	0.11	0.00	0.04
Si/Al	5.13	5.62	5.19	4.78

4.1.3 EDS analysis

The EDS analysis results of KMI and BIT clinoptilolite are presented in Figure 4.3, Figure 4.4, and Table 4.2.

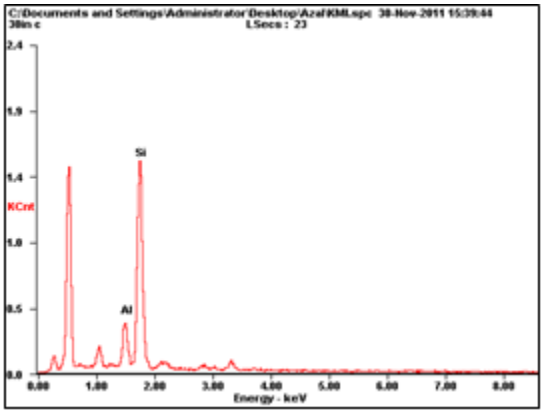

Figure 4.3: EDS analysis of KMI clinoptilolite.

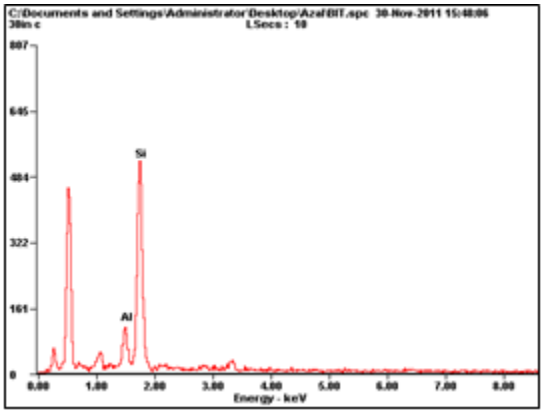

Figure 4.4: EDS analysis of BIT clinoptilolite.

Table 4.2: Composition of Si and Al in KMI and BIT clinoptilolite obtained by EDS analysis.

Element	KMI		BIT	
	wt %	At%	wt %	At%
Si	84.60	84.07	85.89	85.40
Al	15.4	15.93	14.11	14.60
Si/Al	5.49	5.27	6.08	5.85

Although the weight percentages of both Si and Al in both KMI and BIT clinoptilolite given in Table 4.2 does not agree with the values given in Table 4.1, both Tables agree that the Si/Al of BIT is higher than that of KMI.

4.1.4 Surface area and pore size measurements

Surface area and pore size analysis are given in Table 4.3.

Table 4.3: Surface properties and density of KMI and BIT clinoptilolite that used in this work (Data was obtained by the Mineral Lab Inc.)

	KMI	BIT
Bulk density (g/cm^3)	1.394	0.96
Surface area (BET, m^2/g)	40	25
Pore volume (%)	15	-
Pore radius (Å)	3.5	-
Specific gravity	1.89	2.0-2.4

KMI possesses a higher surface area than BIT but both are still low compared to the documented surface area of clinoptilolite from other parts of the world which is typically within the range

172-340 m^2/g [3, 114]. The reported surface area of New Zealand zeolite is similar to that of KMI which is 40 m^2/g [114]. This variation in surface properties is expected as the structure and the surface area properties vary among the same type of zeolite that mined from different deposits [3]. KMI has a mean pore radius of 3.5 Å which is greater than that of the New Zealand clinoptilolite which has a mean pore radius of 2.09 Å [4]. A comparison between the tabulated density values for both samples might support the finding by the SEM analysis which is that the BIT is more porous than KMI.

4.2 Batch equilibrium studies

4.2.1 The uptake capacity

The terms ammonia and ammonium ion are used interchangeably in chapter 4. The theoretical information and background on ion exchange capacity are given in section 1.4.3, while recent studies regarding clinoptilolite's capacity are outlined in section 2.2.2. As discussed earlier, there are several approaches to define the capacity of ion exchange. Here, in this work, the capacity is defined as the number of millimoles of counter ion equivalent per gram of clinoptilolite [3, 58]. Ammonia concentration, either in the solution or in the solid material, is always given in mg N-NH_4^+. The experimental studies in this part were performed following the procedure given in section 3.2.1, and the scope of these studies was designed to quantify the equilibrium uptake behavior of ammonium ion onto KMI and BIT clinoptilolite. It was assumed that all the ammonium ions in the liquid solution were exchanged with Na^+ ions onto clinoptilolite. Literature indicates that equilibrium can be reached within 3 to 4 days for clinoptilolite [58, 98]. The equilibration studies were done using RO, DI, and tap water. The resistivity of RO and DI water were greater than 0.05 and 18 μΩ.cm respectively. The total dissolved solids present in the

tap water (before pass the commercial filter) ranged from 140 to 490 ppm [149]. The reduction of ammonia concentration from the solution containing different ammonium ion concentration for KMI and BIT using RO water is shown in Figure 4.5 and Figure 4.6 respectively.

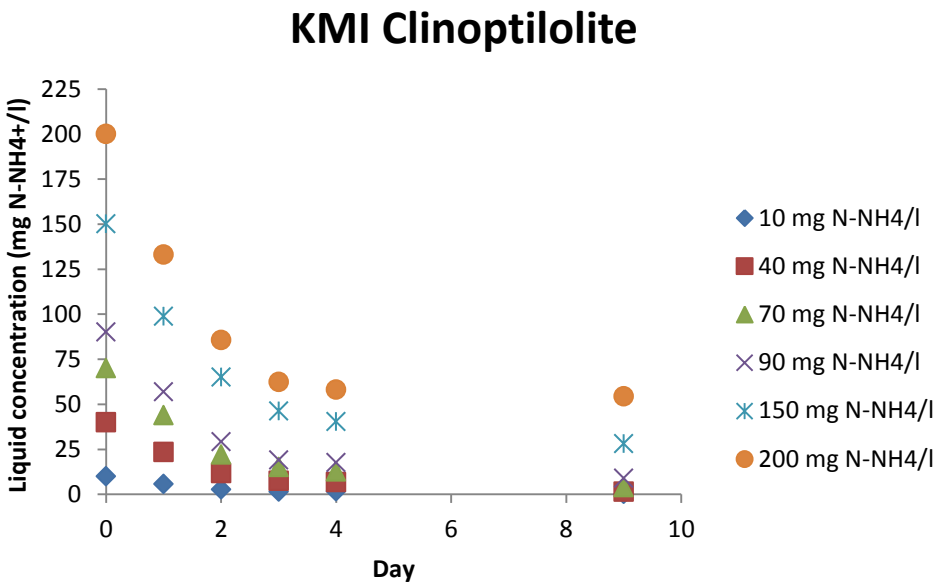

Figure 4.5: Reduction of ammonia concentration over time for different initial ammonia concentrations in 100 ml of solution and 1.0 g of KMI clinoptilolite (T= 23 ºC, particle size 0.42 mm- 1.41 mm, RO water).

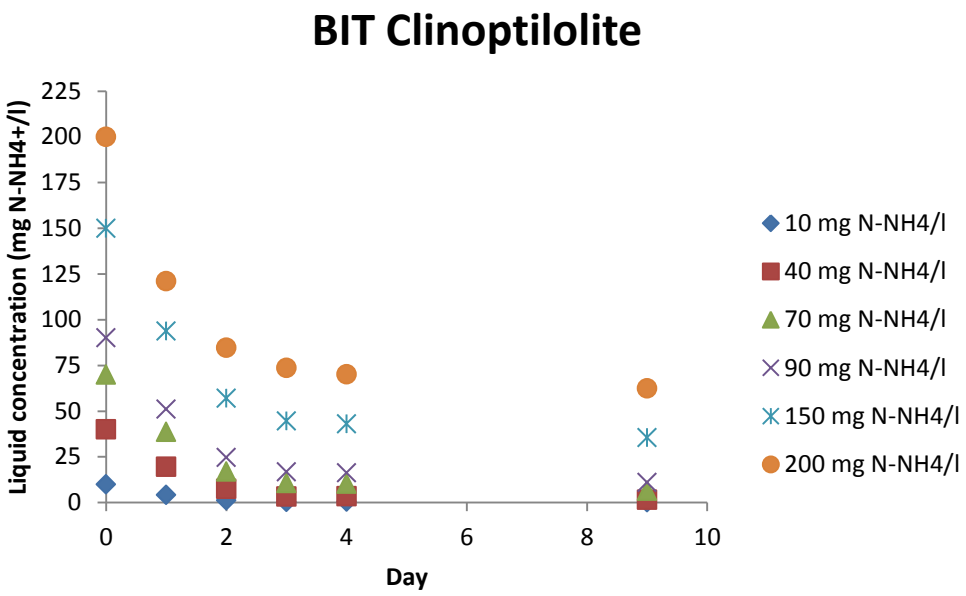

Figure 4.6: Reduction of ammonia concentration over time for different initial ammonia concentrations in 100 ml of solution and 1.0 g of BIT clinoptilolite (T= 23 ºC, particle size 0.42 mm- 1.41 mm, RO water).

From the previous figures, it is clear that the KMI and BIT achieve equilibrium after 4 days of contacting the solution with the material. This result agrees with the equilibrium period Jorgenson and Weatherley [5] found when contacting ammonium ions with clinoptilolite. They only agitated samples by hand four times per day whereas Miladinovic and Weatherley [58] placing the samples on an orbital shaker, and found that it took 3 days for clinoptilolite to reach equilibrium. Clearly, continuous shaking of samples has improved the uptake kinetics.

By performing a mass balance on the ammonium ions, the uptake capacity was calculated. The uptake capacities, solid concentrations, and percentages of ammonia removal after 9 days contact of KMI and BIT are presented in Table 4.4 and Table 4.5.

Table 4.4: The uptake data for ammonium ion onto KMI after 9 days contact.

Initial Ammonium Concentration (mg $N\text{-}NH_4^+$ /l)	KMI Capacity (meq/g)	Q_e, solid concentration, mg $N\text{-}NH_4^+$/g clino	Percentage of removed ammonia
10	0.071	0.99	99.02
40	0.281	3.93	98.30
70	0.485	6.79	96.97
90	0.617	8.64	95.96
150	0.984	13.78	91.84
200	1.257	17.60	88.00

The solid phase concentrations, over the entire work, are based on dry weight of zeolite.

Table 4.5: The uptake data for ammonium ion onto BIT after 9 days contact.

Initial Ammonium Concentration ($N\text{-}NH_4^+$ mg/l)	BIT Uptake capacity (meq/g)	Q_e, solid concentration, mg $N\text{-}NH_4^+$/g clino	Percentage of removed ammonia
10	0.071	0.99598	99.59
40	0.279	3.9088	97.72
70	0.473	6.619	94.56
90	0.596	8.346	92.73
150	0.927	12.984	86.56
200	1.191	16.676	83.38

At low to moderate concentration, 10-90 mg $N\text{-}NH_4^+$ /l, ammonium ions were removed at a high percentage. Above 150 mg $N\text{-}NH_4^+$ /l, the removal percentage decreases significantly. For all concentration levels, KMI exhibited high capacity comparing to BIT and more significantly at 150 and 200 mg $N\text{-}NH_4^+$ /l, where the uptake capacity percentage difference is calculated as 5.8 and 5.3 % respectively. This is expected since BIT clinoptilolite has a higher Si/Al ratio than KMI clinoptilolite, and as a result KMI is expected to have more counter ions ready for exchange. Comparing to previous published results, Miladinovic and Weatherley [58] tested the uptake of New Zealand clinoptilolite whose composition is shown in Table 4.1. For the same

concentration levels, the uptake capacities were 0.07, 0.26, 0.42, 0.49, 0.62, and 0.66 meq/g. They used the same ratio of mass of exchanger to the volume of solution phase, 0.5 g per 50 ml, as the current work, 1 g per 100 ml. For this work, 1 g per 100 ml was chosen for the long period sampling which lasted for 9 days. KMI and BIT reveal higher uptake capacity than the New Zealand clinoptilolite. In fact, KMI and BIT uptake capacities are double that of New Zealand clinoptilolite at the reported levels of concentrations. Jorgenson and Weatherley [5] examined ammonium ion uptake onto Hector clinoptilolite and reported a higher uptake capacity of 1.30 meq/g (obtained from a graph in their work) at initial ammonium concentration of 200 mg N-NH_4^+ /l. Vassileva and Voikova [106] used natural and pretreated Bulgarian clinoptilolite (Si/Al = 5.60), and they reported the uptake capacity as 0.88 and 1.31 meq/g respectively. A possible explanation of high uptake capacity of KMI, BIT, and Hector clinoptilolite comparing to New Zealand and natural Bulgarian clinoptilolite is that those three types of clinoptilolite are commercial market product and thus; they are probably pre-screened and pre-treated with the inert components being removed in order to achieve an optimal performance [4].

At this point, the performance of KMI and BIT are quite promising; therefore, testing these materials at high concentration is required to draw comprehensive conclusion on how these material works at high concentrations. Therefore; Materials were tested at 500 and 1000 mg N-NH_4^+ /l. The results are introduced in Table 4.6 and Table 4.7 for KMI and BIT respectively.

Table 4.6: The uptake data for ammonium ion onto KMI at high concentration.

RO water: Initial Ammonium Concentration (mg $N\text{-}NH_4^+$ /l)	KMI Capacity (meq/g)	Q_e, solid concentration, mg $N\text{-}NH_4^+$/g clino	Percentage of removed ammonia
500	2.62	36.65	73.3
1000	4.66	65.25	65.25

Table 4.7: The uptake data for ammonium ion onto BIT at high concentration.

RO water: Initial Ammonium Concentration (mg $N\text{-}NH_4^+$ /l)	BIT Capacity (meq/g)	Q_e, solid concentration, mg $N\text{-}NH_4^+$/g clino	Percentage of removed ammonia
500	2.47	34.55	69.10
1000	4.42	61.90	61.9

Although both types show high uptake capacity, KMI still exhibited higher uptake capacity compared to BIT clinoptilolite at high concentrations. Dryden and Weatherley [150] reported an ammonium ion uptake capacity of 2.16 meq/g at 900 mg $N\text{-}NH_4^+$/l using Hector clinoptilolite which is less than half of the uptake capacity of KMI and BIT.

It is worthy to note that, the solid concentration (Q_e) of KMI at 500 mg $N\text{-}NH_4^+$ /l is 36.65 mg $N\text{-}NH_4^+$/g clino which means that 13.35 mg ammonia is still remained in the solution, while Q_e of the 1000 mg $N\text{-}NH_4^+$ /l is 61.90 which means that KMI has the capability to adsorb more than 36.65 mg ammonia, and the question is why did not KMI adsorb the remaining 13.35 mg ammonia? The following reasons [5] might answer this question:

- Not all sites are accessible;
- Inert material is included in the weight of resin;
- Other zeolite structures might also present;

- Water of hydration may be different;
- Preconditioning was not complete or material was exposed to different levels of treatment.

Further experiments were carried out to quantify the effect of DI and tap water on the uptake capacity. The concentration levels were 40, 90, 500, and 1000 mg $N\text{-}NH_4^+$ /l. The reduction of ammonia concentration from the solution is shown in Figure 4.7-Figure 4.10.

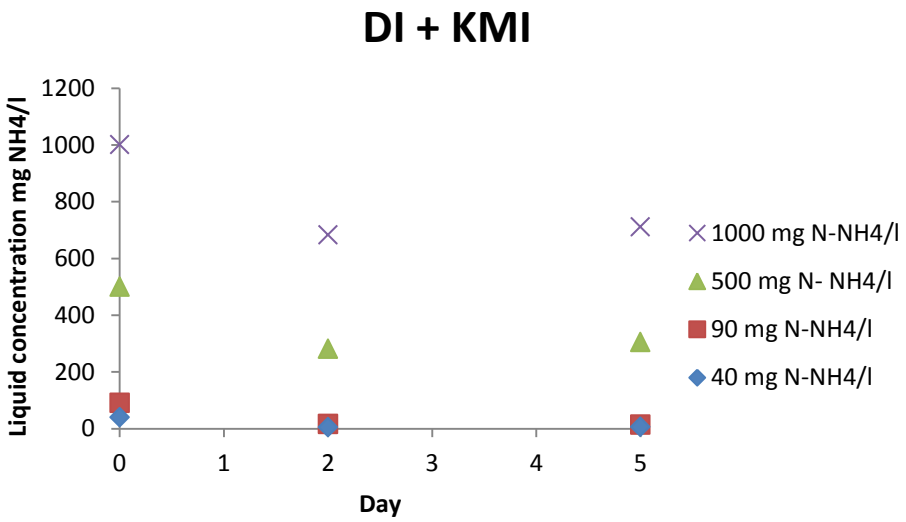

Figure 4.7: Reduction of ammonia concentration over time for different initial ammonia concentrations in 100 ml of solution and 1.0 g of KMI clinoptilolite (T= 23 ºC, particle size 0.42 mm- 1.41 mm, DO water).

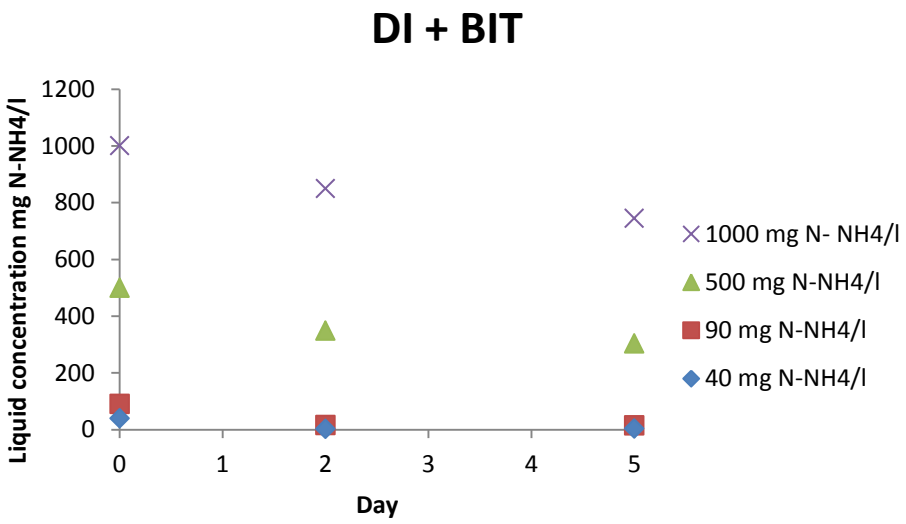

Figure 4.8: Reduction of ammonia concentration over time for different initial ammonia concentrations in 100 ml of solution and 1.0 g of BIT clinoptilolite (T= 23 ºC, particle size 0.42 mm- 1.41 mm, DI water).

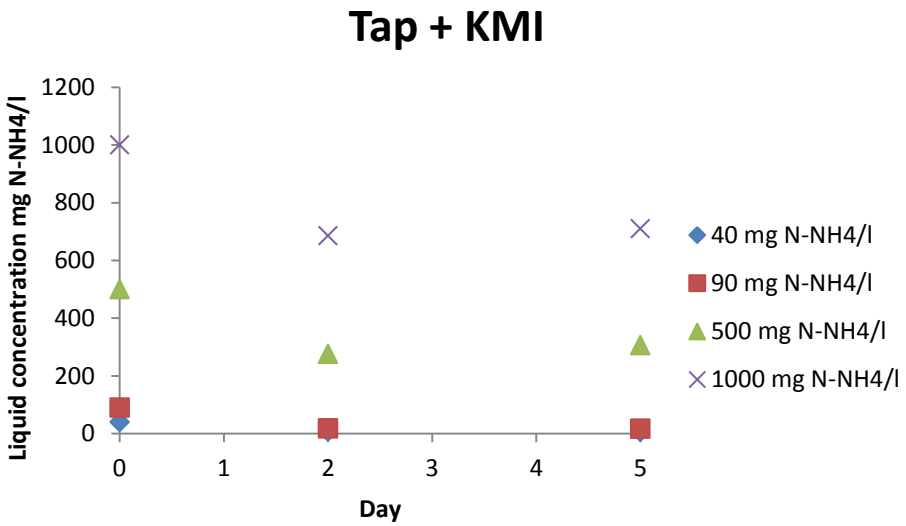

Figure 4.9: Reduction of ammonia concentration over time for different initial ammonia concentrations in 100 ml of solution and 1.0 g of KMI clinoptilolite (T= 23 ºC, particle size 0.42 mm- 1.41 mm, tap water).

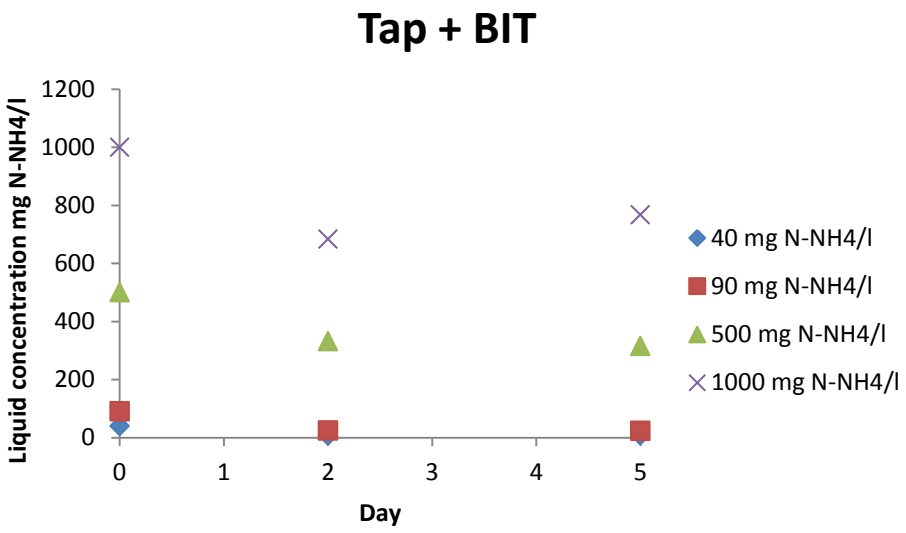

Figure 4.10: Reduction of ammonia concentration over time for different initial ammonia concentrations in 100 ml of solution and 1.0 g of BIT clinoptilolite (T= 23 ºC, particle size 0.42 mm- 1.41 mm, tap water).

Table 4.8, Table 4.9, and Table 4.10 show the solid concentration, uptake capacity, and ammonia percentage removal, respectively, of KMI and BIT in DI and tap water.

Table 4.8: Solid concentration, Q_e, of KMI and BIT in DI and tap water.

Initial Ammonium Concentration ($N\text{-}NH_4^+$ mg/l)	KMI: Q_e, solid concentration, mg $N\text{-}NH_4^+$/g clino		BIT: Q_e, solid concentration, mg $N\text{-}NH_4^+$/g clino	
	DI water	Tap water	DI water	Tap water
40	3.74	3.63	3.74	3.36
90	7.84	7.78	7.83	7.06
500	25.84	25.68	23.92	23.36
1000	42.32	43.2	37.04	39.12

Table 4.9: Uptake capacity of of KMI and BIT in DI and tap water.

Initial Ammonium Concentration ($N\text{-}NH_4^+$ mg/l)	KMI: Q_e, meq/g ,		BIT: Q_e, meq/g	
	DI water	Tap water	DI water	Tap water
40	0.27	0.26	0.27	0.24
90	0.56	0.56	0.56	0.50
500	1.84	1.83	1.71	1.67
1000	3.02	3.08	2.64	2.79

Table 4.10: Ammonia percentage removal fo KMI and BIT in DI and tap water.

Initial Ammonium Concentration ($N\text{-}NH_4^+$ mg/l)	KMI: Percentage of removed ammonia		BIT: Percentage of removed ammonia	
	DI water	Tap water	DI water	Tap water
40	93.58	90.82	93.58	84.1
90	87.11	86.49	87.02	78.4
500	51.68	51.36	47.84	46.72
1000	42.32	43.2	37.04	39.12

The previous results show a slight better performance of KMI and BIT in the presence of tap water comparing to DI water. This is an unexpected result. However, tap water was filtered using a 3-stage PUR commercial filter and this company claimed that this filter has the capability

to remove major ions. The conductivities of DI water, RO water, and filtered tap water are presented in Table 4.11.

Table 4.11: Conductivity of DI, RO, and filtered tap water.

Water type used	Conductivity, μS/cm
DI	9.821
RO	13.970
Filtered tap	502.100

Comparing to the results obtained with RO water, the KMI and BIT have lower uptake capacity in the presence of DI and filtered tap water.

4.2.2 Influence of other cations on the uptake capacity

Major cations that exist in wastewater might affect the ammonium ion uptake capacity especially those which have a high affinity for clinoptilolite such as calcium, potassium and magnesium [4]. Those cations typically exist in wastewater. Therefore; it is important to study the extent to which cations other than ammonium ion will be removed during the ion exchange process. Experiments in this part were done as explained in Section 3.2.1. Results are presented in Figure 4.11.

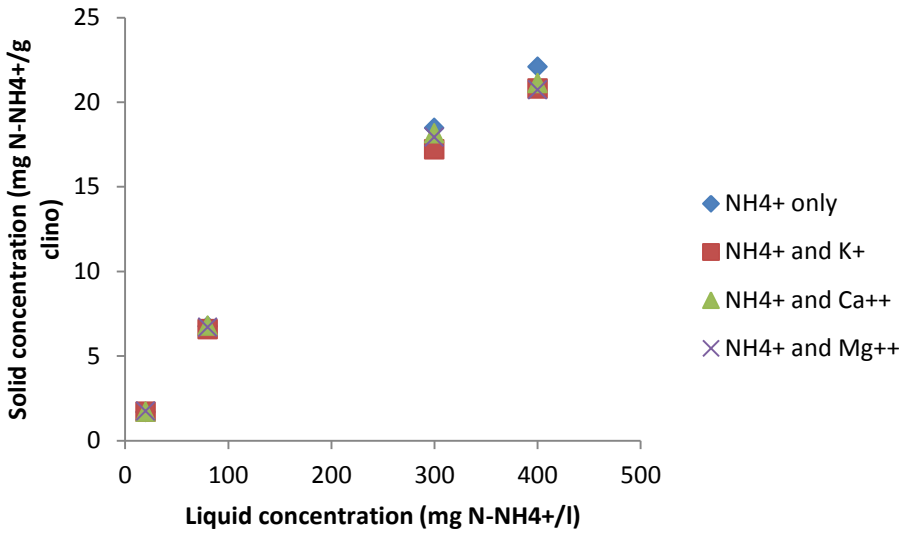

Figure 4.11: Uptake performance of KMI clinoptilolite in presence of potassium, calcium, and magnesium.

The effect of the presence of the other cations was examined separately for each relative to ammonium. Thus, each run was a binary exchange process of ammonium ion and a major cation. In one of these runs, ammonium ion was tested alone to provide comparison. Equivalent concentration for each cation was as follows: 1.0 meq K^{+}/l, 2.0 meq Ca^{++}/l, and 3.3 meq Mg^{++}/l. The ammonium ion concentrations in the solution at equilibrium were measured as explained earlier, and the solid concentrations were determined by mass balance. The uptake data are presented in Table 4.12.

Table 4.12: Influence of presence of other cations on the ammonium ion uptake into KMI clinoptilolite.

Initial $N\text{-}NH_4^+$, mg/l	Percentage of removed ammonia				Uptake capacity, meq/g			
	NH_4^+ only	K^+	Ca^{++}	Mg^{++}	$NH4^+$ only	K^+	Ca^{++}	Mg^{++}
20	91.56	91.47	91.524	91.285	0.12	0.12	0.12	0.12
80	91.56	91.76	91.52	91.62	0.48	0.48	0.48	0.47
300	93.84	94.26	93.94	94.02	1.32	1.28	1.29	1.27
400	94.48	94.8	94.72	94.82	1.58	1.48	1.50	1.47

The uptake capacities are the highest for the solutions containing only the ammonium ions. At lower concentrations, in the range 20 and 80 $N\text{-}NH_4^+$ mg/l, variation in uptake capacity of different cations is scarcely noticed. But at higher levels, in the range 300 and 400 $N\text{-}NH_4^+$ mg/l, variations in uptake capacity are clearly noticed. Overall, the effect of the three cations upon uptake capacity is relatively small at the given amount of cations present in the solutions. Ammonia uptake capacities in the presence of magneisum are always the lowest, as shown in Table 4.12, which indicates that magnesium has the largest effect upon ammonium uptake. The effect of potassium and magnesium are almost identical, although most researchers agree that clinoptilolite has a high affinity for potassium relative to magnesium as discussed in Section 2.2.2. At the given cation concentration, potassium had a higher impact on the ammonium uptake more than calcium had. Miladinovic and Weatherley [58], Table 4.13, and McVeigh and Weatherley [3], Table 4.14, studied the effect of potassium, calcium, and magnesium upon ammonium uptake.

Table 4.13: Ammonium ion uptake onto clinoptilolite in the presence of calcium, magnesium, and potassium at different ammonia concentration, Miladinovic and Weatherley [58].

Initial $N\text{-}NH_4^+$, mg/l	Uptake capacity, meq/g			
	$NH4^+$ only	K^+	Ca^{++}	Mg^{++}
10	0.07	0.07	0.07	0.07
40	0.26	0.26	0.24	0.28
70	0.42	0.40	0.38	0.40
90	0.49	0.46	0.44	0.46
150	0.58	0.56	0.54	0.58
200	0.61	0.60	0.57	0.61

Table 4.14: Ammonium ion uptake onto clinoptilolite in the presence of calcium, magnesium, and potassium at different ammonia concentration, McVeigh and Weatherley [3].

Initial $N\text{-}NH_4^+$, mg/l	Uptake capacity, meq/g			
	$NH4^+$ only	K^+	Ca^{++}	Mg^{++}
40	1.76	1.38	1.58	1.65

Miladinovic and Weatherley [58] found that the order of cations preference was $Ca^{++}>K^+>Mg^{++}$, while McVeigh and Weatherley [3] found the preference as $K^+>Ca^{++}>Mg^{++}$ which agrees with most researchers. For this work, the order of preference is $Mg^{++}\approx K^+>Ca^{++}$.

4.2.2.1 Modeling of the uptake data

The Langmuir and Freundlich models were introduced in Section 1.4.5 and are given in Equation 1.20 and 1.21 respectively. These models were used to compare the equilibrium data obtained. The linear form of these equations is presented in Equation 1.20 and 1.21 respectively:

$$\frac{1}{Q_e} = \frac{1}{KbC_e} + \frac{1}{b} \tag{1.20}$$

$$\log Q_e = \log k + \frac{1}{n}\log C_e \tag{1.21}$$

All terms are explained in Section 1.4.5. After equilibrium was reached, C_e was measured and Q_e was calculated by applying the mass balance on ammonium ions in the solution. Langmuir parameters, K and b, can be determined by plotting $1/C_e$ vs. $1/Q_e$; Intercept =1/b and 1/(Kb)=slope. The Freundlich parameters can be determined by plotting logQ_e against logC_e and by slope and intercept calculation.

Knowing these parameters and using experimental data for C_e, the Langmuir and Freundlich theoretical Q_e can be calculated. Detailed calculations of determining these Langmuir and Freundlich parameters are given in Appendix III. The fit to each model obtained for KMI clinoptilolite without and with other cations present in the solution are given in Figure 4.12-Figure 4.15, and Table 4.15 shows the calculated isotherms' parameters.

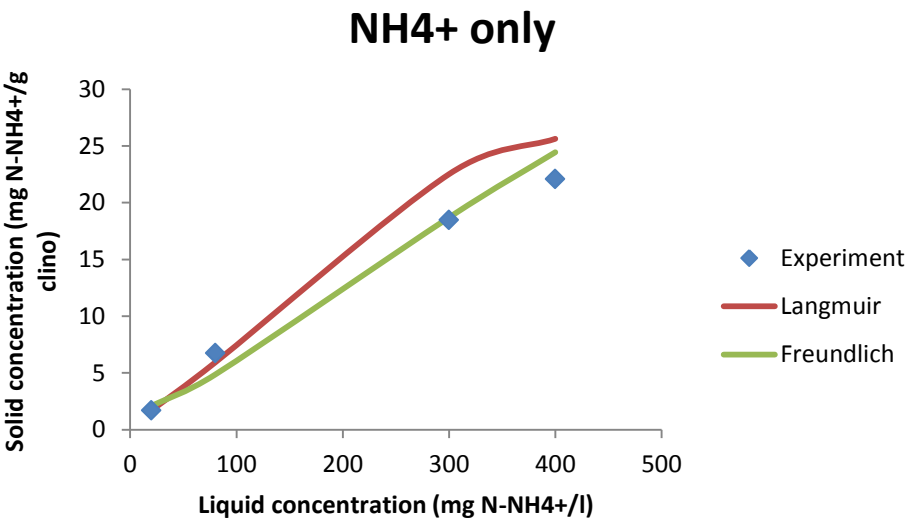

Figure 4.12: Equilibrium isotherm data for ammonium uptake onto KMI clinoptilolite fitted to the Langmuir and the Freundlich adsorption models.

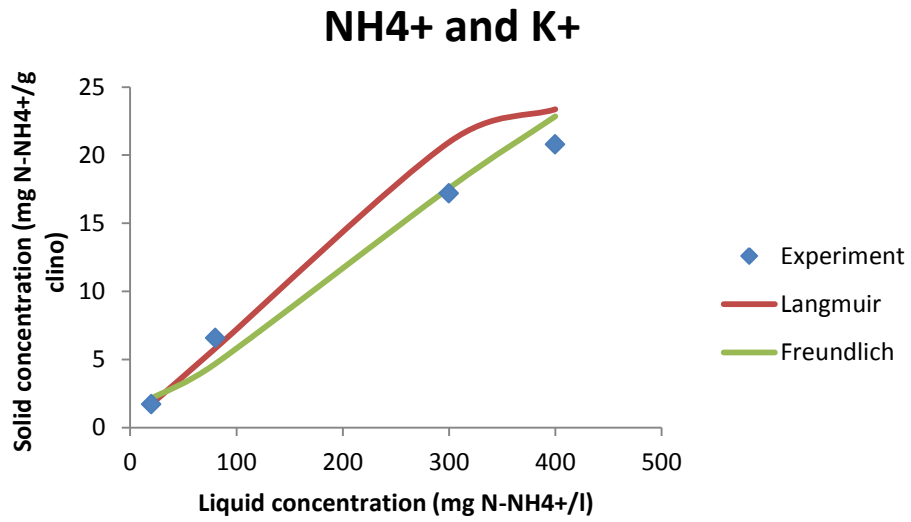

Figure 4.13: Equilibrium isotherm data for ammonium uptake onto KMI clinoptilolite in the presence of potassium fitted to the Langmuir and the Freundlich adsorption models.

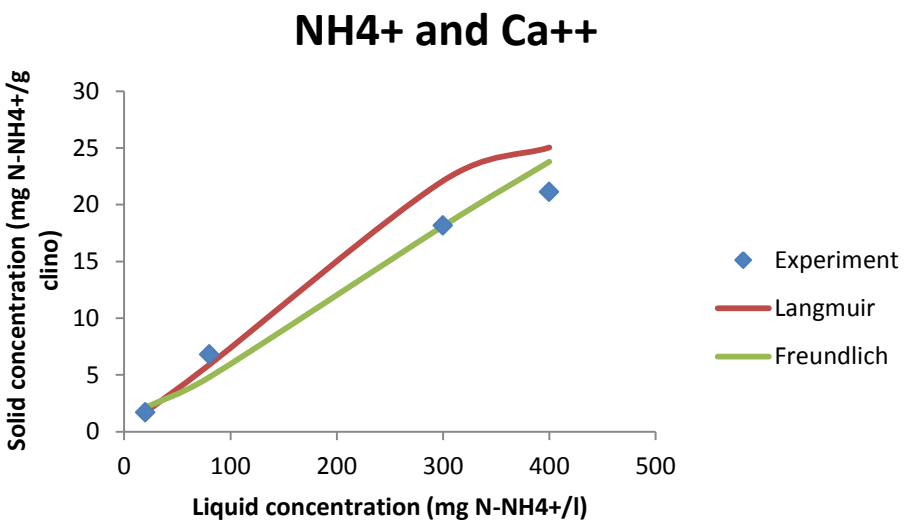

Figure 4.14: Equilibrium isotherm data for ammonium uptake onto KMI clinoptilolite in the presence of calcium fitted to the Langmuir and the Freundlich adsorption models.

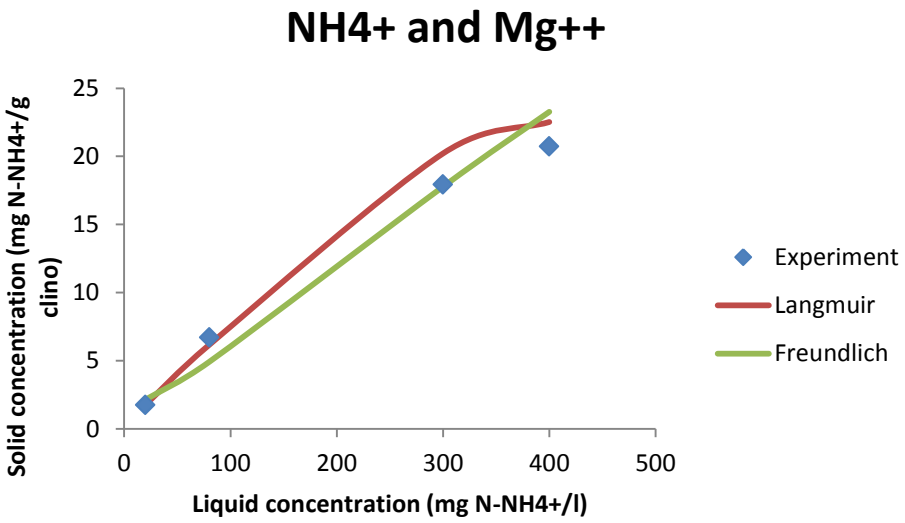

Figure 4.15: Equilibrium isotherm data for ammonium uptake onto KMI clinoptilolite in the presence of magnesium fitted to the Langmuir and the Freundlich adsorption models.

Table 4.15: Langmuir and Freundlich parameters for KMI clinoptilolite.

Langmuir parameters	*b*	*K*	*Kb*	R^2
NH_4^+ only	34.12	0.013457	0.459153	0.997
Mg^{++}	29.06	0.017087	0.496548	0.997
Ca^{++}	32.25	0.014697	0.473978	0.996
K^+	27.85	0.017521	0.48796	0.998
Freundlich parameters	*1/n*	*logk*	R^2	
NH_4^+ only	0.6067	-0.0377	0.960	
Mg^{++}	0.5667	-0.01	0.954	
Ca^{++}	0.5841	-0.0097	0.953	
K^+	0.5764	-0.0062	0.961	

For the adsorption of ammonia with and without the presence of major cations onto KMI clinoptilolite the Langmuir model provides a slightly more consistent fit to the data compared Freundlich model. This is more clear at high liquid concentration, while at low concentrations the fit is acceptable in both cases. This observation was also reported by Miladinovic and Weatherley [58] and Jorgenson and Weatherley [5]. Comparing the parameters obtained and shown in Table 4.15 for different cations present in the solution, the uptake data in the presence of calcium revealed Langmuir parameters are close to the experimental uptake data discussed previously. This finding agrees with the order of preference discussed earlier since calcium exhibited less effect on ammonium uptake performance. The parameter "*Kb*" in the Langmuir model provides an indication of how favorable the adsorption process is. Higher values are obtained when equilibrium is attained at high uptake of adsorbate [3]. The obtained "*Kb*" values confirm the order of uptake performance observed in the experiments.

It is worth mentioning that, besides the impact of the metal ions such as the cationic ions discussed in these experiments on the uptake of ammonia onto clinoptilolite, the presence of organic pollutants in the wastewater might has an impact on the ammonia removal too. Nguyen and Tanner [114] studied the removal of ammonium ions from piggery wastewater and they found that the ammonium ion removal was much less than other waters due to the higher organic content presents in the piggery wastewater as the small suspended solids could block the pores of ion exchangers. Jorgenson and Weatherley [109] studied the impact of the presence of organic pollutants on the ammonium ion removal during ion exchange up to concentration of 50 ppm, and they observed only a minor influence on the ion exchange breakthrough behavior of clinoptilolite.

4.3 Kinetic studies

The removal of ammonium ions from solution into and onto clinoptilolite surface and pores is a mass transfer process. The rate of the physio-chemi sorption mainly depends on internal and/or external diffusional resistances. In most ion exchange processes it is assumed that the actual exchange at the fixed site is very fast. The kinetics of ammonia removal onto KMI and BIT clinoptilolite were conducted based on the procedure explained in Section 3.2.2. Table 3.2 gave a clear description on how the parameters are being varied in kinetics studies. These studies compare the uptake of ammonia onto KMI and BIT clinoptilolite using the internal and external mass transfer models that discussed in Section 1.4.6.

4.3.1 KMI clinoptilolite

Results for the reduction of ammonia concentration over time due to adsorption onto KMI clinoptilolite are presented in Figure 4.16 - Figure 4.19.

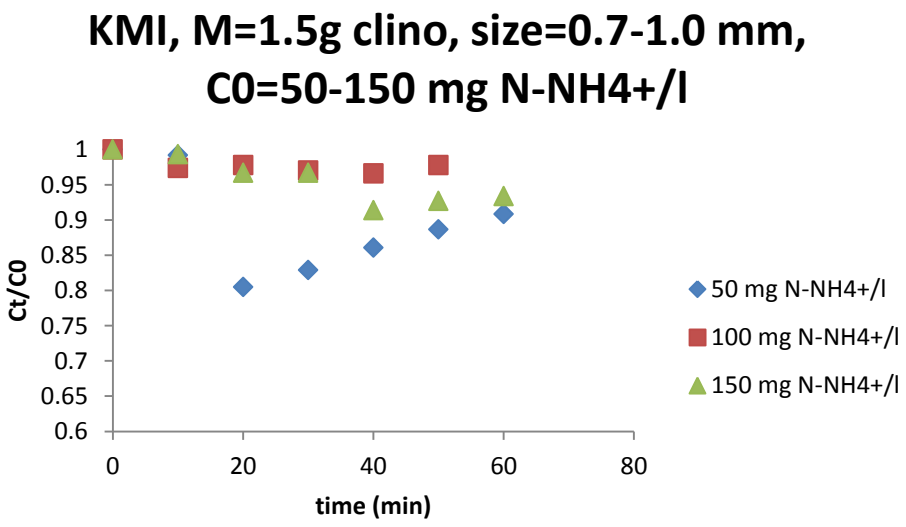

Figure 4.16: Ammonia uptake onto KMI clinoptilolite with different initial ammonia concentrations.

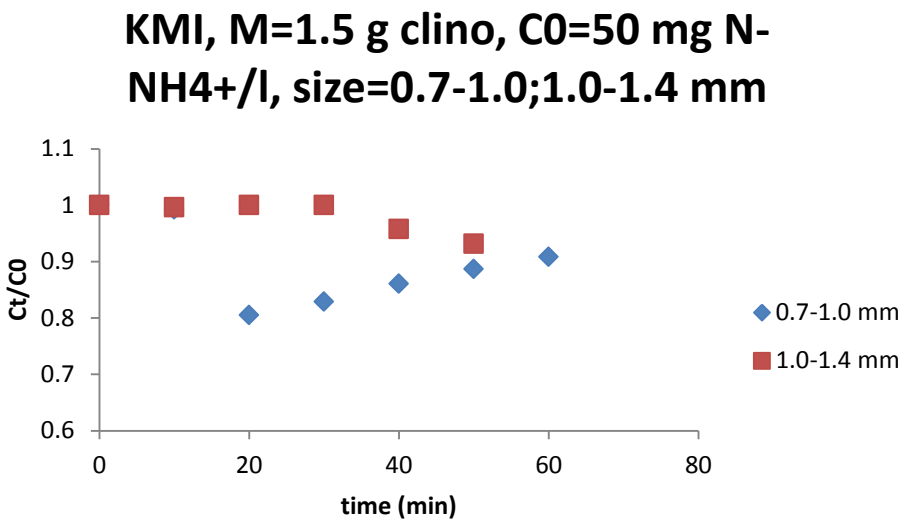

Figure 4.17: Ammonia uptake onto KMI clinoptilolite with different particle size.

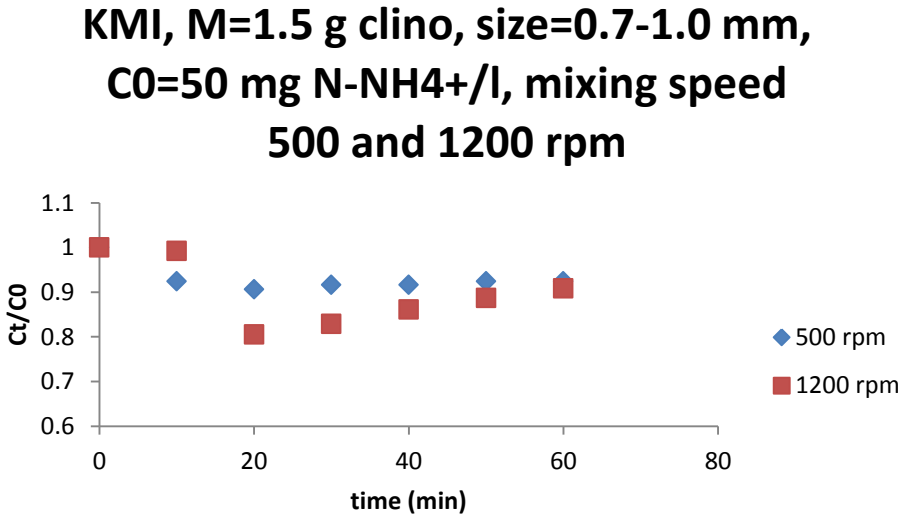

Figure 4.18: Ammonia uptake onto KMI clinoptilolite with different mixing speed.

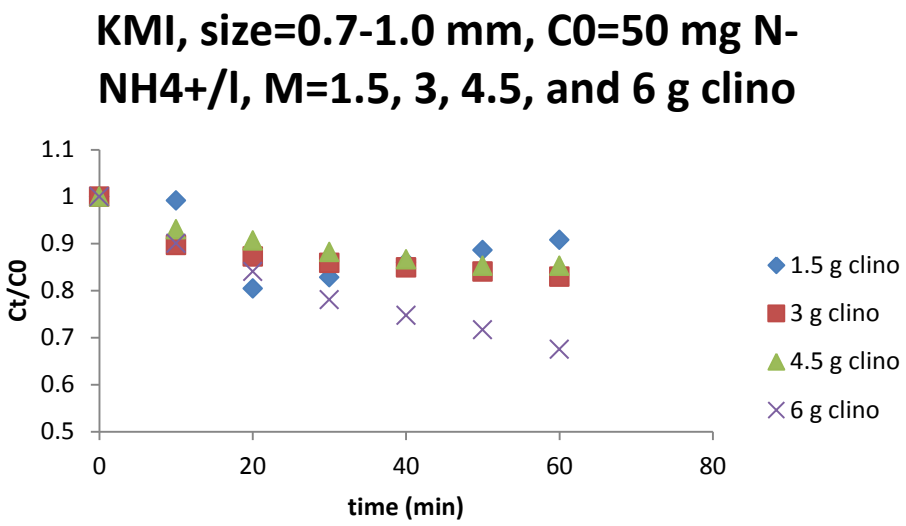

Figure 4.19: Ammonia uptake onto KMI clinoptilolite with different amount of material.

Figure 4.16 suggests that as the initial ammonia increased the uptake removal decreased. This finding is also confirmed by the previous studies [3, 5, 58]. As the surface area is a subject of the diameter of the particles, Figure 4.17 shows a better uptake removal was obtained by the lower particle size where the surface area was higher. High mixing speed was supposed to improve the uptake removal but no significant difference was noticed with both mixing speed used. Figure 4.19 obviously shows that as the amount of zeolite material present increase, the uptake removal is enhanced.

4.3.1.1 External Mass Transfer Model

Evaluation of the external resistance to mass transfer is in need of clinoptilolite particle characteristics and the Langmuir constants which were previously calculated in Section 4.2.2.1. According to Appendix IV, the external diffusion coefficients were calculated based on Furusawa-Smith model, Equation 1.22 and 1.23. Figure 4.20 show how the Furusawa-Smith

model was used to estimate the external mass transfer coefficient, k_f, for KMI clinoptilolite at M = 6.0 g.

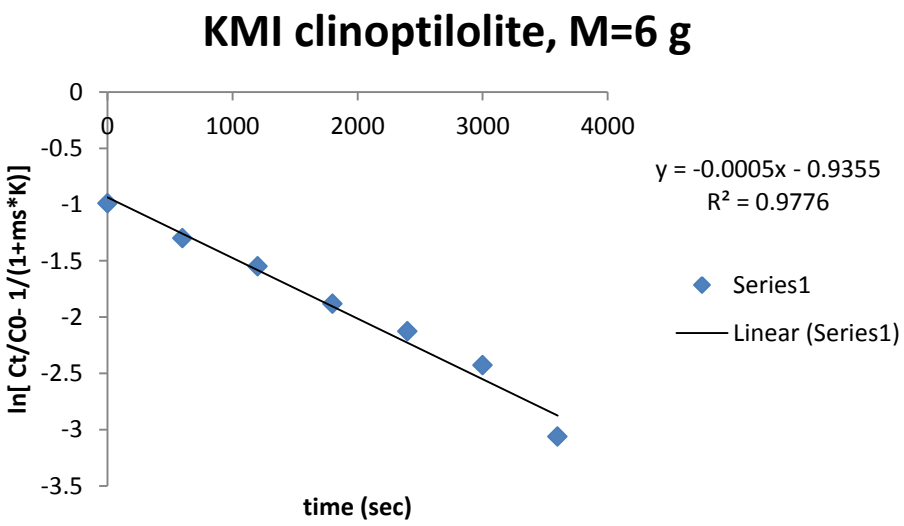

Figure 4.20: Estimation of the external mass transfer coefficient, k_f, for KMI clinoptilolite at M = 6.0 g using Furusawa-Smith model.

Results for KMI clinoptilolite were tabulated in Table 4.16. External mass transfer coefficient, k_f, values for New Zealand clinoptilolite obtained by Miladinovic and Weatherley [4] are reviewed in for comparison.

Table 4.16: External mass transfer coefficient, k_f, for KMI clinoptilolite. If not changed in the table C_0 = 50 mg N-NH_4^+/l, d_p = 0.7-1.0 mm, M = 1.5 g KMI clino, mixing speed = 1200 rpm.

Initial ammonia concentration (mg N-NH_4^+/l)	k_f x10^3 (cm/s)	R^2
50	5.489	0.973
100	0.686	0.979
150	1.372	0.878
Mass of clinoptilolite (g)		
1.5	5.489	0.973
3.0	5.812	0.931
4.5	2.103	0.917
6.0	7.164	0.978
Mixing speed (rpm)		
500	7.547	0.958
1200	5.489	0.973
Particle diameter (mm)		
0.7-1.0	5.489	0.973
1.0-1.4	5.811	0.999

Ideally, the external mass transfer coefficient increased in the following conditions:

- Decrease in the initial ammonia concentration;
- Increase in the mass of the clinoptilolite;
- Increase in the mixing speed;
- Decrease in the particle size.

Based on the calculated values of k_f in Table 4.16, k_f sharply decreased when C_0 was increased from 50 to 100 mg N-NH_4^+/l. The k_f values when the amount of ion exchanger was the varying parameter agrees with how the external mass transfer coefficient behave as statements mentioned above stated except that for M = 4.5 g clino. The k_f value when mixing speed was 500 rpm was higher than k_f when mixing speed was 1200 rpm and this result contradicts the hypothetical assumption stated above. During the experiment, it was noticed that when the mixing speed was 1200 rpm bubbles were created in the vessel and this might affect the mass transfer of uptaking ammonia. Contradictory result also was observed when the particle size was the varying parameter.

Table 4.17: External mass transfer coefficient, k_f, for New Zealand clinoptilolite, Miladinovic and Weatherley [4]. If not changed in the table C_0 = 50 mg N-NH_4^+/l, d_p = 0.7-1.0 mm, M = 1.5 g KMI clino, mixing speed = 2000 rpm.

Initial ammonia concentration (mg N-NH_4^+/l)	k_f x10^3 (cm/s)	R^2
50	18.1	0.978
100	15.4	0.970
150	9.1	0.957
Mass of clinoptilolite (g)		
1.5	35.3	0.876
3.0	18.1	0.978
4.5	7.2	0.934
6.0	6.8	0.954
Mixing speed (rpm)		
500	9.1	0.996
1500	16.3	0.988
2000	18.1	0.978
Particle diameter (mm)		
0.7-1.0	18.1	0.978
1.0-1.4	12.7	0.989

4.3.1.2 Internal Mass Transfer Model

The McKay model was applied to estimate the internal mass transfer coefficient, k_d. The calculated internal mass transfer coefficient values for KMI clinoptilolite are shown in Table 4.18. A detailed calculation example is given in Appendix IV. Figure 4.21 show how the McKay model was used to estimate the internal mass transfer coefficient, k_d, for KMI clinoptilolite at M = 6.0 g.

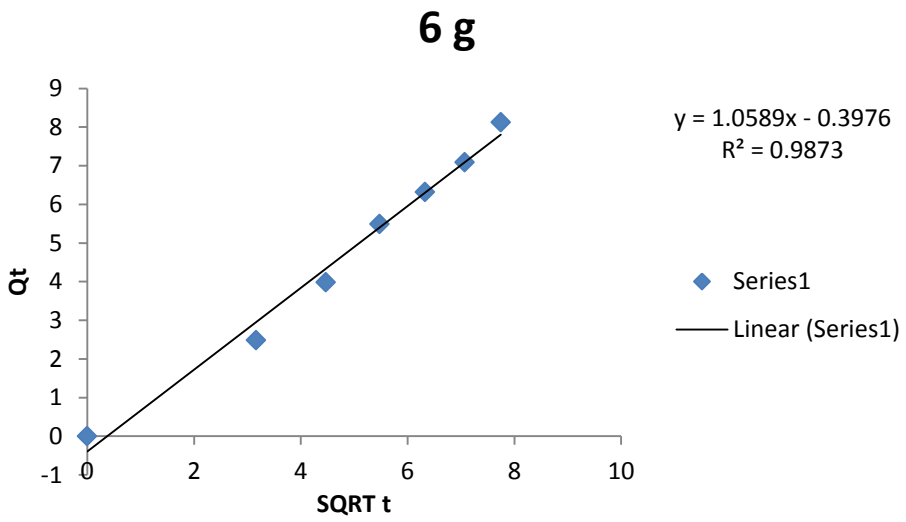

Figure 4.21: Estimation of the internal mass transfer coefficient, k_d, for KMI clinoptilolite at M = 6.0 g using McKay model.

Internal mass transfer coefficient, k_f, values for New Zealand clinoptilolite obtained by Miladinovic and Weatherley [4] are reviewed in Table 4.19 for comparison.

Table 4.18: Internal mass transfer coefficient, k_d, for KMI clinoptilolite. If not changed in the table C_0 = 50 mg N-NH_4^+/l, d_p = 0.7-1.0 mm, M = 1.5 g KMI clino, mixing speed = 1200 rpm.

Initial ammonia concentration (mg N-NH_4^+/l)	k_d (mg/g/$min^{0.5}$)	R^2
50	1.229	0.890
100	1.075	0.994
150	3.870	0.770
Mass of clinoptilolite (g)		
1.5	1.229	0.890
3.0	1.060	0.945
4.5	0.697	0.999
6.0	1.059	0.973
Mixing speed (rpm)		
500	2.158	0.989
1200	1.229	0.890
Particle diameter (mm)		
0.7-1.0	1.229	0.890
1.0-1.4	4.300	0.990

Clearly, the internal mass transfer coefficient, k_d, was changing as the varying parameters (initial concentration of ammonia, mixing speed, particle size, and amount of zeolite) were changing which suggests that the rate of exchange was not exclusively controlled by internal particle diffusion. However, some contradictory results were observed. For example, as the mixing speed increase the external film resistance decreases and the intraparticle become the controlled

resistance; hence, an increase in the internal mass transfer coefficient is expected but the opposite was observed. The values of k_d increase from 1.229 to 3.870 mg/g/min$^{0.5}$ as the initial concentration increased from 50 to 150 mg N-NH_4^+/l respectively, since the liquid film role become less important at high concentrations. Internal mass transfer coefficient decreased as the amount of ion exchanger increased in the solution. The increase of k_d values with the increase in the particles size was unexpected, as the particle size increases the ions have further to travel through the zeolite phase and this is predicted in a higher resistance with increase in size.

Table 4.19: Internal mass transfer coefficient, k_d, for New Zealand clinoptilolite, Miladinovic and Weatherley [4]. If not changed in the table C_0 = 50 mg N-NH_4^+/l, d_p = 0.7-1.0 mm, M = 1.5 g KMI clino, mixing speed = 2000 rpm.

Initial ammonia concentration (mg N-NH_4^+/l)	k_d (mg/g/$min^{0.5}$)	R^2
50	1.67	0.988
100	2.15	0.938
150	2.67	0.901
Mass of clinoptilolite (g)		
1.5	2.18	0.985
3.0	1.67	0.988
4.5	1.33	0.986
6.0	1.29	0.994
Mixing speed (rpm)		
500	1.35	0.868
1500	1.52	0.923
2000	1.67	0.988
Particle diameter (mm)		
0.7-1.0	1.67	0.988
1.0-1.4	1.66	0.985

4.3.2 BIT clinoptilolite

Results for the reduction of ammonia concentration over time due to adsorption onto KMI clinoptilolite are presented in Figure 4.22- 4.25.

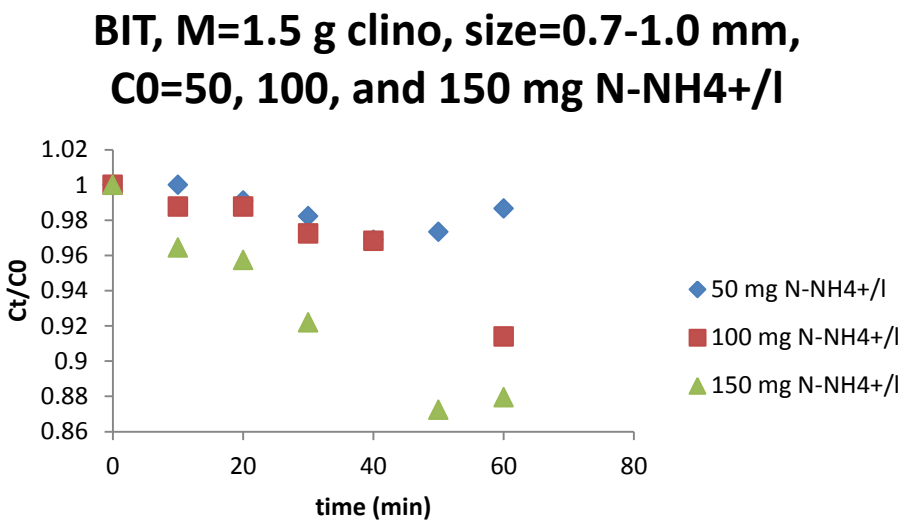

Figure 4.22: Ammonia uptake onto BIT clinoptilolite with different initial ammonia concentrations.

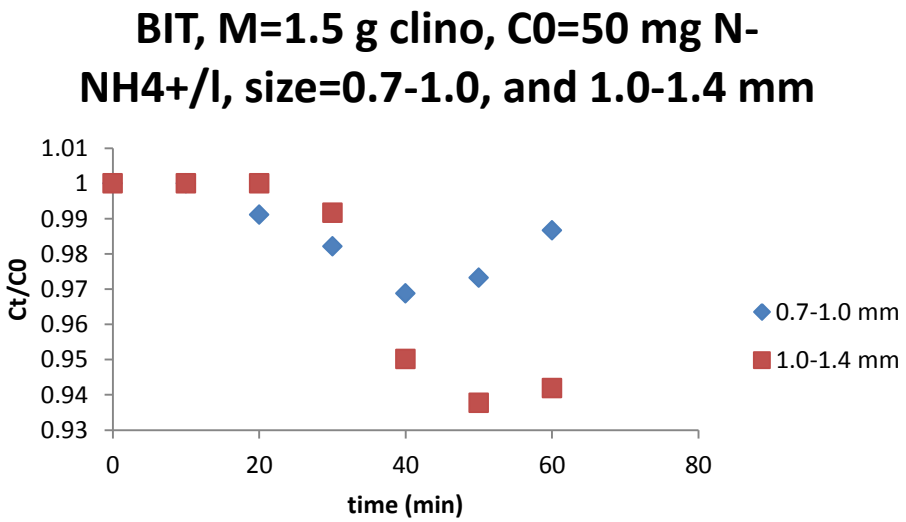

Figure 4.23: Ammonia uptake onto BIT clinoptilolite with different particle size.

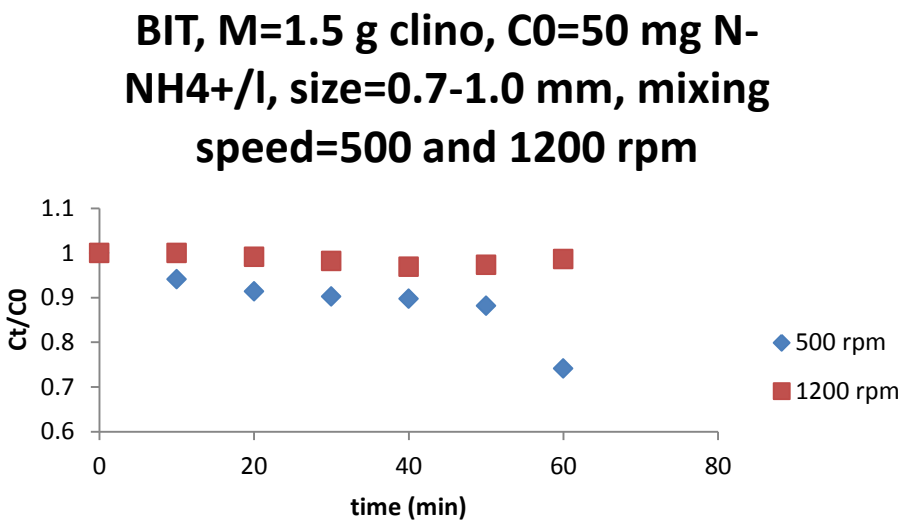

Figure 4.24: Ammonia uptake onto BIT clinoptilolite with different mixing speed.

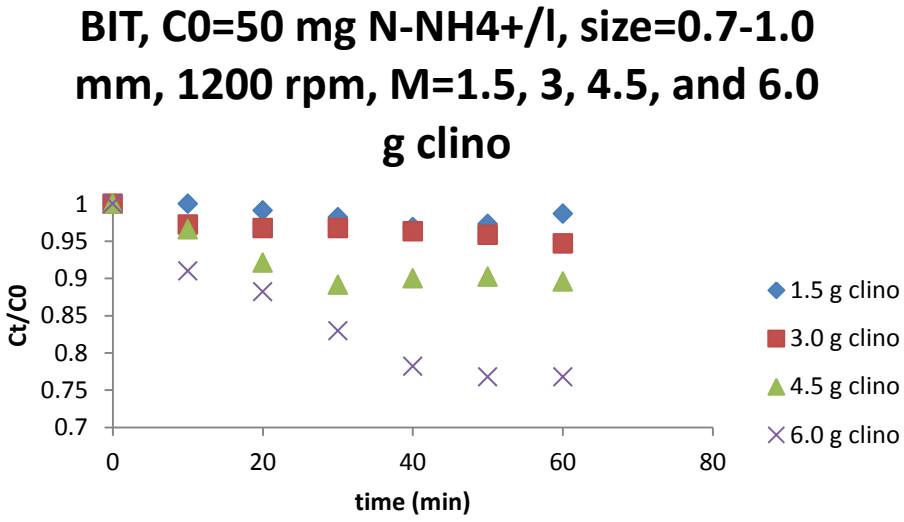

Figure 4.25: Ammonia uptake onto BIT clinoptilolite with different amount of material.

BIT clinoptilolite has contrasting behavior compared to KMI when the ammonia concentration in the solution is increased. The BIT uptake removal is enhanced when the initial ammonia concentration is increased. Also, the uptake removal of BIT is enhanced when the particle size is increased which is opposite to the finding with KMI clinoptilolite. However, Miladinovic and Weatherley [4] noticed the same behavior of BIT when increasing the particle size. BIT uptake removal performance was not enhanced when increasing the mixing speed, and this was not expected.

4.3.2.1 External Mass Transfer Model

For KMI clinoptilolite, the external diffusion coefficients were calculated based on the Furusawa-Smith model, Equations 1.22 and 1.23, and the results are tabulated in Table 4.20.

Table 4.20: External mass transfer coefficient, k_f, for BIT clinoptilolite. If not changed in the table C_0 = 50 mg N-NH_4^+/l, d_p = 0.7-1.0 mm, M = 1.5 g KMI clino, mixing speed = 1200 rpm.

Initial ammonia concentration (mg N-NH_4^+/l)	k_f x10^3 (cm/s)	R^2
50	0.473	0.906
100	0.473	0.937
150	2.362	0.922
Mass of clinoptilolite (g)		
1.5	0.473	0.906
3.0	0.400	0.981
4.5	1.448	0.994
6.0	2.96	0.985
Mixing speed (rpm)		
500	3.307	0.960
1200	0.473	0.906
Particle diameter (mm)		
0.7-1.0	0.473	0.906
1.0-1.4	2.670	0.932

The values of the external mass transfer coefficient, k_f, obtained totally agree with the performance of BIT uptake removal presented in Figure 4.22 to Figure 4.25. The k_f value jumped from 0.473 to 2.362 (cm/s) when the initial concentration increased from 50 to 150 mg N-NH_4^+/l, respectively. Though, no change was observed when the initial concentration increased from 50 to 100 mg N-NH_4^+/l. A significant increase in k_f value was obtained when the amount of BIT

used in the experiment increased above 3 g whereupon a maximum k_f value was obtained at 6 g of KMI. k_f sharply decreased when the mixing speed was increased. And as the particle size was increased, the k_f value was significantly increased, see Table 4.20.

4.3.2.2 Internal Mass Transfer Model

The McKay model was applied to estimate the internal mass transfer coefficient, k_d, for BIT and the calculated coefficients are shown in Table 4.21. A summary of the kinetics experiments is presented in Table 4.22. For initial ammonia concentration, particle size, and mixing speed parameter the internal mass transfer coefficients for BIT had the same behavior of internal mass transfer coefficient for KMI.

Table 4.21: Internal mass transfer coefficient, k_d, for BIT clinoptilolite. If not changed in the table C_0 = 50 mg N-NH_4^+/l, d_p = 0.7-1.0 mm, M = 1.5 g KMI clino, mixing speed = 1200 rpm.

Initial ammonia concentration (mg N-NH_4^+/l)	k_d (mg/g/$min^{0.5}$)	R^2
50	0.958	0.962
100	1.023	0.985
150	5.124	0.890
Mass of clinoptilolite (g)		
1.5	0.958	0.962
3.0	0.281	0.932
4.5	0.645	0.921
6.0	0.841	0.976
Mixing speed (rpm)		
500	1.829	0.996
1200	0.958	0.962
Particle diameter (mm)		
0.7-1.0	0.958	0.962
1.0-1.4	2.616	0.917

Table 4.22: Summary of kinetics studies.

Parameter	KMI	BIT	New Zealand [4]
	Uptake removal rate		
Initial concentration +	-	+	-
Particle size +	-	+	+
Mixing speed +	+	-	+
Amount of clino +	+	+	+
	k_f		
Initial concentration +	-	+	-
Particle size +	+	+	-
Mixing speed +	-	-	+
Amount of clino +	+	+	-
	k_d		
Initial concentration +	+	+	+
Particle size +	+	+	0
Mixing speed +	-	-	+
Amount of clino +	-	+	-

+ means increase, - means decrease, 0 no change

4.4 Aeration studies

4.4.1 SEM analysis for porous membrane

SEM analysis was carried out for all membrane types in the Microscopy and Analytical Imaging Laboratory at KU following the same procedure carried out for analysis of clinoptilolite samples in Section 3.1.1.1. SEM photos for the membranes used in this work are presented in Figure 4.26-Figure 4.29. Very high magnification (14 k X) was used. An important benefit of using SEM analysis is that the foulants do not have to be removed from the membrane in order to be analyzed.

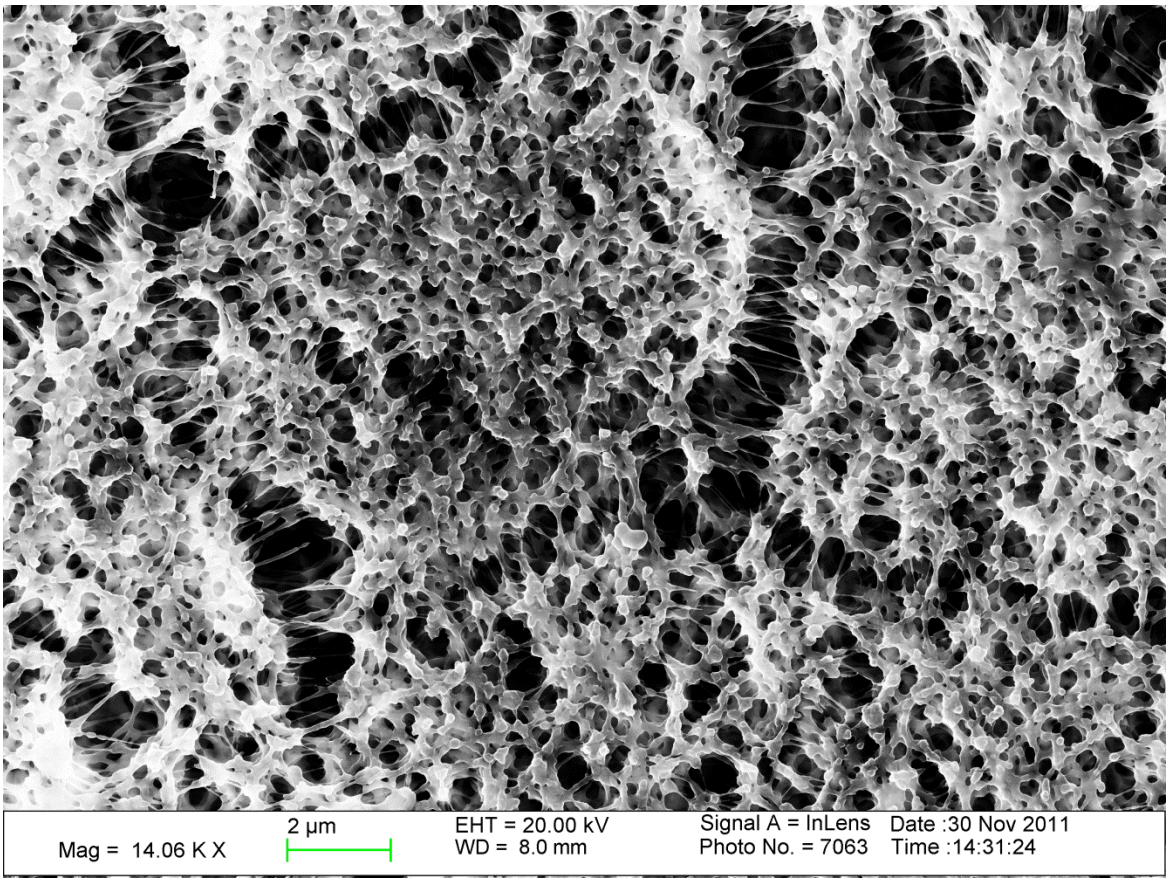

Figure 4.26: SEM analysis of PP membrane.

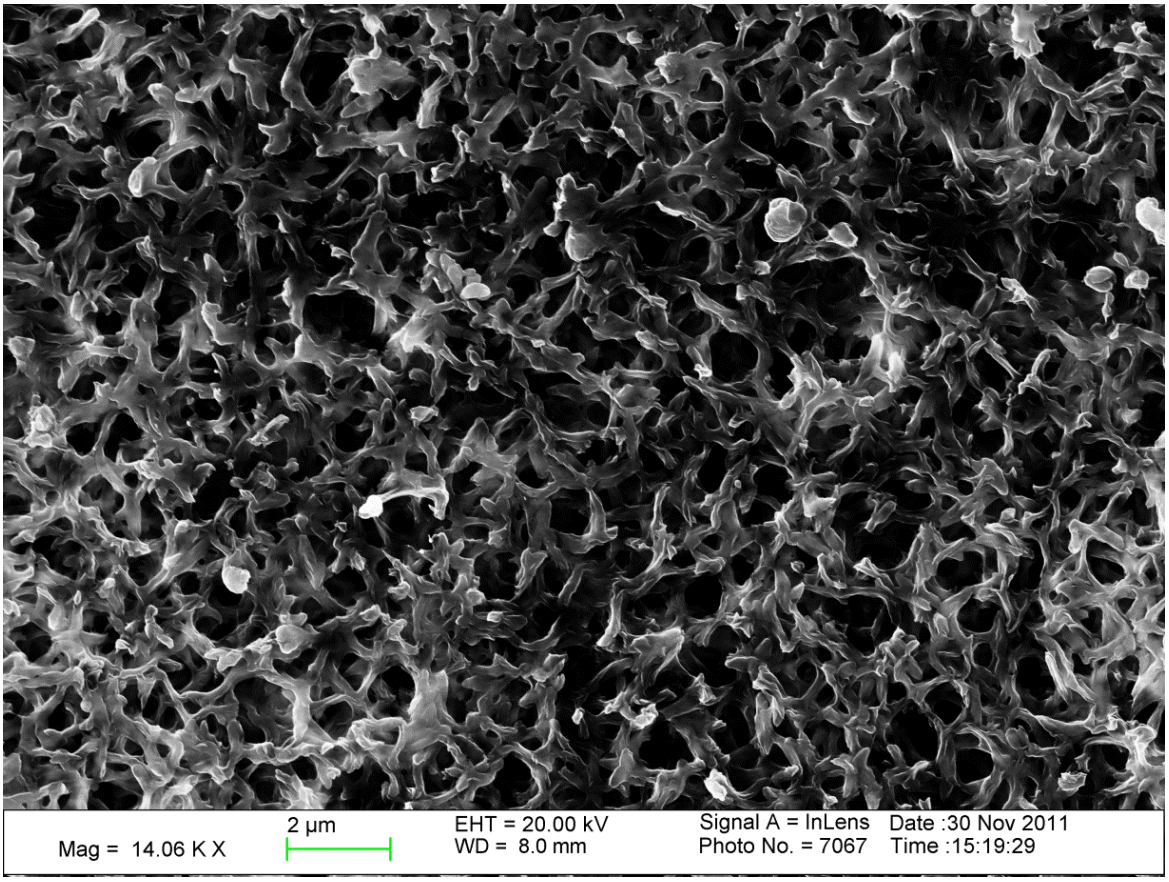

Figure 4.27: SEM analysis of Nylon membrane.

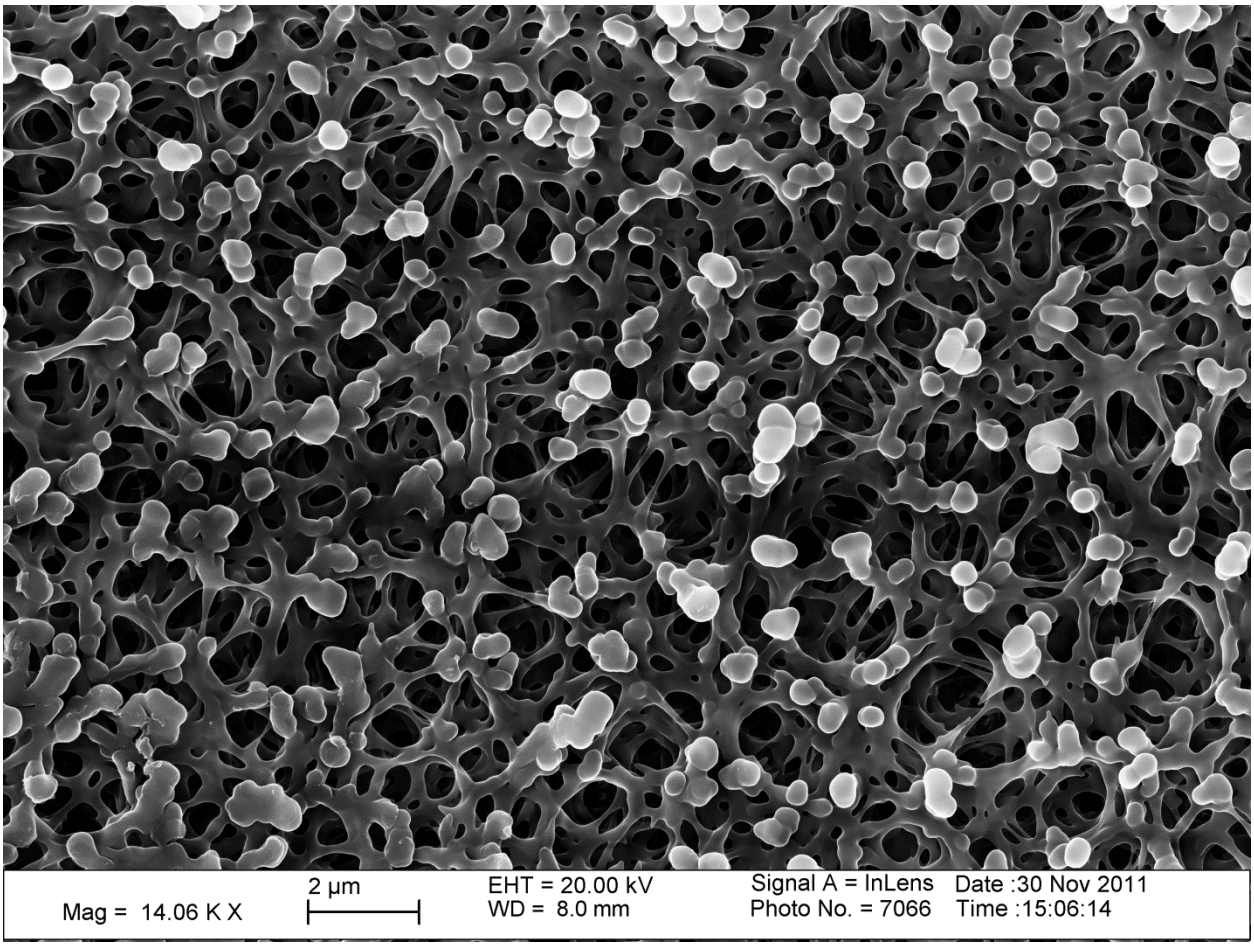

Figure 4.28: SEM analysis of PES membrane.

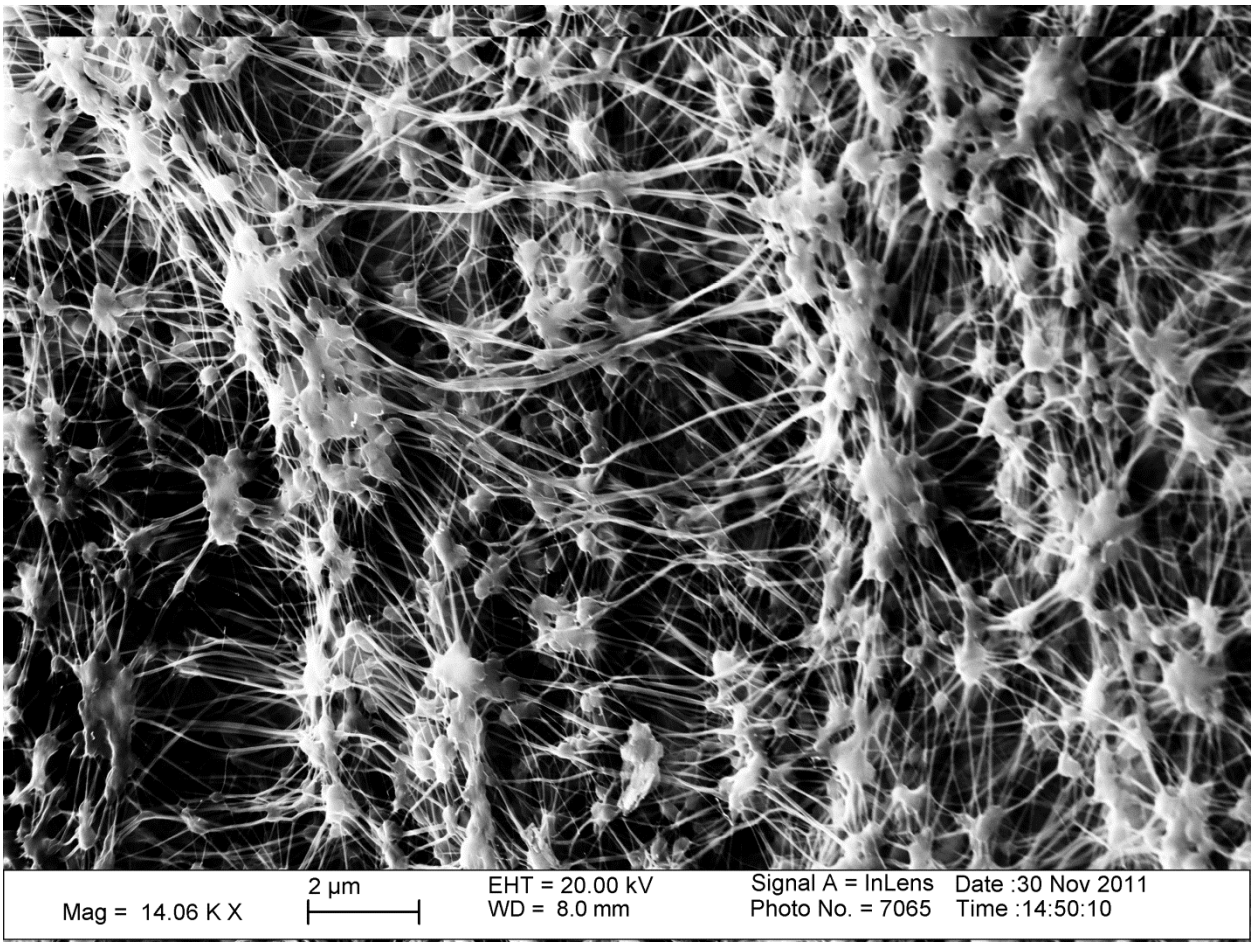

Figure 4.29: SEM analysis of PTFE membrane.

SEM analysis was used to study the morphology of the membranes used in this work. Some parameters can be directly obtained from the SEM images such as the number of pores per surface unit and porosity [151]. Membrane specifications are summarized in Table 3.3. In this work, different pore sizes were selected to test the proper pore size by which the best aeration could be reached. The pore size used in this work was 0.1 µm for PP and Nylon membranes and 0.2 µm for PTFE and PES. Regular pores were recognized in Figure 4.26, Figure 4.27, and Figure 4.28 which are associated with PP, Nylon, and PES membranes respectively. No regular pore was detected for PTFE. Macro pores were observed in PP SEM image. Comparing to PES, obviously both PP and Nylon membranes have smaller pore size which agrees with the data

provided by the manufacturers. Due to the hydrophobic character of the membranes the water droplets repelled and the pores remain dry.

4.4.2 Water deoxygenation

As outlined in Section 3.2.3, filtered tap water was deoxygenated with sodium sulfite, Na_2SO_3. Equation 3.1 was used to determine that 167.5 mg sodium sulfite is needed to deoxygenate 2.5 L of water. On the other hand, Mayernick and Weatherley [152] found after some trial and error, the appropriate amount of sodium sulfite to deoxygenate 2.5 L of tap water for 45 minutes was determined to be approximately 250 mg. However, when 250 mg sodium sulfite was stirred with 2.5 L of tap water it took more than 60 minutes, see Figure 4.30 to achieve a steady state concentration of oxygen. Therefore; 350 mg sodium sulfite was used to deoxygenate 2.5 L of tap water for the rest of the experiments. This amount took approximately 30-40 minutes for a zero DO concentration to be reached.

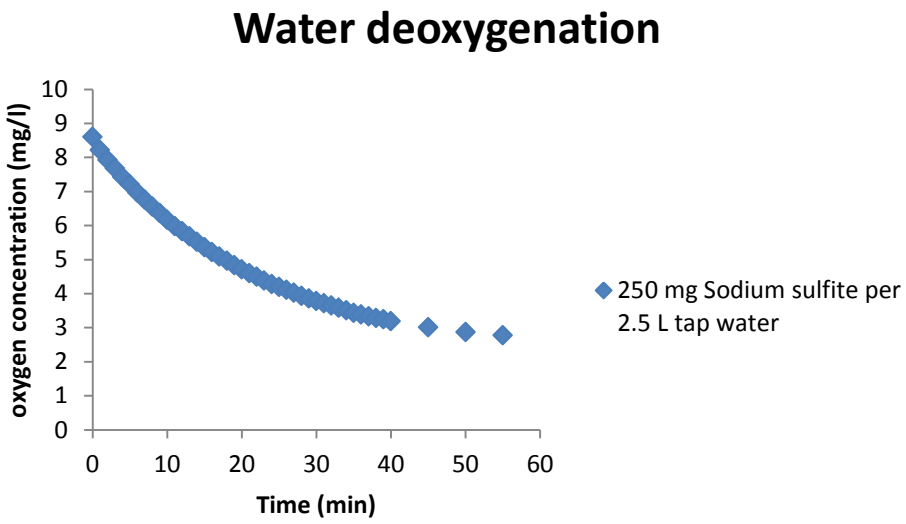

Figure 4.30: Deoxygenation of 2.5 L tap water by 2.5 mg sodium sulfite.

4.4.3 Membranes performance

After deoxygenation, the water vessel was reoxygenated and the DO concentration in water was measured with time. The performance of membranes used in this work is presented in Figure 4.31-Figure 4.34.

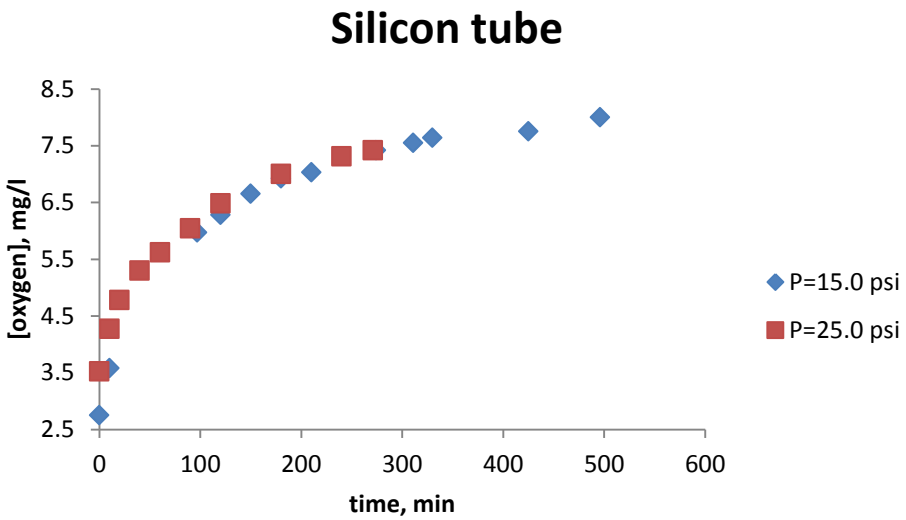

Figure 4.31: Silicon tube membrane oxygenation at different pressures.

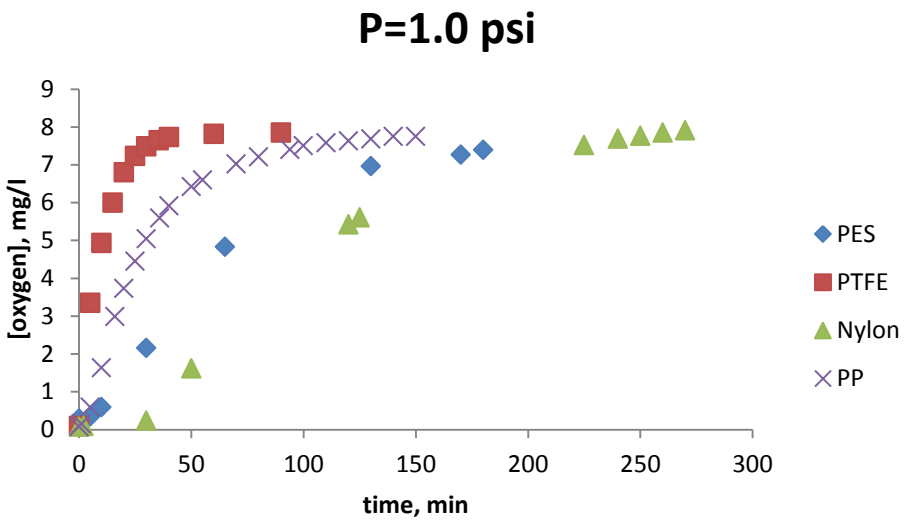

Figure 4.32: Porous membrane oxygenation at P = 1.0 psi.

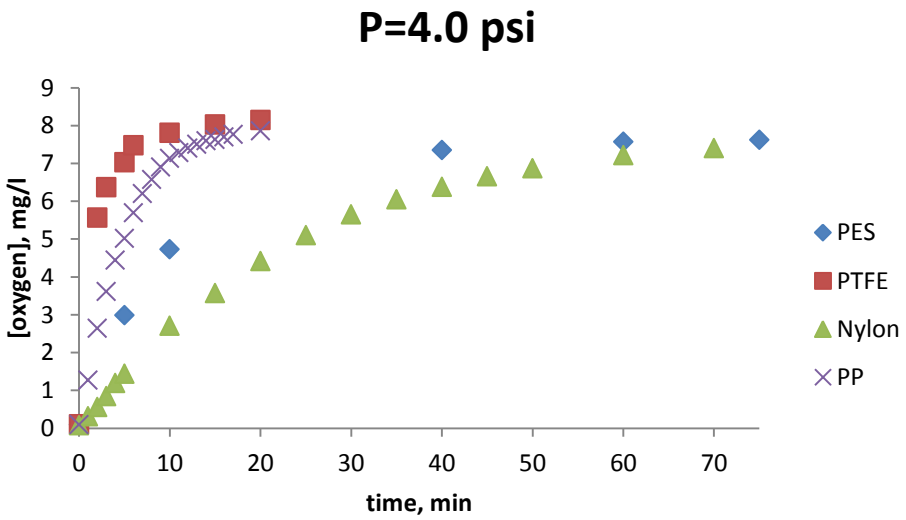

Figure 4.33: Porous membrane oxygenation at P = 4.0 psi.

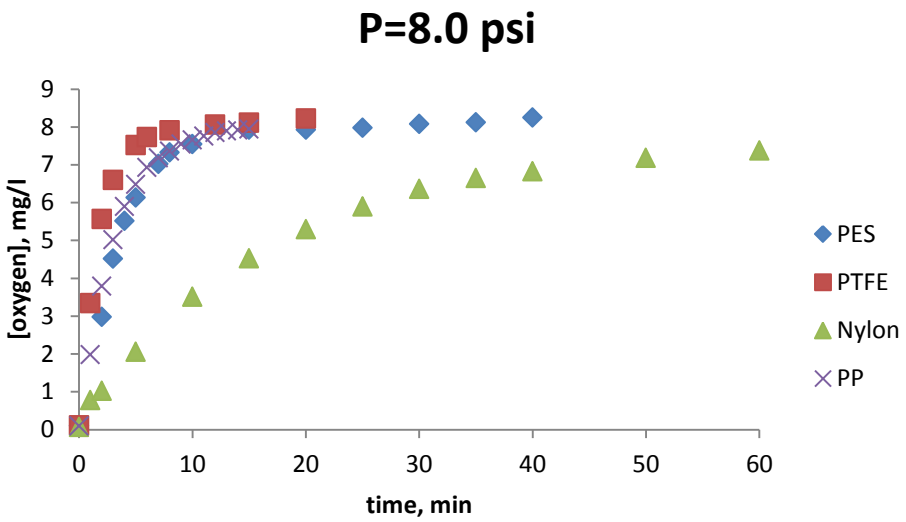

Figure 4.34: Porous membrane oxygenation at P = 8.0 psi.

For the silicon tube membrane, no difference was observed in the oxygen transfer rate when pressure changed from 15 to 25 psi. It took approximately 300 minutes to reach 7.5 mg DO/l at 15 and 25 psi. Compared to the silicon tube membrane, the porous membrane showed a better performance at all pressure levels used.

PTFE showed the best performance at the pressure levels used. At 1.0 and 4.0 psi, PP conducted aeration better than PES but at 8.0 psi, both PP and PES showed identical performance. Nylon gave the worst performance, compared to the other porous membranes, taking more than 60 minutes to reach 7.5 mg DO/l.

Despite having similar pore size, aeration with PTFE reached 100% saturation within 10 minutes while with PES it took 60 minutes to reach 90% saturation at 4.0 psi. At 8.0 psi, PES, and PP reached saturation after 15 minutes.

4.4.4 Overall mass transfer coefficient

The overall mass transfer coefficient, $k_L.a$, was calculated experimentally by measuring the DO concentration over time. Equation 2.36 represents the oxygen flux through the membrane. The oxygen transfer *rate* through the membrane is described in Equation 4.1:

$$\frac{dC_{O_2L}}{dt} = k_l a\left(C^*_{O_2} - C_{O_2L}\right) \tag{4.1}$$

where $\frac{dC_{O_2L}}{dt}$ is the oxygen transfer rate through the membrane. All other parameters in Equation 4.1 are explained previously in Section 2.5.2. Integrating Equation 4.1 results in C_{O_2L} as a function of time as shown in Equation 4.2 and 4.3:

$$\int_{C_0}^{C_t} \frac{dC_{O_2L}}{\left(C^*_{O_2} - C_{O_2L}\right)} = k_l a \int_0^t dt \tag{4.2}$$

$$C_t = C^*_{O_2} - \left(C^*_{O_2} - C_0\right)e^{-k_l a} \tag{4.3}$$

Where,

- C_t- is the oxygen concentration at time t, mg/l;
- C_0- is the initial oxygen transfer, mg/l

Equation 4.3 can be rearranged and by taking the natural log of both sides Equation 4.4 is formed:

$$\ln\left(\frac{C^*_{O_2} - C_t}{C^*_{O_2} - C_0}\right) = -k_l a t \tag{2.37}$$

Plotting $\ln\left(\frac{C_{O_2}^{*}-C_t}{C_{O_2}^{*}-C_0}\right)$ versus time gives a straight line slope equals to - $k_L.a$. A representative diagram of overall mass transfer coefficient for PES membrane is given in Figure 4.35.

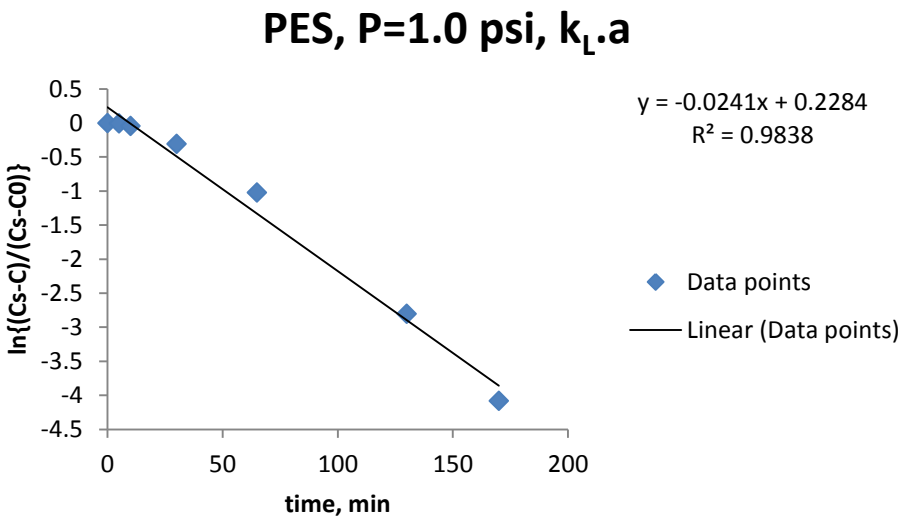

Figure 4.35: Determination of overall mass transfer coefficient of PES membrane at 1.0 psi.

Overall mass transfer coefficients for silicon tube membrane and porous membranes are estimated in the same manner and presented in Table 4.23 and Table 4.24 respectively.

Table 4.23: Overall mass transfer coefficient of silicon tube membrane at 15 and 25 psi.

Silicon tube membrane	
Pressure, P (psi)	$k_L.a$ (min^{-1})
15	0.0073
25	0.0136

Table 4.24: Overall mass transfer coefficients of porous membranes at various pressures.

Pressure, P (psi)	$k_L.a$ (min^{-1})			
	PES	PTFE	Nylon	PP
1	0.0241	0.0961	0.0171	0.0352
4	0.0701	0.2614	0.0342	0.2531
8	0.111	0.2839	0.0578	0.3927

Overall mass transfer coefficients of the porous membranes are higher than that of silicon membrane tube. For the porous membranes, PTFE gave the highest overall mass transfer coefficient at 1.0 and 4.0 psi. At 8.0 psi, PP showed a higher overall mass transfer coefficient than the PTFE. Without the determination of overall mass transfer coefficients, this finding cannot be obtained by oxygenation figure of porous membrane at 8.0 psi. Based on the pore size comparison, the overall mass transfer coefficient for PP was nearly 1 order of magnitude greater than the overall mass transfer coefficient for nylon at 4.0 and 8.0 psi. The overall mass transfer coefficient for the PTFE is 4 times greater than the overall mass transfer coefficient for PES at 1.0 and 4.0 psi, and 2.5 times greater at 8.0 psi.

Equation 4.1 is based on the two-film theory which hypothetically assumes existence of two films, one film exists in the gas phase adjacent to the liquid and the other film exists in the liquid phase adjacent to the gas. The two-films are represented in Figure 4.36.

Based on the argument that made in Section 2.5.2, which stated that the mobility of oxygen molecules in the gas phase is much greater than the mobility of oxygen molecules in the liquid phase and thus the only resistance should be considered is the liquid resistance, and the gas and membrane resistance can be neglected, Figure 4.36 is reduced to Figure 4.37.

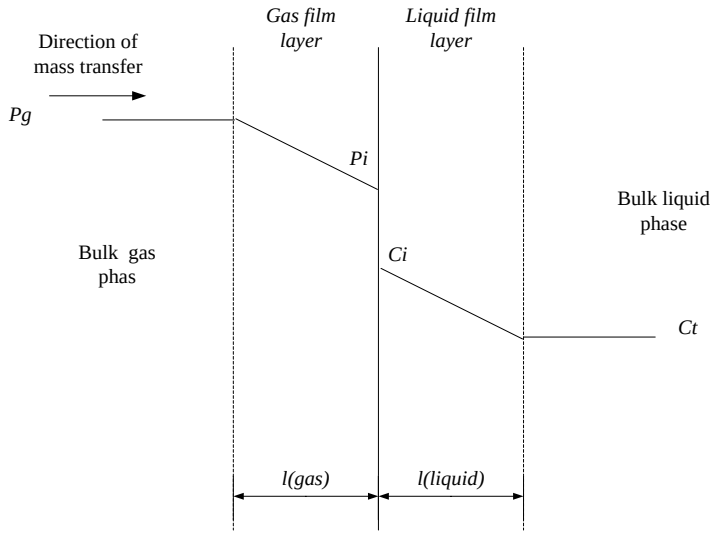

Figure 4.36: Two-film theory for gas transfer.

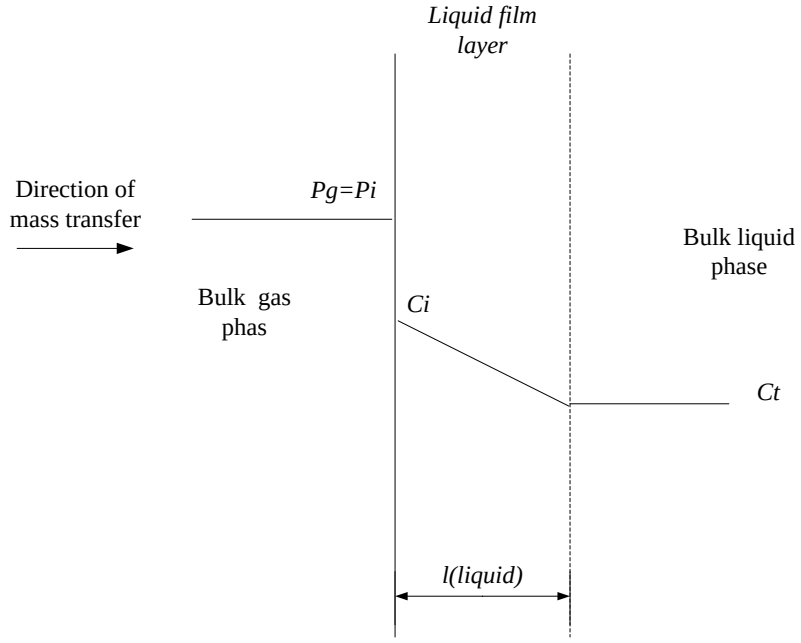

Figure 4.37: Liquid film layer resistance.

In Figure 4.36 and Figure 4.37, *Ci* is the interfacial oxygen concentration and at the same time it is the oxygen saturation concentration$C_{O_2}^*$, and can be determined by Henry's law as discussed in Section 2.5.2. *Ct* is the oxygen concentration in the liquid phase (C_{O_2L}).

Oxygen is transferred to the liquid phase as long as the oxygen saturation concentration is greater than the oxygen concentration in the liquid phase. If both concentrations are equal, then the process is at equilibrium as seen in the oxygenation figures that discussed previously. To attain the highest transfer rate, the following conditions [153] must be met:

- The renewal rate of the interface should be high.
- The liquid film layer should be small.

The first condition simply enhances the driving force, i.e., the difference in concentration, since the rapid circulation of the elemental volumes that reside at the interface results in higher oxygen mass transfer. The second condition enhances the liquid mass transfer coefficient, k_L, as the relation between k_L and the liquid film layer is an inverse relationship.

4.5 Column studies

KMI clinoptilolite in the initial sodium form was used for all the experimental column work, except for the bio-regeneration studies, as this is typical of its use in industry and has been observed to be most effective in the removal of ammonia [3].

4.5.1 Silicon tube membrane column

4.5.1.1 Column without bacteria

In this part, KMI and BIT clinoptilolite were examined. Figure 4.38-Figure 4.39 show a comparison of the performance of KMI and BIT clinoptilolite, respectively, in two runs. As shown in those figures, the performance of these columns was quantified in terms of breakthrough curves where the ratio of effluent/initial ammonium concentration is plotted against the bed volumes treated. The feed solution used was ammonia in filtered tap water.

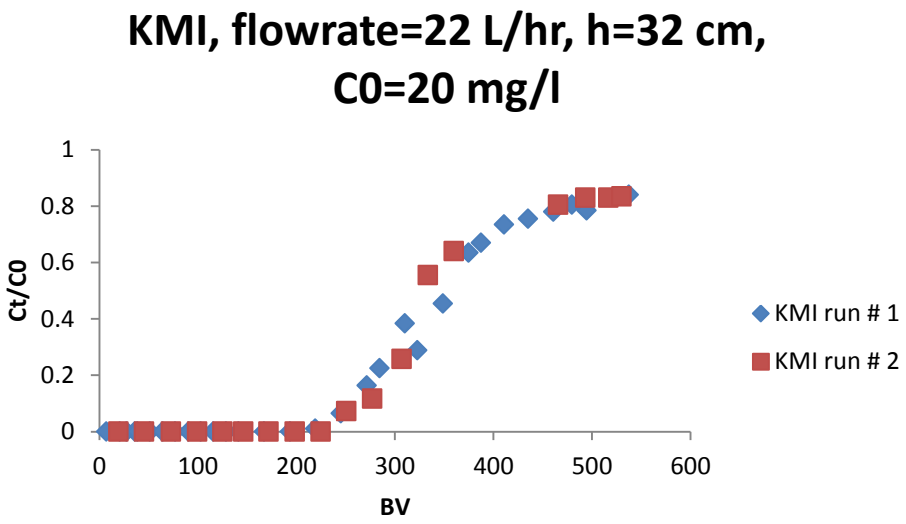

Figure 4.38: The breakthrough charecteristics for ammonium uptake onto KMI clinoptilolite for two runs. Downflow, initial ammonia concentration: 20 mg $N\text{-}NH_4^+$/l, particle size: 0.42-1.41 mm, flowrate: 13.7 BV/hr (22 L/hr), bed height: 32 cm.

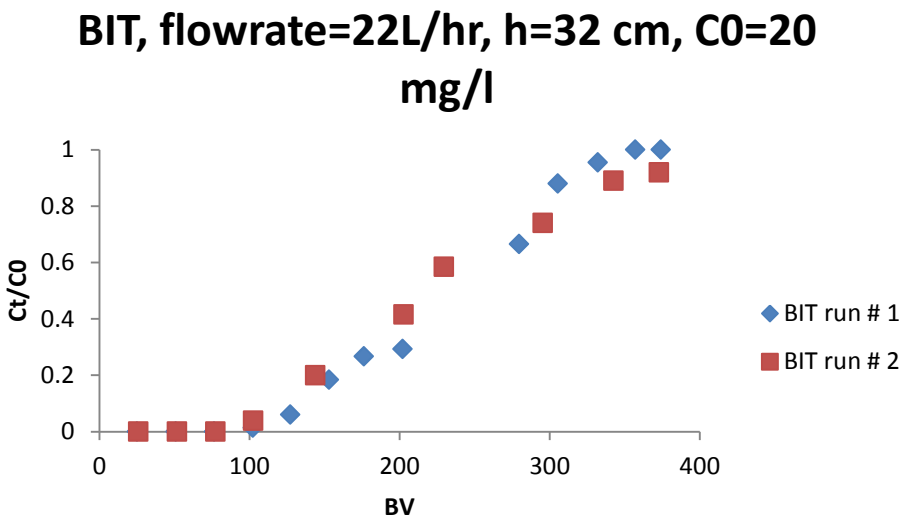

Figure 4.39: The breakthrough charecteristics for ammonium uptake onto BIT clinoptilolite for two runs. Downflow, initial ammonia concentration: 20 mg $N\text{-}NH_4^+$/l, particle size: 0.42-1.41 mm, flowrate: 13.7 BV/hr (22 L/hr), bed height: 32 cm.

One way to compare the breakthrough curves is by finding the breakthrough point which is the point where the column is unable to accommodate the exchange zone length, and it can be found by a specific percentage of C_t/C_0 on the breakthrough curve. It could be at 4% [5] or 5% [58]. For this work, 5% C_t/C_0 was chosen to indicate the breakthrough point. A demonstrative diagram is presented to how to find the breakthrough BV, see Figure 4.40. The uptake capacity was calculated for the KMI and BIT columns based on the calculations given in Appendix V. The breakthrough BV and the uptake capacities for Figure 4.38 and Figure 4.39 are tabulated in Table 4.25.

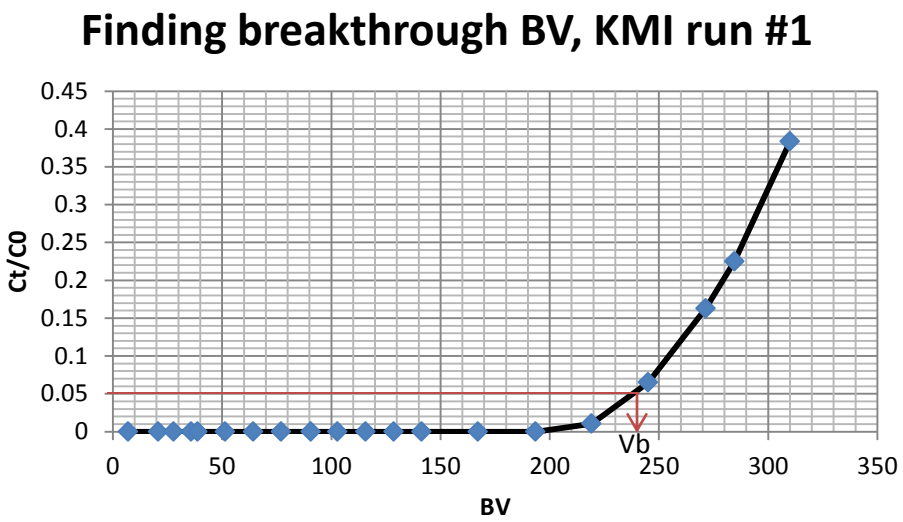

Figure 4.40: A representative figure of how to find the breakthrough BV.

Table 4.25: Breakthrough BV and uptake capacities for Figure 4.38 and Figure 4.39.

	KMI		BIT	
	Run # 1	Run # 2	Run # 1	Run # 2
5% Breakthrough point (BV)	240	240	120	110
Uptake column capacity (meq/g)	0.38	0.38	0.18	0.17

In all runs, batches of fresh KMI and BIT clinoptilolite were used. For the silicon tube column with height of 32 cm, the BV is equal to 1.605 L. The KMI breakthrough curves for both runs are sharper than the BIT breakthrough curves, and that is an indication of better performance of the KMI column over the BIT column. KMI breakthrough BV was found to be 240BV, while BIT breakthrough point started only after 120BV for the first run. This is a significant difference. A number of possible explanations may explain the difference in the breakthrough of KMI and BIT clinoptilolite columns. This may related to capacity differences between the two batches or

perhaps due to different structure characteristics which would influence the kinetics which in turn would be reflected in the breakthrough behavior. For the second run, the BIT column performed less well than in the first run since it was found that only 110BV of feeding solution was enough to saturate the BIT column. The uptake capacity of the KMI column is double the uptake capacity of the BIT column. Even in the batch equilibration uptake experiments, KMI performed better than BIT. Therefore; it was decided to continue the rest of the columns studies with the KMI clinoptilolite as an effective ion exchanger in the packed bed column.

Miladinovic and Weatherley [58], obtained a column capacity of 0.76 for the New Zealand clinoptilolite. However, the BV used in their work was 211.95 cm^3 and they used DI water instead of tap water. Also, the flowrate they used was 4BV/hr.

In the experiments discussed above, the feed solution was assumed to be free of Mg^{++}, K^{+}, and Ca^{++} ions which is not the case when treating real wastewater and thus, the uptake capacity is expected to be dropped.

To examine the effect of the aeration on the hydrodynamics of the silicon tube column, an experiment was conducted to check whether the aeration within the silicon column would have any impact on the ammonia removal. Figure 4.41 shows the comparison between the ammonia uptakes in the silicon tube column packed with KMI clinoptilolite with and without aeration. The breakthrough BV and the uptake capacities are presented in Table 4.26.

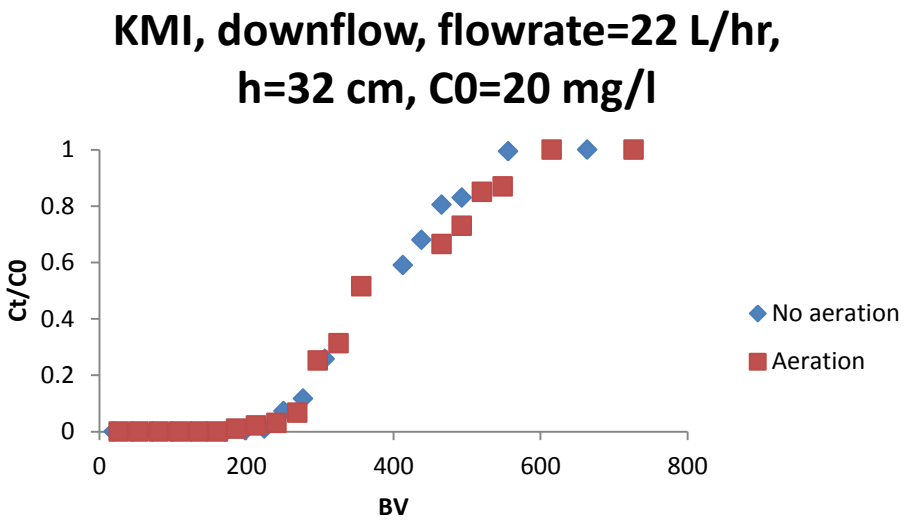

Figure 4.41: The uptake values for column packed with KMI clinoptilolite fitted with the silicon aeration tube. Downflow, initial ammonia concentration: 20 mg $N\text{-}NH_4^+$/l, particle size: 0.42-1.41 mm, flowrate: 13.7 BV/hr (22 L/hr), bed height: 32 cm, P=25.0 psi.

Table 4.26: Breakthrough BV and uptake capacities for Figure 4.41.

	KMI	
	No aeration	Aeration
5% Breakthrough point (BV)	240	260
Uptake column capacity (meq/g)	0.38	0.41

Based on Figure 4.41 and Table 4.26, it was found that the aeration slightly enhanced the uptake removal. It was observed during the experiment that large air bubbles were not formed which may have an impact on the mass transfer within the column. However, air is still introduced to the aerated column and it might enhance the ion exchange process. On the other hand if there is build up of gas hold-up in the column this may inhibit contact between the water and zeolite.

Also the effective residence time for the liquid flow through the column may be reduced in such cases. The previous study [58] showed no impact of aeration on the packed column performance.

The impact of the bed height on the column performance was examined. For the column fitted with the silicon aeration tube, two bed heights used, 27 cm and 32 cm respectively, and the results are presented in Figure 4.42. The breakthrough BV and the uptake capacities are presented in Table 4.27.

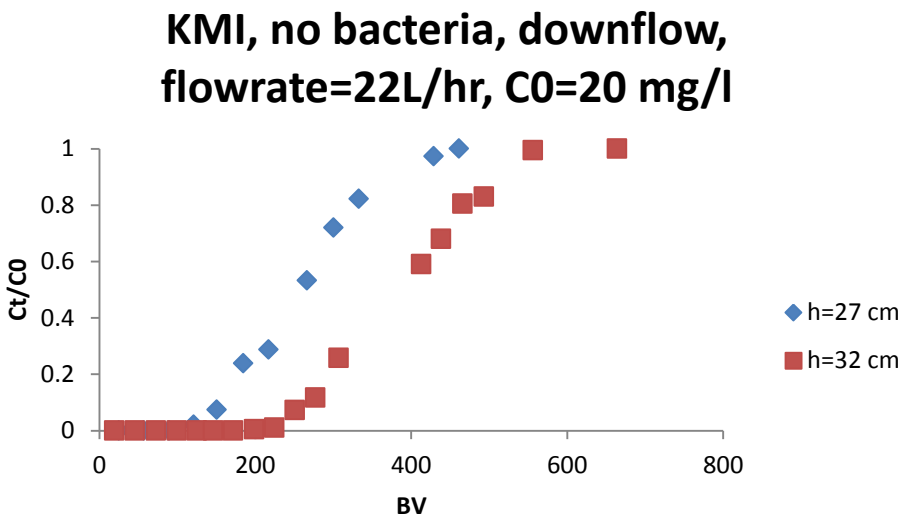

Figure 4.42: The impact of the bed height on the performance column fitted with silicon tube aeration tube. Downflow, initial ammonia concentration: 20 mg $N\text{-}NH_4^+$/l, particle size: 0.42-1.41 mm, flowrate: 13.7 BV/hr (22 L/hr)

Table 4.27: The breakthrough BV and the uptake capacities for Figure 4.42.

	KMI	
	h=32 cm	h=27 cm
5% Breakthrough point (BV)	240	140
Uptake column capacity (meq/g)	0.38	0.22

As expected, the higher the bed was, the more ion exchangers were existed in the column and as a result later breakthrough point was established. The low capacities obtained in Table 4.27 may referred to the high flowrate used (22 L/hr) and to the low initial concentration used in the experiment. Therefore, it was intended to modify the designed experiment parameters and to choose higher initial ammonia concentration. The next figure was conducted to test the flowrate impact on the silicon column performance packed with KMI clinoptilolite at initial ammonia concentration of 40 N-NH_4^+/l.

Table 4.28 shows the breakthrough BV and the uptake capacities for Figure 4.43.

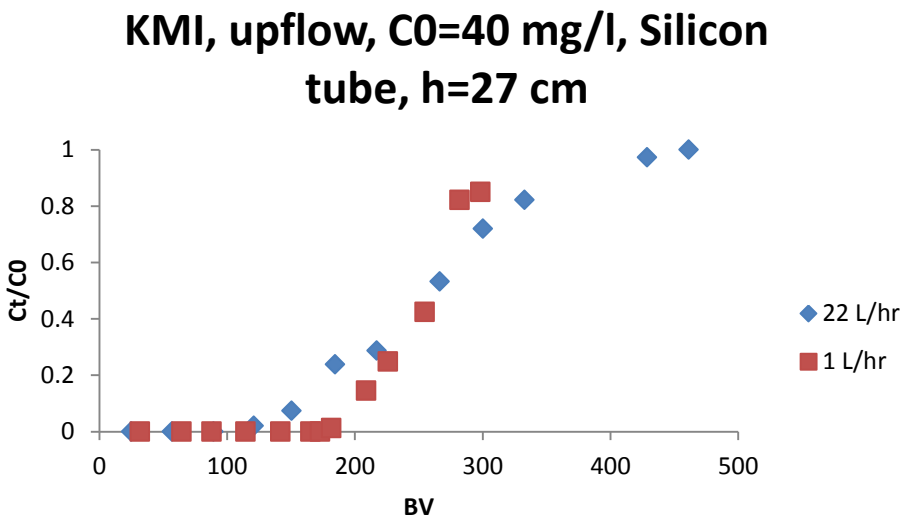

Figure 4.43: The impact of the bed height on the performance column fitted with silicon tube aeration tube. Downflow, initial ammonia concentration: 40 mg $N\text{-}NH_4^+$/l, particle size: 0.42-1.41 mm, bed height: 27 cm.

Table 4.28: The breakthrough BV and the uptake capacities for Figure 4.43.

	KMI	
	Flowrate = 13.7 BV/hr (22 L/hr)	Flowrate = 0.74 BV/hr (1 L/hr)
5% Breakthrough point (BV)	140	195
Uptake column capacity (meq/g)	0.45	0.63

When the flowrate was 0.74 BV/hr (1 L/hr), the start of the breakthrough was shifted towards the higher number of BV (195BV). As discussed in Section 2.2.3, the lower flowrate results in the better breakthrough curve as shown in Figure 4.43. Because of the low flowrate the confronted zone of ion exchanger was highly utilized. Hence, when the confronted zone reached the end of the column, the column was hypothetically 100 % utilized.

Obviously, the initial ammonia concentration has a significant impact on the column uptake capacity which was doubled as the initial ammonia concentration increased to 40 mg $N\text{-}NH_4^+$/l.

4.5.1.2 Silicon tube column with bacteria

In this section, the *Nitrosomonas europea* was loaded on KMI clinoptilolite column. Thus, the column became a biologically active column. Clinoptilolite in this case has a dual function, to support the *Nitrosomonas europea* as a surface and to capture ammonium ions from the feed solution. *Nitrosomonas europea* was supposed to oxidize the ammonium ion existing in the free solution. Figure 4.44 provides a comparison between the biologically active and non active columns which were both fitted silicon aeration tubes. The breakthrough BV and the uptake capacities for Figure 4.44 are presented in Table 4.29. The feed solution used in this part is ammonium chloride dissolved in filtered tap water. Nutrient, which was made of the chemicals that outlined in Section 3.2.4.4, was added to the 120 L storage tank.

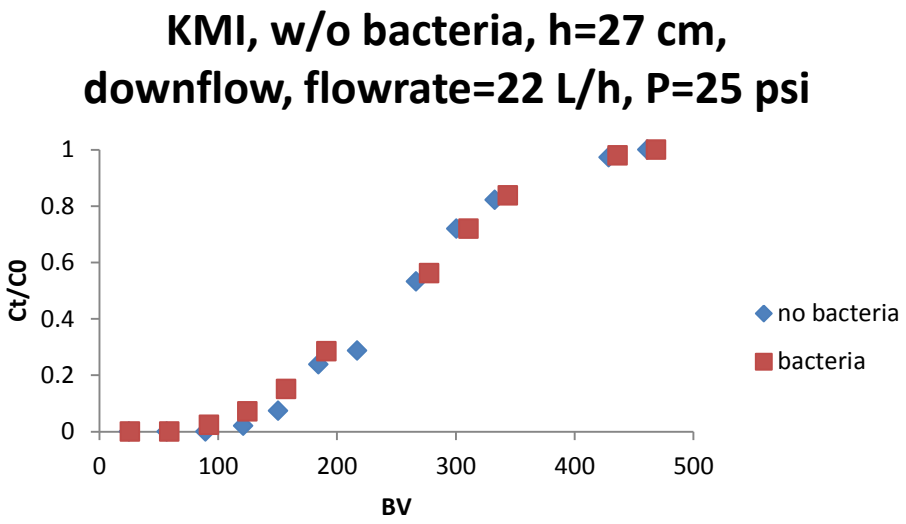

Figure 4.44: Column breakthrough biologically active and non active silicon tube column. Downflow, initial ammonia concentration: 40 mg $N\text{-}NH_4^+$/l, particle size: 0.42-1.41 mm, bed height: 27 cm, P=25 psi.

Table 4.29: The breakthrough BV and the uptake capacities for Figure 4.44.

	KMI	
	No bacteria	Bacteria
5% Breakthrough point (BV)	140	115
Uptake column capacity (meq/g)	0.45	0.37

No improvement was observed in the inoculated column when compared to the non active column. In fact, the uptake capacity of the active column is lower than that of the non active column, and the BV breakthrough was reached at 115BV. A possible explanation for this situation is that the silicon tube membrane was not introducing enough oxygen to the column and therefore the biological material became inactive material and block part of clinoptilolite surface

from exchanging ions. Hence, the performance of the active column reduced. Also, it must be mentioned that the flow rate was high compared to those studies in previous published research [3,5,6,58]. Therefore, it was chosen to reduce the flowrate to 4 BV/hr. The porous membranes exhibited high performance in the aeration studies and were expected to conduct oxygen with acceptable transfer rate. By eliminating these two drawbacks, some enhancement was expected in the porous membrane column when bacteria are loaded onto the column.

4.5.2 Porous membrane columns

Feed solutions, for the porous membrane columns, were exactly same as the feed solutions used for the studies on biological activity in the columns fitted the silicon tube membrane as previously described. The Bed Volume for the porous membrane column was 1.415L, and the flowrate was 4 BV/hr (5.6 L/hr). The air pressure was maintained at 1.5 psi for all columns.

4.5.2.1 PES membrane column

A comparison between the biologically active and non active PES membrane column is shown in Figure 4.45. Also, the breakthrough BV and the uptake capacities for Figure 4.45 are shown in Table 4.30.

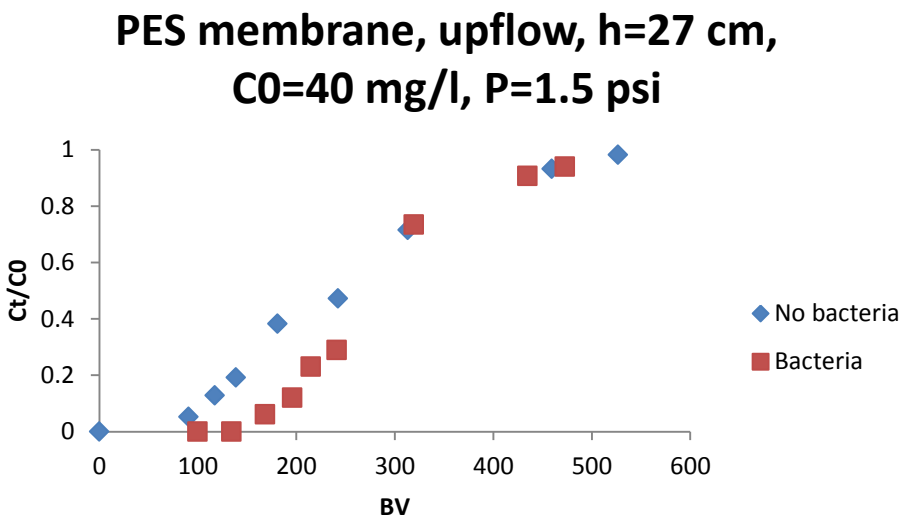

Figure 4.45: Biologically active and non active PES membrane column. Upflow, initial ammonia concentration: 40 mg N-NH_4^+/l, particle size: 0.42-1.41 mm, bed height: 27 cm, P=1.5 psi.

Table 4.30: The breakthrough BV and the uptake capacities for Figure 4.45.

	KMI, PES membrane	
	No bacteria	Bacteria
5% Breakthrough point (BV)	110	165
Uptake column capacity (meq/g)	0.38	0.56

As shown in Figure 4.45, the non active porous membrane column was performed well until 110 BV of synthetic wastewater had passed through the bed, while the biologically active porous column treated a further 55BV before breakthrough. This is a significant improvement, and the presence of bacteria in the column significantly enhanced the columns' performance. The effective breakthrough uptake capacity was increased from 0.38 to 0.56 meq/g. Miladinovic and Weatherley [58] noticed an increase in the breakthrough uptake capacity from 0.15 to 0.22 meq/g

when the bacteria were introduced to the column they used. In Figure 4.45, both curves behaved differently, and they had different slopes, where the active column had a sharper breakthrough curve.

4.5.2.2 PTFE membrane column

The performance of the biologically activated and non activated PTFE membrane columns is compared in Figure 4.46, and the breakthrough uptake capacities are shown in Table 4.31.

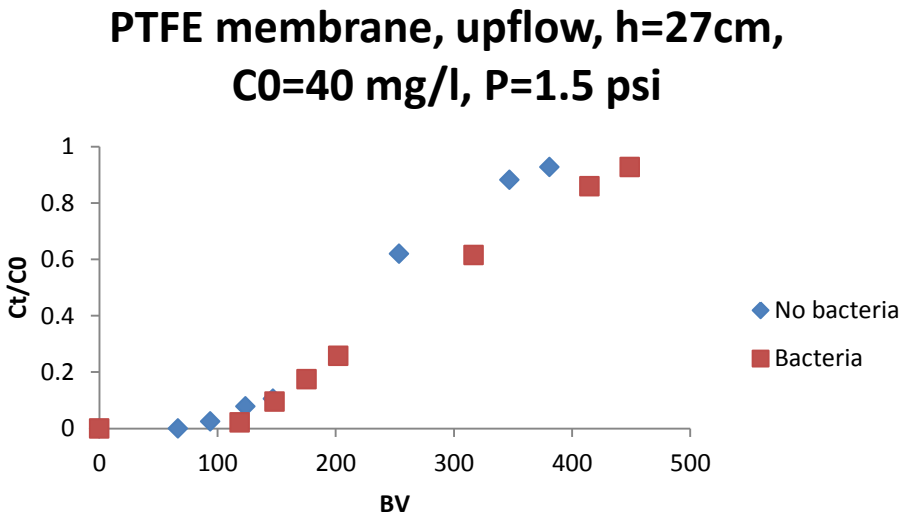

Figure 4.46: Biologically active and non active PTFE membrane column. Upflow, initial ammonia concentration: 40 mg N-NH_4^+/l, particle size: 0.42-1.41 mm, bed height: 27 cm, P=1.5 psi.

Table 4.31: The breakthrough BV and the uptake capacities for Figure 4.46.

	KMI, PTFE membrane	
	No bacteria	Bacteria
5% Breakthrough point (BV)	105	140
Uptake column capacity (meq/g)	0.35	0.47

The PTFE membrane column that contained bacteria performed better than the one without bacteria. The breakthrough capacity calculations in Table 4.31highlight this finding. However, the slope of curves behaved similarly, which means that bacteria only postponed the breakthrough and once it started, the kinetics of the physisorption process was much faster [58].

4.5.2.3 PP membrane column

Figure 4.47 shows the breakthrough curves for both the biologically activated and non activated PP membrane column. The breakthrough BV and the uptake capacities for Figure 4.47 are presented in Table 4.32.

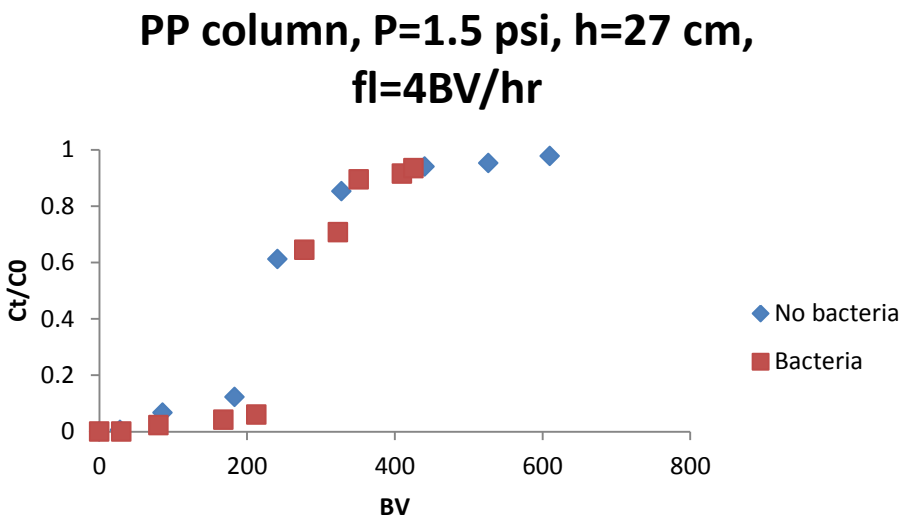

Figure 4.47: Biologically active and non active PP membrane column. Upflow, initial ammonia concentration: 40 mg $N\text{-}NH_4^+$/l, particle size: 0.42-1.41 mm, bed height: 27 cm, P=1.5 psi.

Table 4.32: The breakthrough BV and the uptake capacities for Figure 4.47.

	KMI, PP membrane	
	No bacteria	Bacteria
5% Breakthrough point (BV)	130	200
Uptake column capacity (meq/g)	0.43	0.67

The PP membrane column with the biologically active material performed better than the non active PP membrane column. The breakthrough uptake capacity jumped from 0.43 to 0.67 meq/g. Also, the active PP membrane column had sharper breakthrough column.

4.5.2.4 Nylon membrane column

The performance of the active and non active Nylon membrane column are presented in Figure 4.48, and the breakthrough BV and the uptake capacities based on Figure 4.48 are presented in Table 4.33.

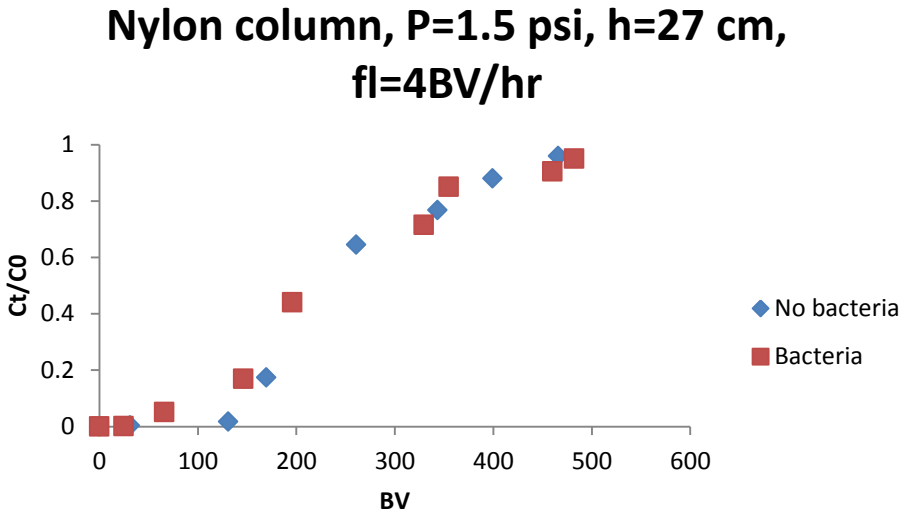

Figure 4.48: Biologically active and non active Nylon membrane column. Upflow, initial ammonia concentration: 40 mg $N\text{-}NH_4^+$/l, particle size: 0.42-1.41 mm, bed height: 27 cm, P=1.5 psi.

Table 4.33: The breakthrough BV and the uptake capacities for Figure 4.48.

	KMI, Nylon membrane	
	No bacteria	Bacteria
5% Breakthrough point (BV)	150	110
Uptake column capacity (meq/g)	0.51	0.37

Unlike other porous membranes columns, the non activated Nylon membrane column performed better than the activated column. Although the slopes of the breakthrough curves are similar. This might be on account of the relatively poor performance of the Nylon membrane as mentioned in the aeration studies described in Section 3.3.2.

The porous membrane columns in the presence of nitrifying bacteria show significant enhancement of ammonia removal as an evidence of the combination process (ion exchange process and nitrification) was being intensified.

4.5.3 Porous membrane columns: Comparison

In this section, a comparison between the porous membranes columns for those with and without biologically active material will be made. Figure 4.49 shows the performance of the porous membranes columns used in this work. Table 4.34 gave the calculated breakthrough capacities and breakthrough BVs.

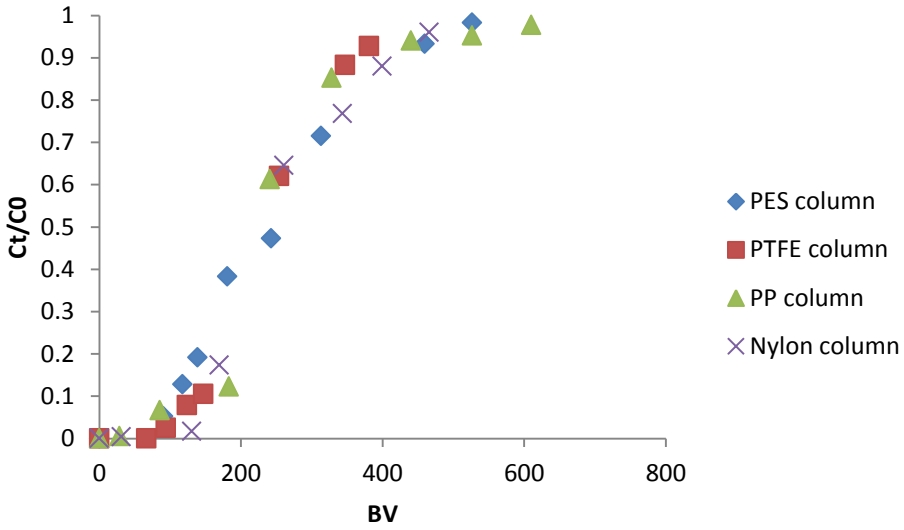

Figure 4.49: Biologically free porous membranes columns.

Table 4.34: The breakthrough BV and the uptake capacities for Figure 4.49.

	KMI, No bacteria			
	PES	PTFE	PP	Nylon
5% Breakthrough point (BV)	110	105	130	150
Uptake column capacity (meq/g)	0.38	0.35	0.43	0.51

The packed beds were set up with the same bed volume and the same particle size so the residence times were similar. Although breakthrough curves shown in Figure 4.49 had slightly different breakthrough points, within the limits of experimental error they share the same breakthrough curve profile. The 0.1 μm pore size membrane, PP and Nylon, had the highest treated volumes of feed solution before the breakthrough took place, while the membrane with the 0.2 μm pore size were the membranes that had the lowest BVs at the breakthrough point. The column fitted with the Nylon membrane had the highest breakthrough capacity of 0.51 meq/g. Since the permeability of the porous membrane is not the same as shown in the aeration studies, the amount of air existing in each column during the cycle was also different. Thus, the presence of air could affect the column hydrodynamics and thus the uptake capacity of each column. During the experiments, bubbles were formed and this observation might support the effect of aeration on the columns hydrodynamics.

It seems, by reviewing the literature, the type of the feed solution has a great impact on the column capacity. Miladinovic and Weatherley [58] used DI and creek water as a feed solution for the non active column and the column capacity dropped from 0.76 to 0.48 meq/g respectively for the New Zealand clinoptilolite column. The batch studies described in this work, where the

effects of presence of other major metal ions were studied, confirmed this finding as the metal ions are expected to compete with ammonium ions for the clinoptilolite vacant sites.

Figure 4.50 introduced the comparison between the biologically activated porous membrane columns, and the breakthrough BV points are given in Table 4.35

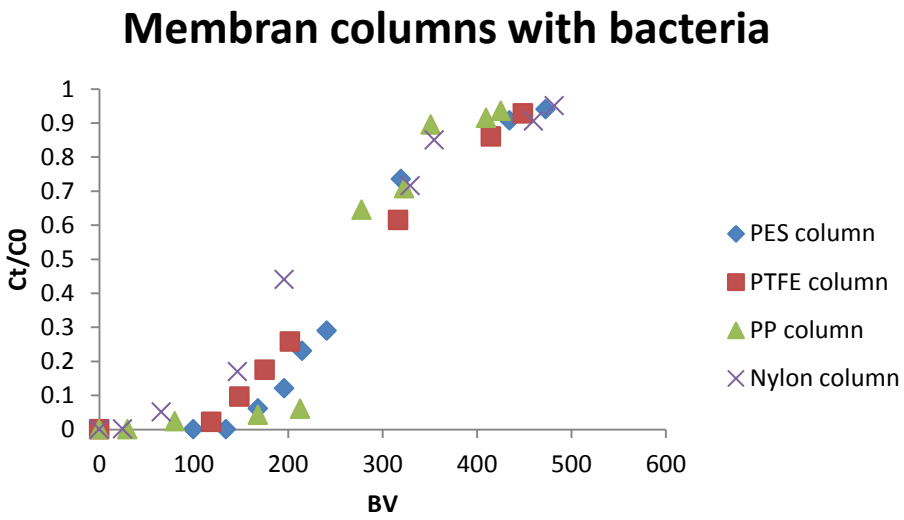

Figure 4.50: Biologically active porous membranes columns.

Table 4.35: The breakthrough BV and the uptake capacities for Figure 4.50.

	KMI, Bacteria			
	PES	PTFE	PP	Nylon
5% Breakthrough point (BV)	165	140	200	110
Uptake column capacity (meq/g)	0.56	0.47	0.67	0.37

The feed solution used for the biologically active and non active porous membrane columns was the same. This was to quantify the impact of presence of nitrifying bacteria on the removal of ammonium ion. The ammonium ion concentration in the inlet feed was chosen to be 40 mg N-NH_4^+/l instead of 20 mg N-NH_4^+/l, since the nitrification kinetics would be improved due to the higher substrate concentration within the ion exchange column. Initially 50 ml of rich nitrifying bacteria were added to a solution of very low ammonia ion concentration (1-0.5 mg N-NH_4^+/l). The bacteria concentration of the combined solution was measured at OD600 by spectrophotometer and then it was circulated in the column to loaded the bacteria on the column. Bacteria concentration of the effluent solution was re-measured at OD600. Time was allowed for bacteria to be attached and immobilized. For example, the biomass of the PP membrane column was measured before the bacteria solution was introduced to the column and the absorbance was found at OD600 equal to 0.062 and after the bacteria solution circulated it was found that its absorbance was 0.023 when measured at OD600. The binding effeciecny of bacteria was then calculated and it was 63%. In all the columns, the attached bacteria were more than 60% of the

circulated bacteria. The remaining bacteria were either washed out or were unable to attach to the clinoptilolite.

The PP membrane column was found to be the best column that had the highest performance and the highest breakthrough capacity of 0.67 meq/g. Followed by PP, PES membrane column came secondly with a breakthrough uptake capacity of 0.56 meq/g. There was a significant difference in the PP and Nylon membrane columns performance, although they shared the same pore size which is 0.1 μm. There are some differences in the profiles of breakthrough curves. The PP breakthrough curve had a sharp S-shaped curve comparing to other porous membrane breakthrough curves, followed by PES membrane column. The PTFE and Nylon breakthrough curves although S-shaped overall are flatter. Obviously, biological material only improved the ammonia removal process before breakthrough was reached since all curves had the same general S-shape. KMI clinoptilolite, apparently, has the ability to act as a support for immobilized bacteria. These results confirmed that the adsorption method as an immobilization technique was found to be an effective method. It was simple to implement and it was found to be an economic method to apply. Table 2.4 provides a summary of the previous researcher's results on the batch and column capacity. Different researchers used different setup design, materials, and operational conditions. However, Table 2.4 was helpful especially in the design stage of this work and most of the provided results in this table were compared to the results in this work.

The nitrite concentration was measured for the porous membrane columns based on the procedure given in Section 3.3.2. Figure 4.51 and Figure 4.52 shows the nitrite production of biologically enhanced PES/PTFE and PP/Nylon membrane columns, respectively.

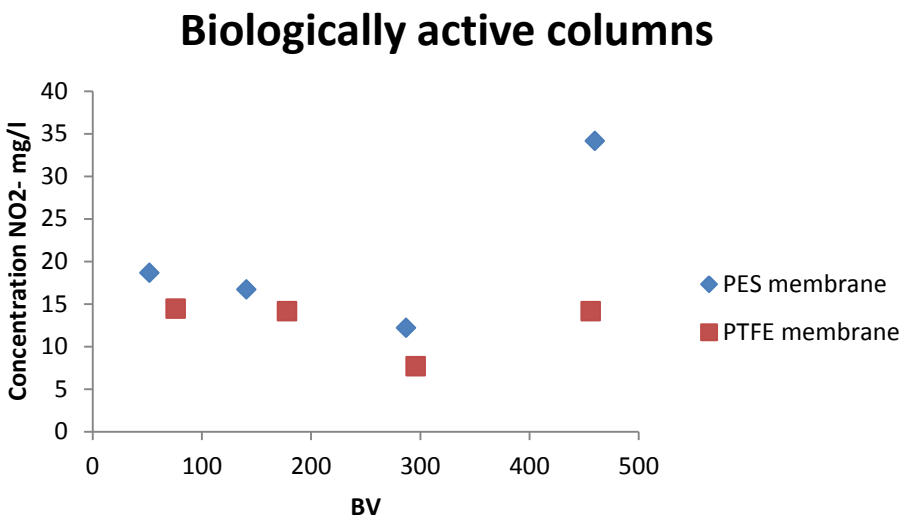

Figure 4.51: Nitrite production of biologically enhanced PES and PTFE membrane columns.

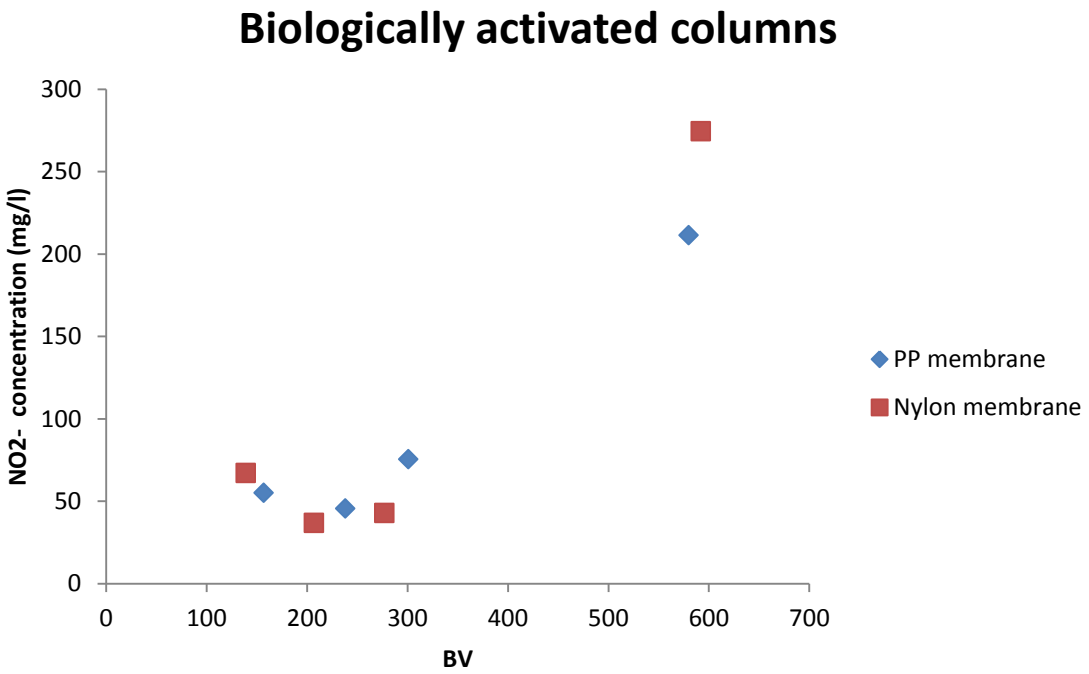

Figure 4.52: Nitrite production of biologically enhanced PP and Nylon membrane column.

Figure 4.51 and Figure 4.52 show the production of nitrite during the uptake runs, comparing columns fitted with each of the four different membranes. The nitrite concentration of the eluents

from the PES and PTFE columns ranged between 5 and 20 mg NO_2^-/l until a sudden exponential increment occurred at approximately 450BV. The same observation was noticed for the PP and Nylon column with an increment occurred at the end of the experiment. More nitrite was produced within the PES column compared to PTFE column. This agrees with breakthrough capacity calculations as PES showed higher breakthrough capacity. More nitrite was produced in the PP and Nylon fitted columns compared to the PES and PTFE columns. For 300BV, as shown in Figure 4.52, PP column had higher nitrite concentration than Nylon column. Around 600BV, nitrite concentration in the Nylon column is higher than the PP column. A possible explanation for this behavior is that Nylon column reached the breakthrough point 90BV earlier than PP, therefore; the Nylon column reached 100 % exhaustion earlier than the PP column. The time required for the PP column to reach 100 % exhaustion was the same as for the experiment in which ammonia was only removed in Nylon column by bacteria. This would help explain why the high nitrite concentration in the eluent occurred in the last stages of the experiment. This was not the case in the PES/PTFE columns, since both columns reached breakthrough closely. Next figure shows the oxygen concentration through biologically active and non active PP and Nylon membrane columns.

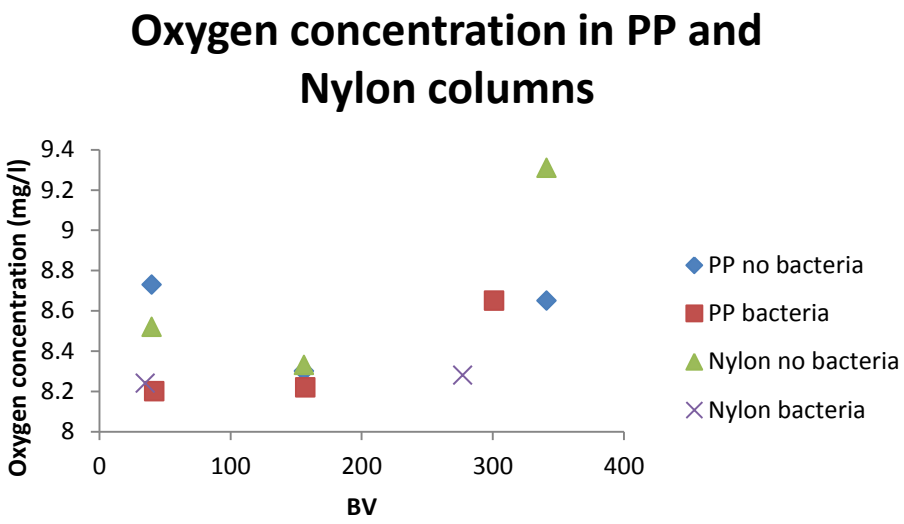

Figure 4.53: Oxygen concentration through biologically active and non active PP and Nylon membrane columns.

There is a significant indication found in Figure 4.53 that the bacteria-free columns, for both PP and Nylon, had higher oxygen concentration than the biologically activated columns. The difference may be readily explained by the lack of nitrification in the bacteria-free columns.

Aeration, in general, is the more expensive element in the wastewater treatment plants. Porous membrane based columns drastically intensify the oxygen concentration in the packed bed column compared to the dense membrane column, and as a result the cost of the overall process will be lower.

Next, the bacteria-free porous membrane columns (PES, PTFE, PP, and Nylon) are modeled with Thomas model and Bohart-Adams model. The uptake models are shown in Figure 4.54-Figure 4.57.

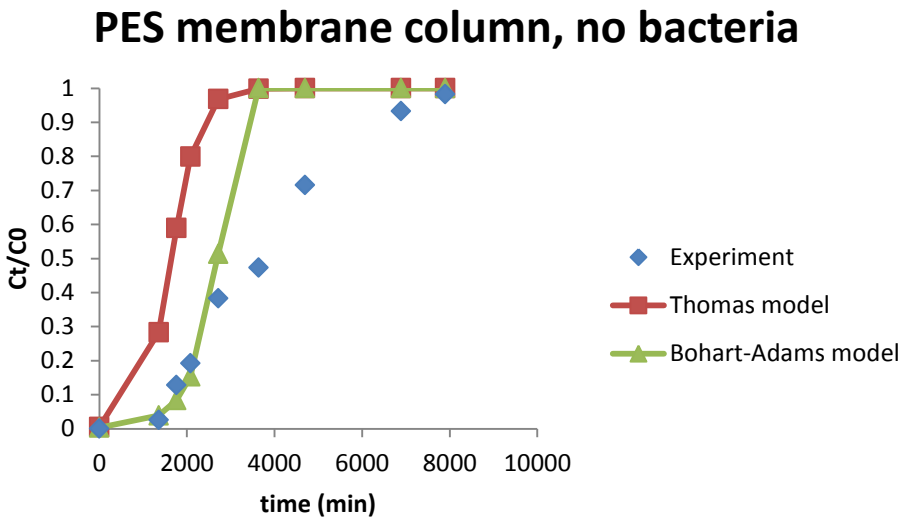

Figure 4.54: Bacteria-free PES membrane column uptake modeling.

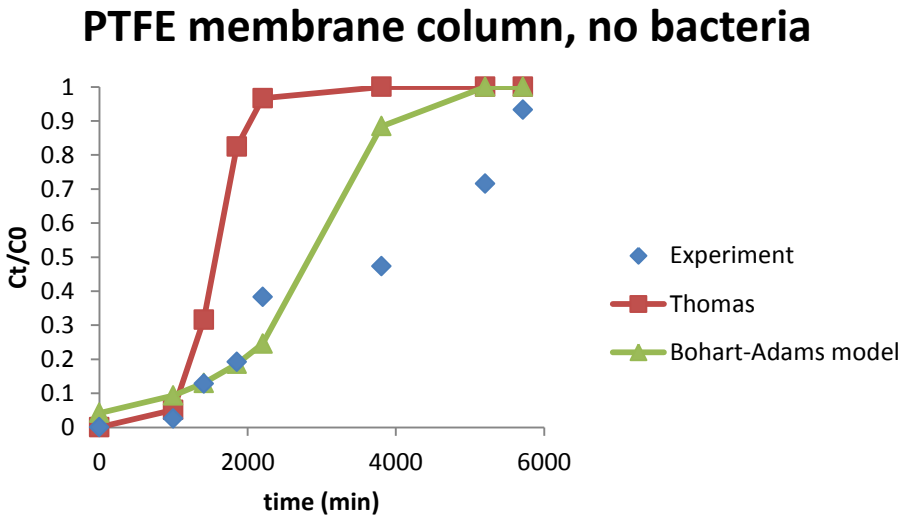

Figure 4.55: Bacteria-free PTFE membrane column uptake modeling.

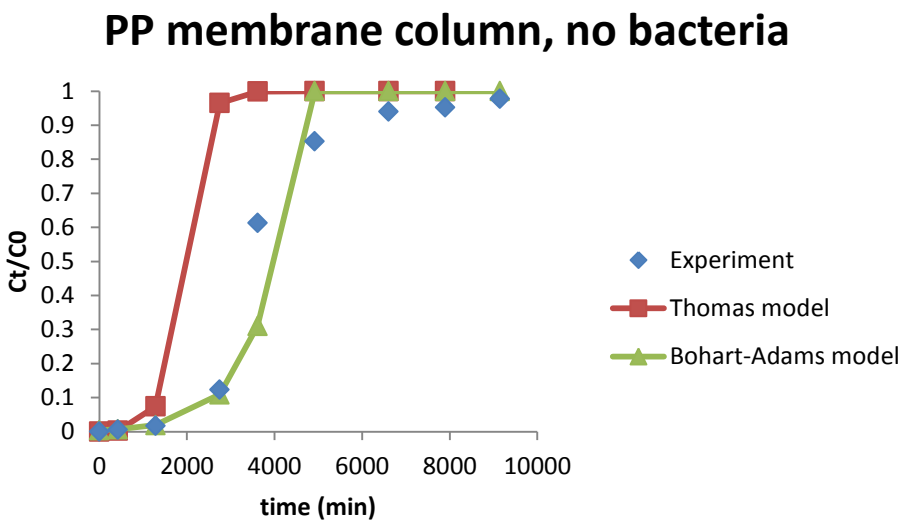

Figure 4.56: Bacteria-free PP membrane column uptake modeling.

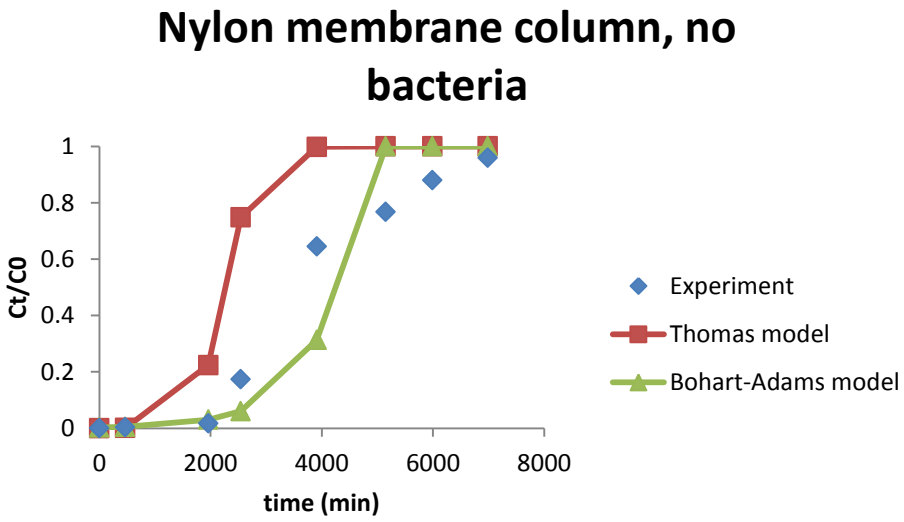

Figure 4.57: Bacteria-free Nylon membrane column uptake modeling.

The Bohart-Adams model and Thomas model for adsorption / ion exchange uptake in columns, were discussed in Section 2.2.3. Appendix VI shows the detailed calculations of both the Bohart-Adams model and the Thomas model. The Bohart-Adams model simulated the experimental data more closely than the Thomas model. The Bohart-Adams model predicted the breakthrough point with high accuracy. After the breakthrough point, the Bohart-Adams model did not reflect the experimental data. Therefore, it is trustable model that can be used during the design of an experiment, such as for determination the needed height of the packed bed to reach certain percentage of exhaustion. On the other hand, the Thomas model did not show significant simulation to the experimental data. The Thomas model prediction for the breakthrough point was not good.

The Thomas model is quite complex and determination of the Thomas model's constants such as k_{TH}, the Thomas rate constant, and q_0, the equilibrium uptake capacity, is not a straight forward step; therefore, these constants were borrowed from the literature. For some figures, manipulation with these constants is required to get the best fit. This might be a possible explanation of the unsatisfied fits that were obtained.

The Bohart-Adams model on the other hand, its constants can be determined using the obtained data. However, most of the published works that used Bohart-Adams model obtained the constants values such as the k_{AB}, the kinetic constant, and N_{AB}, the saturation constants, by running experiments at different flowrates and at different bed depths, thus; these constants help to fit the data better. As the case in this work, only one data point at a specific flowrate and at a specific bed depth was used, therefore; less predicted fit was expected. Moreover, the Bohart-Adams model was first proposed to predict the carbon adsorption column behavior, and applying

this model for an ion exchange column might need further modification to meet the ion exchange process behavior.

4.5.4 Bio-regeneration Columns

Experiments in this part were followed the procedures given in Section 3.2.5. The PP and PES membrane columns had the best performance among the porous membrane columns and it was decided to conduct the bio-regeneration column experiment using these two columns, i.e., PP and PES membrane columns.

As discussed in Section 1.4.7, ion exchange regeneration is an expensive process and improvements to the regeneration process can result in economic benefits.

Batches of exhausted KMI clinoptilolite, i.e., in the ammonium form, were packed within both the PP and PES membrane column. A 50 ml sample of rich bacteria solution was added to 3 L of media solution and the combined solution circulated through each column. The nitrite concentration was taken periodically as explained in Section 3.3.2. After 15 days the experiment stopped, and samples were withdrawn at different heights of each column. Each sample was equilibrated with 100 ml of ammonium ion solution at a concentration of 20 mg $N\text{-}NH_4^+$/l. Figure 4.58 shows the bio-regeneration of exhausted KMI clinoptilolite packed in PP and PES membrane columns.

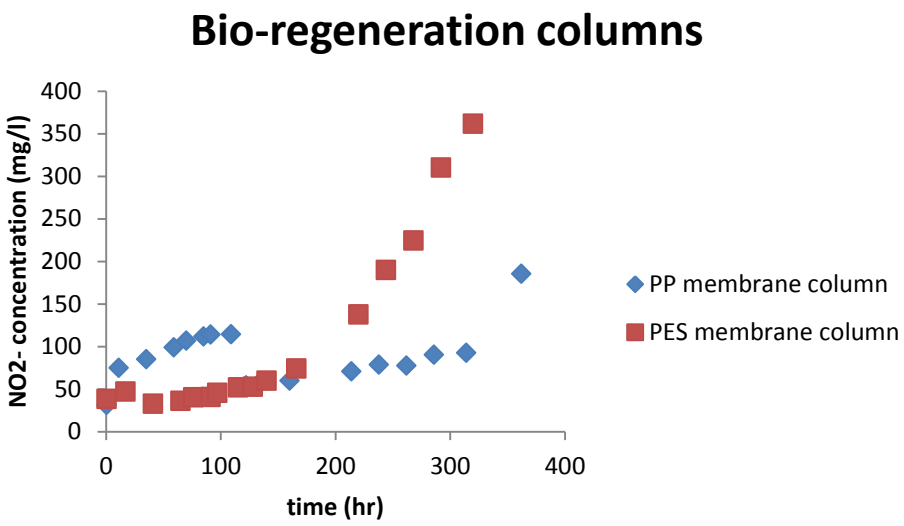

Figure 4.58: Bio-regenerationof exhasuted KMI clinoptilolite packed in PP and PES membrane columns.

Nitrite was detected in the collected samples as shown in Figure 4.58. In PP membrane column, nitrite concentration oscillates between 50 and 130 mg/l. During the experiment, a makeup solution of the inoculation media was added as needed. It was needed to add a makeup solution at t=109 hr. 95% of the media used in the circulation was changed for the PP column and 35 % for the PES column. That was needed as a failure occurred in the pump's tube. This might explain the dome in the PP column curve. After this dome, PP column curve started to increase. For the PES column curve it was not affected so much by the makeup addition.

The batch experiment equilibration data for the biologically regenerated KMI clinoptilolite obtained from the PP and PES column at different height is shown in Figure 4.59 and Figure 4.60 respectively.

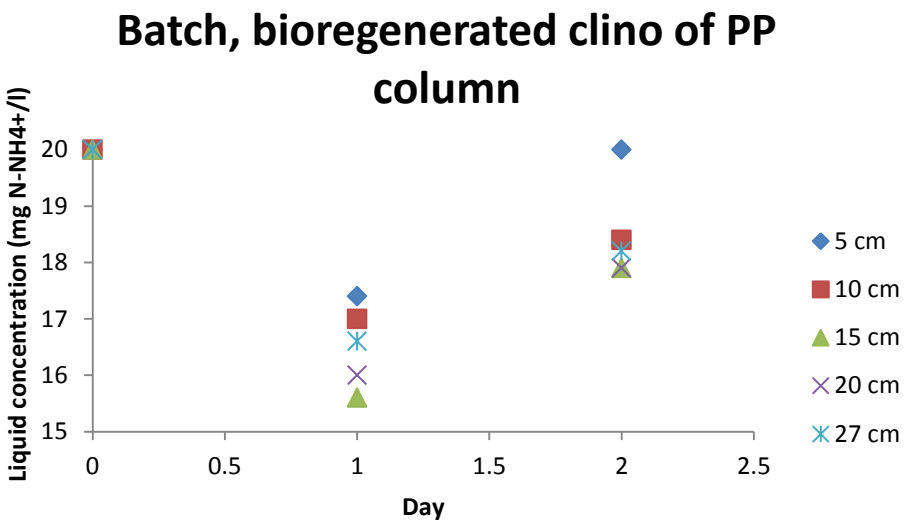

Figure 4.59: Batch experiment equilibration for the biologically regenerated KMI clinoptilolite obtained from the PP column.

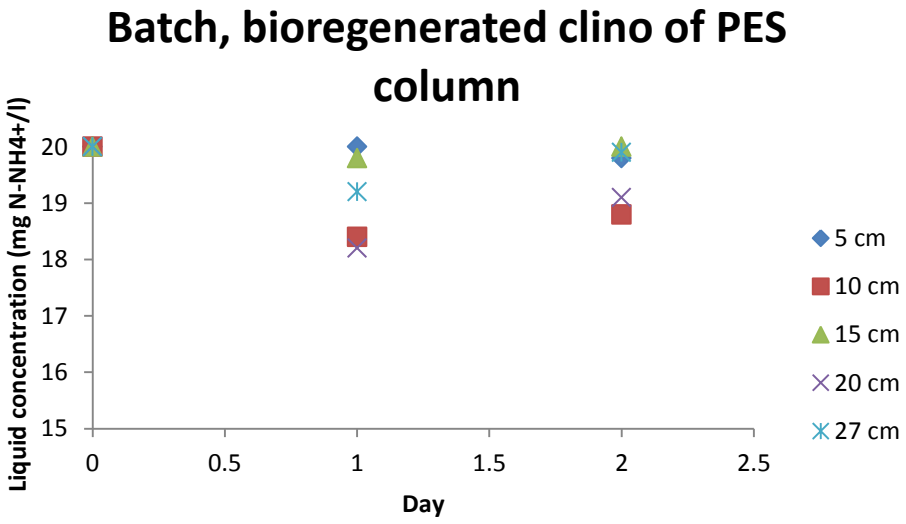

Figure 4.60: Batch experiment equilibration for the biologically regenerated KMI clinoptilolite obtained from the PES column.

It was unknown where exactly the bacteria inoculated inside columns, therefore, samples were taken from different height of the columns. For the PP column, the sample taken at column height of 15 cm gave the best ammonia removal, while that for the PES column it was the sample taken from 10 cm height.

As shown in Figure 4.59 and Figure 4.60, the removal of amminia by the bioregenerated clinoptilolite is not even close to compete with the removal of ammonia by clinoptilolite that chemically conditioned. A possible explaination for this huge difference in the two removal rates is that both columns were packed with 1200 g of zeolite but only 50 ml of rich nitrifying bacteria solution were introduced to each column. The indications are that this amount of bacteria was not enough to fully regenerate the exhausted clinoptilolite biologically. Indeed, literature supported this conclusion as Semmens and Goodrich [31] used 3 L of nitrifying bacteria to bio-regenerate only 5 g saturated with ammonium ions. Therefore, it is concluded that the small amount of nitrifying bacteria used was the primary reason for the ineffective results shown in the two previous figures.

5 Conclusion

5.1 Material analysis

The electron scanning microscope (SEM) analysis indicated that both clinoptilolite types (KMI and BIT) used in this work had available pores, which have sites for ion exchange. The clinoptilolite structure can be seen more clearly for KMI clinoptilolite. From the micrographs, BIT clinoptilolite appears to be more porous than the KMI form. XRF and EDS analysis revealed that both KMI and BIT had an average Si/Al ratio comparing to clinoptilolite from other parts of the world.

5.2 Batch equilibrium studies

In batch equilibrium studies, KMI clinoptilolite exhibited higher ammonia uptake capacities comparing to BIT clinoptilolite. No significant effect on ammonia removal was noticed when using different types of water (DI, RO, filtered tap water) on KMI or BIT clinoptilolite. The presence of the metal ions, K^{+}, Ca^{++}, and Mg^{++} affected the uptake capacity of ammonium ion by KMI clinoptilolite which indicates that metal ions compete with ammonia. KMI clinoptilolite preference was found to be $Mg^{++} \approx K^{+} > Ca^{++}$. To model the uptake data, Langmuir and Freundlich models were used. The Langmuir model provided the best fit for the equilibrium data obtained on KMI and BIT clinoptilolite.

5.3 Kinetics studies

Two analytical models were used to describe the rate behavior of KMI and BIT clinoptilolite. The proposed analytical models were originally used for modeling of the uptake data onto activated carbon; however these models were found to be applicable to describe the ion exchange

process. Two resistances were considered, the film and the intraparticle resistances, and each model described the associated resistance effectively.

5.4 Aeration studies

Five air permeable membranes were used in this part, four porous membranes and a dense membrane. The porous membranes were PES, PTFE, PP, and Nylon. The dense membrane was a silicon tube membrane. SEM analysis was carried out for the porous membrane to examine its structures. Different air pressures were used for aeration. The oxygen transfer rate for the membranes used was in the following order from the highest to the lowest: PTFE, PP, PES, Nylon, and silicon tube.

5.5 Column studies

In this section, all types of membranes listed above were evaluated for with and without the presence of nitrifying bacteria. KMI clinoptilolite, also, was used in the packed beds for evaluation of each type of membranes namely the dense membrane and the porous membranes. Because of its poorer ion exchange performance comparing to KMI, BIT clinoptilolite was used only in the silicon membrane column as a basis for comparison.

Packed bed performance was evaluated using breakthrough curves expressed as the fraction of exhaustion, Ct/C0, plotted against the treated effluent Bed Volumes passed. The breakthrough performance of KMI clinoptilolite packed bed was successfully modeled using the Bohart-Adams model and the Thomas model. However, the Bohart-Adams model seemed to be more reliable in predicting the breakthrough point. The uptake capacities were calculated and tabulated for each run.

A high loading rate for the silicon tube membrane column was used, 0.96 Kg N/(m^3day). In the case of porous membranes columns a lower loading rate of relatively low, 0.25 Kg N/(m^3day), was used.

The combined process in the biologically activated ion exchange column, was successfully applied for the porous membrane columns. This was not the case for the silicon tube membrane column. The PP and PES columns performed well comparing to the other porous membrane column. Comparing to the design of the silicon tube membrane module, porous membrane modules occupied less space. Hence, the column design was intensified toward a compact column.

An attempt was made to regenerate the exhausted clinoptilolite biologically in a packed bed column. It seemed the nitrifying bacteria were functioning but not sufficiently to fully regenerate the entire bed over the duration of the experiment. It is concluded that full regeneration is achievable if a higher concentration of biomass were present.

6 Future work

Below, a number of recommendations that might be useful to extend this research:

- Use different natural zeolite other than clinoptilolite such as mordenite, since mordenite was found by previous researchers as an alternative ion exchanger that might function better than clinoptilolite. Mordenite occurs naturally so economically should cost relatively the same as clinoptilolite. Try the sodium form conditioning of ion exchangers at different temperatures to find the optimum temperature that yields to the highest uptake removal rate of ammonium ions.
- To test the ion exchanger performance in presence of the metal ions, it is suggested to use different concentrations of the metal ions to examine to which extent those ions affect ammonium ion removal. Use high concentrations (500, 1000, 1500 mg NH_4^+/l) of ammonium ions and add 6 ml of metal ions (40, 50, 60, and 80 mg metal ion/l) to obtain high solid concentration, Q_e, in order to examine the performance of Langmuir and Freundlich models.
- One of the most challenging issues in the combined process is knowing the amount and concentration of the biomass that should be loaded to the packed bed column without losing significant capacity of the ion exchanger. Therefore, equilibration of biologically active ion exchanger bench experiments are recommended to test the performance of the uptake ammonium ions removal rate in the presence of bacteria to examine the optimum amount of biomass per gram of clinoptilolite. This can be done using small columns. By knowing the amount of the ion exchanger used and by measuring the inlet and outlet of the bacteria rich solution concentrations (at OD600), the ratio of biomass concentration to the amount of ion exchanger used can be determined. Once the optimum ratio is

determined, it can be used for a scale-up calculation. To check the effectiveness of the scale-up calculations, different ratios can be used within the optimum ([biomass]/g ion exchanger) ratio to find the optimum ratio for packed bed column.

- Instead of using air, use enriched air or pure oxygen with different pressures.
- Try new hydrophobic micropores membranes such as those introduced by W.L. Gore and Associates Inc. (www.gore.com) as these membranes could be cheaper than the porous membrane and more readily applicable to be incorporated into the packed bed column.
- As section 2.5 discussed the transport phenomena, the equations given in this section can be solved using finite element method. Solving those partial differential equations can be an alternative of using Bohart-Adams and Thomas model.
- Use suitable amount of biomass to assess the bio-regeneration column. Nitrate is recommended to be measured even though Nitrobacter were not inoculated into the packed bed column.

7 Appendices

Appendix I: Standard Calibration Curve of Nitrite

Based on the procedure given in the "Simplified Procedures for Water Examination" manual the 5th edition, page 137, the nitrite calibration curve was obtained. Table 7.1 shows the calibration curve data.

Table 7.1: Nitrite standard calibration curve.

Nitrite concentration, mg/l	Absorbance (A.U.)
0	Blank, 0
10	0.032
20	0.062
40	0.124
60	0.183
80	0.253
100	0.307
200	0.622

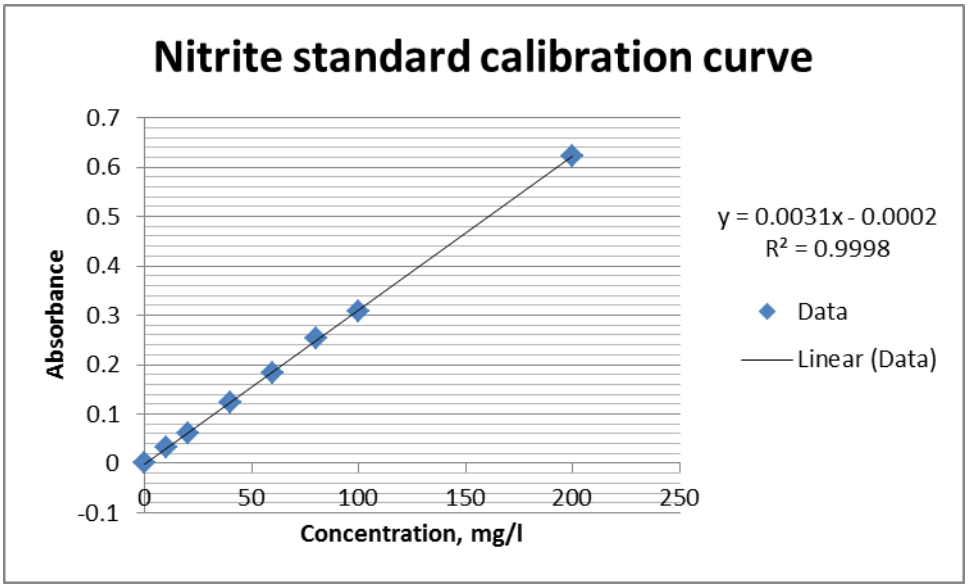

Figure 7.1: Nitrite standard calibration curve.

From the linear regression, the equation of the best fit line is:

$$\text{Absorbance} = 0.0031 * \text{Concentration} - 0.0002$$

Appendix II: Uncertainty calculations of nitrite standard calibration curve

Calculating uncertainties from nitrite standard calibration curve is a process of three steps.

1) Obtain the equation relating absorbance and concentration. This step is done in Appendix I, and the equation of the best fit is found from the linear regression, Equation A1:

   Absorbance = 0.0031*Concentration – 0.0002

2) Calculate the errors in the slope and intercept:

   $x_{avg} = 63.75$; $y_{avg} = 0.198$; $S_{yy} = \sum_{i=1}^{n} (y_i - \bar{y})^2 = 0.286$; $S_{xy} = \sum_{i=1}^{n} (x_i - \bar{x}) * (y_i - \bar{y}) = 91.923$;

   $S_{xx} = \sum_{i=1}^{n} (x_i - \bar{x})^2 = 29587.5$ (with n =8)

   $S = \sqrt{\frac{S_{yy} - m * S_{xy}}{n-2}} = 0.0027$; $SE(b) = S * \sqrt{\frac{1}{n} + \frac{\bar{x}^2}{S_{xx}}} = 0.512$; $SE(m) = S/\sqrt{S_{xx}} = 1.611E\text{-}5$

3) Absorbance = (0.0031 + t*SE(m)) * Concentration+ (0.0002+ t*SE(b))

4) At 95% confidence interval (Degrees of freedom = 8-2 =6) t = 2.45

5) Absorbance = (0.0031 ± 3.95E-5) * Concentration+ (0.0002± 1.2544)

   Reference: D. Neal Boehnke and R. Del Delunyea “Laboratory Experiments in Environmental Chemistry” p. 17-35.

Appendix III: Langmuir and Freundlich

The modeling of the batch experimental results will be explained by using data obtained for KMI clinoptilolite without interfering cations.

Langmuir adsorption isotherm

The soild concentration was calculated based on mass balance, and the next table shows the solid concentration, Q_e, for different initial ammonia concentration along with the equilibrium concentration of ammonia in the solution, C_e:

Initial ammonia concentration, mg N-NH_4^+/l	C_e	Q_e
20	3.90	1.688
80	15.6	6.752
300	144	18.48
400	224	22.08

When the linear form of the Langmuir model was applied:

$$\frac{1}{Q_e} = \frac{1}{KbC_e} + \frac{1}{b}$$

And 1/Qe vs 1/Ce was plotted, the following figure was obtained:

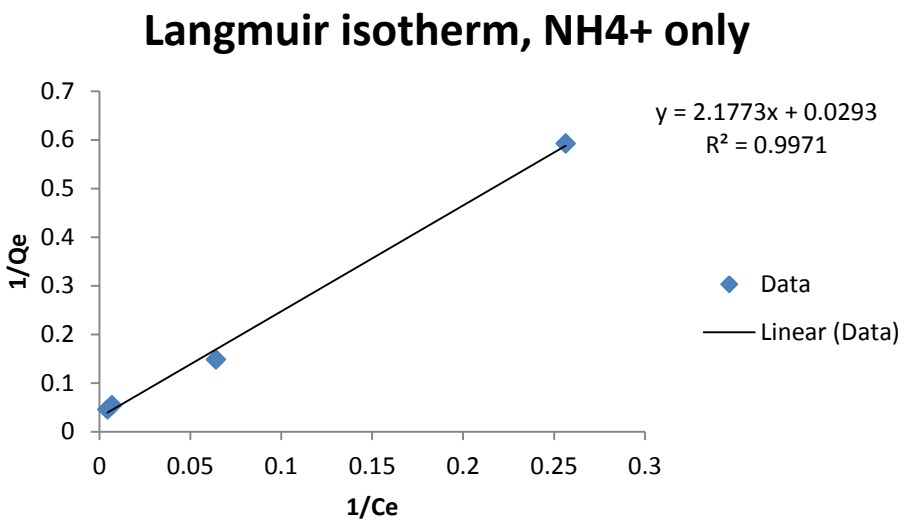

The following values were obtained from the graph:

1/b = 0.0293 ➔ b = 24.13

1/(Kb) = 2.1773 ➔ K=0.0135

By using the constants obtained and the measured concentration C_e, the values for the Qe(Lang) were obtained by using the equations:

$$Q_e(Lang) = \frac{1}{\frac{1}{Kb} + \frac{1}{b}}$$

Freundlich adsorption isotherm

To model the results by using the Freundlich adsorption model the values for C_e and Q_e obtained above were used. The linear shape of the Freundlich isotherm is:

$$\log Q_e = \log k + \frac{1}{n} \log C_e$$

By plotting the logQe vs log C_e the following graph was obtained:

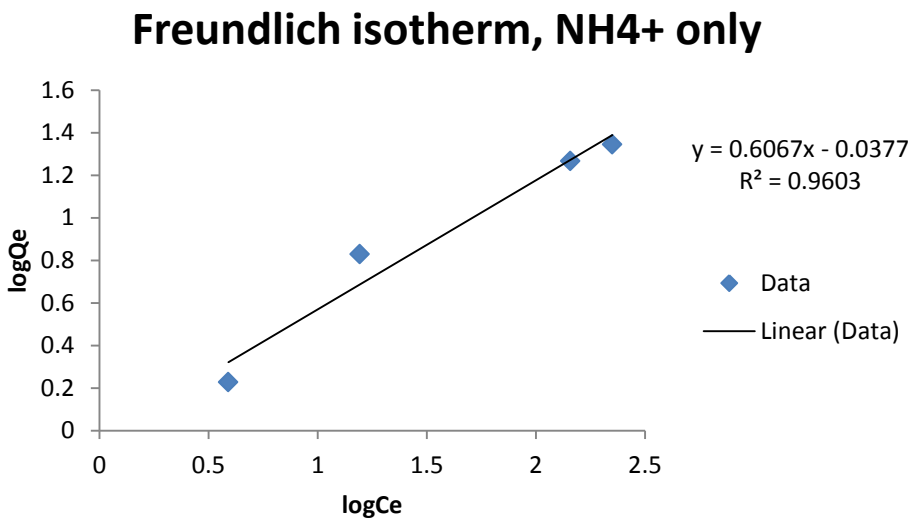

The values for the coefficients obtained from the graph were:

log k = -0.0377

1/n=0.6067

By using the following equation and the obtained values for the coefficients, the values for $Qe_{(Fr)}$ were obtained:

$$\log Q_{e(Fr)} = \log k + \frac{1}{n} \log C_e$$

The calculated values for the whole range of concentrations were as follows:

Ci	*Qexp*	*Qe (Lang)*	*Qe (Fr)*
20	1.688	1.70188997	2.09362501
80	6.752	5.92169695	4.85477038
300	18.48	22.5123114	18.697284
400	22.08	25.6278245	24.4453057

Appendix IV: Modeling of the results obtained for the kinetic experiments

The calculations for the kinetic experiments will be explained by using the data obtained for the ammonia uptake onto KMI clinoptilolite, initial ammonia concentration 50mg/l, particle size 0.7-1mm, mass of the material 6.0 g:

External mass transfer coefficient

The results were correlated using the following equation:

$$\ln\left[\frac{C_t}{C_0}-\frac{1}{1+m_sK}\right]=\ln\left[\frac{m_sK}{1+m_sK}\right]+\left[\frac{-1+m_sK}{m_sK}k_fS_st\right]$$

$$m_s=\frac{M}{V}=2 \quad and \quad S_s=\frac{6m_s}{d_p\rho_p}=0.101$$

Plotting $\ln\left[\frac{C_t}{C_0}-\frac{1}{1+m_sK}\right]$ vs time leads to the following figure:

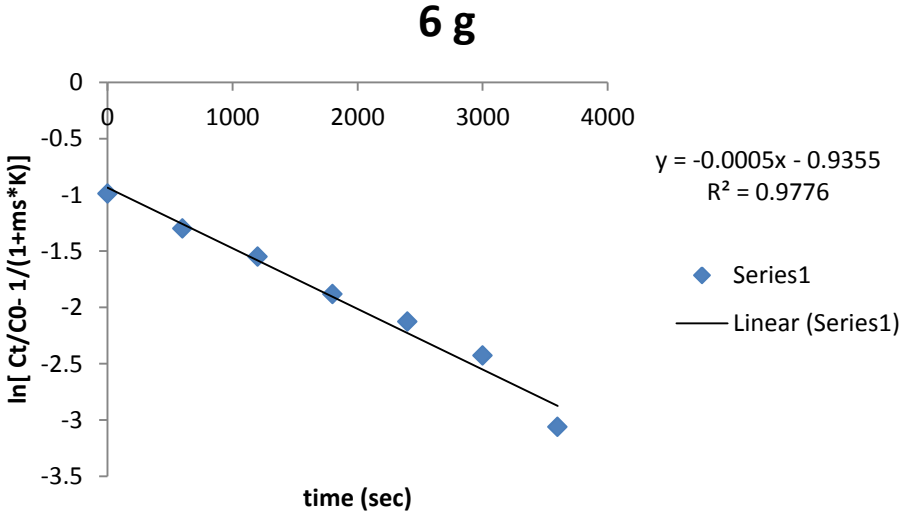

Kf was calculated from slope = 7.163E-3 cm/s

Internal mass transfer coefficient

To test the experimental rate data against the time we used the following equation:

$$k_d = \frac{1}{t^{0.5}} Q_t$$

Qt was calculated by mass balance. The calculated values over 60 minutes were as follows:

t (min)	SQRTt	Ct	Qt
0	0	50	0
10	3.162278	45.03106	2.484472
20	4.472136	42.02899	3.985507
30	5.477226	39.02692	5.486542
40	6.324555	37.3706	6.3147
50	7.071068	35.81781	7.091097
60	7.745967	33.74741	8.126294

When the Qt was plotted versus the square root of the time the following graph was obtained:

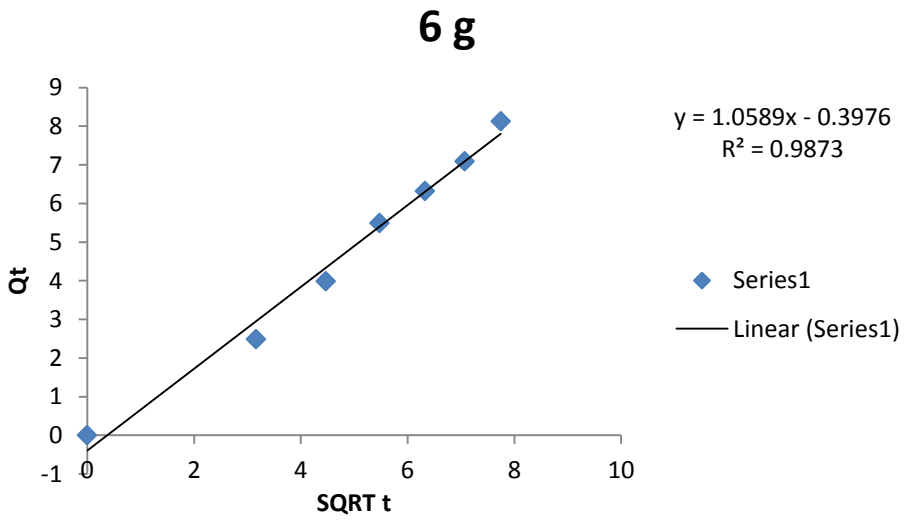

The following value was obtained from the graph:

$k_d = 4.4\ mg/gmin^{0.5}$

Appendix V: The breakthrough uptake capacity calculation

A sample calculatio is made for PES membrane column:

$BV = r^2\pi h = (4.1275\ cm)^2\pi(27\ cm) = 1.455\ L$

Fro PES membrane column, the breakthrough started after 110BV passed through the column;

110BVx1.455 L/BV = 160.05 L

The initial ammonia concentration was 40 mg $N\text{-}NH_4^+$/l ➔ the overall ammonia kept by the KMI clinoptilolite was:

160.05 l x 40 mg/l = 6402 mg $N\text{-}NH_4^+$

The amount of clinoptilolite packed within the column was 1200 g,

- ⇨ The uptake capacity = 6402 mg/1200g = 5.34 mg $N\text{-}NH_4^+$/ g KMI clinoptilolite
- ⇨ = 0.38 meq/g

Appendix VI: Modeling breakthrough curves

The breakthrough curve obtained for the PES membrane column was chosen to show how to apply the Bohart-Adams and Thomas models.

Bohart-Adams model

The Bohart-Adams model used was:

$$\frac{C_t}{C_0} = \exp\left(k_{AB}C_0 t - k_{AB}N_{AB}\frac{Z}{F}\right)$$

The constants, KAB and NAB, sirst were determined by plotting lnCt/C0 vs time; thus, the following figure was obtained:

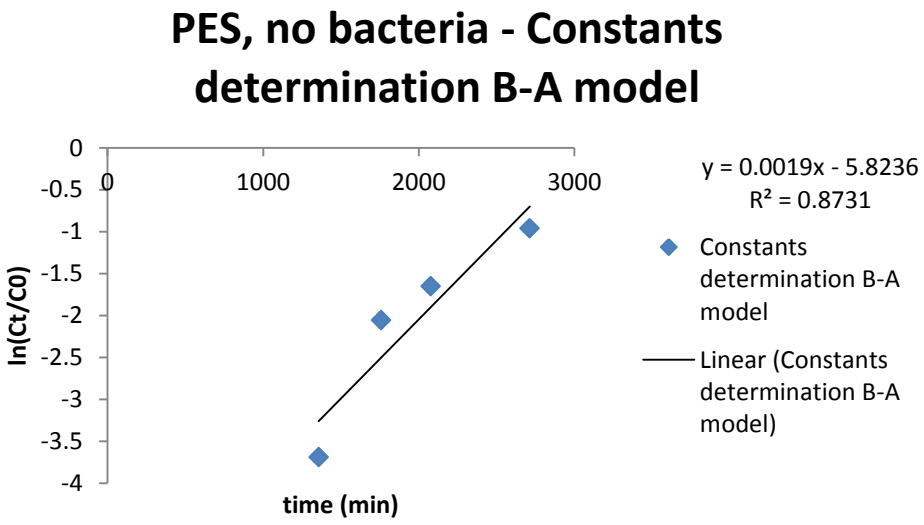

k_{AB} = 4.75E-5, N_{AB}=5657.86

Then, the model was used to estimate the breakthrough profil, and the next table show the Ct/C0 obtained by Bohart-Adams model:

time	C_t/C_0
0	0.002957
1356.89	0.038949
1759.717	0.083732
2077.739	0.153218
2713.781	0.513032
3636.042	2.959087

Thomas model

The Thomas model used is:

$$\frac{C_t}{C_0} = \frac{1}{1 + \exp\left(\frac{k_{Th} q_0 x}{v} - k_{Th} C_0 t\right)}$$

k_{TH} and q_0 was determined by manipulation the model to give the best fit. It was found that by chosing k_{TH} = 0.08 and q_0 = 5.18, the model gave the best fit. These values were compared with values found in the literature. Data obtained is tabulated in the next table:

time	C_t/C_0
0	0.005111453
1356.89	0.283107859
1759.717	0.589027965
2077.739	0.7986079
2713.781	0.968106875

8 References

1. Ferguson, G.A., *Clinoptilolite Zeolite: Effect on Ammonium Exchange Reactions, Nitrification and Plant Nitrogen-Use Efficency*. 1984, The University of Arizona: United States -- Arizona. p. 217.
2. Chalew, T., *Chemical indicators of surface water pollution*. 2006, The University of North Carolina at Chapel Hill: United States -- North Carolina. p. 184.
3. McVeigh, R.J., *The Enhancement of Ammonium Ion Removal Onto Columns of Clinoptilolite In the Presence of Nitrifying Bacteria*. 1999, Department of Chemical Engineering, The Queens University of Belfast: Belfast. p. 239.
4. Miladinovic, N., *Bilogical Interactions During Ion Exchange Removal of Ammonia from Terrestrial and Marine Waste Water* in *Chemical and Process Engineering*. 2005, University of Canterbury: Christchurch. p. 180.
5. Jorgensen, T.C., *Removal of Ammonia from Wastewater by Ion Exchange in the Presence of Organic Compounds* 2002, University of Canterbury Christchurch, New Zealand. p. 174.
6. Dryden, H.T. and L.R. Weatherley, *Aquaculture water treatment by ion exchange: Continuous ammonium ion removal with clinoptilolite.* Aquacultural Engineering, 1989. **8**(2): p. 109-126.
7. Downing, L., *The hybrid membrane-biofilm process: A novel system for achieving nitrogen removal from wastewater*. 2008, University of Notre Dame: United States -- Indiana. p. 352.

8. Preston, K.T., *Co-immobilization of nitrifying bacteria and clinoptilolite*. 1992, Purdue University: United States -- Indiana. p. 232.

9. Preston K. T., A.J.E., *Co-immobilization of Nitrofying Bacteria and Clinoptilolite for Enhanced Control of Nitrification.* roccedings of the 48th Industrial Waste Conference, 1994: p. 407-412.

10. Delatolla, R., *Nitrifying biofilms at cold temperatures: Kinetics and in-situ characterization*. 2009, McGill University (Canada): Canada. p. 292.

11. Lyssenko, C.A., *Impact of operating disturbances on ammonia removal by trickling and submerged-upflow biofilters for intensive recirculating aquaculture*. 2001, University of Maryland College Park: United States -- Maryland. p. 195.

12. Madigan, M., *Brock biology of microorganisms*. 12th ed. 2009: Prentice Hall.

13. Bruce E. Rittmann, P.L.M., *Environmental biotechnology: principles and applications*. 2001: McGraw-Hill.

14. Anthonisen, A.C., et al., *INHIBITION OF NITRIFICATION BY AMMONIA AND NITROUS-ACID.* Journal Water Pollution Control Federation, 1976. **48**(5): p. 835-852.

15. Monod, J., *THE GROWTH OF BACTERIAL CULTURES.* Annual Review of Microbiology, 1949. **3**: p. 371-394.

16. Herbert, D., R. Elsworth, and R.C. Telling, *THE CONTINUOUS CULTURE OF BACTERIA - A THEORETICAL AND EXPERIMENTAL STUDY*. Journal of General Microbiology, 1956. **14**(3): p. 601-622.

17. Chen, S.L., J. Ling, and J.P. Blancheton, *Nitrification kinetics of biofilm as affected by water quality factors.* Aquacultural Engineering, 2006. **34**(3): p. 179-197.

18. Esfandi, A., *INHIBITION OF NITRIFICATION IN BIOLOGICAL SYSTEMS*. 1977, Oklahoma State University: United States -- Oklahoma. p. 218.

19. Helfferich, F.G., *Ion Exchange*. 1962: McGraw-Hill. 624.

20. Kithome, M., *Reducing nitrogen losses during composting of poultry manure using the natural zeolite clinoptilolite*. 1998, The University of British Columbia (Canada): Canada. p. 134.

21. Vemulapalli, G.K., *Simultaneous nitrification and denitrification of septic tank effluents: A comparative pilot-scale study using clinoptilolite and gravel*. 2003, The University of Texas at Arlington: United States -- Texas. p. 99.

22. Larry D. Benefield, J.F.J., Barron L. Weand, *Process chemistry for water and wastewater treatment*. 1982, New Jesey: Prentice-Hall.

23. Lai, R.W.M., *The use of clinoptilolite as permeable reactive barrier substrate for acid rock drainage*. 2005, The University of British Columbia (Canada): Canada. p. 455.

24. Leung, S., *The effect of clinoptilolite properties and supplementation levels on swine performance*. 2005, McGill University (Canada): Canada. p. 117.

25. Dryden, H.T. and L.R. Weatherley, *Aquaculture water treatment by ion-exchange: II. Selectivity studies with clinoptilolite at 0·01*. Aquacultural Engineering, 1987. **6**(1): p. 51-68.

26. Dryden, H.T., *Ammonium ion removal from dilute solutions and fish culture water by ion exchange*, in *Dep't of Chemical & Process Engineering*. 1984, Heriot-Watt University: Edinburgh.

27. Sprynskyy, M., et al., *Heterogeneity and hierarchy of clinoptilolite porosity.* Journal of Physics and Chemistry of Solids, 2010. **71**(9): p. 1269-1277.

28. Aguilar-Armenta, G., et al., *Adsorption kinetics of CO2, O-2, N-2, and CH4 in cation-exchanged clinoptilolite.* Journal of Physical Chemistry B, 2001. **105**(7): p. 1313-1319.

29. Sherwood, D., *Nitrogen loss from cattle feedlots as impacted by the addition of clinoptilolite zeolite to the ration or open-lot surface conditions*. 2007, The University of Nebraska - Lincoln: United States -- Nebraska. p. 125.

30. Furusawa, T. and J.M. Smith, *FLUID-PARTICLE AND INTRAPARTICLE MASS-TRANSPORT RATES IN SLURRIES.* Industrial & Engineering Chemistry Fundamentals, 1973. **12**(12): p. 197-203.

31. Semmens, M.J. and R.R. Goodrich, *BIOLOGICAL REGENERATION OF AMMONIUM-SATURATED CLINOPTILOLITE .1. INITIAL OBSERVATIONS.* Environmental Science & Technology, 1977. **11**(3): p. 255-259.

32. Stankiewicz, A. and J.A. Moulijn, *Re-Engineering the Chemical Processing Plant: Process Intensification*. 2007, Dekker. p. 368.

33. Drioli, E., A.I. Stankiewicz, and F. Macedonio, *Membrane engineering in process intensification--An overview.* Journal of Membrane Science, 2011. **380**(1-2): p. 1-8.

34. Reay D., R.C., Harvey A. , *Process Intensification*. First ed. 2008, MA: Butterworth-Heinemann. 444.

35. Qiu, Z.Y., L.N. Zhao, and L. Weather, *Process intensification technologies in continuous biodiesel production.* Chemical Engineering and Processing, 2010. **49**(4): p. 323-330.

36. Bernardo, P. and E. Drioli, *Membrane gas separation progresses for process intensification strategy in the petrochemical industry.* Petroleum Chemistry, 2010. **50**(4): p. 271-282.

37. Li, J.P., et al., *Long-term partial nitrification in an intermittently aerated sequencing batch reactor (SBR) treating ammonium-rich wastewater under controlled oxygen-limited conditions.* Biochemical Engineering Journal, 2011. **55**(3): p. 215-222.

38. Nittami, T., et al., *Partial nitrification in a continuous pre-denitrification submerged membrane bioreactor and its nitrifying bacterial activity and community dynamics.* Biochemical Engineering Journal, 2011. **55**(2): p. 101-107.

39. Ahn, J.H., T. Kwan, and K. Chandran, *Comparison of Partial and Full Nitrification Processes Applied for Treating High-Strength Nitrogen Wastewaters: Microbial Ecology through Nitrous Oxide Production.* Environmental Science & Technology, 2011. **45**(7): p. 2734-2740.

40. Ahn, J.H., R. Yu, and K. Chandran, *Distinctive microbial ecology and biokinetics of autotrophic ammonia and nitrite oxidation in a partial nitrification Bioreactor.* Biotechnology and Bioengineering, 2008. **100**(6): p. 1078-1087.

41. Cotter, S., *Partial nitrification and oxygen transfer analysis utilizing hollow fiber membrane aeration*. 2010, Iowa State University: United States -- Iowa. p. 75.

42. Shin, S., S.S. Choi, and Y.J. Yoo, *Partial nitrification using an electrolytic aerating bioreactor with ammonia-oxidizing bacteria-dominant activated sludge.* Biotechnology Letters, 2011. **33**(4): p. 699-703.

43. Yan, J. and Y.Y. Hu, *Partial nitrification to nitrite for treating ammonium-rich organic wastewater by immobilized biomass system.* Bioresource Technology, 2009. **100**(8): p. 2341-2347.

44. Edwards, V.H., *INFLUENCE OF HIGH SUBSTRATE CONCENTRATIONS ON MICROBIAL KINETICS.* Biotechnology and Bioengineering, 1970. **12**(5): p. 679-&.

45. Suthersan, S., Ganczarczyk, 1.1., *Inhibition of Nitrite oxidation during nitrification, some observations.* Water Pollution Research Journal of Canada, 1986. **21**(2).

46. Radniecki, T.S. and E.G. Lauchnor, *INVESTIGATING NITROSOMONAS EUROPAEA STRESS BIOMARKERS IN BATCH, CONTINUOUS CULTURE, AND BIOFILM REACTORS,* in *Methods in Enzymology, Vol 46: Research on Nitrification and Related Processes, Pt B*, M.G. Klotz and L.Y. Stein, Editors. 2011. p. 217-246.

47. Gerards, S., H. Duyts, and H.J. Laanbroek, *Ammonium-induced inhibition of ammonium-starved Nitrosomonas europaea cells in soil and sand slurries.* Fems Microbiology Ecology, 1998. **26**(4): p. 269-280.

48. Lauchnor, E., *Inhibition, Gene Expression and Modeling of Ammonia Oxidation in Biofilms of Nitrosomonas europaea*. 2011, Oregon State University: United States -- Oregon. p. 170.

49. Webb, J.L., *Many enzyme conform to Michaelis-Menten kinetics* 1963, Academic Press: New York.

50. Groeneweg, J., B. Sellner, and W. Tappe, *AMMONIA OXIDATION IN NITROSOMONAS AT NH3 CONCENTRATIONS NEAR K-M - EFFECTS OF PH AND TEMPERATURE.* Water Research, 1994. **28**(12): p. 2561-2566.

51. Pambrun, V., E. Paul, and M. Sprandio, *Modeling the partial nitrification in sequencing batch reactor for biomass adapted to high ammonia concentrations.* Biotechnology and Bioengineering, 2006. **95**(1): p. 120-131.

52. Surmacz-Gorska, J., A. Cichon, and K. Miksch, *Nitrogen removal from wastewater with high ammonia nitrogen concentration via shorter nitrification and denitrification.* Water Science and Technology, 1997. **36**(10): p. 73-78.

53. Mauret, M., et al., *Application of experimental research methodology to the study of nitrification in mixed culture.* Water Science and Technology, 1996. **34**(1-2): p. 245-252.

54. Chudoba, J., J.S. ÄŒech, and P. Chudoba, *The Effect of Aeration Tank Configuration on Nitrification Kinetics.* Journal (Water Pollution Control Federation), 1985. **57**(11): p. 1078-1083.

55. Siddiqi, R.H., et al., *Elimination of Nitrification in the BOD Determination with 0.10 M Ammonia Nitrogen.* Journal (Water Pollution Control Federation), 1967. **39**(4): p. 579-589.

56. Ford, D.L., R.L. Churchwell, and J.W. Kachtick, *COMPREHENSIVE ANALYSIS OF NITRIFICATION OF CHEMICAL-PROCESSING WASTEWATERS.* Journal Water Pollution Control Federation, 1980. **52**(11): p. 2726-2746.

57. Tanaka, H. and I.J. Dunn, *KINETICS OF BIOFILM NITRIFICATION*. Biotechnology and Bioengineering, 1982. **24**(3): p. 669-689.

58. Miladinovic, N. and L.R. Weatherley, *Intensification of ammonia removal in a combined ion-exchange and nitrification column.* Chemical Engineering Journal, 2008. **135**(1-2): p. 15-24.

59. Bae, W., et al., *Optimal operational factors for nitrite accumulation in batch reactors.* Biodegradation, 2001. **12**(5): p. 359-366.

60. Chung, J., et al., *Optimization of free ammonia concentration for nitrite accumulation in shortcut biological nitrogen removal process.* Bioprocess and Biosystems Engineering, 2006. **28**(4): p. 275-282.

61. Turk, O. and D.S. Mavinic, *MAINTAINING NITRITE BUILDUP IN A SYSTEM ACCLIMATED TO FREE AMMONIA.* Water Research, 1989. **23**(11): p. 1383-1388.

62. Castens, D.J. and A.F. Rozich, *ANALYSIS OF BATCH NITRIFICATION USING SUBSTRATE-INHIBITION KINETICS.* Biotechnology and Bioengineering, 1986. **28**(3): p. 461-465.

63. Tora, J.A., et al., *Combined effect of inorganic carbon limitation and inhibition by free ammonia and free nitrous acid on ammonia oxidizing bacteria.* Bioresource Technology, 2010. **101**(15): p. 6051-6058.

64. Kim, J.H., X.J. Guo, and H.S. Park, *Comparison study of the effects of temperature and free ammonia concentration on nitrification and nitrite accumulation.* Process Biochemistry, 2008. **43**(2): p. 154-160.

65. Contreras, E.M., F. Ruiz, and N.C. Bertola, *Kinetic Modeling of inhibition of ammonia oxidation by nitrite under low dissolved oxygen conditions.* Journal of Environmental Engineering-Asce, 2008. **134**(3): p. 184-190.

66. Park, S. and W. Bae, *Modeling kinetics of ammonium oxidation and nitrite oxidation under simultaneous inhibition by free ammonia and free nitrous acid.* Process Biochemistry, 2009. **44**(6): p. 631-640.

67. Srinath, E.G., R.C. Loehr, and T.B.S. Prakasam, *NITRIFYING ORGANISM CONCENTRATION AND ACTIVITY.* Journal of the Environmental Engineering Division-Asce, 1976. **102**(2): p. 449-463.

68. Yusof, N., et al., *Nitrification of ammonium-rich sanitary landfill leachate.* Waste Management, 2010. **30**(1): p. 100-109.

69. Aslan, S. and M. Dahab, *Nitritation and denitritation of ammonium-rich wastewater using fluidized-bed biofilm reactors.* Journal of Hazardous Materials, 2008. **156**(1-3): p. 56-63.

70. Ruiz, G., et al., *Nitrification-denitrification via nitrite accumulation for nitrogen removal from wastewaters.* Bioresource Technology, 2006. **97**(2): p. 330-335.

71. Uhl, W. and R. Gimbel, *Dynamic modeling of ammonia removal at low temperatures in drinking water rapid filters.* Water Science and Technology, 2000. **41**(4-5): p. 199-206.

72. Van Hulle, S.W.H., et al., *Engineering aspects and practical application of autotrophic nitrogen removal from nitrogen rich streams.* Chemical Engineering Journal, 2010. **162**(1): p. 1-20.

73. Downing, A.L. and G. Knowles, *POPULATION DYNAMICS IN BIOLOGICAL TREATMENT PLANTS.* Journal Water Pollution Control Federation, 1966. **38**(3P1): p. 352-&.

74. Wang, J.L. and N. Yang, *Partial nitrification under limited dissolved oxygen conditions.* Process Biochemistry, 2004. **39**(10): p. 1223-1229.

75. Wild, H.E., C.N. Sawyer, and T.C. McMahon, *FACTORS AFFECTING NITRIFICATION KINETICS.* Journal Water Pollution Control Federation, 1971. **43**(9): p. 1845-&.

76. Guo, J.H.G.J.H., et al., *Short- and long-term effects of temperature on partial nitrification in a sequencing batch reactor treating domestic wastewater.* Journal of Hazardous Materials, 2010. **179**(1-3): p. 471-479.

77. Farr, S.B. and T. Kogoma, *OXIDATIVE STRESS RESPONSES IN ESCHERICHIA-COLI AND SALMONELLA-TYPHIMURIUM.* Microbiological Reviews, 1991. **55**(4): p. 561-585.

78. Bonazzi, A., *On nitrification V The mechanism of ammonia oxidation.* Journal of Bacteriology, 1923. **8**(4): p. 343-363.

79. Buswell, A.M. and J.F. Pagano, *REDUCTION AND OXIDATION OF NITROGEN COMPOUNDS IN POLLUTED STREAMS.* Sewage and Industrial Wastes, 1952. **24**(7): p. 897-903.

80. Adams, C.E., Jr. and W.W. Eckenfelder, Jr., *Nitrification Design Approach for High Strength Ammonia Wastewaters.* Journal (Water Pollution Control Federation), 1977. **49**(3): p. 413-421.

81. Bryant, C.W., et al., *Biological nitrification of kraft wastewater.* Water Science and Technology, 1997. **35**(2-3): p. 147-153.

82. Montgomery, H., Borne, BJ, *The inhibition of nitrification in the BOD test.* J. Proc. Inst. Sewage Purification, 1966. **357**.

83. Abeliovich, A., *NITRIFYING BACTERIA IN WASTE-WATER RESERVOIRS.* APPLIED AND ENVIRONMENTAL MICROBIOLOGY, 1987. **53**(4): p. 754-760.

84. Haug, R.T. and P.L. McCarty, *NITRIFICATION WITH SUBMERGED FILTERS.* Journal Water Pollution Control Federation, 1972. **44**(11): p. 2086-&.

85. Stenstrom, M.K. and R.A. Poduska, *THE EFFECT OF DISSOLVED-OXYGEN CONCENTRATION ON NITRIFICATION.* Water Research, 1980. **14**(6): p. 643-649.

86. Knowles, G., A.L. Downing, and M.J. Barrett, *DETERMINATION OF KINETIC CONSTANTS FOR NITRIFYING BACTERIA IN MIXED CULTURE WITH AID OF AN ELECTRONIC COMPUTER.* Journal of General Microbiology, 1965. **38**(2): p. 263-&.

87. Sanchez, O., N. Bernet, and J.P. Delgenes, *Effect of dissolved oxygen concentration on nitrite accumulation in nitrifying. Sequencing batch reactor.* Water Environment Research, 2007. **79**(8): p. 845-850.

88. Chung, J., et al., *Comparison of influence of free ammonia and dissolved oxygen on nitrite accumulation between suspended and attached cells.* Environmental Technology, 2005. **26**(1): p. 21-33.

89. Jechalke, S., et al., *Inhibition of Nitrification by Low Oxygen Concentrations in an Aerated Treatment Pond System with Biofilm Promoting Mats.* Water Environment Research, 2011. **83**(7): p. 622-626.

90. Daebel, H., R. Manser, and W. Guer, *Exploring temporal variations of oxygen saturation constants of nitrifying bacteria.* Water Research, 2007. **41**(5): p. 1094-1102.

91. Stankiewich, M., *Biological Nitrification with the High purity Oxygenation Process*, in *27th Purdue Industrial Waste Conference*. 1972.

92. Baykal, B.B., et al., *The effect of initial loading on the removal of ammonium and potassium from source-separated human urine via clinoptilolite.* Water Science and Technology, 2009. **60**(10): p. 2515-2520.

93. Beler-Baykal, B. and A.D. Allar, *Upgrading fertilizer production wastewater effluent quality for ammonium discharges through ion exchange with clinoptilolite.* Environmental Technology, 2008. **29**(6): p. 665-672.

94. de Lima, R.M.G., et al., *Removal of ammonium ions from waters produced in petroleum offshore exploitation by adsorption on clinoptilolite.* Quimica Nova, 2008. **31**(5): p. 1237-1242.

95. Gunay, A., *Application of nonlinear regression analysis for ammonium exchange by natural (Bigadic) clinoptilolite.* Journal of Hazardous Materials, 2007. **148**(3): p. 708-713.

96. Guo, X., et al., *Ammonium and potassium removal for anaerobically digested wastewater using natural clinoptilolite followed by membrane pretreatment.* Journal of Hazardous Materials, 2008. **151**(1): p. 125-133.

97. Hedstrom, A. and L.R. Amofah, *Adsorption and desorption of ammonium by clinoptilolite adsorbent in municipal wastewater treatment systems.* Journal of Environmental Engineering and Science, 2008. **7**(1): p. 53-61.

98. Jorgensen, T.C. and L.R. Weatherley, *Continuous ion-exchange removal of ammonium ion onto clinoptilolite in the presence of contaminants.* Asia-Pacific Journal of Chemical Engineering, 2008. **3**(1): p. 57-62.

99. Karadag, D., et al., *Ammonium Removal from Municipal Landfill Leachate by Clinoptilolite Bed Columns: Breakthrough Modeling and Error Analysis.* Industrial & Engineering Chemistry Research, 2008. **47**(23): p. 9552-9557.

100. Karadag, D., et al., *Ammonium removal from sanitary landfill leachate using natural Gordes clinoptilolite.* Journal of Hazardous Materials, 2008. **153**(1-2): p. 60-66.

101. Mazeikiene, A., M. Valentukeviciene, and J. Jankauskas, *LABORATORY STUDY OF AMMONIUM ION REMOVAL BY USING ZEOLITE (CLINOPTILOLITE) TO TREAT DRINKING WATER.* Journal of Environmental Engineering and Landscape Management, 2010. **18**(1): p. 54-61.

102. Mazeikiene, A., et al., *Removal of nitrates and ammonium ions from water using natural sorbent zeolite (clinoptilolite).* Journal of Environmental Engineering and Landscape Management, 2008. **16**(1): p. 38-44.

103. Rahmani, A.R., M.T. Samadi, and H.R. Ehsani, *INVESTIGATION OF CLINOPTILOLITE NATURAL ZEOLITE REGENERATION BY AIR STRIPPING*

FOLLOWED BY ION EXCHANGE FOR REMOVAL OF AMMONIUM FROM AQUEOUS SOLUTIONS. Iranian Journal of Environmental Health Science & Engineering, 2009. **6**(3): p. 167-172.

104. Siljeg, M., L. Foglar, and M. Kukucka, *The ground water ammonium sorption onto Croatian and Serbian clinoptilolite.* Journal of Hazardous Materials, 2010. **178**(1-3): p. 572-577.

105. Van Nooten, T., L. Diels, and L. Bastiaens, *Microbially Mediated Clinoptilolite Regeneration in a Multifunctional Permeable Reactive Barrier Used to Remove Ammonium from Landfill Leachate Contamination: Laboratory Column Evaluation.* Environmental Science & Technology, 2010. **44**(9): p. 3486-3492.

106. Vassileva, P. and D. Voikova, *Investigation on natural and pretreated Bulgarian clinoptilolite for ammonium ions removal from aqueous solutions.* Journal of Hazardous Materials, 2009. **170**(2-3): p. 948-953.

107. Wang, H.Y., H.F. Huang, and J.Q. Jiang, *The effect of metal cations on phenol adsorption by hexadecyl-trimethyl-ammonium bromide (hdtma) modified clinoptilolite (Ct.).* Separation and Purification Technology, 2011. **80**(3): p. 658-662.

108. Klieve, J.R. and M.J. Semmens, *An evaluation of pretreated natural zeolites for ammonium removal.* Water Research, 1980. **14**(2): p. 161-168.

109. Jorgensen, T.C., Weatherley. *Ion Exchange Removal of Ammonium Ion from Wastewater onto Clinoptilolite in the Presence of Organics*. in *6th World Congress of Chemical Engineering*. 2001. Melbourne.

110. McLaren, J.R. and G.J. Farquhar, *FACTORS AFFECTING AMMONIA REMOVAL BY CLINOPTILOLITE.* Journal of the Environmental Engineering Division-Asce, 1973. **99**(NEE4): p. 429-446.

111. Semmens, M.J. and W.P. Martin, *THE INFLUENCE OF PRETREATMENT ON THE CAPACITY AND SELECTIVITY OF CLINOPTILOLITE FOR METAL-IONS.* Water Research, 1988. **22**(5): p. 537-542.

112. Inglezakis, V.J., et al., *Pretreatment of natural clinoptilolite in a laboratory-scale ion exchange packed bed.* Water Research, 2001. **35**(9): p. 2161-2166.

113. Jorgensen, S.E., et al., *AMMONIA REMOVAL BY USE OF CLINOPTILOLITE.* Water Research, 1976. **10**(3): p. 213-224.

114. Nguyen, M.L., Tanner, C. C., *Ammonia Removal From Wastewaters Using Natural New Zealand Zeolites.* New Zealand Journal of Agricultural Research, 1998. **41**(3): p. 20.

115. Ji, Z.Y., J.S. Yuan, and X.G. Li, *Removal of ammonium from wastewater using calcium form clinoptilolite.* Journal of Hazardous Materials, 2007. **141**(3): p. 483-488.

116. Thomas, H.C., *Heterogeneous ion exchange in a flowing system.* Journal of the American Chemical Society, 1944. **66**: p. 1664-1666.

117. Bohart, G.S. and E.Q. Adams, *Some aspects of the behavior of charcoal with respect to chlorine.* Journal of the American Chemical Society, 1920. **42**: p. 523-544.

118. Lopes, C.B., et al., *Fixed-bed removal of Hg(2+) from contaminated water by microporous titanosilicate ETS-4: Experimental and theoretical breakthrough curves.* Microporous and Mesoporous Materials, 2011. **145**(1-3): p. 32-40.

119. Han, R.P., et al., *Adsorption of methylene blue by phoenix tree leaf powder in a fixed-bed column: experiments and prediction of breakthrough curves.* Desalination, 2009. **245**(1-3): p. 284-297.

120. Hutchins, R.A., *NEW METHOD SIMPLIFIES DESIGN OF ACTIVATED-CARBON SYSTEMS.* Chemical Engineering, 1973. **80**(19): p. 133-138.

121. Webb, C., Black, G.M., Atkinson, B., ed. *Process Engineering Aspects of Immobilized Cell Systems*. 1984: England.

122. Pilkington, P.H., et al., *Fundamentals of immobilised yeast cells for continuous beer fermentation: A review.* Journal of the Institute of Brewing, 1998. **104**(1): p. 19-31.

123. Hill, C.B. and E. Khan, *A comparative study of immobilized nitrifying and co-immobilized nitrifying and denitrifying bacteria for ammonia removal from sludge digester supernatant.* Water Air and Soil Pollution, 2008. **195**(1-4): p. 23-33.

124. Manju, N.J., et al., *Immobilization of nitrifying bacterial consortia on wood particles for bioaugmenting nitrification in shrimp culture systems.* Aquaculture, 2009. **294**(1-2): p. 65-75.

125. Dong, Y.M., et al., *Nitrification performance of nitrifying bacteria immobilized in waterborne polyurethane at low ammonia nitrogen concentrations.* Journal of Environmental Sciences-China, 2011. **23**(3): p. 366-371.

126. Cao, G.M., et al., *Characterization of nitrifying and denitrifying bacteria coimmobilized in PVA and kinetics model of biological nitrogen removal by coimmobilized cells.* Enzyme and Microbial Technology, 2002. **30**(1): p. 49-55.

127. Li, Z.R., et al., *Comparative study of the nitrification characteristics of two different nitrifier immobilization methods.* Biodegradation, 2009. **20**(6): p. 859-865.

128. Ginkel, C.G., et al., *CHARACTERIZATION OF NITROSOMONAS-EUROPAEA IMMOBILIZED IN CALCIUM ALGINATE.* Enzyme and Microbial Technology, 1983. **5**(4): p. 297-303.

129. Sumino, T., et al., *IMMOBILIZATION OF NITRIFYING BACTERIA IN POROUS PELLETS OF URETHANE GEL FOR REMOVAL OF AMMONIUM NITROGEN FROM WASTE-WATER.* Applied Microbiology and Biotechnology, 1992. **36**(4): p. 556-560.

130. Uemoto, H., A. Ando, and H. Saiki, *Effect of oxygen concentration on nitrogen removal by Nitrosomonas europaea and Paracoccus denitrificans immobilized within tubular polymeric gel.* Journal of Bioscience and Bioengineering, 2000. **90**(6): p. 654-660.

131. Tramper, J., G. Suwinskaborowiec, and A. Klapwijk, *CHARACTERIZATION OF NITRIFYING BACTERIA IMMOBILIZED IN CALCIUM ALGINATE.* Enzyme and Microbial Technology, 1985. **7**(4): p. 155-160.

132. Hao, J., *Membrane processes for gas separations: Part I. Removal of carbon dioxide and hydrogen sulfide from low-quality natural gas. Part II. Enrichment of krypton in air*. 1998, Syracuse University: United States -- New York. p. 252.

133. van Reis, R. and A. Zydney, *Bioprocess membrane technology*. Journal of Membrane Science, 2007. **297**(1-2): p. 16-50.

134. Downing, L.S. and R. Nerenberg, *Effect of Oxygen Gradients on the Activity and Microbial Community Structure of a Nitrifying, Membrane-Aerated Biofilm.* Biotechnology and Bioengineering, 2008. **101**(6): p. 1193-1204.

135. Schaffer, R.B., F.J. Ludzack, and M.B. Ettinger, *Sewage Treatment by Oxygenation through Permeable Plastic Films.* Journal (Water Pollution Control Federation), 1960. **32**(9): p. 939-941.

136. Gazola, F.C., et al., *Removal of Cr3+ in fixed bed using zeolite NaY.* Chemical Engineering Journal, 2006. **117**(3): p. 253-261.

137. Ostroski, I.C., et al., *A comparative study for the ion exchange of Fe(III) and Zn(II) on zeolite NaY.* Journal of Hazardous Materials, 2009. **161**(2-3): p. 1404-1412.

138. Ostroski, I.C., et al., *Mass Transfer Mechanism of Ion Exchange in Fixed Bed Columns.* Journal of Chemical and Engineering Data, 2011. **56**(3): p. 375-382.

139. da Silva, E.A., et al., *Modeling of copper(II) biosorption by marine alga Sargassum sp in fixed-bed column.* Process Biochemistry, 2002. **38**(5): p. 791-799.

140. Barrosa, M., et al., *Removal of Cr(III) in the fixed bed column and batch reactors using as adsorbent zeolite NaX.* Chemical Engineering Science, 2004. **59**(24): p. 5959-5966.

141. Ruthven, D.M., *Principles of Adsorption and Adsorption Processes*. 1984, New York: Wiley.

142. Wilson, E.J. and Geankopl.Cj, *LIQUID MASS TRANSFER AT VERY LOW REYNOLDS NUMBERS IN PACKED BEDS.* Industrial & Engineering Chemistry Fundamentals, 1966. **5**(1): p. 9-&.

143. James E. Bailey, D.F.O., *Biochemical engineering fundamentals*. 1986: McGraw-Hill.

144. Wijffels, R.H. and J. Tramper, *Nitrification by immobilized cells.* Enzyme and Microbial Technology, 1995. **17**(6): p. 482-492.

145. Zhu, S.M. and S.L. Chen, *The impact of temperature on nitrification rate in fixed film biofilters.* Aquacultural Engineering, 2002. **26**(4): p. 221-237.

146. Hamdi, M., *BIOFILM THICKNESS EFFECT ON THE DIFFUSION LIMITATION IN THE BIOPROCESS REACTION - BIOFLOC CRITICAL DIAMETER SIGNIFICANCE.* Bioprocess Engineering, 1995. **12**(4): p. 193-197.

147. Meunier, A.D. and K.J. Williamson, *PACKED-BED BIOFILM REACTORS - SIMPLIFIED MODEL*. Journal of the Environmental Engineering Division-Asce, 1981. **107**(2): p. 307-317.

148. (AWWA), A.W.W.A., *Simplified Procedures for Water Examination*. 5 th ed. .

149. Lawrence, C.o., *Water Quality Report.* 2010.

150. Dryden, H.T. and L.R. Weatherley, *Aquaculture water treatment by ion-exchange: I. Capacity of hector clinoptilolite at 0·01-0·05.* Aquacultural Engineering, 1987. **6**(1): p. 39-50.

151. Wu, Q.L. and B.M. Wu, *STUDY OF MEMBRANE MORPHOLOGY BY IMAGE-ANALYSIS OF ELECTRON-MICROGRAPHS.* Journal of Membrane Science, 1995. **105**(1-2): p. 113-120.

152. Adam Mayernick, L.W., *Membrane Aeration studies for Wastewater treatment Applications*. 2005.

153. Droste, R.L., *Theory and practice of water and wastewater treatment*. 1997: J. Wiley.